# Similar and Non-Similar Flows of Nanofluid with Heat and Mass Transfer


*By*

**Muhammad Saleem Iqbal**

**Reg. No. 09-FBAS/PHDMA/S12**

**Department of Mathematics and Statistics**
**Faculty of Basic and Applied Sciences**
**International Islamic University, Islamabad**
**Pakistan**


**2018**

# Similar and Non-Similar Flows of Nanofluid with Heat and Mass Transfer

*By*

**Muhammad Saleem Iqbal**

*Supervised By*

**Dr. Ahmer Mehmood**

**Department of Mathematics and Statistics**
**Faculty of Basic and Applied Sciences**
**International Islamic University, Islamabad**
**Pakistan**
**2018**

# Similar and Non-Similar Flows of Nanofluid with Heat and Mass Transfer

A dissertation

submitted in the partial fulfillment of the

requirements for the degree of

**DOCTOR OF PHILOSOPHY**

**IN**

**MATHEMATICS**

*Submitted By*

**Muhammad Saleem Iqbal**

*Supervised By*

**Dr. Ahmer Mehmood**

**Department of Mathematics and Statistics**

**Faculty of Basic and Applied Sciences**

**International Islamic University, Islamabad**

**Pakistan**

**2018**

# Author’s Declaration

I, **Muhammad Saleem Iqbal** Reg. No. **9-FBAS/PHDMA/S12** hereby state that my Ph.D. thesis titled: **Similar and Non-similar Flows of Nonfluid with Heat and Mass Transfer** is my own work and has not been submitted previously by me for taking any degree from this university, **International Islamic University, Sector H-10, Islamabad, Pakistan** or anywhere else in the country/world.

At any time if my statement is found to be incorrect even after my Graduation the university has the right to withdraw my Ph.D. degree.

Name of Student: ***(Muhammad Saleem Iqbal)***
Reg. No. **9-FBAS/PHDMA/S12**
Dated: **01/08/2018**

# Plagiarism Undertaking

I solemnly declare that research work presented in the thesis titled: **Similar and Non-similar Flows of Nonfluid with Heat and Mass Transfer** is solely my research work with no significant contribution from any other person. Small contribution/help wherever taken has been duly acknowledged and that complete thesis has been written by me.

I understand the zero tolerance policy of the HEC and University, **International Islamic University, Sector H-10, Islamabad, Pakistan** towards plagiarism. Therefore, I as an Author of the above titled thesis declare that no portion of my thesis has been plagiarized and any material used as reference is properly referred/cited.

I undertake that if I am found guilty of any formal plagiarism in the above titled thesis even after award of Ph.D. degree, the university reserves the rights to withdraw/revoke my Ph.D. degree and that HEC and the University has the right to publish my name on the HEC/University Website on which names of students are placed who submitted plagiarized thesis.

Student/Author Signature: ______________________________

Name: **(Muhammad Saleem Iqbal)**

# Certificate of Approval

This is to certify that the research work presented in this thesis, entitled: **Similar and Non-similar Flows of Nonfluid with Heat and Mass Transfer** was conducted by **Mr. Muhammad Saleem Iqbal,** Reg. No. **9-FBAS/PHDMA/S12** under the supervision of **Dr. Ahmer Mehmood** no part of this thesis has been submitted anywhere else for any other degree. This thesis is submitted to the **Department of Mathematics & Statistics, FBAS, IIU, Islamabad** in partial fulfillment of the requirements for the degree of **Doctor of Philosophy in Mathematics, Department of Mathematics & Statistics, Faculty of Basic & Applied Science, International Islamic University, Sector H-10, Islamabad, Pakistan.**

**Student Name: Muhammad Saleem Iqbal** **Signature: ______________**

## Examination Committee:

a) **External Examiner 1:**
**Name/Designation/Office Address** **Signature: ______________**

**Prof. Dr. Muhammad Ayub**
Professor of Mathematics,
Department of Mathematics,
QAU, Islamabad

b) **External Examiner 2:**
**Name/Designation/Office Address)** **Signature: ______________**

**Prof. Dr. Mazhar Hussain**
Professor of Mathematics,
National University of Computer & Emerging Sciences,
Islamabad, Pakistan.

c) **Internal Examiner:**
**Name/Designation/Office Address)** **Signature: ______________**

**Prof. Dr. Muhammad Sajid T.I**
Professor

***Supervisor Name:***
**Dr. Ahmer Mehmood** **Signature: ______________**

***Name of Dean/HOD:***
**Prof. Dr. Muhammad Sajid, T.I** **Signature: ______________**

**My Life**

*may not be going the way*

**I planned**

*it, but it is going*

**Exactly**

*the way*

**ALLAH**

*planned it*

# Acknowledgement

First and foremost, I am grateful to Almighty **Allah** the most merciful and the most beneficent creator who has enabled me to perform this research work. I offer my humblest and sincerest thanks to the Holy Prophet Hazrat **Muhammad** Mustafa (SAW) who is forever a torch of guidance and knowledge for humanity.

It is a great pleasure to acknowledge my supervisor **Dr. Ahmer Mehmood** for his valuable suggestions and guidance during the Ph.D. research work, his experience, tremendous cooperation and valuable comments enabled me to complete my dissertation successfully. I would appreciate the painstaking attitude of my supervisor. He does not forward any draft unless he himself is satisfied with its standard which indicates his professional approach and sincerity to the subject.

I would like to express my gratitude and special thanks to the Chairman Department of Mathematics **Prof. Dr. Muhammad Sajid (T.I)** for his favorable response and valuable suggestions during the whole study. I express my sincere thanks to external examiners **Prof. Dr. Muhammad Ayub** and **Prof. Dr. Mazhar Hussain** for valuable comments and encouragement.

I am thankful to the faculty and staff of Mathematics Department for the co-operation during study. I would also express my sincere appreciation for help received from **Prof. Dr. Tariq Javed** and **Prof. Dr. Nasir Ali**.

I am grateful to all my research colleagues including ‘**Dr. Irfan Mustafa, Dr. Abid Majeed, Dr. Abuzar Ghaffri, Dr. Bilal Ahmed, Dr. Muhammad Asif Javed Rana, Dr. Mubashir Nazeer, Dr. Raja Ziafat Mehmood, Mr. Muhammad Arshad Siddiqui, Mr. Abdul Haleem Hamid, Hafiz Muhammad Atif, Mr. Muhammad Usman, Mr. Sajid Khan, Mr. Ghulam Dastgir Tabassum, Mr. Iqrar Raza, Mr. Muhammad Awais, Mr. Babar shah,** for their encouragement and helping in all affairs especially in my research work. I am thankful to the staff of the **ICB G-6/3 Islamabad**, for their cooperation during the time of research. I pay gratitude to my cousin **Prof. Dr. Muhammad Iqbal** (late) and my PhD fellow **Prof. Dr. Hussain Ahmed** (late).

I express my devoted affection to all my family members for creating a delightful atmosphere and excusing me from family duties in order to complete the research.

# Nomenclature

| | |
|---|---|
| $B_0$ | Magnetic field strength |
| $C$ | Concentration of fluid |
| $c_p$ | Specific heat at constant pressure |
| $C_f, C_{fx}$ | Local skin friction coefficient |
| $C_{f_{avg}}$ | Average skin friction coefficient |
| $D_B$ | Brownian diffusion coefficient |
| $D_m$ | Mass diffusivity |
| $D_T$ | Thermophoretic diffusion coefficient |
| $d, d_1, d_2, d_3, d_4, d_5$ | Material parameters |
| $f$ | Dimensionless stream function |
| $g$ | Acceleration due to gravity |
| $H$ | Heat source/sink parameter |
| $l$ | Reference length |
| $Le$ | Lewis number |
| $M$ | Magnetic parameter |
| $m$ | Temperature /Concentration Power-law index |
| $N_b$ | Brownian motion parameter |
| $N_t$ | Thermophoresis parameter |
| $\hat{n}$ | Unit normal to the wavy surface |
| $Nu, Nu_x$ | Local Nusselt number |
| $Nu_{avg}$ | Average Nusselt number |
| $p$ | Pressure |
| $Pr$ | Prandtl number |
| $Q$ | Uniform heat sink/source |
| $q_r$ | Radiative heat flux |
| $q_w$ | Surface heat flux |
| $r$ | Radius of the cone |
| $Rd$ | Radiation parameter |

| | |
|---|---|
| $Re, Re_x$ | Reynolds number |
| $S$ | Sinusoidal wavy function |
| $Sh, Sh_x$ | Sherwood Nusselt number |
| $T$ | Fluid temperature |
| $T_w$ | Temperature at the surface |
| $T_\infty$ | Ambient fluid temperature |
| $\hat{t}$ | Unit vector normal to the wavy surface |
| $u$ | Velocity component along $x$-direction |
| $U$ | Free stream velocity |
| $u_c$ | Reference velocity |
| $v$ | Velocity component along $y$-direction |
| $\boldsymbol{V}$ | Velocity vector |

**Greek symbols**

| | |
|---|---|
| $\bar{\alpha}$ | Amplitude |
| $\alpha$ | Ratio of the wavy amplitude to the wave length |
| $\alpha^*$ | Thermal diffusivity |
| $\beta$ | Thermal expansion coefficient |
| $\gamma$ | Cone half angle |
| $\delta$ | Boundary layer thickness |
| $\eta, \xi$ | Dimensionless variables |
| $\theta, \theta^*$ | Dimensionless temperature |
| $\kappa$ | Thermal conductivity of fluid |
| $\mu$ | Dynamic viscosity |
| $\nu$ | Kinematic viscosity |
| $\rho$ | Density |
| $\sigma$ | Sinusoidal wavy surface |
| $\sigma^*$ | Electrical conductivity |
| $\tau^*$ | Ratio of heat capacity of nanoparticle to the base fluid |
| $\tau_w$ | Surface shear stress |
| $\varphi, \varphi^*$ | Dimensionless concentration |

| | |
|---|---|
| $\phi$ | Concentration of nanoparticle |
| $\psi$ | Stream function |
| ω | Wavy parameter |

**Subscripts**

| | |
|---|---|
| $f$ | Base fluid |
| $nf$ | Nanofluid |
| $p$ | Nanoparticle |
| $w$ | Condition at the surface |
| $\infty$ | Condition at the Infinity |
| $\eta, \xi$ | Partial derivatives |

**Superscript**

| | |
|---|---|
| $'$ | Ordinary derivative w.r.t $\eta$ |

# Preface

Nanofluids own upgraded thermal properties, especially, higher thermal conductivity and increased convective heat transfer coefficient as compared to their respective base fluid. Nanofluids are therefore a novel class of fluids designed by dispersing nanometer-sized material particles (nanoparticles, nanofibers, nanotubes, nanowires, nano rods, nano sheets) in the base fluids. They may also be regarded as nanoscale colloidal suspensions containing condensed nanomaterials. They are two-phase systems with one phase (solid phase) into another (liquid phase). Nanofluids have also been found to exhibit enhanced thermal diffusivity and viscosity compared to those of base fluids like oil or water etc. In many engineering simulations, including computational fluid dynamics, a nanofluid can be assumed to be single-phase fluid. In the course of mathematical modeling of their convective transport the classical theory of single-phase fluids is usually applied, where the physical properties of the nanofluid are taken as the functions of properties of both the constituents and their concentration.

In the boundary layer flows the concept of self-similarity is of particular importance. For the self-similar flows the governing boundary layer equations, do reduce to ordinary differential equations; thus providing a great facility towards their solution. Particular to the two-dimensional flows the self-similarity is directly associated to the particular forms of the reference velocities; the surface texture and the imposed boundary conditions. In this dissertation the conditions of self-similarity for a two-dimensional convective heat and mass transfer flow problems have been determined. In view of the obtained criteria of self-similar and non-similar solutions have been discussed. By utilizing the famous mathematical nanofluid models namely, the Buongiorno model and the Tiwari and Das model attempts have been made to analyze the heat and mass transfer characteristics along horizontal/vertical flat or non-flat surfaces. Comparisons have been made by calculating the average heat and mass transfer rates for the nanofluid and the pure fluid. These analyses are carried out numerically by the utilization of implicit finite difference schemes.

**Chapter one** covers important information of nanofluid models, heat transfer modes, characteristics of dimensionless parameters, and literature review on self-similar and non-similar flows of nanofluid with heat and mass transfer. In **Chapter two** laminar, incompressible, boundary-layer flow over a vertical flat plate for variable surface temperature (VWT) and variable heat flux (VHF) cases has been investigated. The general form of boundary layer equations, for the Buongiorno nanofluid model, are modeled, which are equally valid for self-similar and non-similar flows. The power-law form of the variable wall temperature, for which the flow is self-similar, is derived by utilizing the conditions of self-similarity. Sherwood number and Nusselt number are calculated numerically for different values of Brownian motion and thermophoresis parameters. The contents of this chapter are submitted to **Canadian Journal of Physics**.

**Chapter three** contains the analysis of nanofluid flow along a circular cone with heat and mass transfer. Buongiorno transport model for nanofluid has been used to model the transport equations. These equation together with boundary data are solved using an explicit finite difference scheme. Effects of thermophoresis and Brownian motion are studied in detail. Important physical quantities of interest have been investigated graphically in the form of heat and mass transfer rates. Thermophoresis and Brownian motion play vital role in the improvement of heat and mass transfer phenomena.

The investigation on heat transfer in the MHD boundary layer flow over the moving wavy plate is considered in **Chapter four**. Due to the presence of metallic nanoparticles in the fluid and enhanced surface area of the plate as a consequence of non-flat surface texture, an increase in the convective heat transfer rate is expected. However, the calculation of these enhanced rates of heat transfer is not straightforward because the convection phenomena becomes more complicated due the motion of nanoparticle in the base fluid and also due to the waviness of the plate surface. The contribution of nanoparticles towards convective heat transfer is many fold which requires a suitable model in order to capture the correct physics. Famous Tiwari and Das model has been utilized in the current study. Percent increase in the average rate of heat transfer is calculated for the nanoparticles of different metals, such as $MWCNT$, $SWCNT$, $Al_2O_3$, $TiO_2$ and $Ag$. The trend of velocity profile, Nusselt number and coefficient of skin friction under applied magnetic field has been shown with the help of graphs. The concentration of the nanoparticles has been limited up to 10%. The contents of this chapter have been published in **Zeitschrift für Naturforschung A, 71(7) (2016) 583-593.**

**Chapter five** contains the study of heat transfer characteristics in natural convection flow of water-based nanofluid near a vertical rough wall. The analysis considers five different nanoparticles, namely, silver ($Ag$), copper ($Cu$), alumina ( $Al_2O_3$), magnetite ($Fe_3O_4$) and silica ($SiO_2$). The concentration has been limited between $0-10\%$ for all types of nanoparticle. The governing equations are modeled using the Boussinesq approximation where the Tiwari and Das model is utilized to represent the nanofluid. The analysis examines the effects of nanoparticle volume fraction, the type of nanoparticle and the wavy surface geometry parameter on the skin friction coefficient and the Nusselt number. It is noticed that Nusselt number for considered nanofluid can be enhanced via an appropriate tuning of the wavy surface geometry parameter along with the adjustment of nanoparticle concentration. The concluded results of this chapter are presented in an article which was published in **Thermal Science, DOI:10.2298/TSCI151008122M.**

**Chapter six** considers the effects of heat generation/absorption and nanoparticle on natural convection heat transfer phenomena along vertical wavy surface. Transport equations have been solved numerically by an accurate implicit finite difference scheme. The skin friction coefficient and the Nusselt number are plotted under the variation of several parameters for two types of nanoparticles namely, alumina ($Al_2O_3$) and magnetite ($Fe_3O_4$). The impact of nanoparticle concentration on flow and heat transfer process has been studied in detail. For heat generation/absorption case percent change in the average skin friction coefficient and the average Nusselt number for two types of nanoparticles is calculated. The article published in **Journal of Molecular Liquids, 222 (2016) 1326-1331,** contains the contents of this chapter.

In **Chapter seven**, the problem of natural convective heat transfer of water-based nanofluid along wavy cone surface is investigated numerically. Analysis is performed to study the heat transfer augmentation due to five different types of nanoparticles, namely, alumina ($Al_2O_3$), copper ($Cu$), silver ($Ag$), copper oxide ($CuO$) and titania ($TiO_2$). Famous Tiwari and Das model of nanofluid has been utilized in this study. The effects of cone half angle $\gamma$ and amplitude of the waviness $\alpha$ on the Nusselt number ($Nu$) and the skin friction coefficient ($C_f$) are studied. These results are the part of an article which has been published in the **Journal of Molecular Liquids, 223 (2016) 1178-1184.**

# Contents

Chapter 1 .......... 5

Introduction and preliminaries .......... 5

1.1 Introduction .......... 5

1.2 Preliminaries .......... 15

1.2.1 Fluid .......... 15

1.2.2 Fluid mechanics .......... 16

1.2.3 Heat transfer phenomenon .......... 16

1.2.4 Nanofluid .......... 17

1.2.5 Thermophysical properties of nanofluid .......... 19

1.2.5.1 Density .......... 19

1.2.5.2 Specific heat .......... 20

1.2.5.3 Thermal conductivity .......... 20

1.2.5.4 Effective electrical conductivity .......... 20

1.2.5.5 Thermal diffusivity .......... 20

1.2.5.6 Viscosity .......... 21

1.2.6 Governing equations .......... 22

1.2.6.1 Equation of continuity .......... 22

1.2.6.2 Momentum equation .......... 22

1.2.6.3 Energy equation .......... 23

1.2.6.4 Concentration equation .......... 23

1.2.7 Wavy surface .......... 24

1.2.8 Heat source/sink .......... 25

1.2.9 Skin friction coefficient .......... 25

1.2.10 Nusselt number .......... 25

1.2.11 Sherwood number ........................................................................ 26

1.2.12 Reynolds number ........................................................................ 26

1.2.13 Prandtl number ........................................................................ 26

1.2.14 Grashof number ........................................................................ 27

1.2.15 Lewis number ........................................................................ 27

1.2.16 Thermophoresis ........................................................................ 27

1.2.17 Brownian motion ........................................................................ 28

1.2.18 Self-similar and non-similar flows ........................................................................ 28

1.2.19 Solution methodology ........................................................................ 29

Chapter 2 ........................................................................ 30

Self-similar natural convection flow of nanofluid past a vertical plate ........................................................................ 30

2.1 Problem formulation ........................................................................ 30

2.1.1 Buongiorno convective transport model ........................................................................ 30

2.1.2 Flow assumptions ........................................................................ 31

2.1.3 Governing equations ........................................................................ 32

2.2 Numerical scheme ........................................................................ 36

2.3 Results and discussion ........................................................................ 41

2.4 Conclusion ........................................................................ 53

Chapter 3 ........................................................................ 54

Self-similar natural convection flow of nanofluid past a circular cone ........................................................................ 54

3.1 Problem formulation ........................................................................ 54

3.2 Numerical scheme ........................................................................ 56

3.3 Results and discussion ........................................................................ 57

3.4 Conclusion ........................................................................ 63

Chapter 4 ........................................................................ 64

Heat transfer analysis of non-similar MHD nanofluid flow along moving wavy surface .. 64

4.1 Problem formulation ........................................................................... 64

4.2 Solution methodology ........................................................................... 69

4.3 Results and discussion ........................................................................... 76

4.4 Conclusion ........................................................................... 89

Chapter 5 ........................................................................... 91

Heat transfer analysis in non-similar natural convection flow of nanofluid along a vertical wavy surface ........................................................................... 91

5.1 Formulation of the problem ........................................................................... 91

5.2 Numerical procedure ........................................................................... 94

5.3 Results and discussion ........................................................................... 94

5.4 Conclusion ........................................................................... 107

Chapter 6 ........................................................................... 108

Effect of heat generation/absorption on non-similar natural convection nanofluid flow along a vertical wavy surface ........................................................................... 108

6.1 Mathematical formulation ........................................................................... 108

6.1.1 Nanofluid: thermo-physical properties ........................................................................... 109

6.1.2 Governing equations ........................................................................... 109

6.2 Computational procedure and validation of results ........................................................................... 111

6.3 Results and discussion ........................................................................... 112

6.4 Concluding remarks ........................................................................... 122

Chapter 7 ........................................................................... 123

Heat transfer phenomena in natural convection flow of nanofluid past a vertical wavy cone ........................................................................... 123

7.1 Mathematical formulation ........................................................................... 123

7.2 Solution procedure ........................................................................... 126

7.3 Results and discussion....126
7.4 Concluding remarks....138
Chapter 8....139
Conclusion and future work....139
References....142

# Chapter 1

# Introduction and preliminaries

This chapter includes two major topics, namely, the introduction and the preliminaries as is reflected in the chapter title. The introduction contains a brief literature review and the background of the problems debated in this thesis. For a better understanding and the convenience of the reader some basics of fluid mechanics, and its fundamental laws; nanofluid and their thermophysical properties and some important definitions are included among the preliminaries.

## 1.1 Introduction

Passive techniques towards the enhancement of convective heat transfer processes have fascinated the numerous investigators and scientists in the most recent couple of decades because of the way that both science and technology are being attracted to passive energy storage systems, such as the cooling of fuel rods in nuclear reactor and the design of solar collectors. In particular, for low power level equipment it might be a substantial cooling mechanism and in such situations the heat exchanger’s surface area may be increased for the augmentation of heat transfer rates. It also appears in the design of material processing, thermal insulation and geothermal systems. It has been found that free convection can induce the thermal stresses which cause serious structural destruction in the piping systems of nuclear reactors. Natural convection flow occurs due to the buoyancy force caused by temperature difference between the solid surface and the ambient fluid. The free convection flows happen frequently in natural and in engineering phenomena. For example, the buoyant flow occurs from heat rejection to the atmosphere, heating and cooling of rooms and buildings, flow driven by temperature and salinity differences in oceans, and flows generated by fire. In weather systems convection cells formed from air raise above from the heated land or water etc., in natural processes. The cooling of molten metals and fluid flows around shrouded heat-dissipation fins and solar ponds are also the examples of natural convection applications in engineering processes. Furthermore, the natural convection also takes place in various phenomena such as fire engineering, combustion modeling, nuclear reactor cooling, heat exchangers, petroleum reservoirs etc.

The study of heat transfer in natural convection flows belongs to an important class of boundary layer flows. The quantity of heat transferred (to or from the fluid) is highly dependent upon the flow character and surface texture of the bounding surface. Examples can be given of heat transfer devices like heat exchangers and radiators etc., where the heat transferring surface is made intentionally rough and irregular in order to enhance the heat transfer rates. The waviness and the increased surface area affect the heat transfer process significantly because of the increased conduction and convection. Moreover, the consideration of nanofluid also contributes significantly towards heat transfer enhancement as a consequence of its enhanced material properties. Buoyancy driven convective flows over heated or cooled bodies have been investigated for many years. A detailed account on these flows can be found in [1-6]. The free convection flow problems produced by a heated/cooled vertical plate offer one of the most fundamental situations of natural convection heat transfer phenomena and thus is of substantial practical and theoretical importance. The boundary layer natural convection flow over the surface placed vertically is possibly the first flow problem in which buoyancy force is the main source to drive the flow, which has been examined since long. After the leading work of Schmidt and Beckmann [7], Ostrach [8], Schetz and Eichhorn [9], their experimental and theoretical results have been developed, regularly refined and enhanced. Some recent works related to natural convection flows with different geometries and various boundary conditions can be seen in [1, 4, 10-26].

Expedition of heat transfer processes had been a topic of interest for researchers and scientists since the very first studies on the heat transfer phenomenon. More than a century ago, some scientists had been using the idea of suspending solid micrometer sized metallic particles and other highly conductive materials in the fluids. Extensive experimental and theoretical studies were carried out to investigate the heat transfer enhancement. In 1881 Maxwell [27] presented the foremost models for solid-liquid mixture of micro/millimeter particles but the drawbacks of these micro/millimeter particles were the rapid sedimentation, erosion, high pressure drop and clogging. Consequently, such an intelligent idea was impossible to be accommodated in the practical applications convective transport phenomenon. This idea of mixing metallic particles to the fluid could be of any success if one could avoid the sedimentation and clogging etc. issues of the metallic particles in the base fluid. This can, however, be done if the size of the additive particles is of nanoscale. During the last decade of the nineteenth century Masuda et al. [28] and Choi et al. [29] attract the scientists towards the nanofluid. They showed that the nanoparticles are strong agents to enhance the thermal conductivity of ordinary fluids. At Argonne National Lab., Choi et al. [29] developed the innovative idea of nanofluids. These nanofluids were prepared by scattering nanometer-sized material particles in ordinary base fluids. Since the size of the particles was 1000 times smaller than the particles utilized before, hence, issues of clogging and erosion were diminished. Because of the higher surface region to volume proportions of nanofluids, they were anticipated to indicate higher thermal conductivities [30]. Low pressure drop and stability were extra alluring characteristics of the nanofluids. Once the experimentation proved the utility of the nanoparticles the next task was the development of the mathematical nanofluid model so that further exploration could be done in theory. In this regards there exist two types of models in literature, namely, homogenous and the non-homogenous nanofluid models. Among these two major classes of theoretical models the homogenous models have a greater acceptability because of their simple nature. The most famous available homogenous models of nanofluid are Buongiorno [31] and Tiwari & Das [32] models. In the Buongiorno nanofluid model, the basic transport equations for fluid flow and heat transfer are appended with a transport equation for nanoparticle concentration. Buongiorno distinguished the succeeding dominating phenomena: Brownian diffusion (stochastic motion of nanoparticles), thermophoresis (particle diffusion due to the temperature gradient) and the Brownian motion; while the Tiwari and Das [32] model focuses upon the thermophysical properties of the nanoparticles [33-34]. For the description of physical properties of nanofluid, different mathematical relations are used. However, the majority of the researchers involved in the research of heat and mass transfer prefer to use the Buongiorno [31] and the Tiwari and Das [32] models for the theoretical investigations in various flow geometries. The implementation of these nanofluid models in different flow situation have been discussed in many in last few decades, some famous studies are [35-43].

During the past few decades, a lot of work has been done on convective flow along vertical stretching surface with variable surface temperature. Vajravelu and Nayfeh [44] investigated natural convection along the stretching surface placed in vertical direction with VWT case. Vajravelu [45] considered convective flow near infinite porous vertical stretching plate with VWT case in the presence of suction/blowing. It was noticed that heat transfer rate is reduced with the increase of exponent of variable surface temperature. Vajravelu and Soewono [46] studied the combined free and forced convection flow of second order fluid with linearly varying surface temperature and observed that Nusselt number decreases with the increase of index parameter *m.* Fan et al. [47] studied free convective flow along vertical stretching surface with variable surface temperature and found that Nusselt number increases with the increase of index parameter *m.* Devi and Thiyagarajan [48] considered power-law temperature profile to investigate MHD the flow and heat transfer phenomenon over a stretching sheet. Ali and Yousef [49] investigated mixed convection through moving vertical surface by considering power-law surface temperature and wall suction/injection. Javaherdeh et al. [50] studied convective flow along vertical surface placed in a porous medium. They also assumed that the surface is moving and has variable temperature. They found that the increase in the power-law index for wall variable temperature or wall variable concentration is seen to increase the temperature and concentration gradients on the surface. Mehrizi et al. [51] investigated free convection flow in boundary layer regime over the horizontal wall of variable temperature and established that the temperature gradient at the surface and exponent of variable temperature values have a direct relationship.

Uddin et al. [52] discussed natural convective flow along vertical plate in nanofluid. They used Buongiorno model and studied the Brownian motion of nanoparticles and thermophoresis effects. They found the mass transfer rate as increasing function of convective heat transfer parameter and Lewis number, while it is decreasing function of thermophoresis parameter. Qasim et al. [53] studied heat and mass transfer in nanofluid over an unsteady stretching sheet and concluded that the nanofluid parameters reduce the heat transfer rate. Uddin et al. [54] numerically investigated the MHD flow of a nanofluid with thermal and mass convective boundary conditions and showed that the surface slip causes to decrease the skin friction whereas it enhances the local Nusselt number.

Ghalambaz et al. [55] utilized the combined similarity and numerical approach to investigate the natural convection nanofluid flow over a heated vertical plate in a porous medium and observed that the Brownian motion parameter increases the velocity and temperature profile. Ramzan and Yousaf [56] considered three-dimensional viscoelastic nanofluid flow with Newtonian heating and noticed that concentration and temperature profiles are decreasing and increasing functions of the Brownian motion parameter respectively. Das et al. [57] studied thermophoresis and Brownian effects on stretched surface and observed that the mass transfer is increasing function of thermophoretic parameter whereas the effect is reversed for Brownian motion parameter. Khan et al. [58] discussed double diffusive free convective nanofluid flow along the vertical plate with thermal and momentum boundary conditions and found that the Nusselt number and the Sherwood number decrease with thermal slip condition. In view of these studies it could be concluded that the nanofluid enhances the heat transfer rate in convective flows which have numerous applications in engineering and industry. Due to this importance, the study of natural convection flow of nanofluid past a vertical plate with variable surface is included in **Chapter 2**.

Self- similar solutions for natural convection flows over vertical cone have received much attention from many researchers and scientists. Hering and Grosh [59] and Hering [60] studied the natural convection phenomenon in the vertical cone and found the similarity solution. Roy [61] investigated the solution for the large Prandtl number in natural convection from the vertical cone. Vajravelu and Nayfeh [62] investigated heat transfer phenomenon along a cone and wedge surface and concluded that the flow and heat transfer characteristic have smaller values at the cone surface as compared to the wedge surface. Kafoussias [63] discussed mass transfer flow in free convection along vertical isothermal cone and analyzed that heat and mass transfer is strongly effected by bouncy parameter and Schmidt number. Yih [64] studied free convection flow over isothermal truncated cone in the presence of thermal radiation and observed that radiation plays vital role in the enhancement of heat transfer rate. Behrang et al. [65] considered free convection of Darcian fluid over a vertical cone in porous medium and established that numerical values of Nusselt number obtained by analytical solution show remarkable accuracy when compared with those computed numerically. Cheng [66] discussed natural convection flow from non-isothermal permeable vertical cone in Newtonian fluid with suction and variable properties and noted that Nusselt number rises with increase of suction and viscosity variation parameter. Duwari et al. [67] considered MHD mixed convection flow over a cone embedded in a porous medium and observed that the Nusselt number increases with the increase of cone angle. Elbashbeshy et al. [68] examined natural convection from a vertical circular cone with pressure work and variable heat flux in the presence of heat generation source. They observed that the skin friction increases and the Nusselt number reduces with the increment in the heat generation parameter. Braun et al. [69] studied free convection similarity flows of bodies with closed lower ends and observed that body shape parameter enhances the heat transfer. Grosan [70] examined free convection flow over a vertical cone surrounded by a viscoelastic fluid with heat source in porous medium. Chamkha et al. [71] discussed the effects of combined chemical reactions and pressure work in natural convection flows and concluded that the Nusselt number reduces with the increase of heat generation, chemical reaction parameter and Schmidt number. Sohouli et al. [72] studied free convection of Darcian fluid along vertical cone embedded in porous medium analytically.

The study of nanofluids over the cone have attracted many researchers in last few decades. Mahdy [73] was among the few researchers who paid their attention to investigate the flow along the cone placed in the vertical direction having vertex at origin. Mahdy [73] considered gyro-tactic microorganisms in porous medium and noticed that the Sherwood number enhances and Nusselt number reduces with an increase in thermophoresis and Brownian motion parameters. Behseresht et al. [74] investigated convective flow in the presence of nanoparticles along cone placed in the vertical direction in porous medium. They noticed that heat transfer due to migration of nanoparticles is negligible in comparison to convection and heat conduction phenomena. Noghrehabadi et al. [75] considered isothermal cone placed vertically in non-Darcy porous medium and noticed that the increase in the non-Darcy parameter would reduce the heat and mass transfer rates. Keshtkar and Hadizadeh [76] investigated boundary layer nanofluid flow along a vertical cone in porous medium. Considering porous medium Fauzi et al. [77] studied mixed convection in nanofluid flow over a cone and noticed that in forced convection and the assisting flow the Nusselt number enhances as the concentration of nanoparticle intensifies.

The study of natural convection flow over a vertical cone has been the area of interest for many researchers due to dynamic importance of nanofluids. Important studied published in last decades have achieved much attention of the researchers, few of them are [78-88] **Chapter 3** is aimed to study the natural convection flow of nanofluid over a circular cone using Buongiorno model.

Heat transfer enhancement through irregular surface shapes is a topic of fundamental importance in the studies of heat transfer processes. In practice, the surface irregularities occur frequently in several manufacturing and engineering mechanisms. The working body surface is sometimes intentionally roughened to enhance heat and mass transfer as a consequence of enhanced convection phenomena. Flat plate solar collectors and flat plate condensers in refrigerators are examples where the roughening elements are intentionally placed on a uniform body surface. The presence of roughing elements disturbs the flow which in turn expedites the convective mixing of the fluid. Consequently, the rate of heat transfer is increased. The gain in convective heat transfer rate as a result of increased surface area is usually not simple because of enhanced conduction between the fluid and the solid surface. Enhanced surface area also contributes towards increased vorticity transport which in turn results in increased rate of heat transfer. Keeping this fact in mind the idea of surface roughening came in reality in order to establish enhanced vorticity transport to get the heat transfer augmentation. Mathematical handling of irregular rough surfaces is far more difficult as compared to the regular rough surfaces. In this way a smooth wavy roughness of the flat plate is quite easy to model due to its differentiable nature. Moreover, the wavy surface contributes towards symmetry breaking where the scaling symmetry does not leave the governing system (equations and the boundary conditions) invariant as it does for the flat plate case. Consequently, the self-similar solution does not persist anymore and the flow becomes completely non-similar. Rees and Pop [89-90] investigated free convective boundary layer flow and heat transfer due to a moving wavy horizontal plate. Hossain and Pop [91] studied the MHD effects on momentum and thermal boundary layer over a moving wavy plate. Narayana et al. [92] considered horizontal wavy surface to investigate cross-diffusion and double diffusive effects in porous regime. More information about flow and heat transfer along wavy texture can be seen in published studies [93-106].

In several practical applications, the fluids are assumed to be electrically conducting and their interaction with the applied magnetic field gives rise to the study of magnetohydrodynamics. Such situations frequently occur in the cooling of nuclear reactor, electromagnetic casting and ship propulsion etc. Based on these interesting applications the field of magnetohydrodynamics is an active area of research. Chamkha and Ahmed [107-108] studied time dependent hydromagnetic effects and chemical reaction of species in convective flow near stagnation point region. Sheremet et al. [109] analyzed time dependent hydromagnetic effects in a wavy-walled cavity using Buongiorno's mathematical model. Mahdy and Ahmed [110] investigated Soret and Dufour effects on thermo solutal Marangoni boundary layer magnetohydrodynamics flow along a vertical flat plate. In all above mentioned studies, the authors considered pure fluid for the computation of increased rate of heat transfer due to the wavy surface. Further increase in the rate of heat transfer is expected if one considers nanofluid instead of pure fluid over a wavy plate. Based on this motivation **Chapter 4** is aimed to study the hydromagnetic flow and heat transfer in nanofluids over moving wavy surface.

Free convection flow over vertical plate was first studied by Pohlhausen [111] who analyzed the steady free convection flow of a viscous incompressible fluid past a semi-infinite vertical plate by using an integral method. Ostrach [112] presented the similarity solution of natural convection flow along vertical isothermal plate. The flow over vertical rough wavy surface was first initiated by Yao [113]. He numerically simulated the problem by means of finite difference method. Before employing the numerical scheme he first reduced the problem of wavy surface to a relatively simple form through a coordinate transformation. Moulic and Yao [114] extended the work of Yao [113] by assuming the free stream velocity and concluded that heat transfer rate in case of flat surface is higher than the wavy surface. Rees and Pop [115] studied fluid flow and heat transfer over a horizontal surface with sinusoidal texture where the medium of the flow is assumed to be a Darcy porous medium. They use the Keller-box scheme to perform the computational task. Hossain and Rees [116] considered the isothermal surface of wavy texture placed in vertical direction and analyzed the heat and mass transfer phenomena. Cheng [117] considered the convective heat transfer in the porous regime along the vertical surface of wavy texture. Gorla and Kumari [118] studied free convection phenomena near a vertical wavy plate in a nanofluid. Ahmed et al. [119] studied natural convection flow along the wavy surface in porous regime by assuming local thermal non-equilibrium condition. The transfer of heat in solid and fluid phase is modeled by separate equations. Intensification of surface roughness enhances the effective heat transfer rate without increasing the overall volume of the equipment significantly. Rough surfaces for example, fins; non-flat surfaces and micro channels have been found to increase heat transfer rates considerably. Keeping this fact in view heat transfer analysis of natural convection flow of nanofluid along a vertical wavy surface has been investigated and the details of this study are included in **Chapter 5**.

The real heat transfer processes associated with the change of some form of energy into thermal energy have the possibility of involving internal heat generation/absorption. Heat transfer and fluid flow phenomena with heat generation/absorption are associated with large temperature gradients which is frequently met in several engineering and thermal processes such as, in the combustion chamber, thermal control of space ships, casting or blading of gas turbines and spent fuel storage [120], post-accident heat removal [121], engine cooling system and insulation of buildings etc. Vajravelu and Hadjinicolaou [122] considered an internal heat source over a stretching surface. Molla et al. [123] studied magneto hydrodynamic free convection flow on a sphere under the influence of heat source. Alam et al. [124] investigated hydromagnetic convective flow over a sphere. Mamun et al. [125] analyzed the heat source effects along a vertical plate. Mamun et al. [126] discussed the impact of viscous dissipation and heat source on heat transfer over a vertical plate. Mansoor and Ahmed [1279] explored natural convection in porous triangular enclosure using nanofluid and heat generation. Molla et al. [128] used isothermal wavy surface and heat generation effects to examine the heat transfer phenomena. Hady et al. [129] studied MHD natural convective flow through a vertical wavy sheet by considering heat source. Alim et al. [130] analyzed natural convective flow through a vertical wavy sheet by taking into account the viscosity depending upon temperature and heat source. Parveen and Alim [131-132] discussed MHD natural convective flow through a vertical wavy sheet with heat source/sink, joule heating, viscosity depending upon temperature and temperature dependent thermal conductivity. Kabir et al. [133] discussed heat source impact on MHD free convection flow along a heated vertical wavy plate. Saddiqa et al.

[134] studied the radiation effects on natural convection flow along vertical wavy surface. Natural convection flow occurs in many practical phenomena caused by heat source/sink. The importance of heat source/sink is more significant in those flows where the chemical reaction occurs. Due to heat generation/absorption changes occur in temperature distribution, particle decomposition rate in semiconductor products and nuclear reactors. Some studies about heat generation/absorption can be seen in published articles [135-147]. Due to this fundamental importance **Chapter 6** is optimized with the inclusion of heat generation/absorption in nanofluid flow over a vertical wavy surface.

Convective heat transfer phenomena over a cone is applicable in various designs of thermal equipment like heat exchangers, geothermal reservoirs, nuclear reactor cooling, solar energy plants, design of space crafts, drying dehydration process in chemical and food process and steam generators etc. Heat and mass transfer augmentation has evolved into an important component of thermal sciences and engineering. This poses a great challenge for choosing appropriate design and application information to achieve the industrial and technology goals. Regarding the cone geometry the phenomena of natural convection heat transfer over vertical cone has been studied by several researchers and scientists. Merk and Prins [148-149] discussed natural convection flow along a cone for pure fluid. Roy [150] investigated natural convection over an isothermal cone. Lin [151] discussed the heat transfer due to uniform surface heat flux from a vertical cone. Alamgir [152] investigated free heat transfer characteristics from vertical cone using approximate technique. Pop et al. [153] paid their attention to analyze the effects of compressibility in convective flow over the vertical cone. Yih [154] analyzed free convection along a vertical cone in porous medium under uniform mass flux. Cheng [155] examined the effects of variable wall temperature in free convection flow of a micro-polar fluid over a vertical permeable cone. Hossain and Paul [156-157] discussed the non-uniform wall temperature and uniform heat flux along the vertical cone of circular type. Cheng [158] discussed free convection heat transfer from a non-isothermal permeable cone with suction. Pullepu [159] explained uniform heat flux case for unsteady convective flow over vertical cone.

Most of the authors in the above mentioned studies have considered the circular cone with uniform surface texture to study the flow and heat transfer characteristics but very little attention has been given to the cone having non-uniform surface texture. Pop and Na [160-

162] discussed the natural convection flow along a vertical frustum of a wavy cone in porous medium. Cheng [163] investigated heat and mass transfer phenomena in natural convection along wavy cone in porous media. Considering viscosity dependent temperature Hossain et al. [164] examined free convection flow over a vertical wavy cone. Taking viscosity as an exponential function of temperature into account, Rahman et al. [165] discussed free convection flow beside the vertical wavy cone. Since the irregular surface shape changes the flow pattern and hence the heat transfer rate. Therefore the wavy shaped surface occurs frequently in many industrial processes. Because of this reason, the investigation of natural convection flow of nanofluid over a wavy cone has been included in **Chapter 7**.

## 1.2 Preliminaries

In this section some fundamental knowledge, necessary for the subsequent chapters, has been presented. It includes basic definitions and terminologies; the dimensionless numbers of physical importance and the governing equations.

### 1.2.1 Fluid

There are three states of matter namely, solid, liquid and gas, among which the liquid and gas both are fluids. A fluid is a substance (gas or liquid) which modifies its shape continuously under the action of external forces or any material that flows continuously is known as fluid. Due to the fact that a fluid can’t withstand deformation pressure, it moves or flows under the action of the force and its shape changes continuously as long as the force is implemented. It can easily be seen that the fluid flow is a universal phenomenon which occurs frequently in our everyday life. On the other hand a solid can resist a deforming force as long as at rest, while the force may produce some displacement however, the solid does not move indefinitely [6, 166].

To the ancient Greeks, the four fundamental elements are earth, air, fire, and water; among these three, air, fire and water, are fluids. Fluids have been further sub-categorized into ideal and viscous fluids. In ideal or inviscid fluids the most effective internal force is the pressure, which acts in such a way that the fluid flows from high stress to low. In Newtonian fluids the viscosity is independent of shear rate, means that the viscosity is constant at given temperature and pressure. Moreover, these are the fluids which obey Newton's law of viscosity which states that the shear stress is directly and linearly related to the shear rate.

### 1.2.2 Fluid mechanics

Fluid mechanics is concerned with the understanding, prediction, and controlling the behavior of a fluids [6, 166]. Fluid mechanics is one of the engineering sciences that forms the basis for all forms of engineering [167]. This subject branches out into various specialties such as aerodynamics, hydraulic engineering, marine engineering, gas dynamics, and manufacturing processes. It includes the statics, kinematics and dynamics of fluids. Fluid mechanics studies the dynamic properties (e.g. motion) of fluid. In other words, fluid mechanics is the study of the nature of fluids under the action of applied forces. Generally, we are interested in finding the force required to move a fluid through a device, or the force required to move a solid body through a fluid. The speed of the resulting motion, pressure, density and temperature variations within the fluid is also of extremely great interest.

### 1.2.3 Heat transfer phenomenon

Heat transfer processes assume a key part in many natural, industrial and biological systems. Heat transfer is actually the transition of energy in accordance with the provided temperature differences. Conduction, convection and radiation are the three modes of heat transfer as shown in Fig. 1.1. **Conductive** heat transfer takes place in solids via molecular energetic movement due to the temperature gradient within a medium. **Radiative** heat transfer is the interchange of thermal energy between two or more bodies by electromagnetic waves. Interestingly, it does not require any medium. **Convective** heat transfer is the shift of energy through liquids and gases or fluids in general moving near the surface. Heat transfer due to convection can further be subdivided into three major types namely; forced convection, natural convection and mixed convection. In **forced convention** process the fluid movement is due to external source like fan; suction devices and pump etc. In many cases, only natural buoyancy forces are accountable for fluid motion when the fluid is heated and this phenomenon is called **natural or free convection**. Natural convection flow is caused by density variance in different sections of the fluid. This density change, along with the influence of the gravity, generates a buoyancy force, due to which the heavier fluid travels downwards and the lighter fluid moves upwards, generating buoyancy driven flow. The density variance in natural convection flows may result from a temperature variance or from the changes in the concentration of chemical species. The most common buoyant flows may be seen as air flows around our rooms and other engineering applications [30,168]. When these two phenomena of heat transfer (forced and natural convection) are occurring at the same time the situation is commonly known as **mixed convection**.

Heat transfer is most important phenomenon where the involvement of fluid plays a crucial role to expedite this process. Inclusion of solid nanoparticles in the base fluid is another important source to enhance the heat transfer rate. The mixture of nanoparticles and the base fluid is known as nanofluid. The details of nanofluid are presented in the next section.

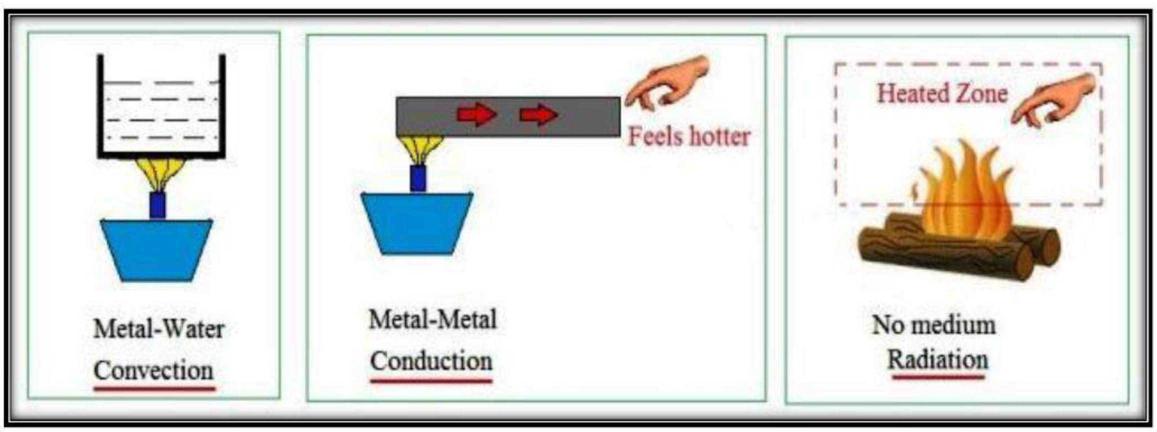


**Figure 1.1:** Modes of Heat Transfer (Image Source: Study Channel Website).

### 1.2.4 Nanofluid

Convective heat transfer process can be improved by modifying the flow geometry, adjusting the boundary conditions or enhancing the thermal conductivity of the base fluid. In 1881, Maxwell [27] succeeded in exploring that the heat transfer rate can be augmented by mixing micro sized particles in the base fluid. After Maxwell, it was observed that although the addition of micro sized material particles in the base fluid do result in some enhancement in the rate of heat transfer but the issues of clogging; rapid sedimentation;

erosion, and high pressure drop, produced due to these particles, retained the technology away from the practical usage of this strategy for a long time.

**Table 1.1:** Potential usage of the nanomaterials [169].

| **Nanomaterial** | **General applications** |
|---|---|
| $Ag$ | Microelectronic industry, antibacterial and disinfecting agent, anti-corrosive coating, catalysis. |
| $Al, Al_2O_3$ | Heat transfer fluid, catalyst support, water-proof material, antibacterial and disinfecting agent, transparent conductive and optical coating, wear-resistant additive, cosmetic filler. |
| $Cu, CuO$ | Superconductors, antibacterial and disinfecting agent, catalysis, gas sensors, thermo-electronics, microelectronic industry. |
| $Fe, Fe_2O_3$, $Fe_3O_4$ | Biomedical applications, environment remediation, magnetic data storage, semiconductor, microwave devices. |
| $TiO_2$ | Solar cells, photo-catalysis, antibacterial and disinfecting agent, cosmetics, air purification, semiconductors, UV resistors, astronautics. |
| $SiO_2$ | Construction industry, production of glass, sensitive optical fiber, ceramics, food and pharmaceutical applications. |
| $SWCNT$, $MWCNT$ | Supercapacitor, catalysts, energy conversion, sensors, electromagnetic-wave absorption and shielding, lithium-battery anodes, nanotube composites (by filling or coating), nanolithography, nano-electrodes, drug delivery, hydrogen storage. |

Masuda et al. [28] firstly conveyed that addition of nanoparticles enhances thermal conductivity of the base fluid. In 1995, while working at the Argonne National Laboratory in U.S.A, Choi [29] introduced the term nanofluid. Nanofluid is a suspension of solid nanoparticles (of size 1-100 nm diameter) in conventional liquids like water, oil or ethylene glycol etc. Nanofluids improved the heat transfer phenomena that made them potentially supportive in various applications of heat transfer including fuel cells, microelectronics, hybrid powered engines and pharmaceutical processes. Nanofluids show improved convective heat transfer coefficient and thermal conductivity in comparison to the pure fluid. Nanofluid can be made from various combinations of nanoparticles and base fluid. Particles can be of different types such as, metals, non-metals, metallic oxides and non-metallic oxides etc. The common base fluids are water, ethylene glycol and oil. In industries, commonly used nanoparticles are $Al_2O_3, Fe_3O_4, TiO_2, CuO, SiO_2$ in compound form and $Ag, Au,\ Cu, Fe$ in elemental form.

Some important applications of nanomaterials are given in Table 1.1. The heat transfer rate of nanofluid depends upon the thermophysical properties of the nanoparticles. Physical properties of the nanoparticles are viscosity, density, specific heat, thermal diffusivity and thermal conductivity etc. The numerical values of these properties vary with the change of nanoparticle material and the base fluid. The scientists and researchers use well known predictive correlations for the material properties of the nanofluids. Therefore, the thermophysical properties of nanoparticles and base fluid have been discussed in detail in the next section.

### 1.2.5 Thermophysical properties of nanofluid

Thermophysical properties of nanofluid strongly affect the solution of the considered flow problems. There are different types of models for the description of thermophysical properties of nanofluid which are derived by various scientist. Thermophysical properties such as thermal conductivity, electrical conductivity, density, viscosity and specific heat are calculated by employing the formulas 170-172, which are adopted as empirical relation among the base fluid and nanoparticles.

#### 1.2.5.1 Density

Using the physical principle of the mixture law the density of nanofluid may be calculated analytically. Using this law measuring weight and volume of amalgamation density of nanofluid can be determined. The particle volume fraction $\phi$ can be assessed by knowing the densities of both components and nanofluid density can be described as (see [170-172])

$$\rho_{nf} = (1-\phi)\rho_f + \phi\rho_p. \tag{1.1}$$

### 1.2.5.2 Specific heat

The amount of heat to raise the temperature of one Kg mass of a substance by one Kelvin is known as Specific heat capacity. Specific heat of nanofluid depends upon simple mixing theory [170-172] in convective heat transfer nanofluid flows and is written as

$$\left(\rho c_p\right)_{nf} = (1-\phi)\left(\rho c_p\right)_f + \phi\left(\rho c_p\right)_p. \tag{1.2}$$

### 1.2.5.3 Thermal conductivity

In 1873, Maxwell [27] established that thermal conductivity of a liquid is increased by the addition of solid particles in the liquid and introduced a classical relation between the thermal conductivity of nanoparticle and the base fluid, described as

$$\frac{\kappa_{nf}}{\kappa_f} = \frac{(\kappa_p + 2\kappa_f) - 2\phi(\kappa_f - \kappa_p)}{(\kappa_p + 2\kappa_f) + \phi(\kappa_f - \kappa_p)}. \tag{1.3}$$

### 1.2.5.4 Effective electrical conductivity

The electrical conductivity of nanofluid enhances with a rise in concentration and temperature of the particle. Electrical conductivity is observed to be higher for smaller sized particles in nanofluid by fixing concentration of nanoparticles. Effective electric conductivity of nanofluid presented by Maxwell [170-172] is given as

$$\frac{\sigma_{nf}}{\sigma_f} = 1 + \frac{3\left((\sigma_p/\sigma_f) - 1\right)\phi}{\left((\sigma_p/\sigma_f) + 2\right) + \phi\left((\sigma_p/\sigma_f) - 1\right)}. \tag{1.4}$$

### 1.2.5.5 Thermal diffusivity

It is the measure of speed of carrying heat away from the hot body. Mathematically, it is the ratio of thermal conductivity to the volumetric heat capacity. The thermal diffusivity of nanofluid in convective heat transfer phenomena is written as (due to [170-172])

$$\alpha_{nf}^{*} = \frac{\kappa_{nf}}{\left(\rho c_p\right)_{nf}}. \tag{1.5}$$

### 1.2.5.6 Viscosity

Engineers and scientists utilize different models for effective dynamic viscosity of nanofluid which is a function of solid volume fraction. Einstein [174-176] determined the effective viscosity of a suspension of spherical solid particles as a function of low volume fraction (less than 2%). Later-on, Brinkman [177] presented a new relation by modifying the Einstein's equation of viscosity correlation with particle volume fraction less than 4%. Viscosity of the nanofluid can be computed by the simple mixture theory [170-172] and is expressed as

$$\mu_{nf} = \frac{\mu_f}{(1-\phi)^{2.5}}\ . \tag{1.6}$$

The thermophysical properties of the different nanoparticles and the base fluids used in this dissertation are presented in Table 1.2.

**Table 1.2:** Thermophysical properties of different nanoparticles and water.

| Properties / Nano-particle | Density $\rho(Kg/m^3)$ | Specific heat $c_p(J/KgK)$ | Thermal conductivity $\kappa(W/mK)$ | Thermal expansion $\beta \times 10^{-5}(1/K)$ | Electrical conductivity $\sigma(S/m)$ |
|---|---|---|---|---|---|
| Fluid (water) | 997.1 | 4179 | 0.613 | 21.0 | 0.05 |
| $Ag$ | 10500 | 235 | 429 | 1.89 | $6.3 \times 10^7$ |
| $Au$ | 19320 | 128 | 318 | 0.01416 | $4.10 \times 10^7$ |
| $Al_2O_3$ | 3970 | 765 | 40 | 0.85 | $3.5 \times 10^7$ |
| $Cu$ | 8954 | 383.1 | 386 | 1.67 | $5.96 \times 10^7$ |
| $CuO$ | 6500 | 535.6 | 20 | 1.80 | $-$ |
| $Fe_3O_4$ | 5180 | 670 | 9.7 | 0.5 | $2.5 \times 10^3$ |
| $SiO_2$ | 2200 | 703 | 1.2 | 0.056 | $-$ |
| $TiO_2$ | 4250 | 686.2 | 8.9538 | 0.90 | $0.26 \times 10^7$ |
| $SWCNT$ | 2600 | 425 | 6600 | $-$ | $1 \times 10^4$ |
| $MWCNT$ | 1600 | 796 | 3000 | $-$ | $1 \times 10^5$ |

### 1.2.6 Governing equations

The basic governing equations for the nanofluid flow are the same as they are for the pure fluid, that is, the laws of conservation of mass, momentum and energy. However, the consideration of nanofluid does modifies these laws to some extent. Since we intend to use the two famous nanofluid models, namely, Buongiorno model and Tiwari and Das mod. Therefore, the modification in the governing laws shall be mentioned with regard to these two models.

#### 1.2.6.1 Equation of continuity

Principle of conservation of mass for fluid flow is commonly known as the continuity equation, which in vector notation is given as follows

$$\frac{1}{\rho_f}\frac{\partial \rho_f}{\partial t} + \nabla . \boldsymbol{V} = 0. \tag{1.7}$$

The above equation is valid pure fluid and Buongiorno model, for Tiwari and Das model, $\rho_f$ has been replaced by $\rho_{nf}$. For an incompressible fluid the density is constant due to which the equation of continuity (1.7) simplifies to

$$\nabla . \boldsymbol{V} = 0. \tag{1.8}$$

#### 1.2.6.2 Momentum equation

For an incompressible viscous fluid the law of conservation of linear momentum reads as

$$\frac{\partial \boldsymbol{V}}{\partial t} + (\boldsymbol{V}.\nabla)\boldsymbol{V} = -\frac{1}{\rho_f}\nabla p + \nu_f \nabla^2 \boldsymbol{V} + \frac{1}{\rho_f}\boldsymbol{b}, \tag{1.9}$$

where $\boldsymbol{b}$ denotes the body forces, $\boldsymbol{V}$ is velocity vector, $\nabla$ is the vector operator. The Eq. (1.9) is valid for pure fluid and Buongiorno model, for Tiwari and Das model, $\rho_f, \nu_f$ have been replaced by $\rho_{nf}, \nu_{nf}$ respectively.

In view of the problems considered in this dissertation the expected body forces are the bouncy force or magnetic force. $\frac{\partial}{\partial t}$ represents local time derivative and $\boldsymbol{V}.\nabla$ denotes convective derivative. The bouncy force is given by

$$\boldsymbol{b}_{bou} = \boldsymbol{g}\beta(T - T_\infty), \tag{1.10}$$

where $\boldsymbol{g}$ denotes the gravitational acceleration The magnetic body force caused due to the application of wall-normal magnetic field and is calculated as

$$\boldsymbol{b}_{Mag}=\boldsymbol{J} \times \boldsymbol{B}, \tag{1.11}$$

where $(\boldsymbol{J} \times \boldsymbol{B})$ is the Lorentz force, $\boldsymbol{B}$ is the applied magnetic field and $\boldsymbol{J}$ is the current charge density.From Ohm's law:

$$\boldsymbol{J} = \sigma(\boldsymbol{E} + \boldsymbol{V} \times \boldsymbol{B}), \tag{1.12}$$

and due to the Maxwell's equations

$$\nabla.\boldsymbol{B} = 0, \nabla.\boldsymbol{E} = \frac{\rho_f}{\epsilon_0}, \nabla \times \boldsymbol{B} = \mu_0 \boldsymbol{J}, \nabla \times \boldsymbol{E} = 0, \tag{1.13}$$

where σ is the electrical conductivity, $\boldsymbol{E}$ is the electric field, $\mu_0$ denotes the magnetic permeability and $\epsilon_0$ is the permittivity of free space. It is assumed that the magnetic Reynold number is so small such that the induced magnetic field can be ignored. In the present dissertation applied electric field $\boldsymbol{E}$ is zero ($\boldsymbol{E} = \boldsymbol{0}$) and constant magnetic field of strength $B_0$ is applied perpendicular to the surface ($\boldsymbol{B} = (0, B_0, 0)$) (see for instance [27]).

#### 1.2.6.3 Energy equation

For a viscous incompressible fluid having constant fluid conductivity, zero internal heat generation and negligible viscous dissipation effect, the energy equation (law of conservation of energy) is given as

$$\frac{\partial T}{\partial t} + \boldsymbol{V}.\nabla T = \alpha_f^* \nabla^2 T. \tag{1.14}$$

The Eq. (1.14) is valid for pure fluid, for Tiwari and Das model, $\alpha_f^*$ has been replaced by $\alpha_{nf}^*$.For the Buongiorno model [31] which utilizes the Brownian motion and thermophoresis effects in the fluid flow, the energy equation is written as

$$\frac{\partial T}{\partial t} + \boldsymbol{V}.\nabla T = \alpha_f^* \nabla^2 T + \tau^* \left( D_T \frac{\nabla T.\nabla T}{T_\infty} + D_B \nabla C.\nabla T \right). \tag{1.15}$$

where $D_T$, $D_B$ and $\tau^*$ are the thermophoretic diffusion coefficient; the Brownian diffusion coefficient and the ratio of heat capacity of a nanoparticle to the base fluid, respectively.

#### 1.2.6.4 Concentration equation

Usually, the convective processes 'usually' and 'often' go along with the mass transfer. Therefore, by the transport of materials that act as components (constituents, species) in the fluid mixture. In mathematical formulation this phenomena can be written as

$$\frac{\partial C}{\partial t} + \boldsymbol{V}.\nabla \mathrm{C} = D_m \nabla^2 \mathrm{C}, \tag{1.16}$$

and in view of Buongiorno nanofluid model [31] eq.(1.16) modifies as

$$\frac{\partial C}{\partial t} + \boldsymbol{V}.\nabla C = D_B \nabla^2 C + \left(\frac{D_T}{T_\infty}\right)\nabla^2 T. \tag{1.17}$$

Equations (1.16) and (1.17) show that the concentration $C$ occupies the place of temperature, while, the mass diffusivity $D_m$ replaces the thermal diffusivity $\alpha_f^*$ where $\alpha_f^* = \kappa_f/(\rho c_p)_f$ in the energy equation. The above equations are in general form where $C$ denotes the fluid concentration for mass transfer. The subscript $\infty$ denotes the values in the ambient fluid.

### 1.2.7 Wavy surface

In majority of the chapters of this dissertation we shall be considering the viscous boundary layers formed upon a wavy surface. Interestingly, for every such wavy surface the flow is essentially non-similar in nature. For example a non-flat wavy sheet extended in $x$ −directions is defined as

$$\bar{y} = \bar{S}(\bar{x}) = \bar{\alpha} sin\left(\frac{\pi \bar{x}}{l}\right), \tag{1.18}$$

where $l$ is the wave length and $\bar{\alpha}$ is the fixed amplitude . This wavy surface is assumed to be semi-infinite starting from $x$ in the $xz$ −plane and is assumed to be surrounded by the ambient nanofluid. The schematic of the wavy surfaces considered in the subsequent chapters has been shown in Figure 1.2.

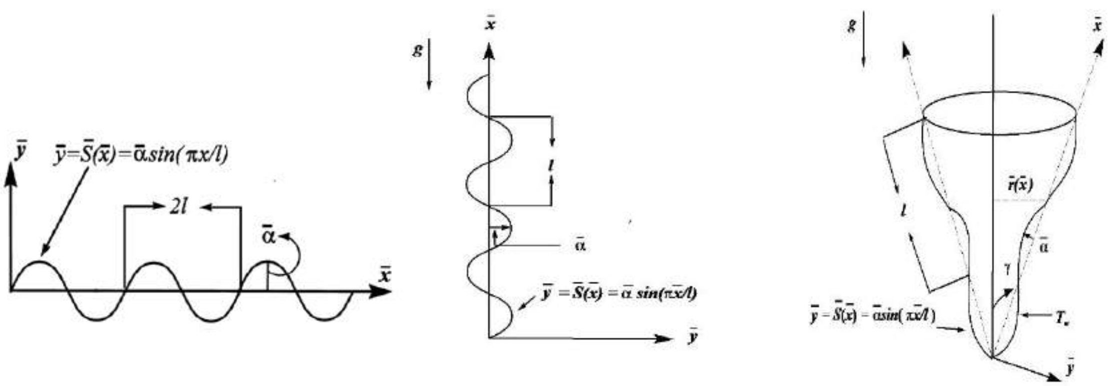


**Figure 1.2:** Schematic of the wavy surfaces considered in this dissertation.

### 1.2.8 Heat source/sink

Volumetric heat source/sink $q^*(W/m^3)$ can be written as

$$q^* = \begin{cases} Q(T - T_\infty) & T \geq T_\infty \\ 0 & T < T_\infty \end{cases}, \tag{1.19}$$

while the constant $Q \gtreqless 0$ represents the heat source/sink.

### 1.2.9 Skin friction coefficient

The coefficient of skin friction at the wavy surface in two-dimensional flow is defined as

$$C_{fx} = \frac{\tau_w}{\rho_f U^2}, \tag{1.20}$$

where $\tau_w$ is the wall shear stress which is given by

$$\tau_w = \mu_f (\nabla \overline{u}\,.\,\hat{n})_{\bar{y}=0}, \tag{1.21}$$

where $\hat{n} = \left(n_x, n_y\ \right) = (-\frac{S_\xi}{\omega}, \frac{1}{\omega})$ is the unit vector normal to the wavy surface and $\omega = \sqrt{1 + S_\xi^2}$ is the wavy parameter. The coefficient of skin friction for the case of flat plate takes the form

$$C_{fx} = \mu_f (\nabla \overline{u})_{y=0} / \rho_f U^2. \tag{1.22}$$

### 1.2.10 Nusselt number

Dimensionless heat transfer coefficient is known as Nusselt number which is an important physical parameter in the process of convective heat transfer. It is the ratio of convective to conductive heat transfer in the fluid. In convective heat transfer phenomena the heat transfer rate is described as

$$Nu_x = \frac{\bar{x} q_w}{\kappa_f (T_w - T_\infty)}, \tag{1.23}$$

where $q_w$ is the wall heat flux and is calculated as

$$q_w = -\kappa_f (\nabla T.\hat{n})_{\bar{y}=0}\,. \tag{1.24}$$

The Nusselt number for the flat surface is defined as

$$Nu_x = -(\nabla T)_{\bar{y}=0} / (T_w - T_\infty). \tag{1.25}$$

### 1.2.11 Sherwood number

The local Sherwood number is a measure of the rate of convective mass transfer. It is the ratio of the convective to diffusive mass transfer can be describe as

$$Sh_x = \frac{\bar{x} q_m}{D_B (C_w - C_\infty)}, \tag{1.26}$$

where $q_m$ is the wall mass flux which is given by

$$q_m = -D_B (\nabla C . \hat{n})_{\bar{y}=0} . \tag{1.27}$$

The Sherwood number for the flat surface is given by

$$Sh_x = -(\nabla C)_{\bar{y}=0} / (C_w - C_\infty). \tag{1.28}$$

### 1.2.12 Reynolds number

The Reynolds number, named after the famous British fluid dynamicist of the late nineteenth century, Osborne Reynolds is the ratio of inertial forces to viscous forces in a flow, i.e.

$$Re = \frac{Ul}{\nu_f}, \tag{1.29}$$

where $U$ represents the reference velocity $l$ represents the characteristic length, and $\nu_f$ is dynamic viscosity. The Reynolds number is used to characterize the flow as laminar or turbulent.

### 1.2.13 Prandtl number

Prandtl number ($Pr$), named after a German scientist, Ludwig Prandtl, who has a dominant role in the research on viscous flow in the first half of 20$^{th}$ century. $Pr$ is the ratio of the coefficient of diffusion of momentum to the coefficient of diffusion of heat, that is

$$Pr = \frac{\nu_f}{\alpha_f^*} = \frac{\mu_f c_p}{\kappa_f} = \frac{\mu_f / \rho_f}{\kappa_f / \left(\rho c_p\right)_f}, \tag{1.30}$$

where $\alpha_f^*$ is the thermal diffusivity. For gases $Pr \backsim 0.7$; for liquids such as water, $Pr \backsim 7.0$ and for liquid metals, $Pr << 1$.

### 1.2.14 Grashof number

The dimensionless number which arises from the ratio of the buoyancy to the viscous forces is known as Grashof number. It is frequently used in the study of natural or mixed convection flows. Mathematically,

$$Gr = \frac{g\beta\Delta T l^3}{\nu_f^2}, \tag{1.31}$$

where $\beta$ is the coefficient of the volumetric change, $\Delta T$ is the temperature difference, $\nu_f$ is kinematic viscosity of fluid and $l$ is characteristic length.

### 1.2.15 Lewis number

For the combined studies of heat and mass transfer Lewis number is an important physical quantity. It is a ratio between the characteristic lengths of diffusion of heat and diffusion of mass. Lewis number is also regarded as the ratio of thermal diffusivity to the mass diffusivity and is defined as

$$Le = \frac{\alpha_f^*}{D_m}, \tag{1.32}$$

where $D_m$ is the mass diffusivity.

### 1.2.16 Thermophoresis

Thermophoresis is related to temperature gradient. Solid particles suspended in a fluid exert a force in the direction opposite to the existing temperature gradient. This phenomena is termed as thermophoresis. Heat transfer is the transfer of thermal energy from one place to the other. The fundamental requirement for heat transfer is the existence of temperature difference. The transfer of energy in the form of heat always occurs from the higher temperature region to the lower temperature region until both regions reach the same temperature.


**Figure 1.3:** Schematic of the thermophoresis phenomenon.

### 1.2.17 Brownian motion

The random movement of particles suspended in a liquid (gas) due to the collisions of surrounding molecules in the base fluid is called Brownian motion. It is recognized that the strength of these disordered motions increases with temperature. The increase in temperature affects thermal conductivity and due to Brownian motion, diffusion of small particles will occur which is governed by Fick's law. Therefore, the Brownian motion is an important feature in the thermal augmentation of nanofluid.

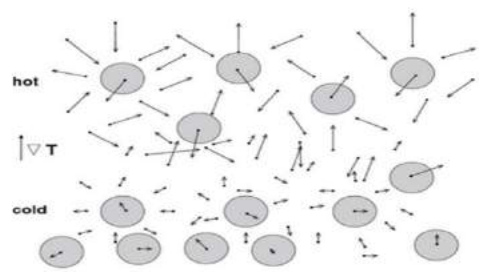


**Figure 1.4:** Brownian motion of the molecules causes the migration of particles to the colder region of the system.

### 1.2.18 Self-similar and non-similar flows

The boundary layer flows have mainly been divided into two categories, namely, the self-similar and non-similar flows. Self-similar solutions have intensively been studied in fluid mechanics. A similarity solution in boundary layer flows make it easier to solve the momentum and energy equations by transforming them to ordinary differential equations, but when such type of similarity does not exist, one had ultimately to determine the solution of the nonlinear partial differential equations (PDEs). Generally, it is tough to solve the nonlinear PDEs for this type of flow problems. The physical situations where it is impossible to find the self-similar solutions; the flows are designated as non-similar flows. The principle of similarity states that the solution is invariant after scaling of the dependent and independent variables. Therefore, the existence of self-similar solution immediately implies the absence of characteristic length (s) in certain direction (s). All the invariant solutions of a PDE can be found with the help of the theory of Lie Groups. Without basic sound knowledge of algebra it is difficult to find those solutions, but its weak form "the scaling group of transformation" is a very useful and powerful tool to explore the self-similarity. By applying such transformations, the new stretched and scaled variables do not change the associated physics. The fact that this one-parameter family of transformations maintains the invariance of the governing PDE's divulges the existence of self-similarity.

### 1.2.19 Solution methodology

Researchers and scientists are more interested in solving systems of nonlinear differential equations related to physical problems. In the field of engineering and technological industries, we come up with highly nonlinear partial differential equations that cannot be tackled analytically. However, noteworthy progress has been done in constructing new and advanced techniques for solving the nonlinear differential equations, particularly in the fields of fluid mechanics, finance, biology, chemistry, aerospace engineering and control engineering. In 1970, Keller [178] constructed a scheme for slow speed aerodynamic boundary layer flows. This scheme is used in various industrial and physical fluid dynamics problems. The essential basic phases in Keller-box scheme [179-185] are described as:

Step I. Reduction of higher order differential equations into first order.

Step II. Reduced first order differential equations are transformed to a system nonlinear

Step III. The system of nonlinear difference algebraic equations are linearized using Newton's method.

Step IV. Linearized algebraic equations are solved by means of block tri-diagonal algorithm.

The obtained numerical values are strongly influenced by the number of mesh points in *x*-direction and *y*-direction. The mesh points are suitably taken to fulfill the suggested boundary conditions asymptotically. Mesh independence must be done while computing the solution. The computer program of the algorithm is developed in "MATLAB" software. This technique validates outstanding stability, convergence and reliability as explained by Keller (1970). This algorithm is unconditionally stable and has second order convergence. We have used this technique (Keller-box method) for the problems discussed in **Chapters 2 to 7**. The detailed procedure of this method for ODE's is explained in **Chapter 2** and for PDE's in **Chapter 4.**

# Chapter 2

# Self-similar natural convection flow of nanofluid past a vertical plate

In the study of natural convection flow past a vertical plate there arises an important question that for what kind of wall temperature or the wall heat flux the flow will be self-similar or non-similar? Keeping this question in mind the laminar, incompressible, boundary-layer flow over a vertical flat plate for variable surface temperature (VWT) and variable heat flux (VHF) cases has been considered in this chapter. The general form of the boundary layer equations, for the Buongiorno nanofluid model is developed, which is equally valid for self-similar and non-similar flows. The power-law form of the variable wall temperature and variable wall heat flux, for which the flow is self-similar, is derived by utilizing the conditions of self-similarity. The obtained ordinary differential equations are solved by employing the Keller-box method. The solution procedure for the integration of obtained ordinary differential equations is elaborated in detail in this chapter. The Sherwood number and the Nusselt number are calculated for different values of the Brownian motion parameter and thermophoresis parameter. It is observed that the heat transfer rate decreases and mass transfer rate increases with the increase of Brownian motion and thermophoresis parameters respectively, provided the Lewis number and the Prandtl number are kept fixed. The power-law index $m$ influences the heat and mass transfer rates significantly.

## 2.1 Problem formulation

### 2.1.1 Buongiorno convective transport model

There are two famous homogenous nanofluid models, namely, Buongiorno model [31] and Tiwari & Das model [32] for the modeling of nanofluid flow problems. In the presence of temperature gradient, the thermophoresis force produces a concentration gradient of nanoparticles in the base fluid. According to Buongiorno, Brownian diffusion and thermophoresis were found to be important for nanoparticle transport mechanism. Therefore, the steady state transport equations for an incompressible nanofluid model which includes the effects of Brownian motion and thermophoresis are described as

$$\nabla . \boldsymbol{V} = 0, \tag{2.1}$$

$$\rho_f (\boldsymbol{V}.\nabla)\boldsymbol{V} = -\nabla p + \mu_f \nabla^2 \boldsymbol{V} + \boldsymbol{g}\beta\rho_f (T - T_\infty), \tag{2.2}$$

$$\boldsymbol{V}.\boldsymbol{\nabla} T = \alpha_f^* \nabla^2 T + \tau^* [D_B (\nabla T.\nabla C) + \frac{D_T}{T_\infty} (\nabla T.\nabla T)], \tag{2.3}$$

$$\boldsymbol{V}.\nabla C = D_B \nabla^2 C + \frac{D_T}{T_\infty} \nabla^2 T, \tag{2.4}$$

where $p$ is pressure and $\boldsymbol{V}(\bar{u}, \bar{v})$ is the velocity vector whose components $\bar{u}$ and $\bar{v}$ are along $\bar{x}-$ and $\bar{y}-$ directions, respectively.

### 2.1.2 Flow assumptions

Consider a steady, two-dimensional boundary layer flow of incompressible nanofluid along vertical heated surface as shown in Fig. 2.1. Two types of the boundary conditions for the heated wall have been considered, namely, VWT (variable wall temperature) and VHF (variable heat flux) (See for instance [186]) described as

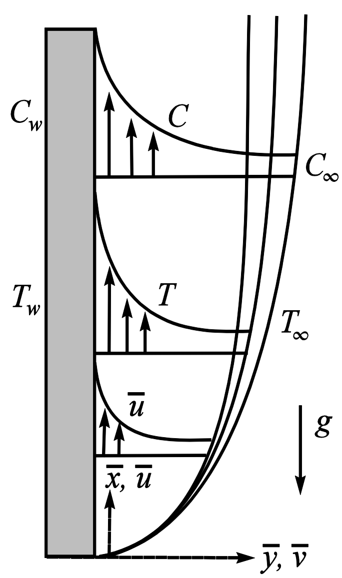


**Figure 2.1:** Schematic diagram and coordinate system.

**VWT** case

$$\left.\begin{array}{ll} \bar{u}=0, T=T_{\infty},\;\; C=C_{\infty}, & at\;\; \bar{x}=0, \bar{y}\neq 0, \\ \bar{u}=0, \bar{v}=v_w(\bar{x}), T=T_w(\bar{x}), C=C_w(\bar{x}) & at\;\; \bar{x}>0, y=0, \\ \bar{u}\to 0, \quad \bar{p}\to p_{\infty}, T\to T_{\infty},\;\; C\to C_{\infty}, & at\;\; \bar{x}>0, \bar{y}\to\infty, \end{array}\right\} \tag{2.5a}$$

**VHF** case

$$\left.\begin{array}{ll} \bar{u}=0, T=T_{\infty},\;\; C=C_{\infty}, & at\;\; \bar{x}=0, \bar{y}\neq 0, \\ \bar{u}=0, \dfrac{\partial T}{\partial \bar{y}}=-\dfrac{q_w}{\kappa}, \quad \dfrac{\partial C}{\partial \bar{y}}=-\dfrac{q_m}{D_B} & at\;\; \bar{x}>0, y=0, \\ \bar{u}\to 0, \quad \bar{p}\to p_{\infty}, T\to T_{\infty},\;\; C\to C_{\infty} & at\;\; \bar{x}>0, \bar{y}\to\infty. \end{array}\right\} \tag{2.5b}$$

### 2.1.3 Governing equations

**Case I (VWT)**

Incorporating the above stated suppositions in Section 2.1.2; and the Boussinesq approximation the constitutive equations for Buongiorno nanofluid model for VWT case [186] can be represented in differential form as

$$\frac{\partial u}{\partial x}+\frac{\partial v}{\partial y}=0, \tag{2.6}$$

$$u\frac{\partial u}{\partial x}+v\frac{\partial u}{\partial y}=\nu\,\frac{\partial^2 u}{\partial y^2}+\theta^*, \tag{2.7}$$

$$u\frac{\partial \theta^*}{\partial x}+v\frac{\partial \theta^*}{\partial y}=\frac{1}{Pr}\frac{\partial^2\theta^*}{\partial y^2}+Nt\left(\frac{\partial\theta^*}{\partial y}\right)^2+Nb\frac{\partial\theta^*}{\partial y}\frac{\partial C}{\partial y}, \tag{2.8}$$

$$u\frac{\partial \varphi^*}{\partial x}+v\frac{\partial \varphi^*}{\partial y}=\frac{1}{Le}\left(\frac{Nt}{Nb}\frac{\partial^2\theta^*}{\partial y^2}+\frac{\partial^2\varphi^*}{\partial y^2}\right), \tag{2.9}$$

where

$$\left.\begin{array}{c} Pr=\dfrac{\nu_f}{\alpha_f^*}, \quad Le=\dfrac{\nu_f}{D_B}, \quad Gr=\dfrac{g\beta(T_w-T_\infty)l^3}{\nu_f^2}, \quad \tau^*=\dfrac{(\rho c_p)_p}{(\rho c_p)_f}, \\ Nt=\dfrac{\tau^* D_T(C_w-C_\infty)}{T_\infty \nu_f}, \quad Nb=\dfrac{\tau^* D_B(T_w-T_\infty)}{\nu_f}, \end{array}\right. \tag{2.10}$$

are the Prandtl number, Lewis number, Grashof number, ratio of heat capacity of a nanoparticle to the base fluid, thermophoresis parameter and Brownian motion parameter, respectively. The dimensionless variables utilized to obtain the system (2.6) – (2.9) are defined as

$$
\begin{gathered}
x=\frac{\bar{x}}{l}\,, \qquad y=\frac{\bar{y}}{l}Gr^{\frac{1}{4}}\,, \qquad u=\frac{\bar{u}}{u_c}\,,\ u_c=Gr^{\frac{1}{2}}\frac{\nu_f}{l} \quad v=Gr^{-\frac{1}{4}}\frac{\bar{v}}{u_c},\\
p=\frac{l^2}{\nu_f^2\rho_f}Gr^{-\frac{1}{4}}\,\bar{p}\,, \qquad \theta^*=\frac{T-T_\infty}{T_w-T_\infty},\ \ \varphi^*=\frac{C-C_\infty}{C_w-C_\infty}.
\end{gathered} \tag{2.11}
$$

In order to satisfy the equation of continuity identically, we define the stream function $\psi$ such that $u=\frac{\partial\psi}{\partial x},\ v=-\frac{\partial\psi}{\partial y}$ and introduce the transformations

$$
\begin{gathered}
\xi=x, \qquad \eta=T_w(x)^{1/4}\xi^{-\frac{1}{4}}y\,, \qquad \theta(\xi,\eta)=T_w(x)\,\theta^*,\\
\varphi(\xi,\eta\,)=C_w(x)\varphi^*, \qquad \psi(\xi,\eta)=T_w(x)^{\frac{1}{4}}\xi^{\frac{3}{4}}f(\xi,\eta)\,,
\end{gathered} \tag{2.12}
$$

due to which the governing system (2.6) – (2.9) transforms to

$$
f'''+\frac{1}{4}\big(3+P(x)\big)ff''+\frac{1}{2}\big(1+P(x)\big){f'}^2+\theta=\xi\left(f'\frac{\partial f'}{\partial\xi}-f''\frac{\partial f}{\partial\xi}\right), \tag{2.13}
$$

$$
\begin{gathered}
\frac{1}{Pr}\theta''+\frac{1}{4}\big(3+P(x)\big)f\theta'-P(x)f'\theta+\left(Nb\theta'\varphi'+Nt{\theta'}^2\right)\\
=\xi\left(f'\frac{\partial\theta}{\partial\xi}-\theta'\frac{\partial f}{\partial\xi}\right),
\end{gathered} \tag{2.14}
$$

$$
\frac{1}{Le}(\varphi''+\frac{Nb}{Nt}\theta'')+\frac{1}{4}\big(3+P(x)\big)f\varphi'-P(x)f'\varphi=\xi\left(f'\frac{\partial\varphi}{\partial\xi}-\varphi'\frac{\partial f}{\partial\xi}\right), \tag{2.15}
$$

subject to the boundary conditions (due to Eq. (2.5a))

$$
\begin{gathered}
\xi\frac{\partial f(\xi,0)}{\partial\xi}+\frac{1}{4}\big(3+P(x)\big)f(\xi,0)=-M(x)\\
f'(\xi,0)=\ 0,\ \ \varphi(\xi,0)=1,\ \ \theta(\xi,0)=1,\\
f'(\xi,\infty)=0, \qquad \varphi(\xi\,,\infty)=0,\theta(\xi\,,\infty)=0,
\end{gathered} \tag{2.16}
$$

here $P(x)=\frac{x}{T_w(x)}\frac{dT_w(x)}{dx}, M(x)=v_w(x)\left(\frac{x}{T_w(x)}\right)^{\frac{1}{4}}$ and the “ ′ ” denotes ordinary derivative with respect to $\eta$.

The system (2.13) – (2.16) is in the general form which is equally valid for self-similar and non-similar flows. When the coefficient of the terms on left hand side are pure constants the situation refers to self-similar flow; otherwise it will be non-similar in nature. The function $P(x)$ could be a pure constant if the wall temperature follows the power-law form that is $T_w(x) = x^m$. For an impermeable surface, as in the present case, the function $M(x)$ becomes zero; hence a pure constant. In view of this reasoning the self-similar form of the system (2.13) – (2.16) reads as:

$$f''' + \frac{(m+3)}{4} f f'' + \frac{(m+1)}{2} f'^2 + \theta = 0, \tag{2.17}$$

$$\frac{1}{Pr}\theta'' + \frac{1}{4}(3+m) f\theta' - m f'\theta + \left(Nt\theta'^2 + Nb\theta'\varphi'\right) = 0, \tag{2.18}$$

$$\frac{1}{Le}\left(\varphi'' + \frac{Nb}{Nt}\theta''\right) + \frac{1}{4}(3+m) f\varphi' - m f'\varphi = 0, \tag{2.19}$$

with boundary conditions

$$\begin{gathered} f(0) = 0, \qquad f'(0) = 0, \qquad \theta(0) = 1, \;\; \varphi(0) = 1, \\ f'(\infty) = 0, \qquad \theta(\infty) = 0, \varphi(\infty) = 0, \end{gathered} \tag{2.20}$$

here $m$ is the power-law index. The quantities of physical nature such as the coefficient of skin friction, the Nusselt number and the Sherwood number defined in Eqs. (1.22), (1.25) and (1.28) respectively, take the following form (for the self-similar flow) in view of Eqs. (2.11) and (2.12):

$$\begin{gathered} C_f = C_{fx}(Gr/x^{3m+1})^{\frac{1}{4}} = f''(0), \\ Nu = Nu_x (Gr\, x^{5m-1})^{-\frac{1}{4}}/l^2 = -\theta'(0), \\ Sh = Sh_x (Gr\, x^{5m-1})^{-\frac{1}{4}}/l^2 = -\varphi'(0). \end{gathered} \tag{2.21}$$

**Case II (VHF)**

Analogous to case I, dimensionless transformations for the VHF case (in view of the WVT case) read as

$$x = \frac{\bar{x}}{l}, y = \frac{\bar{y}}{l} Gr^{\frac{1}{5}}, u = \frac{\bar{u}}{u_c}, u_c = Gr^{\frac{2}{5}} \frac{\nu_f}{l}, v = Gr^{-\frac{1}{5}} \frac{\bar{v}}{u_c}, \tag{2.22}$$

$$p = \frac{l^2}{\nu_f^2 \rho_f} Gr^{-\frac{1}{5}} \overline{p}, \theta(\xi,\eta) = Gr^{\frac{1}{5}} \kappa \frac{(T - T_\infty)}{q_w\, l} q_w(x)^{\frac{4}{5}},$$

$$\varphi(\xi,\eta) q_w(x)^{\frac{4}{5}} = Gr^{\frac{1}{5}} \kappa \frac{(C - C_\infty)}{q_w\, l}, Gr = \frac{g\beta q_w l^4}{\kappa\, \nu^2}.$$

Accordingly the transformations (2.12) modify in this case as

$$\xi = x, \qquad \psi(\xi,\eta) = q_w(x)^{1/5} \xi^{\frac{3}{4}} f(\xi,\eta), \qquad \eta = q_w(x)^{1/5} \xi^{-\frac{1}{4}} y, \tag{2.23}$$

due to which the governing system for Buongiorno nanofluid model in terms of dimensionless variables comes out of the form

$$f''' + \frac{1}{5}\big(4 + Q(x)\big) f f'' + \frac{1}{5}\big(3 + 2Q(x)\big) f'^2 + \theta = \xi \left( f' \frac{\partial f'}{\partial \xi} - f'' \frac{\partial f}{\partial \xi} \right), \tag{2.24}$$

$$\begin{aligned} &\frac{1}{Pr}\theta'' + \frac{1}{5}\big(4 + Q(x)\big) f\theta' - \frac{1}{5}\big(1 + 4Q(x)\big) f'\theta + \big(Nb\theta'\varphi' + Nt\theta'^2\big) \\ &\qquad = \xi \left( f' \frac{\partial \theta}{\partial \xi} - \theta' \frac{\partial f}{\partial \xi} \right), \end{aligned} \tag{2.25}$$

$$\begin{aligned} &\frac{1}{Le}\Big(\varphi'' + \frac{Nb}{Nt}\theta''\Big) + \frac{1}{5}\big(4 + Q(x)\big) f\varphi' - \frac{1}{5}\big(1 + 4Q(x)\big) f'\varphi \\ &\qquad = \xi \left( f' \frac{\partial \varphi}{\partial \xi} - \varphi' \frac{\partial f}{\partial \xi} \right), \end{aligned} \tag{2.26}$$

with the following boundary conditions (due to Eq. (2.5b))

$$\begin{aligned} &\xi \frac{\partial f(\xi,0)}{\partial \xi} + \frac{1}{5}\big(4 + Q(x)\big) f(\xi,0) = -N(x), \\ &f'(\xi,0) = 0, \ \varphi'(\xi,0) + 1 = 0, \ \theta'(\xi,0) + 1 = 0, \\ &f'(\xi,\infty) = 0, \qquad \varphi(\xi,\infty) = 0, \qquad \theta(\xi,\infty) = 0, \end{aligned} \tag{2.27}$$

where

$$Q(x) = \frac{x}{q_w(x)} \frac{dq_w(x)}{dx}, N(x) = v_w(x) \left( \frac{x}{q_w(x)} \right)^{1/5}.$$

Again, the system (2.24) – (2.27) is equally valid for the self-similar and non-similar flows, in general. The similarity can be ensured for the cases when the coefficients of the terms on the left hand side of Eqs. (2.24) – (2.26) become pure constants. This restriction results in the power- law form of the wall heat flux function. The absence of any normal wall velocity makes the function $N(x)$ identically equal to zero. Under these restrictions, the self-similar form of the system (2.24) – (2.27) read as

$$f''' + \frac{1}{5}(4+m)ff'' + \frac{1}{5}(3+2m)f'^2 + \theta = 0, \tag{2.28}$$

$$\frac{1}{Pr}\theta'' + \frac{1}{5}(4+m)f\theta' - \frac{1}{5}(1+4m)f'\theta + \left(Nb\theta'\varphi' + Nt\theta'^2\right) = 0, \tag{2.29}$$

$$\frac{1}{Le}(\varphi'' + \frac{Nb}{Nt}\theta'') + \frac{1}{5}(4+m)f\varphi' - \frac{1}{5}(1+4m)f'\varphi = 0, \tag{2.30}$$

where $m$ is the power-law index, $Nb$ and $Nt$ represent Brownian motion parameter and thermophoresis parameter respectively. In this way the boundary conditions (2.27) modify as

$$\begin{gathered} f(0) = 0, \quad f'(0) = 0, \quad \varphi'(0) = -1, \quad \theta'(0) = -1, \\ f'^{(\infty)} = 0, \quad \varphi(\infty) = 0, \quad \theta(\infty) = 0. \end{gathered} \tag{2.31}$$

Similar to the previous case the physical quantities such as the skin friction, the Nusselt number, and the Sherwood number, defined in equations (1.22), (1.25) and (1.28), transform as (due to Eq. (2.22 and (2.23))

$$\begin{gathered} C_f = C_{fx}(Gr/x^{3m+1})^{\frac{1}{4}} = f''(0), \\ Nu = Nu_x(Gr\, x^{5m+3})^{-\frac{1}{4}}/l^2 = -\theta\,'(0), \\ Sh = Sh_x(Gr\, x^{5m+3})^{-\frac{1}{4}}/l^2 = -\varphi\,'(0). \end{gathered} \tag{2.32}$$

## 2.2 Numerical scheme

The solution of nonlinear system of PDE's (2.17) – (2.19) under the constraints (2.20) is obtained by the second order finite difference scheme [178-185] commonly known as the Keller-box scheme. The governing equations for the VHF case are also solved by the Keller-box technique but the details of the procedure are given only for VWT case. According to this scheme the differential equations (2.17) – (2.19) are firstly converted into form of first order by introducing new variables $\mathbb{u}, \mathbb{v}, \mathbb{q}$ and $\mathbb{p}$ such as

$$f' = \mathbb{u}, \mathbb{u}' = \mathbb{v}, \theta' = \mathbb{q}, \text{ and } \varphi' = \mathbb{p}. \tag{2.33}$$

The independent variable $\eta$ is discretized as

$$\eta_j = \eta_{j-1} + \Delta\eta \text{ where } \eta_0 = 0, \eta_J = \eta_\infty, \quad ; j = 1,2,\dots,J-1, \tag{2.34}$$

here $\Delta\eta = h$ is the constant step size and $j$ represents the positive integer. The derivatives w.r.t. $\eta$ are reduced to the difference equations using central difference formula and functions are changed by their mean values at $\eta_{j-1/2}$. After this process the obtained difference equations look like:

$$\begin{gathered}\left(\frac{1}{h}\right)\left[\left\{\left(\mathbb{v}_j - \mathbb{v}_{j-1}\right)\right\}\right] + \frac{1}{4}(3+m)\left(\frac{1}{4}\right)\{\left((f_j + f_{j-1})(\mathbb{v}_j + \mathbb{v}_{j-1})\right)\}] \\ -\frac{1}{2}(1+m)\left(\frac{1}{4}\right)\{\left((\mathbb{u}_j + \mathbb{u}_{j-1})^2\right)\}] + \left(\frac{1}{2}\right)[\left\{\left(\theta_j + \theta_{j-1}\right)\right\} = 0,\end{gathered} \tag{2.35}$$

$$\begin{gathered}\left(\frac{1}{h\,Pr}\right)\left[\left\{\left(\mathbb{q}_j - \mathbb{q}_{j-1}\right)\right\}\right] + \frac{1}{4}(3+m)\left(\frac{1}{4}\right)\{\left((f_j + f_{j-1})(\mathbb{q}_j + \mathbb{q}_{j-1})\right)\}] \\ -m\left(\frac{1}{4}\right)\{\left((\mathbb{u}_j + \mathbb{u}_{j-1})(\theta_j + \theta_{j-1})\right)\}] \\ +Nb\left(\frac{1}{4}\right)\{\left((\mathbb{q}_j + \mathbb{q}_{j-1})(\mathbb{p}_j + \mathbb{p}_{j-1})\right)\}] \\ +Nt\left(\frac{1}{4}\right) + \{\left((\mathbb{q}_j + \mathbb{q}_{j-1})^2\right)\}] = 0,\end{gathered} \tag{2.36}$$

$$\begin{gathered}\left(\frac{1}{h\,Le}\right)\left[(\mathbb{p}_j - \mathbb{p}_{j-1}) + \frac{Nt}{Nb}(\mathbb{q}_j - \mathbb{q}_{j-1})\right] \\ +\frac{(3+m)}{16}\{\left((f_j + f_{j-1})(\mathbb{p}_j + \mathbb{p}_{j-1})\right)\}] \\ -m\left(\frac{1}{4}\right)\{\left((\mathbb{u}_j + \mathbb{u}_{j-1})(\varphi_j + \varphi_{j-1})\right)\}] = 0.\end{gathered} \tag{2.37}$$

Accordingly the boundary conditions are also discretized which finally take the form

$$\begin{gathered}\frac{2}{h}\left(f_j - f_{j-1}\right) - \mathbb{u}_j - \mathbb{u}_{j-1} = 0\,, \\ \frac{2}{h}\left(\mathbb{u}_j - \mathbb{u}_{j-1}\right) - \mathbb{v}_j - \mathbb{v}_{j-1} = 0, \\ \frac{2}{h}\left(\theta_j - \theta_{j-1}\right) - \mathbb{q}_j - \mathbb{q}_{j-1} = 0, \\ \frac{2}{h}\left(\varphi_j - \varphi_{j-1}\right) - \mathbb{p}_j - \mathbb{p}_{j-1} = 0\,.\end{gathered} \tag{2.38}$$

The obtained equations (2.35) – (2.37) are non-linear algebraic equations. To solve these equations, we first reduced them to linear form by using Newton’s method in this scheme unknown function is replaced by sum of known $\left(f_j^{(i)}\right)$ and unknown $\left(\delta f_j^{(i)}\right)$ function such as $f_j^{i+1}$ at $(i+1)^{th}$ iterates can be written as

$$f_j^{i+1} = f_j^{(i)} + \delta f_j^{(i)}, \tag{2.39}$$

also other variable are replaced in the similar fashion. Further during the linearization process the ${\delta f_j^{(i)}}^2$ and higher order terms are neglected. Same for the case of other variables $\delta \mathbb{u}_j^{(i)}, \delta \mathbb{v}_j^{(i)}, \delta \theta_j^{(i)}, \delta \mathbb{q}_j^{(i)}, \delta \varphi_j^{(i)}$ and $\delta \mathbb{p}_j^{(i)}$, is adopted and the following system of linear algebraic equations is obtained:

$$\delta f_j - \delta f_{j-1} - \frac{\Delta\eta\left(\delta \mathbb{u}_j + \delta \mathbb{u}_{j-1}\right)}{2} = (r_{11})_j,$$

$$(s_{11})_j \delta f_{j-1} + (s_{12})_j \delta f_j + (s_{13})_j \delta \mathbb{u}_{j-1} + (s_{14})_j \delta \mathbb{u}_j + (s_{15})_j \delta \mathbb{v}_{j-1} + (s_{16})_j \delta \mathbb{v}_j$$
$$+ (s_{17})_j \delta \theta_{j-1} + (s_{18})_j \delta \theta_j = (r_{12})_j,$$

$$(s_{21})_j \delta \theta_{j-1} + (s_{22})_j \delta \theta_j + (s_{23})_j \delta \mathbb{q}_{j-1} + (s_{24})_j \delta \mathbb{q}_j + (s_{25})_j \delta \varphi_{j-1} + (s_{26})_j \delta \varphi_j$$
$$+ (s_{27})_j \delta \mathbb{p}_{j-1} + (s_{28})_j \delta \mathbb{p}_j = (r_{13})_j,$$

$$(s_{31})_j \delta \theta_{j-1} + (s_{32})_j \delta \theta_j + (s_{33})_j \delta \mathbb{q}_{j-1} + (s_{34})_j \delta \mathbb{q}_j + (s_{35})_j \delta \varphi_{j-1} + (s_{36})_j \delta \varphi_j$$
$$+ (s_{37})_j \delta \mathbb{p}_{j-1} + (s_{38})_j \delta \mathbb{p}_j = (r_{14})_j,$$

$$\delta \mathbb{u}_j - \delta \mathbb{u}_{j-1} - \tfrac{h}{2}\left(\delta \mathbb{v}_j + \delta \mathbb{v}_{j-1}\right) = (r_{15})_j, \delta \theta_j - \delta \theta_{j-1} - \tfrac{h}{2}\left(\delta \mathbb{q}_j + \delta \mathbb{q}_{j-1}\right) = (r_{16})_j,$$

$$\delta \varphi_j - \delta \varphi_{j-1} - \frac{h}{2}\left(\delta \mathbb{p}_j + \delta \mathbb{p}_{j-1}\right) = (r_{17})_j.$$

The boundary conditions also undergo the same procedure and finally appear in the form

$$\delta f_0 = \delta \mathbb{p}_0 = \delta \theta_0 = \delta \varphi_0 = 0,$$
$$\delta \mathbb{p}_J = \delta \mathbb{q}_J = \delta s_J = \delta \theta_J = \delta \varphi_J = 0.$$

Before iterating the numerical procedure, the linearized system of algebraic equations are written in matrix for under the given constraints.

**Coefficients of momentum equation:**

The coefficients of unknown functions $\delta f_{j-1}, \delta \mathbb{u}_{j-1}, \delta \mathbb{v}_{j-1}, \delta \theta_{j-1}, \delta \mathbb{q}_{j-1}, \delta \varphi_{j-1}$ and $\delta \mathbb{p}_{j-1}$ and the non-homogeneous parts are written as

coefficient of $\delta f_{j-1}$:

$$(s_{11})_j = \frac{1}{16}(3+m)\left\{\left((\mathbb{v}_j + \mathbb{v}_{j-1})\right)\right\},$$

coefficient of $\delta f_j$:

$$(s_{12})_j = \frac{1}{16}(3+m)\{((\mathbb{v}_j + \mathbb{v}_{j-1}))\},$$

coefficient of $\delta \mathbb{u}_{j-1}$:

$$(s_{13})_j = -\frac{m}{4}(\mathbb{u}_j + \mathbb{u}_{j-1}),$$

coefficient of $\delta \mathbb{u}_j$:

$$(s_{14})_j = -\frac{m}{4}(\mathbb{u}_j + \mathbb{u}_{j-1}),$$

coefficient of $\delta \mathbb{v}_{j-1}$:

$$(s_{15})_j = -\frac{1}{h} + \frac{1}{16}(3+m)(f_j + f_{j-1}),$$

coefficient of $\delta \mathbb{v}_j$:

$$(s_{16})_j = \frac{1}{h} + \frac{1}{16}(3+m)(f_j + f_{j-1}),$$

coefficient of $\delta \theta_{j-1}$:

$$(s_{17})_j = \frac{1}{2},$$

coefficient of $\delta \theta_j$:

$$(s_{18})_j = \frac{1}{2}.$$

**Coefficients of energy equation:**

coefficient of $\delta \theta_{j-1}$:

$$(s_{19})_j = -\frac{m}{4}(\mathbb{u}_j + \mathbb{u}_{j-1}),$$

coefficient of $\delta \theta_j$:

$$(s_{20})_j = -\frac{m}{4}(\mathbb{u}_j + \mathbb{u}_{j-1}),$$

coefficient of $\delta \mathbb{q}_{j-1}$:

$$(s_{21})_j = -\frac{1}{Pr\, h} + \frac{1}{16}(3+m)(f_j + f_{j-1}) + \frac{Nt}{2}(\mathbb{q}_j + \mathbb{q}_{j-1}),$$

coefficient of $\delta \mathbb{q}_j$:

$$(s_{22})_j = \frac{1}{Pr\, h} + \frac{1}{16}(3+m)(f_j + f_{j-1}) + \frac{Nt}{2}(\mathbb{q}_j + \mathbb{q}_{j-1}),$$

coefficient of $\delta \mathbb{p}_{j-1}$:

$$(s_{23})_j = \frac{Nb}{4}\left(\mathbb{q}_j + \mathbb{q}_{j-1}\right),$$

coefficient of $\delta \mathbb{p}_j$:

$$(s_{24})_j = \frac{Nb}{4}\left(\mathbb{q}_j + \mathbb{q}_{j-1}\right).$$

**Coefficients of concentration equation:**

coefficient of $\delta \mathbb{q}_{j-1}$:

$$(s_{25})_j = -\frac{Nt}{Nb\ Le\, h},$$

coefficient of $\delta \mathbb{q}_j$:

$$(s_{26})_j = -\frac{Nt}{Nb\ Le\, h},$$

coefficient of $\delta \varphi_{j-1}$:

$$(s_{27})_j = -\frac{m}{4}\left(\mathbb{u}_j + \mathbb{u}_{j-1}\right)$$

coefficient of $\delta \varphi_j$:

$$(s_{28})_j = -\frac{m}{4}\left(\mathbb{u}_j + \mathbb{u}_{j-1}\right),$$

coefficient of $\delta \mathbb{p}_{j-1}$:

$$(s_{29})_j = -\frac{1}{Le\, h} + \frac{1}{16}(3+m)\left(f_j + f_{j-1}\right),$$

coefficient of $\delta \mathbb{p}_j$:

$$(s_{30})_j = \frac{1}{Le\, h} + \frac{1}{16}(3+m)\left(f_j + f_{j-1}\right).$$

**The non-homogeneous terms:**

$$(r_{11})_j = f_j - f_{j-1} - \frac{h}{2}\left(\mathbb{u}_j + \mathbb{u}_{j-1}\right),$$

$$(r_{21})_j = -\frac{1}{h}\left(\mathbb{v}_j + \mathbb{v}_{j-1}\right) - \frac{(3+m)}{16}\left(f_j + f_{j-1}\right)\left(\mathbb{v}_j + \mathbb{v}_{j-1}\right)$$
$$+ \frac{(1+m)}{8}\left(\mathbb{u}_j + \mathbb{u}_{j-1}\right)^2 - \frac{1}{2}\left(\theta_j + \theta_{j-1}\right),$$

$$(r_{31})_j = -\frac{1}{\Pr h}(\mathbb{q}_j + \mathbb{q}_{j-1}) - \frac{(3+m)}{16}(f_j + f_{j-1})(\mathbb{q}_j + \mathbb{q}_{j-1})$$
$$+\frac{m}{4}(\mathbb{u}_j + \mathbb{u}_{j-1})(\theta_j + \theta_{j-1}) - \frac{Nb}{4}(\mathbb{q}_j + \mathbb{q}_{j-1})(\mathbb{p}_j + \mathbb{p}_{j-1}) - \frac{Nt}{4}(\mathbb{u}_j + \mathbb{u}_{j-1})^2,$$
$$(r_{41})_j = -\frac{1}{Le\,h}\left((\mathbb{p}_j - \mathbb{p}_{j-1}) + \frac{Nt}{Nb}(\mathbb{q}_j - \mathbb{q}_{j-1})\right)$$
$$-\frac{(3+m)}{16}(f_j + f_{j-1})(\mathbb{p}_j + \mathbb{p}_{j-1}) + \frac{m}{4}(\mathbb{u}_j + \mathbb{u}_{j-1})(\varphi_j + \varphi_{j-1}),$$
$$(r_{51})_j = \delta\mathbb{u}_j - \delta\mathbb{u}_{j-1} - \frac{\Delta\eta}{2}(\delta\mathbb{v}_j + \delta\mathbb{v}_{j-1}),$$
$$(r_{61})_j = \delta\theta_j - \delta\theta_{j-1} - \frac{\Delta\eta}{2}(\delta\mathbb{q}_j + \delta\mathbb{q}_{j-1}),$$
$$(r_{71})_j = \delta\varphi_j - \delta\varphi_{j-1} - \frac{\Delta\eta}{2}(\delta\mathbb{p}_j + \delta\mathbb{p}_{j-1}).$$

Block-tridiagonal elimination technique is used to solve the obtained matrix vector form for which the algorithm is written in Matlab software. The results are displayed through graphs and tables for different parameters. Comparison of the computed numerical values of $f''(0)$ and $-\theta'(0)$ with the already available results is presented in Table 2.1. These results are in perfect agreement with those of Pop and Ingham [161] which guarantees the accuracy of the present solution.

## 2.3 Results and discussion

Following the above explained procedure numerical computations were performed for several combinations of the values of pertinent parameters namely, the Prandtl number ($Pr$), the power-law index ($m$), the Brownian motion parameter ($Nb$), the Lewis number ($Le$), and the thermophoresis parameter ($Nt$). Graphical representation of velocity, temperature, concentration, skin friction, Nusselt number, and the Sherwood number have been displayed for different parameters.

Figures 2.2 and 2.3 depict the velocity distribution for various values of $Nb$ and $Nt$. It is noticed that the velocity enhances with the increment in the values of $Nb$ and $Nt$. Reduction in the velocity profiles is observed for increasing the power-law index $m$. Figures 2.4 – 2.7 show the influence of $Nt$ and $Nb$ on temperature and concentration distributions. It is noticed that the temperature distribution enhances with the rise of the $Nt$

and $Nb$ while concentration distribution reduces with the increase of $Nt$ and $Nb$. Reduction of these profiles is seen for increasing values of the power-law index $m$. Because $Nt$ and $Nb$ lead to the thickening of the thermal boundary layer while thinning the concentration boundary layer.

**Table 2.1:** Comparison of $C_f$ and $Nu$ data for different $m$ when $Nt = Nb = 0, Pr = 1.0$.

| $m$ | $C_f$ | | $Nu$ | |
|---|---|---|---|---|
| | Present | [186] | Present | [186] |
| 1.0 | 1.009694 | 1.0097 | 1.514716 | 1.5148 |
| 1.25 | 0.959708 | 0.9597 | 1.466989 | 1.4671 |
| 1.5 | 0.917387 | 0.9174 | 1.426671 | 1.4628 |
| 1.75 | 0.880924 | 0.8809 | 1.391951 | 1.3920 |
| 2.0 | 0.849057 | 0.8491 | 1.361583 | 1.3617 |
| 2.25 | 0.820879 | 0.8209 | 1.334685 | 1.3347 |
| 2.5 | 0.795715 | 0.7957 | 1.310607 | 1.3106 |
| 2.75 | 0.773054 | 0.7729 | 1.288859 | 1.2897 |
| 3.0 | 0.752497 | 0.7524 | 1.269066 | 1.2699 |
| 3.25 | 0.733731 | 0.7336 | 1.250933 | 1.2517 |
| 3.5 | 0.716504 | 0.7164 | 1.234225 | 1.2349 |
| 3.75 | 0.700613 | 0.7005 | 1.218752 | 1.2194 |
| 4.0 | 0.685889 | 0.6858 | 1.204358 | 1.2050 |
| 4.25 | 0.672193 | 0.6721 | 1.190914 | 1.1915 |
| 4.5 | 0.659408 | 0.6594 | 1.178312 | 1.1789 |
| 41.75 | 0.647434 | 0.6474 | 1.166462 | 1.1670 |
| 5.0 | 0.636188 | 0.6361 | 1.155285 | 1.1558 |

Moreover, thermal and concentration distributions decrease when the power-law index is increased. Figures 2.8 & 2.9 depict heat and mass transfer rate versus $Nt$ and $Nb$ at two values of the power-law index $m$. Figure 2.8 shows that the Nusselt number decreases with the increase in the values of $Nb$ and $Nt$. However, it rises for increasing values of of $m$. Figure 2.9 illustrates that Sherwood number rises with the increase of $Nt$ and $Nb$; and is also observed to be as an increasing function of $m$. Figures 2.10 – 2.12 depict the influence of $Nt$ and $Nb$ versus power-law index $m$ on skin friction, Nusselt number and Sherwood number, respectively.

Figure 2.10 reveals that the skin friction increases with the increment in $Nb$ and $Nt$ however, skin friction reduces as $m$ is increased. Figure 2.11 illustrates that the Nusselt number decreases with the increase in $Nb$ and $Nt$. Also the Nusselt number increases as $m$ increases. Figure 2.12 predicts that the Sherwood number enhances with the increase of $Nb$ and $Nt$ where an increasing trend can also be seen for the power-law index $m$. Corresponding to these graphs some numerical values have also been written in Table 2.2. For the VHF case, influence of $Nt$ and $Nb$ on velocity, temperature and concentration distributions are depicted in Figs. 2.13 to 2.18. Figures 2.13 and 2.14 demonstrate the impact of $Nt$ and $Nb$ on velocity profiles. It is noticed that velocity increases with the increase of $Nt$ and $Nb$. Figures 2.15 and 2.16 illustrate the effect of $Nt$ and $Nb$ on temperature profiles. It is seen that temperature profile rises with the increase of $Nt$ and $Nb$ near the plate and decreases gradually as one moves away from the plate. Variation of concentration distribution due to the change in $Nt$ and $Nb$ is recorded in Figs. 2.17 and 2.18. Figure 2.17 depicts that concentration distribution reduces adjacent to the plate surface as one increases $Nt$ and enhances subsequently as one moves to the upper part of the concentration boundary layer on increasing $Nt$. Figure 2.18 shows that concentration distribution reduces by incrementing $Nb$. From these figures it is also observed that overall depreciation of these profiles is noted for increasing values of the power-law index $m$.

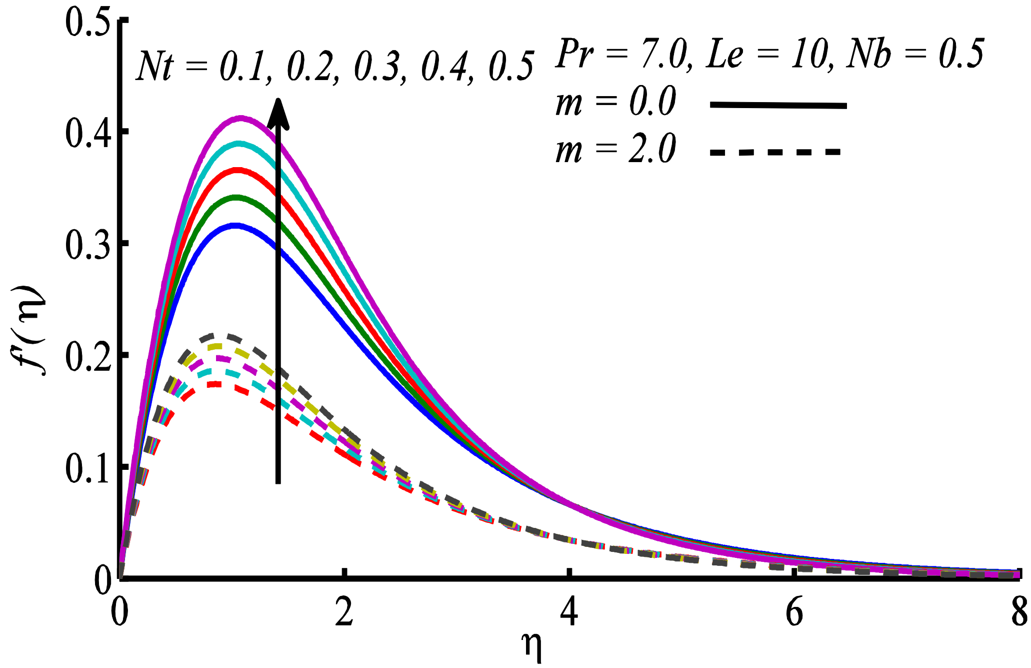


**Figure 2.2:** Velocity graphs for different $Nt$ and $m$.

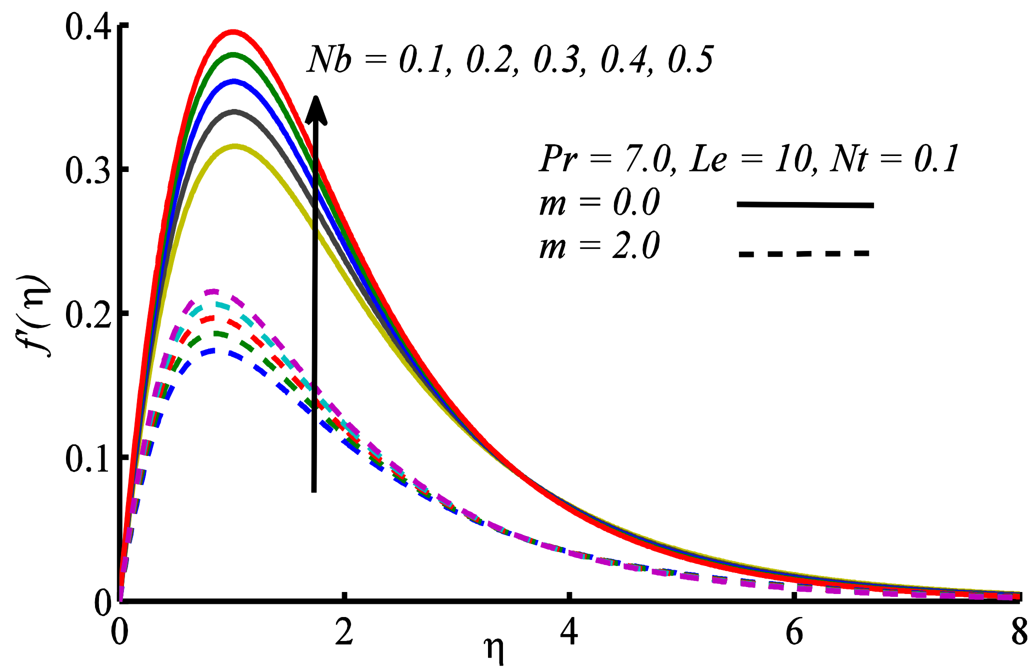


**Figure 2.3:** Variation in velocity profile corresponding to different $m$ and $Nb$ .

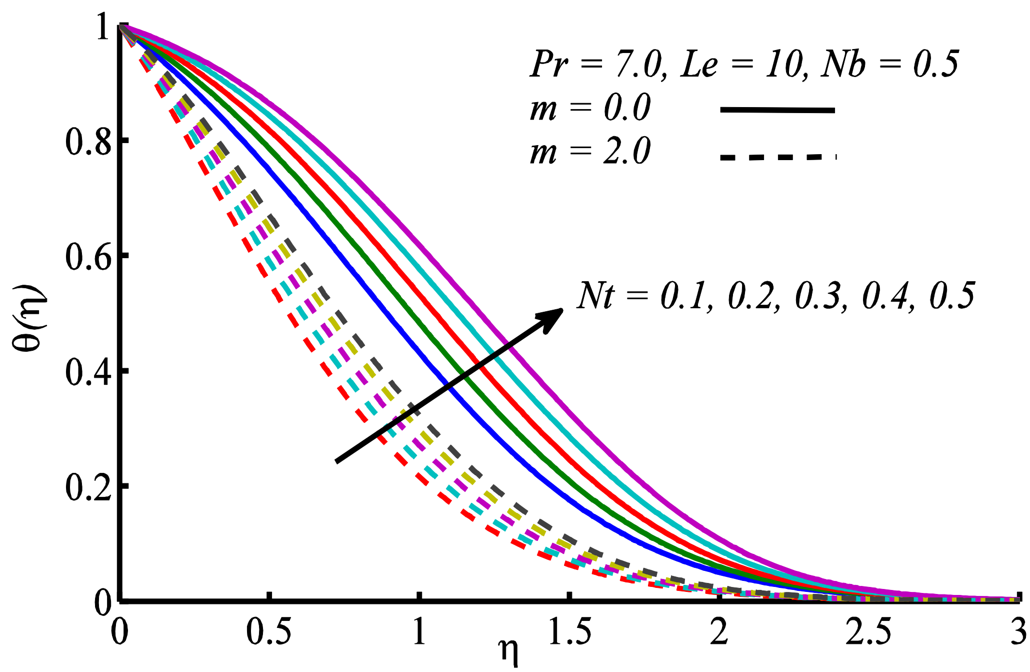


**Figure 2.4:** Effect of varying $Nt$ and $m$ on temperature profile.

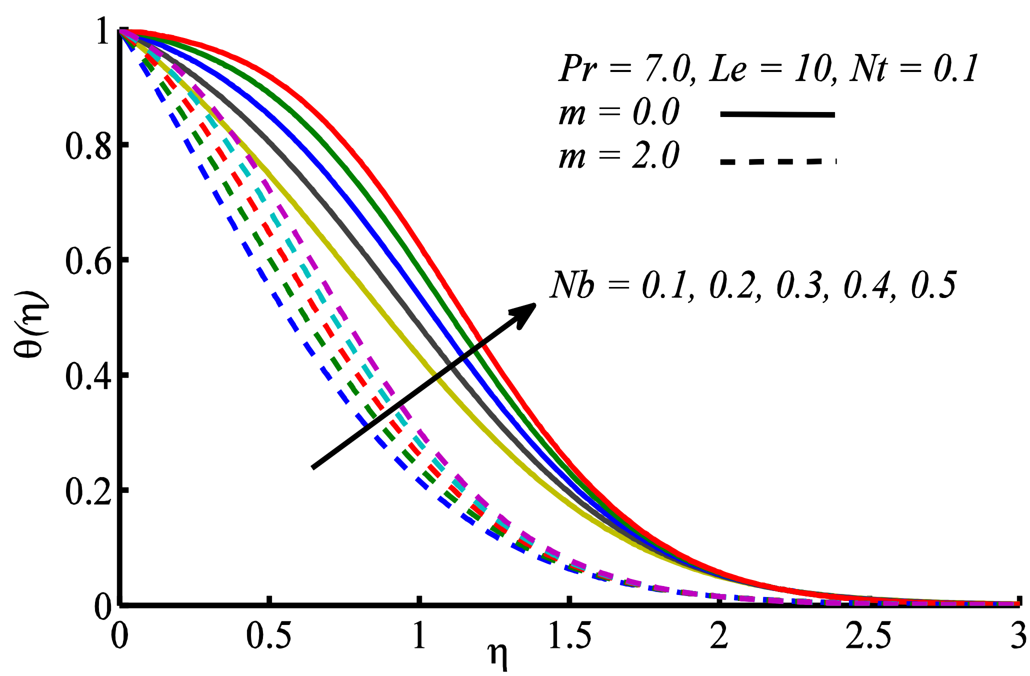


**Figure 2.5:** Temperature profile plotted against different $Nb$ and $m$.

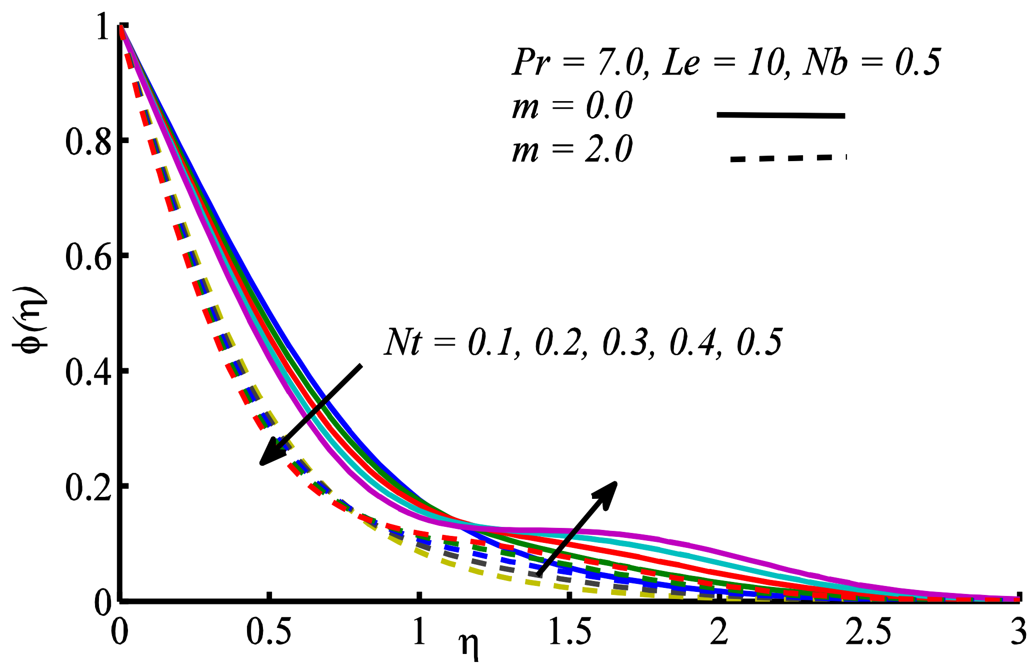


**Figure 2.6:** Effect of varying $Nt$ and $m$ on concentration profile.

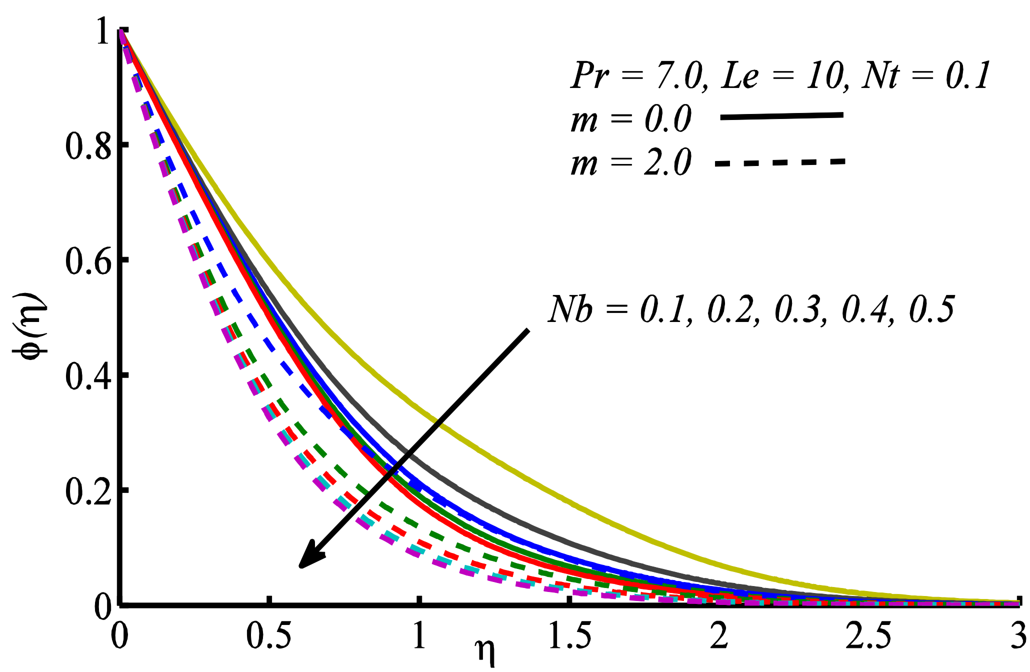


**Figure 2.7:** Concentration distribution for different $m$ and $Nb$.

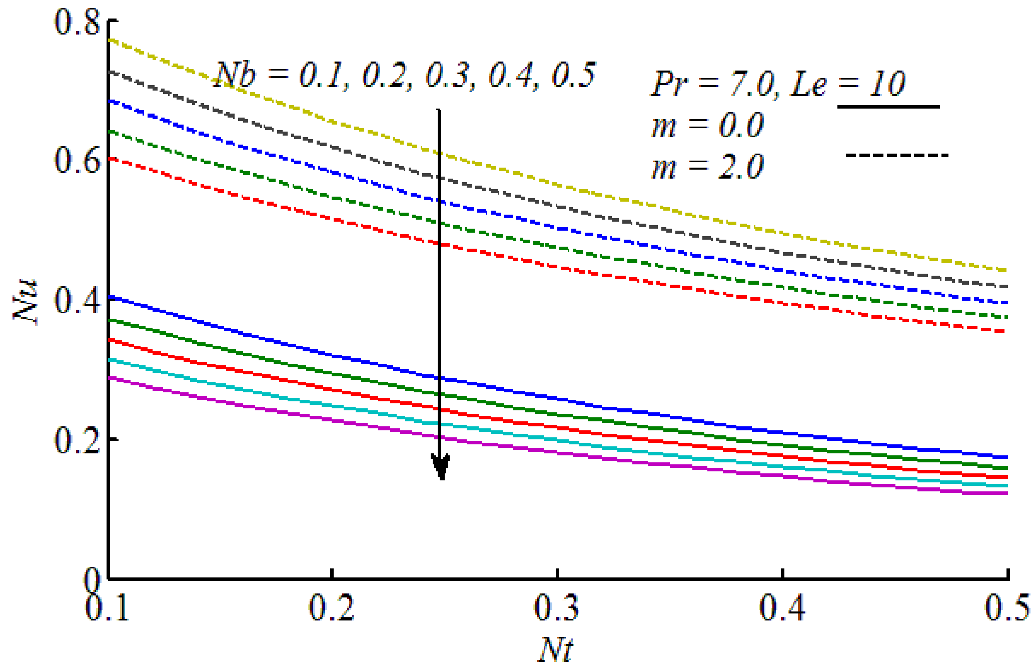


**Figure 2.8:** Nusselt number graph versus $Nt$ and $m$.

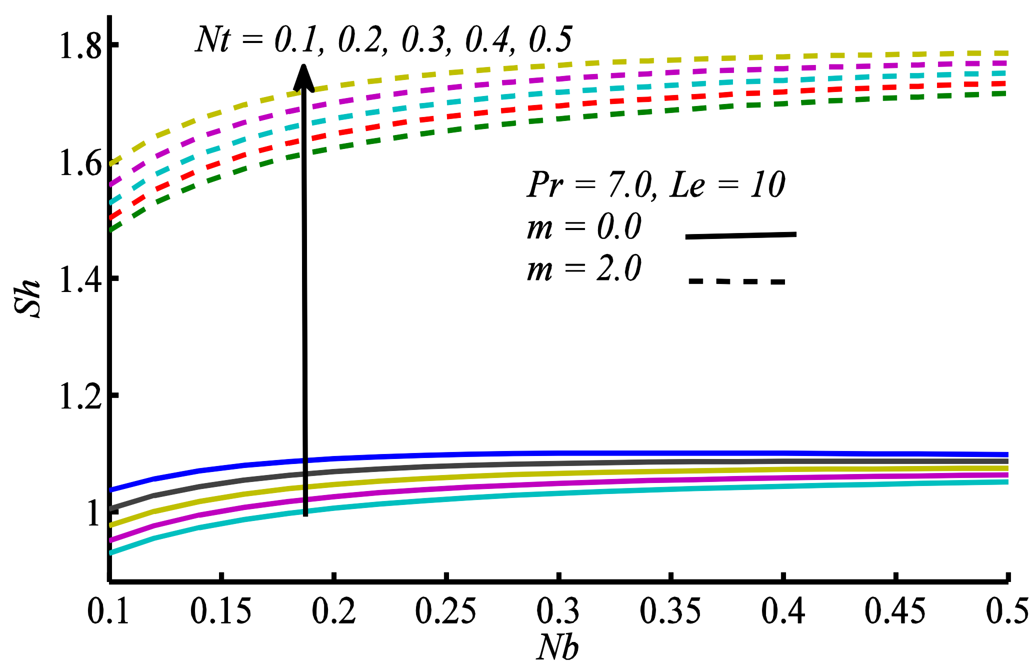


**Figure 2.9:** Sherwood number plotted against $Nb$ and $m$ for different $Nt$.

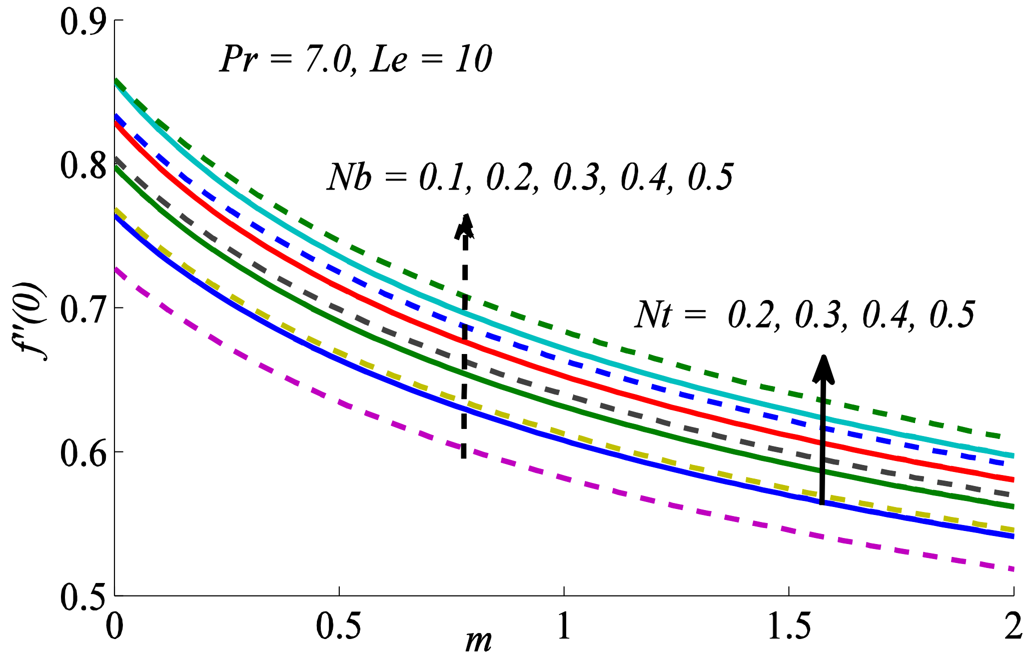


**Figure 2.10:** Skin friction graph against $m$ for different $Nt$ *and* $Nb$.

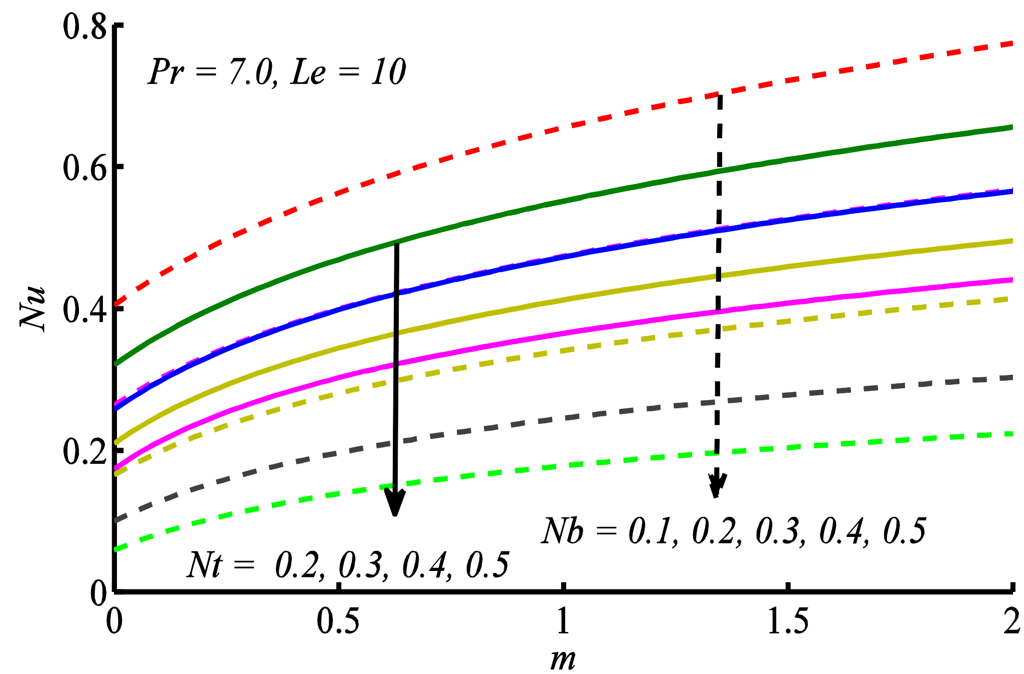


**Figure 2.11:** Nusselt number plotted against $m$ for different $Nb$ and $Nt$.

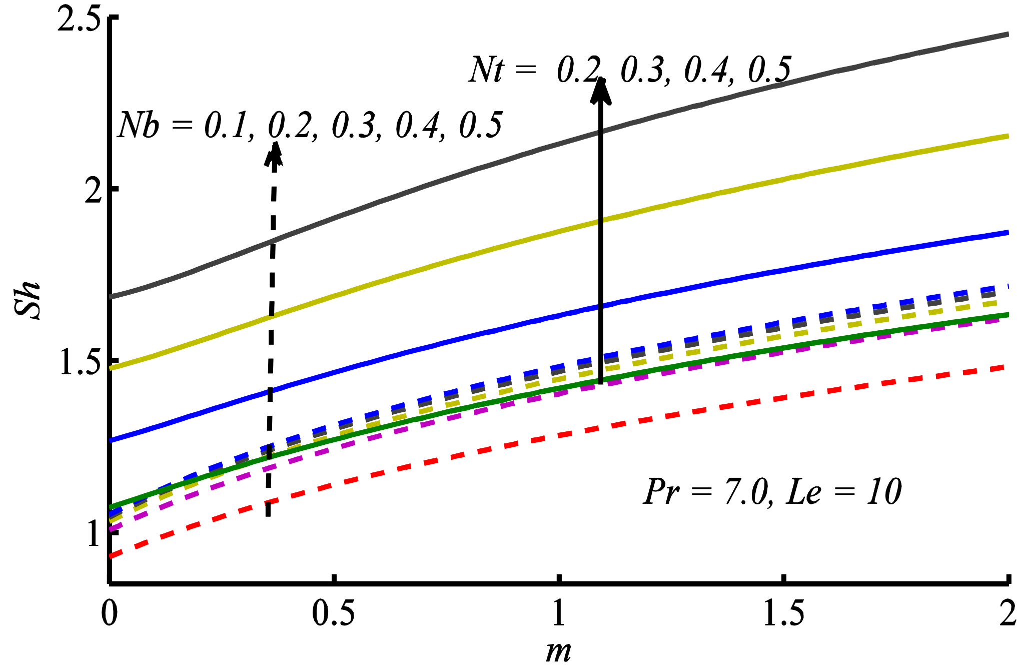


**Figure 2.12:** Variation of Sherwood number at different $Nt$ and $Nb$ against $m$.

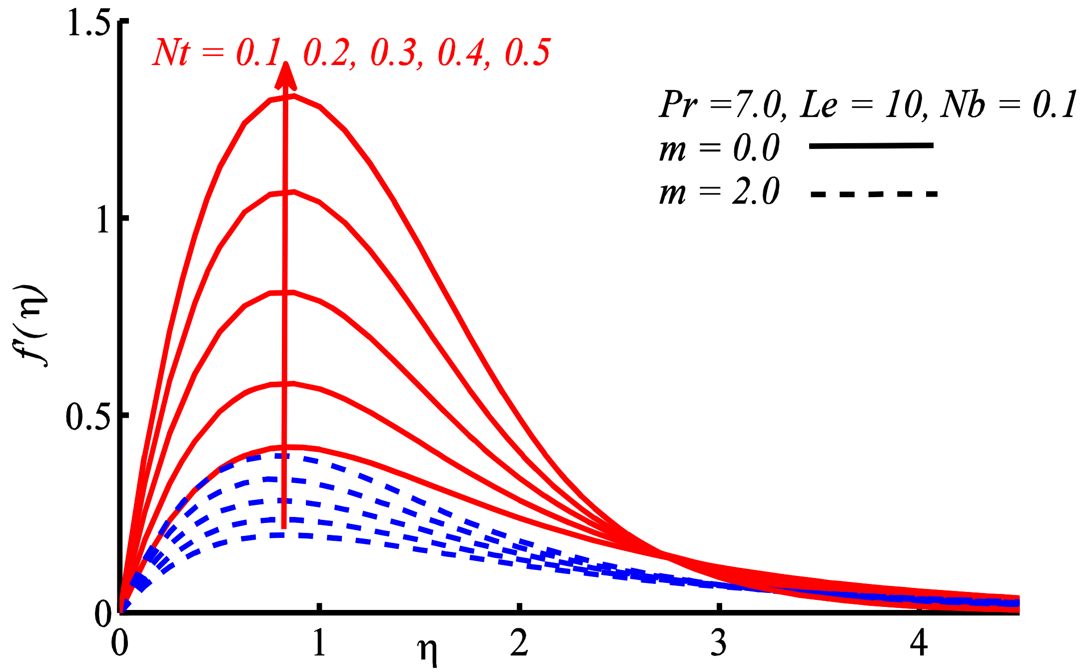


**Figure 2.13:** Velocity graph plotted against different $Nt$ and $m$.

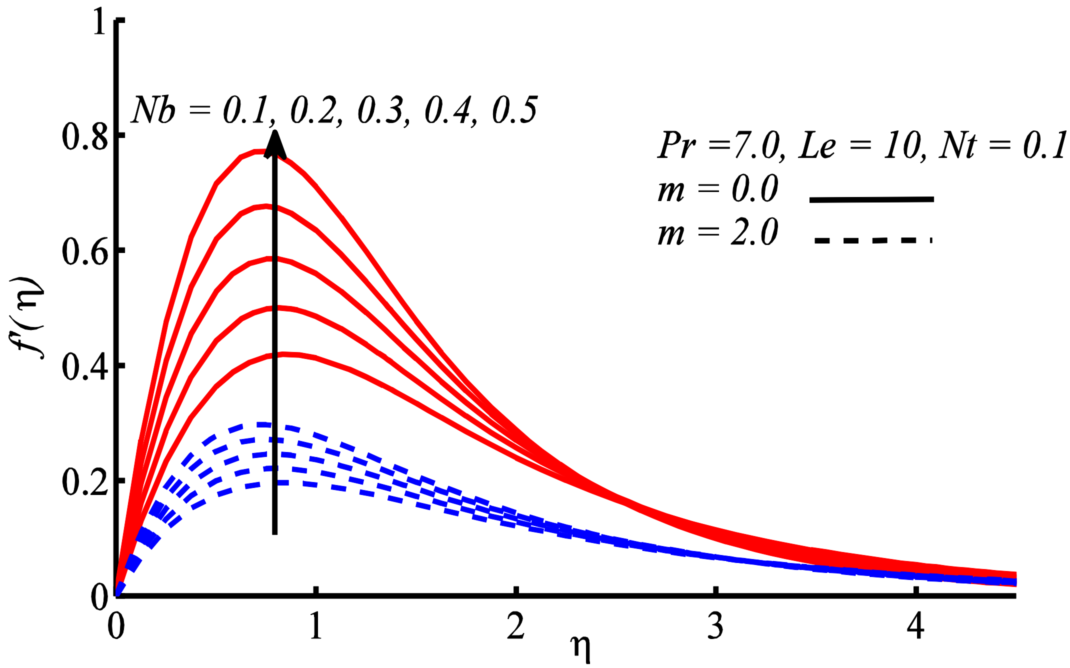


**Figure 2.14:** Velocity profile for different $Nb$.

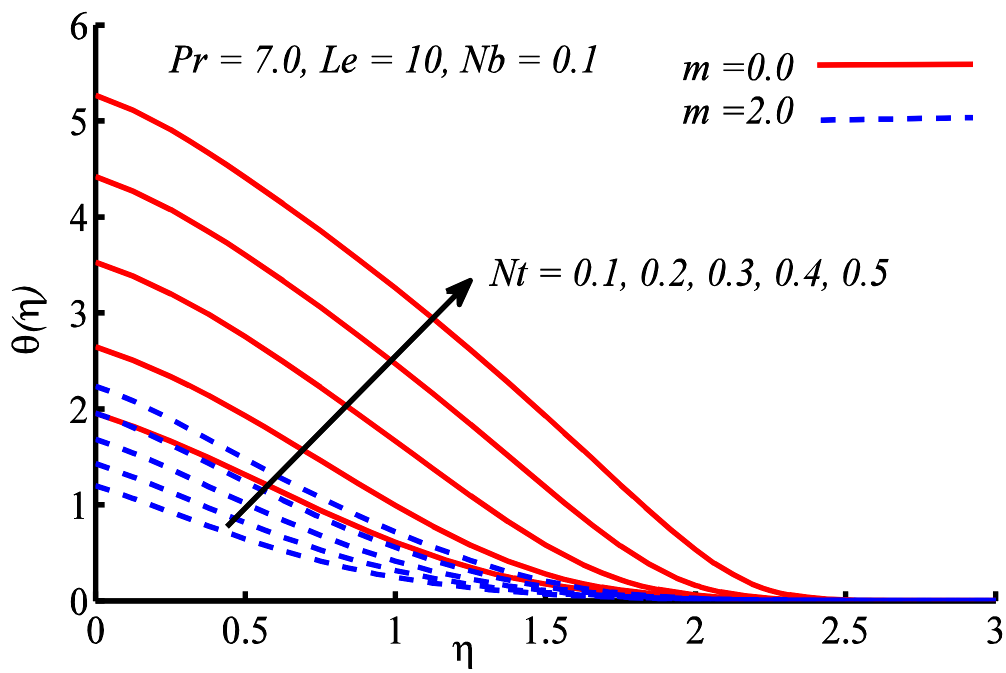


**Figure 2.15:** Temperature graph for different $Nt$.

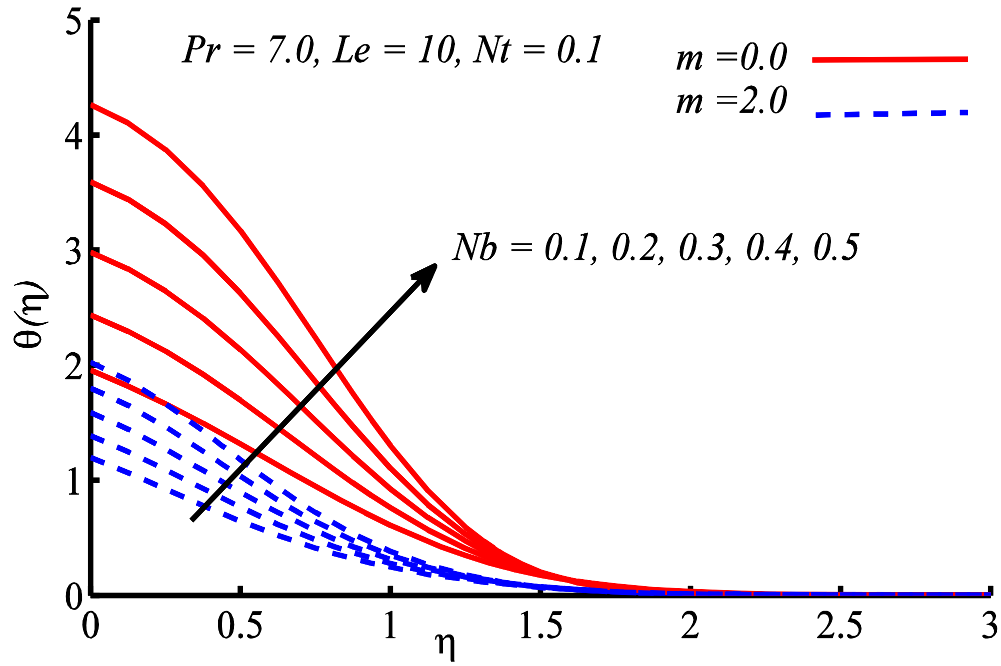


**Figure 2.16:** Temperature profile plotted for different $Nb$ and $m$.

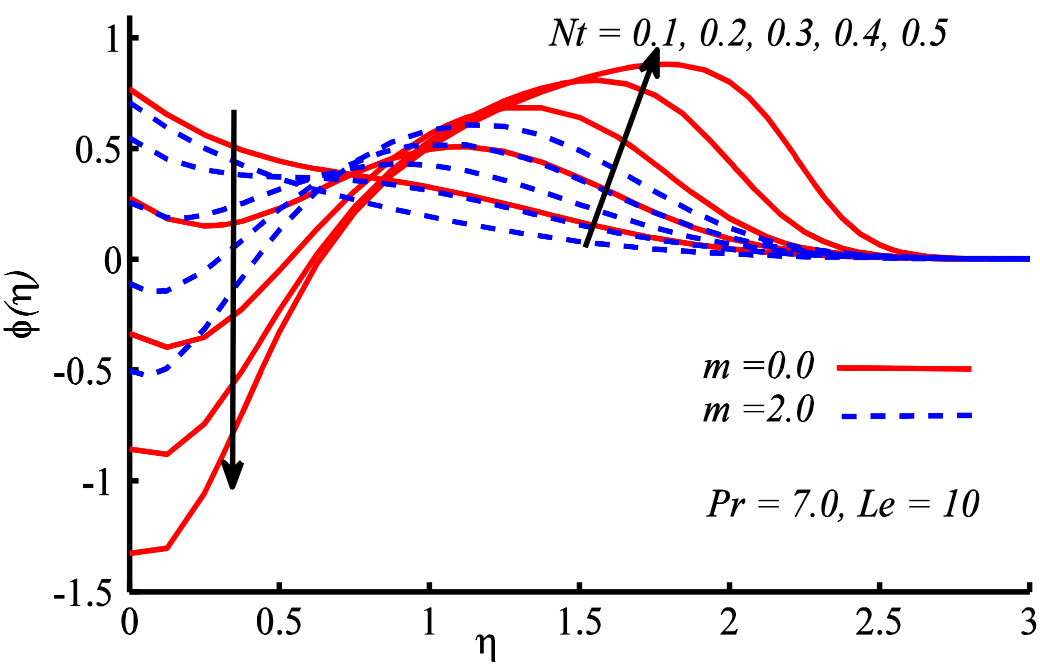


**Figure 2.17:** Effect of $Nt$ and $Nb$ on concentration distribution.

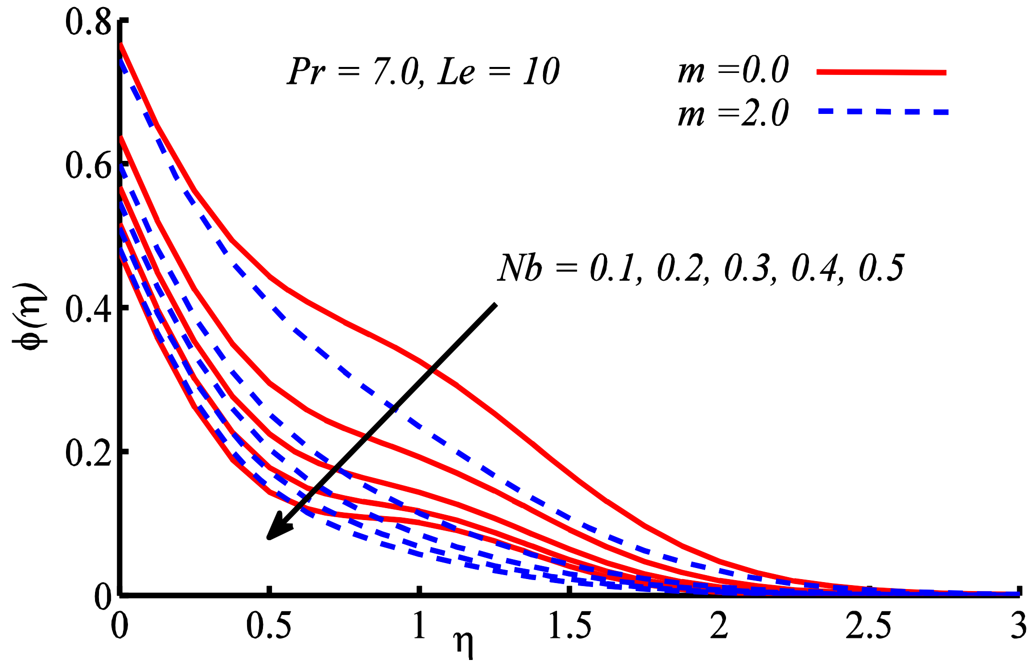


**Figure 2.18:** Variation of concentration profile for different $Nb$ and $m$ .

**Table 2.2:** $Nu$ and $Sh$ data for different $Nt$ and $Nb$ at fixed $Le = 10,$ and $Pr = 7.0$.

| $m = 0$ | | | | | | | | | | |
|---|---|---|---|---|---|---|---|---|---|---|
| $Nt$ /$Nb$ | 0.1 | | 0.2 | | 0.3 | | 0.4 | | 0.5 | |
| | $Nu$ | $Sh$ | $Nu$ | $Sh$ | $Nu$ | $Sh$ | $Nu$ | $Sh$ | $Nu$ | $Sh$ |
| 0.1 | 0.40469 | 0.9286 | 0.3207 | 1.0707 | 0.25745 | 1.2656 | 0.2098 | 1.4771 | 0.17367 | 1.6847 |
| 0.2 | 0.2636 0 | 1.0064 | 0.2071 | 1.1136 | 0.16525 | 1.2298 | 0.1341 | 1.3441 | 0.11066 | 1.4508 |
| 0.3 | 0.16513 | 1.0317 | 0.1289 | 1.1176 | 0.10207 | 1.2020 | 0.0829 | 1.2809 | 0.06827 | 1.3525 |
| 0.4 | 0.09997 | 1.0439 | 0.0777 | 11142 | 0.06164 | 1.1799 | 0.0498 | 1.2398 | 0.04093 | 1.2935 |
| 0.5 | 0.05881 | 1.0511 | 0.0456 | 1.1095 | 0.03612 | 1.1629 | 0.0291 | 1.2108 | 0.02399 | 1.2254 |
| $m = 2$ | | | | | | | | | | |
| 0.1 | 0.77394 | 1.4816 | 0.6557 | 1.6338 | 0.5622 | 1.8732 | 0.4952 | 2.1540 | 0.44027 | 2.4503 |
| 0.2 | 0.56728 | 1.6230 | 0.4848 | 1.7572 | 0.4219 | 1.9125 | 0.3734 | 2.0747 | 0.33517 | 2.2363 |
| 0.3 | 0.41380 | 1.6726 | 0.3579 | 1.7883 | 0.31525 | 1.9079 | 0.2821 | 2.0260 | 0.25592 | 2.1403 |
| 0.4 | 0.30257 | 1.6989 | 0.2654 | 1.7986 | 0.23691 | 1.8962 | 0.2146 | 1.9899 | 0.19677 | 2.0790 |
| 0.5 | 0.22322 | 1.7160 | 0.1988 | 1.8022 | 0.17990 | 1.8844 | 0.1649 | 1.9620 | 0.15286 | 2.0352 |

## 2.4 Conclusion

In this chapter, mathematical formulation has been presented for self-similar flow and heat and mass transfer in incompressible nanofluid flow over a vertical plate. Numerical procedure has been explained in detail. The cases of VWT and VHF has been discussed in detail. The effects of physical parameters like skin friction coefficient, Nusselt number and Sherwood number have been displayed graphically and discussed in detail. The main outcomes of this study are:

- Temperature enhances by strengthening the thermophoresis $Nt$ and Brownian motion $Nb$ effects.
- Nusselt number reduces by increasing $Nb$ and $Nt$ parameters.
- Sherwood number rises by incrementing $Nb$ and $Nt$ parameters.
- Sherwood number and Nusselt number enhance by increasing the power-law index.

# Chapter 3

# Self-similar natural convection flow of nanofluid past a circular cone

In continuation of the previous chapter, self-similar natural convection flow of nanofluid along a circular cone is considered here. Buongiorno transport model for nanofluid has been utilized in the development of transport equations. Using the proper similarity transformations the constitutive equations are converted to the ordinary differential equations. These equations with the boundary data are then solved numerically. Effects of thermophoresis and Brownian motion on the transport phenomena are studied thoroughly. Physical quantities such as skin friction coefficient and Nusselt number are investigated and shown graphically in the presence of heat and mass transfer phenomena. It is observed that Brownian motion and thermophoresis play a vital role in the improvement of heat and mass transfer rates. Results for friction factor and Nusselt number in the absence of thermophoresis and Brownian motion parameter are compared with the published data for pure fluid and are observed to be in good agreement.

## 3.1 Problem formulation

Consider a two-dimensional steady, natural convection, incompressible, viscous flow past a vertical circular cone. The radius of the cone is denoted by $\bar{r}$ and the internal half angle of the cone is denoted by $\gamma$. The surface of the cone is maintained at a constant temperature $T_w$ and a constant concentration $C_w$ whereas, the constant ambient temperature is symbolized by $T_\infty$ and the ambient concentration by $C_\infty$. It is further assumed that the wall values of the temperature and concentration functions are greater than the ambient values, that is $T_w > T_\infty, C_w > C_\infty$ which cause the bouncy effects. The flow is developed along the cone surface in the upward direction. The $x$ −axis is taken along the surface of the cone and the $y$ −axis is taken orthogonal to it as depicted in Fig. 3.1.

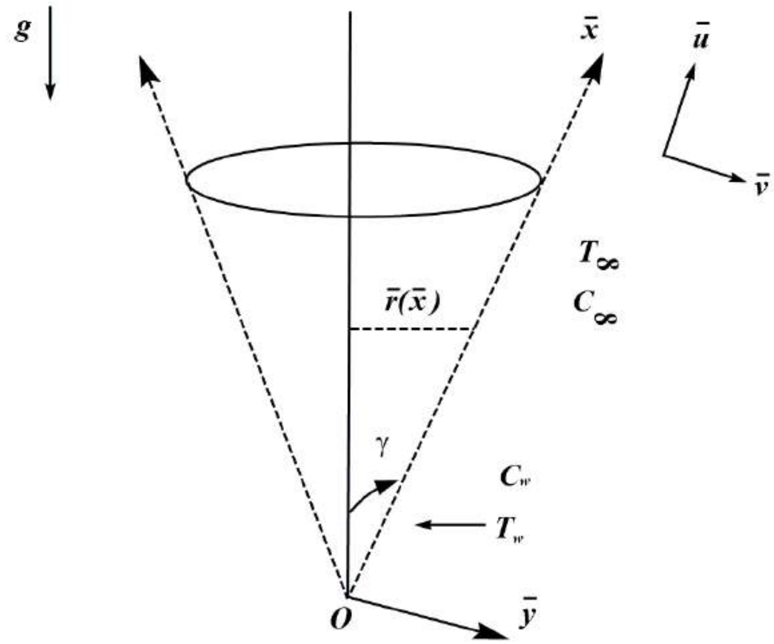


**Figure 3.1:** Cone geometry and coordinate system.

Brownian motion and the thermophoresis effects of nanoparticle are considered which are modelled due to the famous and widely acceptable Buongiorno nanofluid model. According to the Buongiorno mathematical model [31] the mass, momentum, concentration and energy conservation laws after the consideration of above assumptions, respectively read as:

$$\frac{\partial(\bar{r}\bar{u})}{\partial\bar{x}} + \frac{\partial(\bar{r}\bar{v})}{\partial\bar{y}} = 0, \tag{3.1}$$

$$\bar{u}\frac{\partial\bar{u}}{\partial\bar{x}} + \bar{v}\frac{\partial\bar{u}}{\partial\bar{y}} = \nu\ \frac{\partial^2\bar{u}}{\partial\bar{y}^2} + \boldsymbol{g}\beta(T - T_\infty), \tag{3.2}$$

$$\bar{u}\frac{\partial T}{\partial\bar{x}} + \bar{v}\frac{\partial T}{\partial\bar{y}} = {\alpha^*}_f\frac{\partial^2 T}{\partial\bar{y}^2} + \tau^*\left(\frac{D_T}{T_\infty}\left(\frac{\partial T}{\partial\bar{y}}\right)^2 + D_B\frac{\partial T}{\partial\bar{y}}\frac{\partial C}{\partial\bar{y}}\right), \tag{3.3}$$

$$\bar{u}\frac{\partial C}{\partial\bar{x}} + \bar{v}\frac{\partial C}{\partial\bar{y}} = \frac{D_T}{T_\infty}\frac{\partial^2 T}{\partial\bar{y}^2} + D_B\frac{\partial^2 T}{\partial\bar{y}^2}. \tag{3.4}$$

The local radius $\bar{r}$ of the cone body is defined by the relation $\bar{r}(\bar{x}) = \bar{x}sin\gamma$, as shown in Fig. 3.1. The appropriate boundary conditions are written as

$$\begin{gathered}\bar{y} = 0:\ \bar{u} = 0, \qquad \bar{v} = 0, \qquad C = C_w, \qquad T = T_w, \\ \bar{y} \to \infty:\ \bar{u} \to 0, \quad C \to C_\infty, \qquad T \to T_\infty\ .\end{gathered} \tag{3.5}$$

In accordance with the cone geometry which involves circular symmetry we relate the stream function with the velocity components as $\bar{r}\bar{v} = -\partial\psi/\partial\bar{x}$, $\bar{r}\bar{u} = \partial\psi/\partial\bar{y}$, which satisfy the continuity equation identically. In order to normalize the system, we utilize the suitable set of variables (see [62]), given by

$$\xi = x = \frac{\bar{x}}{l}, \qquad r = \frac{\bar{r}}{l} = \xi\, sin\gamma, \eta = \xi^{-\frac{1}{4}} \frac{\bar{y}}{l} Gr^{\frac{1}{4}}, v = \frac{\rho_f l}{\mu_f} Gr^{-\frac{1}{4}}(\bar{v}),$$

$$u = \frac{\rho_f l}{\mu_f} Gr^{-\frac{1}{2}}\, \bar{u}, Pr = \frac{\nu_f}{\alpha^*{}_f}, \ \ \varphi(\eta) = \frac{C - C_\infty}{C_w - C_\infty}, \tag{3.6}$$

$$\theta(\eta) = \frac{T - T_\infty}{T_w - T_\infty}, \qquad \psi(\eta) = \xi^{\frac{3}{4}} f(\eta),$$

which transforms the system (3.2) – (3.5) to the form

$$f''' + \frac{7}{4} f f'' - \frac{1}{2} f'^2 + \theta = 0, \tag{3.7}$$

$$\frac{1}{Pr}\theta'' + \frac{7}{4} f\theta' + Nb\theta'\varphi' + Nt\varphi'^2 = 0, \tag{3.8}$$

$$\frac{1}{Le}\left(\varphi'' + \frac{Nt}{Nb}\,\theta''\right) + \frac{7}{4} f\varphi' += 0. \tag{3.9}$$

$$\begin{gathered} f(0) = 0,\ f'(0) = 0,\ \ \varphi(0) = 1, \qquad \theta(0) = 1, \\ f'(\infty) \to 0, \qquad \varphi(\infty) \to 0, \qquad \theta(\infty) \to 0\ . \end{gathered} \tag{3.10}$$

Physical quantities are the wall shear stress, the surface heat flux and the surface mass flux which are used in the calculation of local skin friction coefficient, local Nusselt number and local Sherwood number as defined in equations (1.22), (1.25) & (1.28) respectively. Incorporating the non-dimensional transformations (3.6) the expressions for the coefficient of skin friction, the Nusselt number and the Sherwood number in dimensionless form, respectively, given by

$$\begin{gathered} C_f = C_{fx}(Gr/x)^{\frac{1}{4}} = f''(0), \qquad Nu = -Nu_x(Grx^3)^{-\frac{1}{4}} = -\theta'(0), \\ Sh = -Sh_x(Grx^3)^{-\frac{1}{4}} = -\varphi'(0), \end{gathered} \tag{3.11}$$

where $Gr$ denotes the Grashof number.

## 3.2 Numerical scheme

The self-similar equations of natural convection flow along the vertical circular cone has been solved numerically by employing the Keller-box method which has already been explained in the previous chapter. The present results of skin friction coefficient

$C_{fx}(Gr/x)^{\frac{1}{4}}$ and heat transfer rate $Nu_x(Grx^3)^{-1/4}$ have been compared with the available results of Hearing [60], Roy [61], Yih [64], Pop and Na [160-161] and Singh et al. [187] in Table 3.1. An excellent agreement is achieved, which authenticates our solution and allows for the further analysis.

**Table 3.1:** Comparison of numerical values of $f''(0,0)$ and $-\theta'(0,0)$ for $Nt = Nb = 0$.

| $Pr$ | $f''(0,0)$ | | | | | | $-\theta'(0,0)$ | | | | | |
|---|---|---|---|---|---|---|---|---|---|---|---|---|
| | present | Pop and Na [160-161] | Singh et al. [187] | Hering [60] | Roy [61] | Yih [64] | Present | Pop and Na [160-161] | Singh et al.[187] | Yih [64] | Hering [60] | Roy [61] |
| 0.0001 | 1.452616 | – | – | – | – | 1.6006 | 0.033845 | – | – | 0.0079 | – | – |
| 0.001 | 1.440436 | – | – | 1.5166 | – | 1.5135 | 0.038402 | – | – | 0.0246 | 0.0247 | – |
| 0.01 | 1.348483 | – | – | 1.3550 | – | 1.3551 | 0.075460 | 0.07493 | – | 0.0749 | 0.0748 | – |
| 0.1 | 1.095916 | – | – | 1.0960 | – | 1.0960 | 0.211345 | – | – | 0.2116 | 0.2113 | – |
| 0.7 | 0.819591 | 0.81959 | 0.81959 | – | – | – | 0.451095 | 0.45101 | 0.45109 | – | – | – |
| 1 | 0.769428 | – | – | 0.7694 | 0.8600 | 0.7699 | 0.510399 | 0.51039 | – | 0.5109 | 0.5104 | 0.5275 |
| 10 | 0.487697 | – | – | – | 0.4899 | 0.4877 | 1.033989 | 1.03397 | – | 1.0339 | – | 1.0354 |
| 100 | 0.289635 | – | – | – | 0.2897 | 0.2896 | 1.922854 | 1.92197 | – | 1.9226 | – | 1.9229 |
| 1000 | 0.166145 | – | – | – | 0.1661 | 0.1661 | 3.470171 | 3.470882 | – | 3.4696 | – | 3.4700 |
| 10000 | 0.094042 | – | – | – | 0.0940 | 0.09400 | 6.2100679 | 6.204813 | – | 6.1984 | – | 6.1998 |

## 3.3 Results and discussion

The graphical presentation of the dimensionless temperature $\theta(\eta)$, and nanoparticle concentration $\varphi(\eta)$ in addition to the local Sherwood number $Sh = -\varphi'(0)$ and local Nusselt number $Nu = -\theta'(0)$ has been made in this section. The influence of involved parameters on the graphs of above named quantities have been discussed in detail. Some numerical values of $Sh$ and $Nu$ against various values of parameters $Nb$, $Le, Nt$ and $Pr$ have been displayed in Tables 3.2 and 3.3.

Figures 3.2 and 3.3 depict the influence of $Nb$ and $Nt$ on $\theta(\eta)$ and $\varphi(\eta)$ distributions. These figures show that an increase in the values of the parameters $Nb$ and $Nt$ enhances the $\theta(\eta)$ profile whereas, $Nt$ causes to increase and $Nb$ results in a decrease in the $\varphi(\eta)$ distribution. Figures 3.4 and 3.5 illustrate the impact of $Pr$ and $Le$ on temperature and concentration profiles. Figure 3.4 shows that the temperature reduces while concentration enhances by strengthening the $Pr$. Figure 3.5 depicts that both the temperature and the concentration boundary layers reduces due to the increase in $Le$ number values where the decrease in concentration profile is more prominent as compared to temperature profile. $Nu$ and $Sh$ are plotted against $Nb$ by varying $Nt$, $Pr$ and $Le$ in Figs. 3.6 and 3.7. Figure 3.6 shows that $Nu$ decreases with the increase of $Nt$, $Pr$ and $Le$. Figure 3.7 reveals that $Sh$ rises with the increase of $Nt$, $Pr$ and $Le$ and this increase becomes linear with the increase of $Nb$ parameter whereas, this increase is more prominent in the case of $Nt$ and $Le$. This is due to the reason that an increase in $Le$ is equivalent to a decrease in Brownian diffusion, due to which $\varphi(\eta)$ profile reduces and $\varphi'(0)$ increases. Incrementing the $Pr$ values results in the reduction of thermal diffusivity, consequently $\varphi(\eta)$ distribution reduces and $\varphi'(0)$ enhances. The coefficient of skin friction $C_f$ is plotted against $Nb$ for variation of $Nt, Pr$ and $Le$ in Fig. 3.8. Figure 3.8 depicts that $C_f$ increases with the increase of $Nt$ and $Pr$ but reduces as $Le$ increases.

Tables 3.2 and 3.3 are constructed for the results of $Nu$ and $Sh$ for different values of $Nt$, $Nb, Pr$ and $Le$. Table 2.2 reveals that $Nu$ reduces with the increase of $Nt$ and $Nb$ where on the other hand $Sh$ rises with the increase of $Nt$ and $Nb$. It is further observed from Table 3.2 that $Sh$ decreases for higher values of $Nt$ and $Nb$. Table 3.3 provides numerical results for the impact of $Pr$ and $Le$ on heat transfer rate $Nu$ and mass transfer rate $Sh$. It is noted that $Nu$ is decreased and $Sh$ is increased due to an increase in $Pr$ and $Le$ values.

**Table 3.2:** $Nu$ and $Sh$ data for different $Nt$ and $Nb$ when $Le = 10, Pr = 7.0$.

| $Nt$ /$Nb$ | 0.1 | | 0.2 | | 0.3 | | 0.4 | | 0.5 | |
|---|---|---|---|---|---|---|---|---|---|---|
| | $Sh$ | $Nu$ | $Sh$ | $Nu$ | $Sh$ | $Nu$ | $Sh$ | $Nu$ | $Sh$ | $Nu$ |
| 0.1 | 1.1670 | 0.50734 | 1.3499 | 0.40194 | 1.5996 | 0.32264 | 1.8701 | 0.26289 | 2.1357 | 0.21761 |
| 0.2 | 1.2632 | 0.33067 | 1.4005 | 0.25969 | 1.5492 | 0.20718 | 1.6955 | 0.16808 | 1.8322 | 0.13876 |
| 0.3 | 1.2950 | 0.20722 | 1.4048 | 0.16176 | 1.5128 | 0.12852 | 1.6134 | 0.10396 | 1.7061 | 0.08559 |
| 0.4 | 1.3104 | 0.12550 | 1.4003 | 0.09597 | 1.4846 | 0.07733 | 1.5615 | 0.06243 | 1.6307 | 0.05133 |
| 0.5 | 1.3196 | 0.07357 | 1.3945 | 0.05730 | 1.4630 | 0.04533 | 1.5247 | 0.036558 | 1.5801 | 0.03003 |

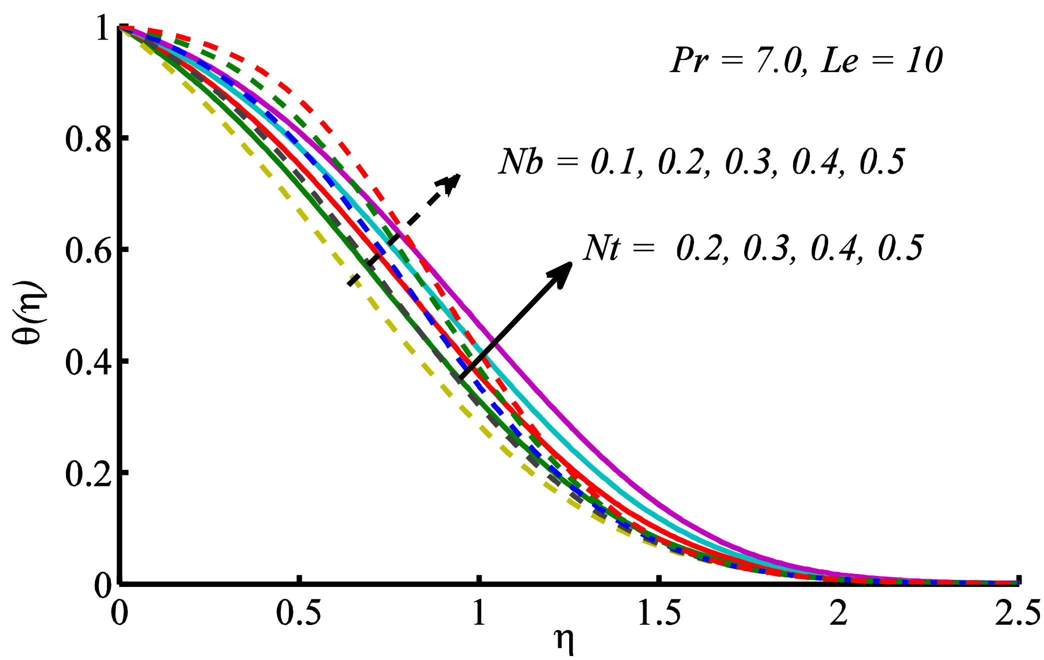


**Figure 3.2:** Influence of $Nb$ and $Nt$ on temperature distribution.

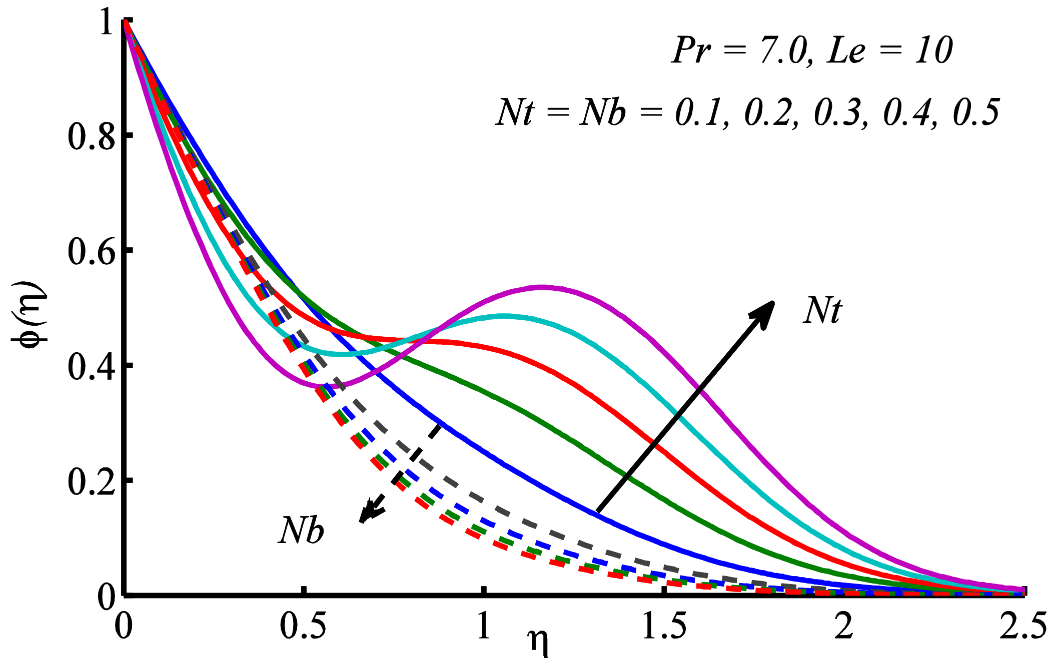


**Figure 3.3:** Concentration distribution at various $Nt$ and $Nb$ values.

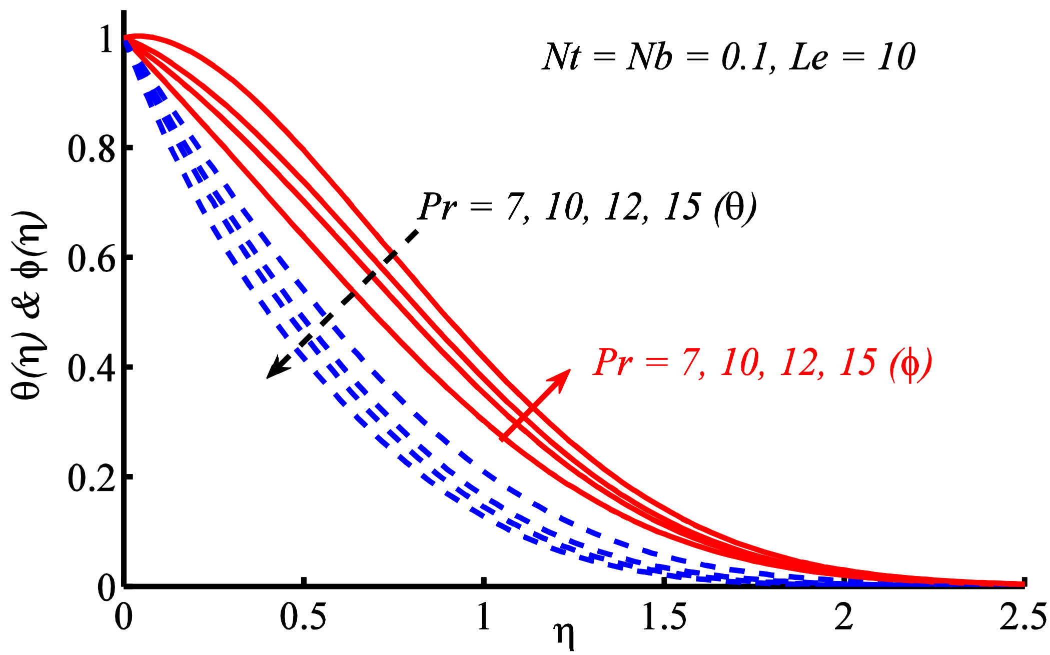


**Figure 3.4:** Influence of $Pr$ on temperature and concentration profiles.

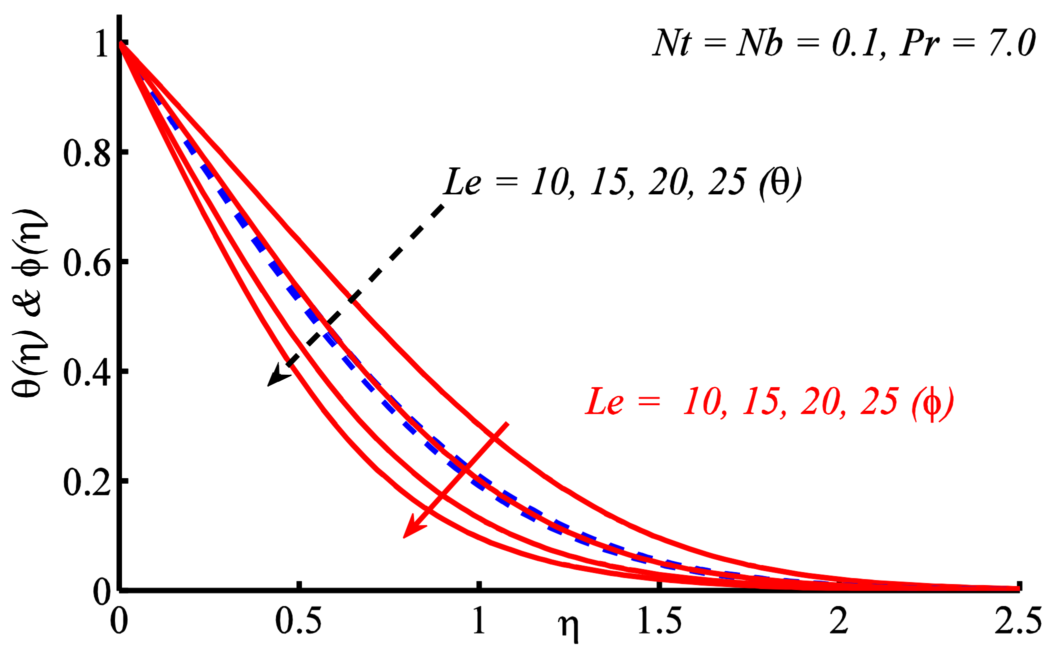


**Figure 3.5:** Variation of temperature and concentration profiles due to $Le$ .

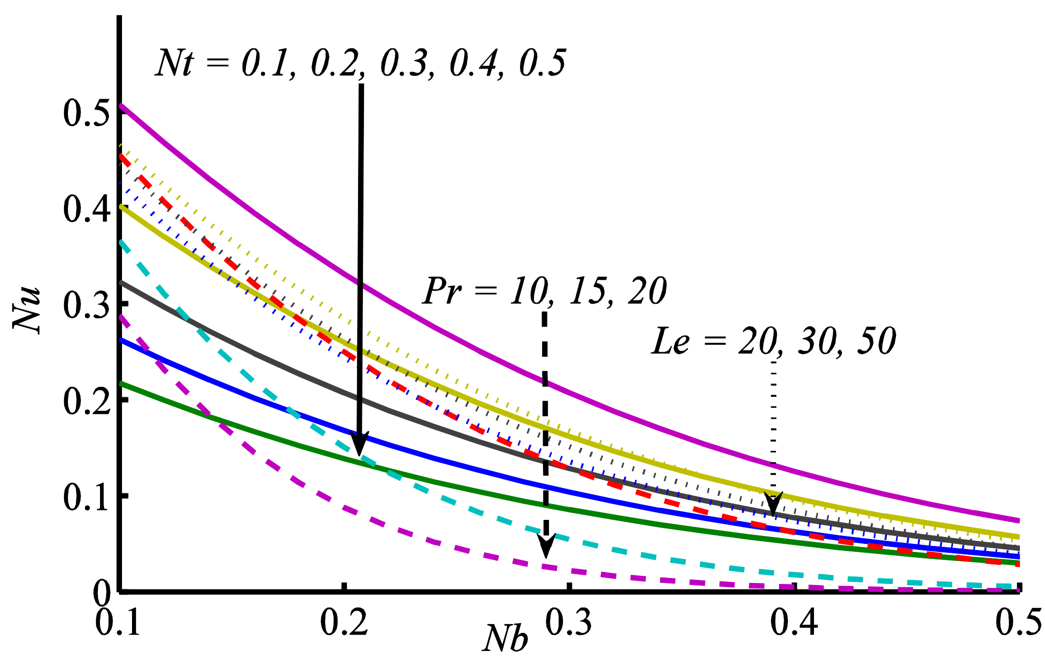


**Figure 3.6:** Plot of Nusselt number against $Nb$ for different $Nt, Pr$ and $Le$.

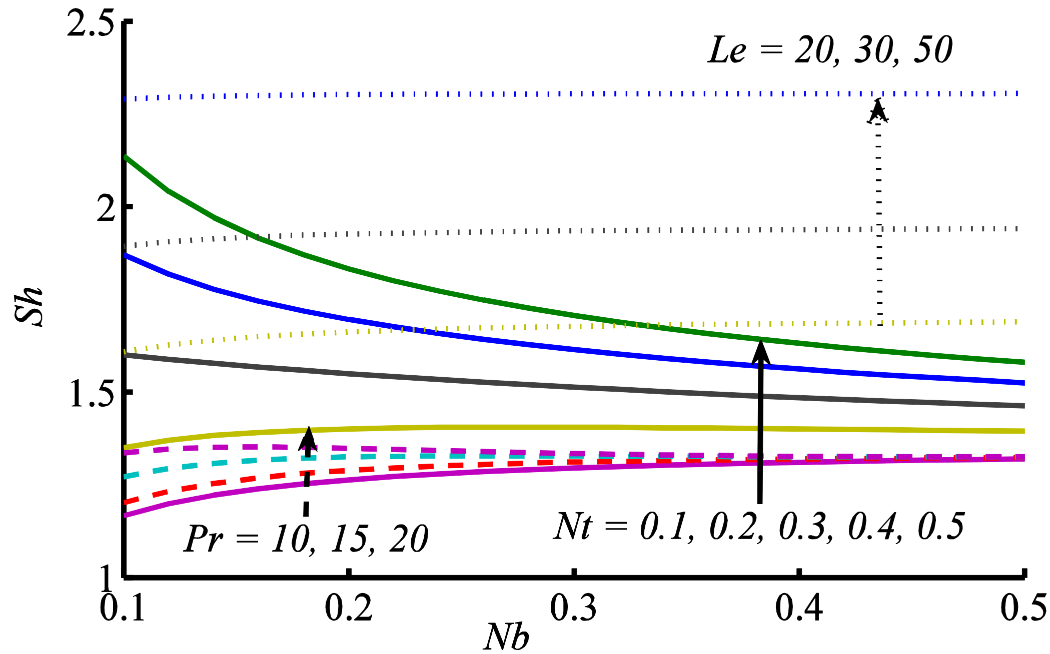


**Figure 3.7:** Sherwood number plotted against $Nb$ for different $Nt, Pr$ and $Le$.

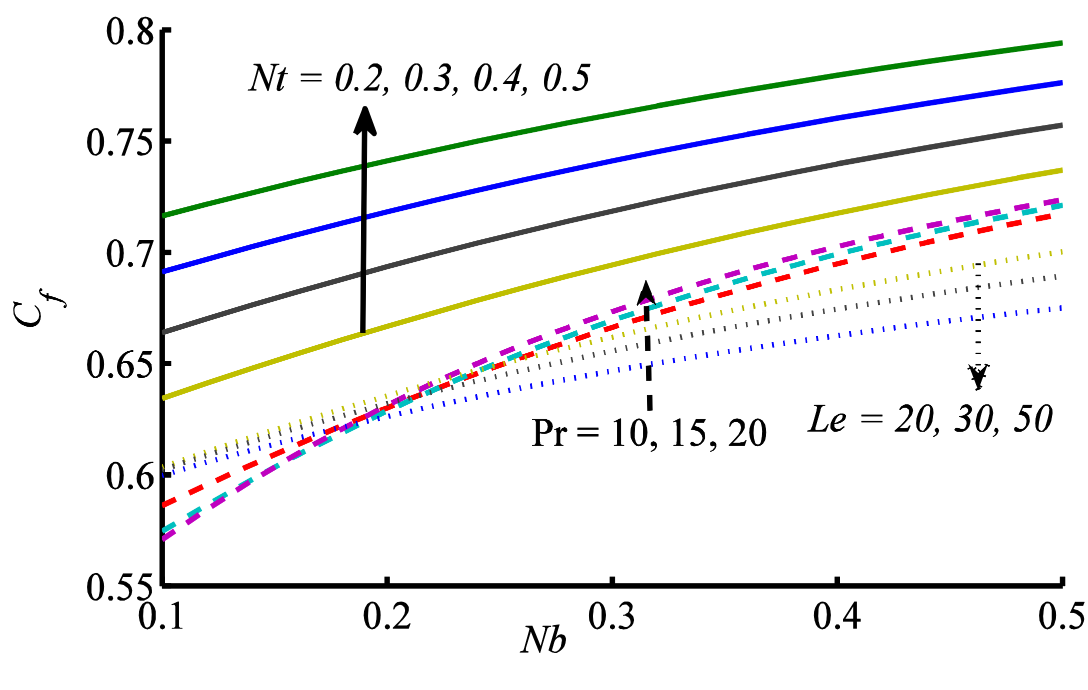


**Figure 3.8:** Skin friction coefficient plotted against $Nb$ for different $Nt, Pr$ and $Le$.

**Table 3.3:** $Nu$ and $Sh$ data for different $Pr\ and\ Le$ when $Nt = Nb = 0.1$.

| $Pr/Le$ | 7.0 | | 10.0 | | 15.0 | |
|---|---|---|---|---|---|---|
| | $Nu$ | $Sh$ | $Nu$ | $Sh$ | $Nu$ | $Sh$ |
| 10 | 0.50734 | 1.1670 | 0.45482 | 1.2020 | 0.36552 | 1.2712 |
| 20 | 0.46481 | 1.6088 | 0.39824 | 1.6747 | 0.29638 | 1.7318 |
| 30 | 0.44529 | 1.8931 | 0.37278 | 1.9401 | 0.26661 | 1.0171 |

## 3.4 Conclusion

In this chapter, natural convection flow along a vertical circular cone is investigated theoretically considering the Brownian motion and thermophoresis effects of nanoparticles. Implicit finite difference technique is used to solve the transformed ordinary differential equations together with the assumed boundary conditions. Computational outcomes are displayed for important quantities of physical nature, such as, Sherwood and Nusselt numbers. An increase in the values of Brownian motion and thermophoresis parameters result in the increase of local Sherwood number, but the decrease is observed for the Nusselt number. Further reduction in heat transfer rate is noted by increasing the values of Prandtl and Lewis numbers whereas, enhancement in the Sherwood number is observed by incrementing the Prandtl and Lewis numbers.

# Chapter 4

# Heat transfer analysis of non-similar MHD nanofluid flow along moving wavy surface

The study of heat transfer analysis in hydromagnetic boundary layer flow near the wavy rough plate is carried out in this chapter. Due to the presence of metallic nanoparticle in the fluid and the enhanced surface area of the plate, as a consequence of surface texture, an increase in heat transfer rate is expected. However, the calculation of this enhancement is not any straightforward because the convection phenomena becomes more complicated due to the motion of nanoparticle in the base fluid and also due to the waviness of the plate surface. The contribution of nanoparticle towards convective heat transfer is manifold which requires a suitable model in order to capture the correct physics. Famous Tiwari and Das model has been utilized in the current study. The wavy nature of the boundary surface makes the flow non-similar in nature. Such a non-similar flow can also be handled by the famous Keller-box scheme. For the self-similar flow the procedure has already been explained in Ch. 2 which requires certain modifications (for non-similar flows) that have been explained in the current chapter. Percent increase in the rate of heat transfer is calculated for the nanoparticle of different metals, such as $MWCNT$, $SWCNT$, $Al_2O_3, TiO_2$ and $Ag$. Appreciable increase in the rate of heat transfer is observed which is $24\%$ at the most for $Al_2O_3$ nanoparticle. The effects of applied magnetic field on the velocity profile, skin friction coefficient and Nusselt number have also been presented through graphs. Throughout this analysis the concentration of the nanoparticle has been limited up to 10%.

## 4.1 Problem formulation

Consider a non-flat wavy sheet extended in $\bar{x}-$ and $\bar{z}-$directions whose surface is described by the function defined in Eq. (1.18). The wavy surface starts from the line $x =$

0 in the $xz$ −plane and is assumed to be surrounded by the ambient nanofluid. The schematic diagram of the coordinate system and wavy plate is shown in Fig. 4.1.

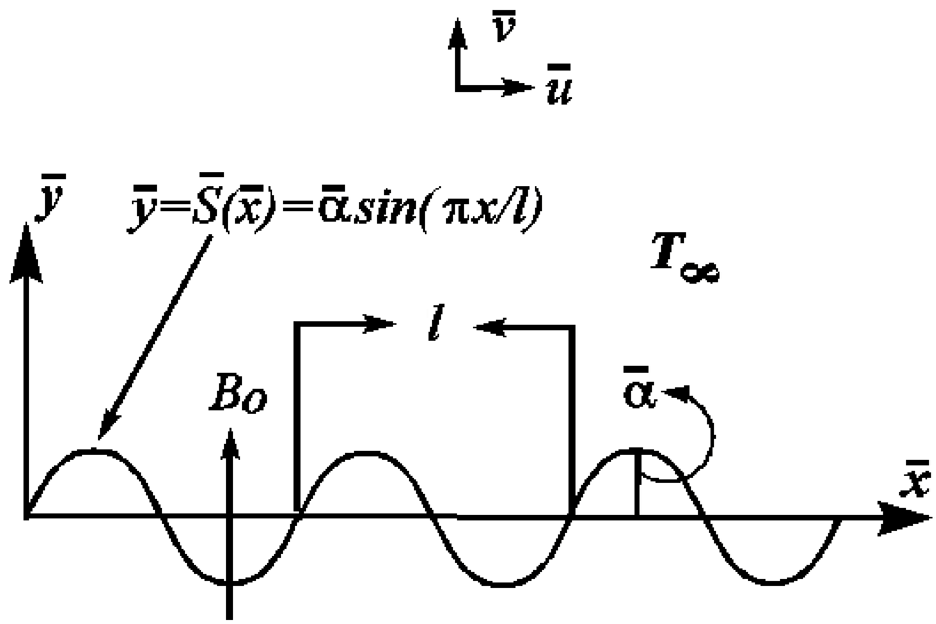


**Figure 4.1:** Physical model and coordinate system.

Because of the wavy plate surface and the location of $\bar{x}$ −axis it is reasonable to investigate the convection phenomena in the domain $\bar{y} \geq \bar{S}(\bar{x})$. Furthermore, the plate surface follows the same texture in $\bar{z}$ −direction. Therefore, the flow can be taken independent of $\bar{z}$ −axis as does for the flat plate in two-dimensional flow. Therefore the assumed flow is two-dimensional in nature and due to wavy surface of the plate the velocity varies continuously with the variable '$\bar{x}$' which makes the flow non-similar. In this way the domain of $\bar{x}$ ($\bar{x} \geq 0$) is of fundamental importance. The flow is assumed to be caused due to the uniform motion of the wavy plate in positive $\bar{x}$ −direction. Along the $\bar{y}$ −direction a uniform magnetic field of strength $B_0$ is applied and further it is assumed that the magnetic Reynolds number to be very small so that the induced magnetic field can be ignored.

The study of convective transport in nanofluid requires a suitable model that can successfully capture the contribution of nanoparticle in flow and heat transfer phenomena. The aforementioned Tiwari and Das model [32] considers the improved material properties of the nanofluid. Practically, the nanoparticles contribute during the convective phenomena in two ways: first by changing the material properties of the base fluid and secondly through their Brownian motion within the base fluid.

Since (as mentioned above) the ambient fluid is assumed to be nanofluid described by the Tiwari and Das model. According to this model the mass, momentum and energy conservation laws in vector form read as

$$\nabla.\boldsymbol{V} = 0, \tag{4.1}$$

$$(\boldsymbol{V}.\nabla)\boldsymbol{V} = -\left(1/\rho_{nf}\right)\nabla p + \nu_{nf}\nabla^{2}\boldsymbol{V} - \frac{\sigma_{nf}^{*}B_0^2}{\rho_{nf}}\boldsymbol{V}, \tag{4.2}$$

$$\boldsymbol{V}.\nabla T = \alpha^{*}{}_{nf}\nabla^2 T. \tag{4.3}$$

For two-dimensional flow the above mass, momentum and energy conservation laws in component form are written as

$$\frac{\partial\bar{u}}{\partial\bar{x}} + \frac{\partial\bar{v}}{\partial\bar{y}} = 0, \tag{4.4}$$

$$\bar{u}\frac{\partial\bar{u}}{\partial\bar{x}} + \bar{v}\frac{\partial\bar{u}}{\partial\bar{y}} = -\frac{1}{\rho_{nf}}\frac{\partial\bar{p}}{\partial\bar{x}} + \nu_{nf}\nabla^2\bar{u} - \frac{\sigma_{nf}^{*}B_0^2}{\rho_{nf}}\bar{u}, \tag{4.5}$$

$$\bar{u}\frac{\partial\bar{v}}{\partial\bar{x}} + \bar{v}\frac{\partial\bar{v}}{\partial\bar{y}} = -\frac{1}{\rho_{nf}}\frac{\partial\bar{p}}{\partial\bar{y}} + \nu_{nf}\nabla^2\bar{v}, \tag{4.6}$$

$$\bar{u}\frac{\partial T}{\partial\bar{x}} + \bar{v}\frac{\partial T}{\partial\bar{y}} = \alpha_{nf}^{*}\nabla^2 T, \tag{4.7}$$

where $\rho_{nf}$ denotes the density, $\alpha_{nf}^{*}$ the thermal diffusivity, $\sigma_{nf}^{*}$ the effective electric conductivity of the nanofluid [163] and $B_0$ the strength of uniform magnetic field. The subscripts "$f$", "$nf$" and "$p$" refer to pure fluid, nanofluid and nanoparticle, respectively. The relations for $\mu_{nf}$, $\rho_{nf}$, $\sigma_{nf}^{*}$, $\alpha_{nf}^{*}$ and $(\rho c_p)_{nf}$ are described in Sec. 1.5.

The wavy plate is assumed to be moving with uniform velocity in $\bar{x}$ −direction. Keeping in view the flow schematic and the associated coordinate system, along with the assumed flow conditions, the resultant velocities along the wavy surface and along the normal to the wavy surface are $\bar{u}\bar{t}_{\bar{y}} + \bar{v}\bar{t}_{\bar{x}}$ and $\bar{u}\bar{t}_{\bar{y}} - \bar{v}\bar{t}_{\bar{x}}$ , respectively. The appropriate boundary conditions for the velocity components and temperature function are described as (see for instance [91])

$$\bar{y} = \bar{S}(\bar{x}): \ \bar{u}\bar{t}_{\bar{y}} - \bar{v}\bar{t}_{\bar{x}} = 0, \bar{u}\bar{t}_{\bar{y}} + \bar{v}\bar{t}_{\bar{x}} = U, T = T_w, \qquad \text{for all} \quad \bar{x} > 0,$$
$$\bar{y} \to \infty: \bar{u} = \bar{v} = 0, \bar{p} = p_\infty, T = T_\infty, \quad \text{for all} \quad \bar{x} > 0, \tag{4.8a}$$

where $\hat{t} = \left(\hat{t}_x, \hat{t}_y\right) = (\frac{1}{\omega}, \frac{\bar{S}_x}{\omega})$ is unit vector tangent to the wavy surface, for further details the reader is referred to follow [91]. Since the boundary layer starts to develop at $\bar{x} > 0$, therefore at the leading edge $\bar{x} = 0$, the ambient flow conditions are assumed to be valid which are given as

$$\bar{x} = 0: \bar{p} = p_\infty, T = T_\infty \text{ , for all } \bar{y} \neq 0 \, . \tag{4.8b}$$

In this case the characteristic length is the wave length '$l$' and the reference velocity is the plate velocity $U$. All the lengths are non-dimensionalized by '$l$' and all the velocities are non-dimensionalized by the reference velocity $U$. Temperature difference $T_w - T_\infty$ is used to non-dimensionalize the temperature function. Let us introduce the following dimensionless variables:

$$x = \frac{\bar{x}}{l}, u = \frac{\bar{u}}{U}, S = \frac{\bar{S}(\bar{x})}{l}, y = \frac{\sqrt{Re}\left(\bar{y} - \bar{S}(\bar{x})\right)}{l}, v = \frac{\sqrt{Re}\left(\bar{v} - S_\xi \bar{u}\right)}{U},$$
$$\theta(\xi, \eta) = \frac{T - T_\infty}{T_w - T_\infty}, \qquad p = \frac{\bar{p}}{\rho_f U^2}, \tag{4.9}$$

due to which the equations (4.5) – (4.7) after certain manipulation, in dimensionless form read as

$$u\frac{\partial u}{\partial x} + v\frac{\partial u}{\partial y} + \frac{\omega_\xi}{\omega}u^2 = \frac{\omega^2}{d_1}\frac{\partial^2 u}{\partial y^2} - \frac{Md_4}{\omega^2 d_2}u, \tag{4.10}$$

$$u\frac{\partial \theta}{\partial x} + v\frac{\partial \theta}{\partial y} = \frac{d\omega^2}{d_3 Pr}\frac{\partial^2 \theta}{\partial y^2}. \tag{4.11}$$

In the problem under consideration, the inviscid flow field is at rest. The surface undulations are assumed to be small such that $\alpha \ll \delta$ where $\delta$ denotes the boundary layer thickness. This leads to the assumption that variations in pressure along $x$ −direction may be ignored which leads to the assumption that $\partial p/\partial x = 0$. On this basis the elimination of $\partial p/\partial y$ between (4.5) and (4.6) results in Eq. (4.10). To get the system (4.10) – (4.11) in a further convenient form, we introduce the following transformations

$$\xi = x,\ \ \psi(\xi,\eta) = \sqrt{\xi} f(\xi,\eta), \qquad \eta = \frac{y}{\omega\sqrt{\xi}},\ \ \theta = \theta(\xi,\eta), \tag{4.12}$$

where continuity equation is identically satisfied by $\psi$ the stream-function. In this way the governing equations under the boundary layer assumptions read as

$$\frac{1}{d_1} f''' + \frac{1}{2} f f'' - 2\frac{\omega_\xi}{\omega} f'^2 - \frac{M d_4 \xi}{d_2} f' = \xi \left[ f' \frac{\partial f'}{\partial \xi} - f'' \frac{\partial f}{\partial \xi} \right], \tag{4.13}$$

$$\frac{d}{d_3 Pr} \theta'' + \frac{1}{2} f\theta' = \xi \left[ f' \frac{\partial \theta}{\partial \xi} - \theta' \frac{\partial f}{\partial \xi} \right], \tag{4.14}$$

in which the variables $\eta$ and $f$ are being stretched by $\sqrt{\xi}$ in order to facilitate the numerical computations. Here $Re = Ul/\nu_f$ denotes the Reynolds number, $M = \sigma_f B_0^2/\rho_f U$ is the magnetic parameter, and $Pr$ is the Prandtl number. The subscript $\xi$ denotes derivative w. r. t $\xi$. The parameter $\omega = \sqrt{1 + S_\xi^2}$ and $\omega_\xi = d\omega/d\xi$ denotes the wavy contribution in the governing equations. The material parameters $d$ , $d_1$, $d_2$ , $d_3$, and $d_4$ are defined as (see for instance [170-173])

$$\begin{gathered} d = \frac{\kappa_{nf}}{\kappa_f},\ d_1 = \left[1 - \phi + \phi\left({}^{\rho_p}/_{\rho_f}\right)\right](1-\phi)^{2.5}, \\ d_2 = \left[1 - \phi + \phi\left({}^{\rho_p}/_{\rho_f}\right)\right], d_3 = \left[1 - \phi + \phi\left((\rho c_p)_p/(\rho c_p)_f\right)\right], \\ d_4 = 1 + \left(\frac{3\left((\sigma_p^*/\sigma_f^*) - 1\right)\phi}{\left((\sigma_p^*/\sigma_f^*) + 2\right) - \phi\left((\sigma_p^*/\sigma_f^*) - 1\right)}\right). \end{gathered} \tag{4.15}$$

In view of Eqs. (4.9) & (4.12), the boundary conditions (4.8a) (in dimensionless form) read as

$$\begin{gathered} f(\xi,0) = 0, \qquad f'(\xi,0) - \omega = 0, \qquad \theta(\xi,0) - 1 = 0, \\ f'(\xi,\infty) = 0, \qquad \theta(\xi,\infty) = 0. \end{gathered} \tag{4.16}$$

The physical quantities of interest such as the local skin friction coefficient and local Nusselt number are defined in Eqs. (1.20) and (1.23). After using Eqs. (4.9) and (4.12) in Eqs. (1.21) & (1.23), the skin friction coefficient and local Nusselt number come out of the form

$$C_f = C_{fx} Re^{\frac{1}{2}} = \frac{x^{-\frac{3}{2}}}{\omega^{\frac{3}{2}}(1-\phi)^{2.5}} f''(\xi ,0),$$
$$Nu = Nu_x Re^{-\frac{1}{2}} = -\frac{x^{\frac{1}{2}}}{\omega^{\frac{1}{2}}} d\theta'(\xi ,0), \tag{4.17}$$

respectively. Due to non-similar nature of the solution the mean values of these quantities are therefore preferred which are defined as

$$C_{f_{avg}} = \frac{1}{\mathbb{S}} \int_0^{\xi} \frac{x^{-\frac{3}{2}} \omega^{-\frac{1}{2}}}{(1-\phi)^{2.5}} f''(\xi ,0) d\xi,$$
$$Nu_{avg} = -\frac{1}{\mathbb{S}} \int_0^{\xi} d x^{\frac{1}{2}} \omega^{\frac{1}{2}} \theta'(\xi ,0) d\xi, \tag{4.18}$$

where $\mathbb{S} = \int_0^{\xi} \omega \, d\xi$ is the surface area of the wavy sheet over a unit dimension measured along the $z$ −coordinate. The average skin friction $C_{f_{avg}}$ and average Nusselt number $Nu_{avg}$ in Eq. (4.18) have been evaluated numerically.

## 4.2 Solution methodology

The governing non-similar equations (4.13) and (4.14) under the constraints (4.16) are solved by a second order finite difference scheme [178-185]. According to this procedure the partial differential equations (4.13) and (4.14) are first reduced to a system of first order differential equations as

$$f' = \mathbb{u}, \mathbb{u}' = \mathbb{v}, \theta' = \mathbb{q}. \tag{4.19}$$

In this way differential equations (4.13) and 4.14) are rewritten as

$$\frac{1}{d_1} \mathbb{v}' + \frac{1}{2} f \mathbb{v} - 2 \frac{\omega_{\xi}}{\omega} \mathbb{u}^2 - \frac{M d_4 \xi}{d_2} \mathbb{u} = \xi \left[ \mathbb{u} \frac{\partial \mathbb{u}}{\partial \xi} - \mathbb{u} \frac{\partial f}{\partial \xi} \right], \tag{4.20}$$

$$\frac{d}{d_3 Pr} \mathbb{q}' + \frac{1}{2} f \mathbb{q} = \xi \left[ \mathbb{u} \frac{\partial \theta}{\partial \xi} - \mathbb{q} \frac{\partial f}{\partial \xi} \right], \tag{4.21}$$

under the constraints

$$f(0,\xi)=0, \qquad \mathbb{u}(0,\xi)-1=0, \qquad \theta(0,\xi)-1=0,$$
$$f(\infty,\xi)=0, \quad \theta(\infty,\xi)=0. \tag{4.22}$$

The uniform net in the $(\xi,\eta)$ plane is described as

$$\eta_l=\eta_{l-1}+\Delta\eta, \eta_0=0, \eta_l=\eta_\infty, \qquad l=1,2,\dots,L-1,$$
$$\xi^n=\xi^{n-1}+\Delta\xi, \qquad \xi^0=0, \qquad n=1,2,\dots, \tag{4.23}$$

where $l$ and $n$ represents the position of grid points along $\eta$ and $\xi$-directions. The step size along $\xi$ is $\Delta\xi=k$ and along $\eta$ is, $\Delta\eta=h$.The unknown functions $f,\mathbb{u},\mathbb{v},\theta,$and $\mathbb{q}$ are replaced by the mean values and their derivatives with central differences given by

$$\frac{\partial}{\partial\xi}\left(f_l^{n-1/2}\right)=\frac{(f_l^n-f_l^{n-1})}{k}, \quad \frac{\partial}{\partial\xi}\left(f_{l-1/2}^n\right)=\frac{(f_l^n-f_{l-1}^n)}{h},$$

and

$$f_{l-1/2}^n=\frac{(f_l^n+f_{l-1}^n)}{2}, \qquad f_l^{n-1/2}=\frac{(f_l^n+f_l^{n-1})}{2}.$$

In view of the above relations, the non-linear PDE's can be read as

$$\left(\frac{1}{2hd_1}\right)(\mathbb{v}_l^n-\mathbb{v}_{l-1}^n)+\frac{1}{16}(\mathbb{v}_l^n-\mathbb{v}_{l-1}^n)(f_l^n+f_{l-1}^n)-\xi\left(\frac{\omega_\xi}{4\omega}\right)[(\mathbb{u}_l^n+\mathbb{u}_{l-1}^n)^2]$$
$$-\xi\left(\frac{Md_4}{4d_2}\right)[(\mathbb{u}_l^n+\mathbb{u}_{l-1}^n)]-\left(\frac{1}{8k}\right)\xi^{n-\frac{1}{2}} \tag{4.24}$$
$$\left\{\begin{matrix}\left(\mathbb{u}_l^n+\mathbb{u}_{j-1}^n\right)^2-(f_l^n+f_{l-1}^n)(\mathbb{v}_l^n+\mathbb{v}_{l-1}^n)\\ +(f_l^{n-1}+f_{l-1}^{n-1})(\mathbb{v}_l^n+\mathbb{v}_{l-1}^n)-(f_l^n+f_{l-1}^n)(\mathbb{v}_l^{n-1}+\mathbb{v}_{l-1}^{n-1})\end{matrix}\right\}=r_{l-\frac{1}{2}}^{n-1},$$

$$\left(\left(\frac{d}{hd_3Pr}\right)+\frac{1}{4}\left(\frac{f_l^n+f_{l-1}^n}{2}\right)\right)\left(\frac{\mathbb{q}_l^n+\mathbb{q}_{l-1}^n}{2}\right)$$
$$-\frac{\xi^{n-\frac{1}{2}}}{8k}\left[\begin{matrix}(\theta_l^n+\theta_{l-1}^n)(\mathbb{u}_l^n+\mathbb{u}_{l-1}^n+\mathbb{u}_l^{n-1}+\mathbb{u}_{l-1}^{n-1})\\ -\left((f_l^n+f_{l-1}^n)-(f_l^{n-1}+f_{l-1}^{n-1})\right)(\mathbb{q}_l^n+\mathbb{q}_{l-1}^n)\end{matrix}\right]=m_{l-\frac{1}{2}}^{n-1}, \tag{4.25}$$

$$f_l^n-f_{l-1}^n=\frac{h}{2}(\mathbb{u}_l^n+\mathbb{u}_{l-1}^n), \tag{4.26}$$

$$\mathbb{u}_l^n-\mathbb{u}_{l-1}^n=\frac{h}{2}(\mathbb{v}_l^n+\mathbb{v}_{l-1}^n), \tag{4.27}$$

$$\theta_l^n-\theta_{l-1}^n=\frac{h}{2}(\mathbb{q}_l^n+\mathbb{q}_{l-1}^n), \tag{4.28}$$

where

$$r_{l-\frac{1}{2}}^{n-1} = -\left(\frac{1}{2d_1h}\right)[(\mathbb{v}_l^{n-1} - \mathbb{v}_{l-1}^{n-1})] - \left(\frac{1}{16}\right)[(f_l^{n-1} + f_{l-1}^{n-1})(\mathbb{v}_l^{n-1} + \mathbb{v}_{l-1}^{n-1})]$$
$$+\xi\left(\frac{\sigma_\xi}{4\sigma}\right)[(\mathbb{u}_l^{n-1} + \mathbb{u}_{l-1}^{n-1})^2] + \xi\left(\frac{Md_4}{4d_2}\right)[(\mathbb{u}_l^{n-1} + \mathbb{u}_{l-1}^{n-1})] + \left(\frac{\xi^{n-\frac{1}{2}}}{8k}\right) \tag{4.29}$$
$$([-(\mathbb{u}_l^{n-1} + \mathbb{u}_{l-1}^{n-1})^2] + [(\mathbb{v}_l^{n-1} - \mathbb{v}_{l-1}^{n-1})][(f_l^{n-1} + f_{l-1}^{n-1})]),$$

$$m_{l-\frac{1}{2}}^{n-1} = \left(\frac{1}{2Prh}\right)[(\mathbb{q}_l^{n-1} - \mathbb{q}_{l-1}^{n-1})] + \left(\frac{1}{16}\right)[(f_l^{n-1} + f_{l-1}^{n-1})(\mathbb{q}_l^{n-1} + \mathbb{q}_{l-1}^{n-1})]$$
$$-\xi\left(\frac{1}{8k}\right)\begin{pmatrix}[\{-(\theta_l^{n-1} + \theta_{l-1}^{n-1})\}\{(\mathbb{u}_l^{n} + \mathbb{u}_{l-1}^{n}) + (\mathbb{u}_l^{n-1} + \mathbb{u}_{l-1}^{n-1})\}] - \\ [\{(f_l^{n} + f_{l-1}^{n}) - (f_l^{n-1} + f_{l-1}^{n-1})\}(\mathbb{q}_l^{n-1} + \mathbb{q}_{l-1}^{n-1})]\end{pmatrix}. \tag{4.30}$$

The boundary conditions (4.22) written as

$$f_0^n = 0, \mathbb{u}_0^n = 1, \theta_0^n = 1, \mathbb{u}_L^n = \theta_L^n = 0. \tag{4.31}$$

These obtained equations (4.24) and (4.25) are non-linear algebraic equations. To solve these equations, we first reduced them to linear form by using Newton's method in this scheme unknown function is replaced by sum of known $\left(f_l^{(i)}\right)$ and unknown $\left(\delta f_l^{(i)}\right)$ function such as $f_l^{i+1}$ at $(i+1)^{th}$ iterates can be written as

$$(f_l^n)^{(i+1)} = (f_l^n)^{(i)} + (\delta f_l^n)^{(i)}, \tag{4.32}$$

also other variable are replaced in the similar fashion. Further during the linearization process the $\delta f_l^{(i)^2}$ and higher order terms are neglected. Same for the case of other variables $\delta\mathbb{u}_l^{(i)}, \delta\mathbb{v}_l^{(i)}, \delta\theta_l^{(i)}, \delta\mathbb{q}_l^{(i)}, \delta\varphi_l^{(i)}$ and $\delta\mathbb{p}_l^{(i)}$, is adopted and the following system of linear algebraic equations is obtained:

$$\delta f_l^n - \delta f_{l-1}^n - \frac{\mathrm{h}}{2}(\delta\mathbb{u}_l^n + \delta\mathbb{u}_{l-1}^n) = (r_{11})_l,$$
$$(s_{11})_l\delta f_{l-1}^n + (s_{12})_l\delta f_l^n + (s_{13})_l\delta\mathbb{u}_{l-1}^n + (s_{14})_l\delta\mathbb{u}_l^n + (s_{15})_l\delta\mathbb{q}_{l-1}^n + (s_{16})_l\delta\mathbb{q}_l^n$$
$$= (r_{12})_l,$$
$$(s_{21})_l\delta\theta_{l-1}^n + (s_{22})_l\delta\theta_l^n + (s_{23})_l\delta\mathbb{q}_{l-1}^n + (s_{24})_l\delta\mathbb{q}_l^n = (r_{13})_l,$$
$$\delta\mathbb{u}_l^n - \delta\mathbb{u}_{l-1}^n - \frac{h}{2}(\delta\mathbb{v}_l^n + \delta\mathbb{v}_{l-1}^n) = (r_{14})_l,$$
$$\delta\theta_l^n - \delta\theta_{l-1}^n - \frac{h}{2}(\delta\mathbb{q}_l^n + \delta\mathbb{q}_{l-1}^n) = (r_{15})_l,$$

where the boundary conditions (4.31) written as

$$\delta f_0^n = 0, \delta \mathbb{u}_0^n = 1, \delta \theta_0^n = 1, \delta \mathbb{u}_L^n = \delta \theta_L^n = 0.$$

The obtained linear algebraic system under the given constraints is written in matrix form. The non-homogeneous part and coefficient matrix containing the coefficients of $\delta f_{l-1}, \delta \mathbb{u}_{l-1}, \delta \mathbb{v}_{l-1}, \delta \theta_{l-1}, \delta \mathbb{q}_{l-1}, \delta \varphi_{l-1}$ and $\delta \mathbb{p}_{l-1}$ are written as

**Coefficients of momentum equation**

Coefficient of $\delta f_{l-1}^n$:

$$(s_{11})_l = \frac{1}{16}(\mathbb{v}_l^n + \mathbb{v}_{l-1}^n) + \frac{\xi^{n-\frac{1}{2}}}{8\mathrm{k}}[(\mathbb{v}_l^n + \mathbb{v}_{l-1}^n) + (\mathbb{v}_l^{n-1} + \mathbb{v}_{l-1}^{n-1})],$$

Coefficient of $\delta f_l^n$:

$$(s_{12})_l = \frac{1}{16}(\mathbb{v}_l^n + \mathbb{v}_{l-1}^n) + \frac{\xi^{n-\frac{1}{2}}}{8\mathrm{k}}[(\mathbb{v}_l^n + \mathbb{v}_{l-1}^n) + (\mathbb{v}_l^{n-1} + \mathbb{v}_{l-1}^{n-1})],$$

Coefficient of $\delta \mathbb{u}_{l-1}^n$:

$$(s_{13})_l = -\xi \frac{\sigma_\xi}{2\sigma}(\mathbb{u}_l^n + \mathbb{u}_{l-1}^n) - \frac{\xi^{n-\frac{1}{2}}}{4\mathrm{k}}(\mathbb{u}_l^n + \mathbb{u}_{l-1}^n),$$

Coefficient of $\delta \mathbb{u}_l^n$:

$$(s_{14})_l = -\xi \frac{\sigma_\xi}{2\sigma}(\mathbb{u}_l^n + \mathbb{u}_{l-1}^n) - \frac{\xi^{n-\frac{1}{2}}}{4\mathrm{k}}(\mathbb{u}_l^n + \mathbb{u}_{l-1}^n),$$

Coefficient of $\delta \mathbb{v}_{l-1}^n$:

$$(s_{15})_l = -\left(\frac{1}{2d_1 h}\right) + \frac{(f_l^n + f_{l-1}^n)}{8} + \xi^{n-\frac{1}{2}}\frac{[(f_l^n + f_{l-1}^n) + (f_l^{n-1} + f_{l-1}^{n-1})]}{8\mathrm{k}},$$

Coefficient of $\delta \mathbb{v}_l^n$:

$$(s_{16})_l = \left(\frac{1}{2d_1 h}\right) + \frac{(f_l^n + f_{l-1}^n)}{8} + \xi^{n-\frac{1}{2}}\frac{[(f_l^n + f_{l-1}^n) + (f_l^{n-1} + f_{l-1}^{n-1})]}{8\mathrm{k}},$$

**Coefficients of energy equation**

Coefficient of $\delta \theta_{l-1}^n$:

$$(s_{21})_l = -\xi^{n-\frac{1}{2}}\frac{[\mathbb{u}_l^n + \mathbb{u}_{l-1}^n + \mathbb{u}_l^{n-1} + \mathbb{u}_{l-1}^{n-1}]}{8\mathrm{k}},$$

Coefficient of $\delta \theta_l^n$:

$$(s_{22})_l = -\xi^{n-\frac{1}{2}}\frac{[\mathbb{u}_l^n + \mathbb{u}_{l-1}^n + \mathbb{u}_l^{n-1} + \mathbb{u}_{l-1}^{n-1}]}{8\mathrm{k}},$$

Coefficient of $\delta\mathbb{q}_{l-1}^{n}$:

$$(s_{23})_l = -\left(\frac{1}{2Prh}\right) + \frac{(f_l^n + f_{l-1}^n)}{16} + \xi^{n-\frac{1}{2}}\frac{[(f_l^n + f_{l-1}^n) - (f_l^{n-1} + f_{l-1}^{n-1})]}{8\mathrm{k}},$$

Coefficient of $\delta\mathbb{q}_{l}^{n}$:

$$(s_{24})_l = \left(\frac{1}{2Prh}\right) + \frac{1}{16}(f_l^n + f_{l-1}^n) + \xi^{n-\frac{1}{2}}\frac{[(f_l^n + f_{l-1}^n) - (f_l^{n-1} + f_{l-1}^{n-1})]}{8\mathrm{k}},$$

**The non-homogeneous terms**

$$(r_{11})_{\boldsymbol{l}} = (f_{l-1}^n - f_l^n) + \frac{\mathrm{h}}{2}\,(\mathbb{u}_l^n + \mathbb{u}_{l-1}^n),$$

$$(r_{12})_{\boldsymbol{l}} = r_{l-\frac{1}{2}}^{n-1} = -\left(\frac{1}{2d_1h}\right)[(\mathbb{v}_l^n - \mathbb{v}_{l-1}^n) + (\mathbb{v}_l^{n-1} - \mathbb{v}_{l-1}^{n-1})] - \left(\frac{1}{16}\right) +$$

$$[(f_l^n + f_{l-1}^n)(\mathbb{v}_l^n + \mathbb{v}_{l-1}^n) + (f_l^{n-1} + f_{l-1}^{n-1})(\mathbb{v}_l^{n-1} + \mathbb{v}_{l-1}^{n-1})]$$

$$+\xi\left(\frac{\omega_\xi}{4\omega}\right)[(\mathbb{u}_l^n + \mathbb{u}_{l-1}^n)^2 + (\mathbb{u}_l^{n-1} + \mathbb{u}_{l-1}^{n-1})^2] +$$

$$\xi\left(\frac{Md_4}{4d_2}\right)[(\mathbb{u}_l^n + \mathbb{u}_{l-1}^n) + (\mathbb{u}_l^{n-1} + \mathbb{u}_{l-1}^{n-1})]$$

$$+\xi\left(\frac{1}{8k}\right)\left(\begin{array}{c}[(\mathbb{u}_l^n + \mathbb{u}_{l-1}^n)^2 + (\mathbb{u}_l^{n-1} + \mathbb{u}_{l-1}^{n-1})^2] + \\ [(\mathbb{v}_l^n - \mathbb{v}_{l-1}^n) + (\mathbb{v}_l^{n-1} - \mathbb{v}_{l-1}^{n-1})][(f_l^n + f_{l-1}^n) - (f_l^{n-1} + f_{l-1}^{n-1})]\end{array}\right),$$

$$(r_{13})_{\boldsymbol{l}} = -\left(\frac{1}{2Prh}\right)[\{(\mathbb{q}_l^n - \mathbb{q}_{l-1}^n) + (\mathbb{q}_l^{n-1} - \mathbb{q}_{l-1}^{n-1})] - \left(\frac{1}{16}\right) +$$

$$[(f_l^n + f_{l-1}^n)(\mathbb{q}_l^n + \mathbb{q}_{l-1}^n) + (f_l^{n-1} + f_{l-1}^{n-1})(\mathbb{q}_l^{n-1} + \mathbb{q}_{l-1}^{n-1})]$$

$$+\xi\left(\frac{1}{8k}\right)([\{(\mathbb{u}_l^n + \mathbb{u}_{l-1}^n) + (\mathbb{u}_l^{n-1} + \mathbb{u}_{l-1}^{n-1})\} * \{(T_l^n + T_{l-1}^n) - (T_l^{n-1} + T_{l-1}^{n-1})\}]$$

$$-[\{(f_l^n + f_{l-1}^n) - (f_l^{n-1} + f_{l-1}^{n-1})\}\{(\mathbb{q}_l^n + \mathbb{q}_{l-1}^n) + (\mathbb{q}_l^{n-1} + \mathbb{q}_{l-1}^{n-1})\}]).$$

The whole system can simply be written in matrix form, as

$$\bar{A}\bar{\delta} = \bar{r}, \tag{4.33}$$

where

$$\bar{A} = \begin{bmatrix} C_0 & D_0 & & & & & & \\ B_1 & C_1 & D_1 & & & & & \\ & B_2 & C_2 & D_2 & & & & \\ & & \ddots & \ddots & \ddots & & & \\ & & & \ddots & \ddots & \ddots & & \\ & & & & \ddots & \ddots & \ddots & \\ & & & & & B_{L-1} & C_{L-1} & D_{L-1} \\ & & & & & & B_L & C_L \end{bmatrix}, \bar{\delta} = \begin{bmatrix} \delta_0 \\ \delta_1 \\ \delta_2 \\ \vdots \\ \vdots \\ \vdots \\ \delta_{L-1} \\ \delta_L \end{bmatrix}, \bar{r} = \begin{bmatrix} r_0 \\ r_1 \\ r_2 \\ \vdots \\ \vdots \\ \vdots \\ r_{L-1} \\ r_L \end{bmatrix}, \qquad (4.34)$$

and

$$C_0 = \begin{bmatrix} 1 & & & & \\ 0 & 1 & & & \\ 0 & 0 & 0 & & \\ & -1 & -h/2 & 0 & \\ & & 0 & -1 & -h/2 \end{bmatrix}, D_j = \begin{bmatrix} 0 & & & & \\ 0 & 0 & & & \\ 0 & 0 & 0 & & \\ & 1 & -h/2 & 0 & \\ & & 0 & 1 & -h/2 \end{bmatrix};$$

$$l = 0,1,..L-1,$$

$$B_l = \begin{bmatrix} -1 & -h/2 & 0 & 0 & 0 \\ (s_{11})_l & (s_{13})_l & (s_{15})_l & 0 & 0 \\ 0 & 0 & 0 & (s_{21})_l & (s_{23})_l \\ & & & & \\ & & & & \end{bmatrix}; \quad l = 1,2, \dots L,$$

$$C_j = \begin{bmatrix} 1 & -h/2 & 0 & & \\ (s_{12})_l & (s_{14})_l & (s_{16})_l & 0 & 0 \\ 0 & 0 & 0 & (s_{22})_l & (s_{24})_l \\ & -1 & -h/2 & 0 & 0 \\ & & & -1 & -h/2 \end{bmatrix}; \; l = 1,2, \dots L-1,$$

$$C_J = \begin{bmatrix} 1 & -h/2 & 0 & & \\ (s_{12})_l & (s_{14})_l & (s_{16})_l & 0 & \\ 0 & 0 & 0 & (s_{22})_l & (s_{24})_l \\ & 1 & 0 & 0 & 0 \\ & & 0 & 1 & 0 \end{bmatrix},$$

$$r_0 = \begin{bmatrix} 0 \\ 0 \\ 0 \\ (r_{14})_1 \\ (r_{15})_1 \end{bmatrix}, r_j = \begin{bmatrix} (r_{11})_l \\ (r_{12})_l \\ (r_{13})_l \\ (r_{14})_{l+1} \\ (r_{15})_{l+1} \end{bmatrix}, r_J = \begin{bmatrix} (r_{11})_L \\ (r_{12})_L \\ (r_{13})_L \\ 0 \\ 0 \end{bmatrix},$$

$$\delta_j = \begin{bmatrix} \delta f_l^n \\ \delta \mathbb{u}_l^n \\ \delta \mathbb{v}_l^n \\ \delta \theta_l^n \\ \delta \mathbb{q}_l^n \end{bmatrix}; l = 0,1,2, \dots, L; n = 0,1, \dots, N.$$

The obtained coefficient matrix is tri-diagonal which is solved by block tri-diagonal algorithm, using forward and the backward sweep. The grid independence of the present numerical solution has also been verified by making several runs for different step sizes of $\eta$ and $\xi$. It is observed that the numerical solution does not change when $\Delta\eta < 0.005$ and $\Delta\xi < 0.005$. Finally, the present solution has been calculated by choosing $\Delta\eta = 0.005$ and $\Delta\xi = 0.005$. Table 4.1 contains a grid independent test for the present problem.

In order to investigate the accuracy and validity of the present results, a comparison with the data available in literature has been made. It is clear from Table 4.2 that the numerical values of the skin friction coefficient $C_f$ and local Nusselt number $Nu$ for $Pr = 0.7$ (with $M = \alpha = 0.0$) are in excellent agreement with the result published by Rees and Pop [90] and Hossain and Pop [91]. Another comparison of the present results for the values of $f''(\xi, 0)$ with those published by Chaim [189] is given in Table 4.3. Again an excellent agreement is observed which authenticates the present numerical procedure.

**Table 4.1:** Gird independence test for pure fluid ($\phi = 0.0$) when $\alpha = 0.2, M = 0.5$.

| No of grid points in $\eta$ direction and $\eta_\infty = 15$. | No of grid points in $\xi$ −direction and $\xi = 2$. | $-C_f$ | $Nu$ |
|---|---|---|---|
| 100 | 10 | 0.60881 | 1.7097 |
| 300 | 20 | 0.54728 | 1.7150 |
| 600 | 50 | 0.51177 | 1.7193 |
| 1000 | 100 | 0.50023 | 1.7205 |
| 1500 | 200 | 0.49450 | 1.7212 |
| 2000 | 400 | 0.49461 | 1.7215 |
| 3000 | 400 | 0.49461 | 1.7215 |

**Table 4.2:**.Comparison of $C_f$ and $Nu$ with already published data when $Pr = 0.7, M = \alpha = 0.0$.

| | Present | Rees and Pop [90] | Hossain and Pop [91] |
|---|---|---|---|
| $C_f$ | $-0.44375$ | $-0.4438$ | $-0.4439$ |
| $Nu$ | $-0.34924$ | $-0.3492$ | $-0.3509$ |

**Table 4.3:** Comparison of $f''(\xi, 0)$ when $Pr = 0.7, M = 0.5,\ \alpha = 0.0$.

| | Present | Chaim [189] |
|---|---|---|
| $\xi$ | $f''(\xi, 0)$ | $f''(\xi, 0)$ |
| 0.0 | $-0.443748$ | $-0.343751$ |
| 0.1 | $-0.478389$ | $-0.47696$ |
| 0.5 | $-0.605687$ | $-0.604488$ |
| 1.0 | $-0.751703$ | $-0.752938$ |

## 4.3 Results and discussion

In most of the part of this section we take $Pr = 7.0,\ M = 0.5,\ \alpha = 0.2,$ and $\phi = 0.1$, otherwise mentioned. In graphical representations, solid lines correspond to the solution at $\xi = 0.5$ (crest), broken lines at $\xi = 1.0$ (node), and the dotted lines at $\xi = 1.5$ (trough). It is observed that these quantities vary periodically in the direction of $\xi$ when $\alpha \neq 0$ (wavy surface) and wavy effects become more pronounced when the values of $\alpha$ are increased.

Velocity graphs are plotted in Figs. 4.2 and 4.3 against $\eta$ for different values of $M$ and $\alpha$, respectively. Figure 4.2 shows that velocity decreases by increasing the magnetic field strength which in turns reduces the boundary layer thickness. This is a well-known effect of the magnetic field on the boundary layer flow. Due to the reason that the applied magnetic field generates the Lorentz force which acts as a retarding force due to which the momentum boundary layer thickness decrease. Figure 4.2 also depicts that the velocity is maximum at the crest and minimum at trough. Figure 4.3 highlights the impact of amplitude to wavelength ratio parameter $\alpha$ on velocity profile at crest; node and trough locations on the wavy surface. Clearly, the velocity increases by increasing the values of $\alpha$ which highlights the role of surface undulation height towards enhanced convective phenomena. The velocity character at different values of $\xi$ is the same as it was in previous Fig. 4.2. The effect of $\alpha$ on temperature profile is shown in Fig. 4.4. It is seen that the variation in $\alpha$ does not bring significant change in the temperature profile, however, the temperature is observed to be minimum at crest and maximum at the node. This is because of the slow convection in the trough region as depicted in Fig. 4.2. The effect of concentration parameter $\phi$ on velocity and temperature profiles is shown in Figs. 4.5 and 4.6, respectively. Clearly, by increasing the concentration of nanoparticle the velocity decreases and temperature increases. This is an obvious consequence of the enhanced gravity of the nanofluid because of the increased density. The $C_f$ and $Nu$ are plotted in Figs. 4.7 and 4.8 respectively at different amplitude $(\alpha)$ . It judged that at different amplitude $(\alpha)$, $Nu$ decreases and $C_f$ increases. This fact can simply be understood from Figs. 4.3 and 4.4 where the velocity and temperature increases by increasing the values of $\alpha$. It is seen that at crest position the velocity is maximum and at trough it is minimum. The current analysis has been carried out for five different types of nanoparticles, namely, alumina ( $Al_2O_3$), silver ( $Ag$), single wall carbon nanotube ( $SWCNT$), multiple wall carbon nanotube ($MWCNT$) and titanium oxide ($TiO_2$). Table 1.2 shows the thermophysical properties of water and the chosen five elements $MWCNT$, $SWCNT, Al_2O_3, TiO_2\ Ag$. The Prandtl number of the base fluid (water) is taken as 7.0. This analysis aims to investigate the effects of different nanoparticle on $C_f$ and $Nu$ on a continuous moving wavy surface in a quiescent electrically conducting fluid with a constant transverse magnetic field. To compare the $C_f$ and $Nu$ for different nanoparticles, base liquid is considered to be water. It is worth mentioning that this study reduces the governing equations (4.8) – (4.9) to those of a viscous or regular fluid when $\phi = 0$. The $C_f$ and $Nu$ are plotted against the solid volume fraction $\phi$ and wavy amplitude $\alpha$ for different type of nanoparticles ($MWCNT,\ SWCNT,\ Al_2O_3,\ TiO_2,\ Ag$) in Figs. 4.9 – 4.12. The effect of solid volume fraction $\phi$ and wavy amplitude $\alpha$ on the $C_f$ are shown in Figs. 4.9 and 4.10. Clearly, the $C_f$ decreases by increasing $\phi$ and increases for increasing values of $\alpha$, in both cases the magnitude of $C_f$ is maximum for $Ag$ and minimum for $MWCNT$. The effect of solid volume fraction $\phi$ and wavy amplitude $\alpha$ on the $Nu$ are shown in Figs. 4.11 and 4.12. In both cases $Nu$ is maximum for $Al_2O_3$ and minimum for $SWCNT$ having increasing behavior against the solid volume fraction $\phi$, but opposite behavior against wavy amplitude $\alpha$. It is worth mentioning that according to Eq. (4.15) the $Nu$ is a product of the temperature gradient and the thermal conductivity ratio. Increasing $\phi$ leads to an increase in the thermal conductivity ratio which in turn increases the Nusselt number . Figure 4.12 depicts that the $Nu$ decrease by increasing the parameter $\alpha$, reason behind this is the increase of temperature due to increase of amplitude ($\alpha$). Stream lines and isotherms are plotted in Figs. 4.13 and 4.14, respectively. The wavy pattern can easily be seen in the stream lines and the isotherm graphs.

Numerical values of $C_f$ and $Nu$ for different values of $\alpha$ and $\phi$ when $Pr = 7.0, M = 0.5$ for alumina ( $Al_2O_3$) on the wavy surface at $x = 0.5, x = 1.0$ and $x = 1.5$ are presented in Table 4.4. It is observed that the $Nu$ decreases with the increase of $\alpha$ and increases with the increase of $\phi$, on the other hand opposite behavior is seen in the case of $C_f$.

Percent increase in the magnitude of the $C_f$ and $Nu$ is calculated in Table 4.5 at three different locations: crest, node and trough on the wavy surface. It is observed that at crest the $C_f$ increases by increasing the wavy amplitude at fixed concentration of nanoparticle whereas the $Nu$ decreases. Similarly for a fixed value of $\alpha$ the $C_f$ increases by increasing the nanoparticle concentration, the behavior of $Nu$ is little bit reverse as it can be seen from Table 4.5. The similar behavior is followed by the $C_f$ and $Nu$ at the node and trough locations, however with different numerical values. The nature of nanoparticle has fundamental role in enhancing the convective heat transfer phenomena. Table 4.6 shows percent change in $C_f$ and $Nu$ for different nanoparticle ($MWCNT$, $SWCNT, Al_2O_3, TiO_2$ $Ag$) when $Pr = 7.0, M = 0.5, \alpha = 0.2, \phi = 0.1$ , in comparison to the cases of pure fluid flow past a flat plate and the pure fluid flow past a wavy plate pure flat and wavy plate. It is observed that maximum increase of about 47.3% in magnitude of $C_f$ is obtained for $Ag$ with 10% concentration in the base fluid and minimum increase of about 27.2% in the value of $C_f$ is obtained for $SWCNT$ with 10% concentration when the present results are compared with the value $f''(0.5,0) = 0.87458$ at $\alpha = 0.2$ and $\phi = 0.0$. On the other hand maximum gain of 10.8% in $Nu$ is obtained for $Al_2O_3$ and minimum of 8.1% for $Ag$ with 10% concentration in the base fluid when the present results are compared with $Nu = 0.90201$ at $\alpha = 0.2$ and $\phi = 0.0$. The percent increase in magnitude of $C_f$ and $Nu$ is also calculated in comparison to $f''(0) = 0.8539$ and $Nu = 0.9531$ at $\alpha = 0.0$ and $\phi = 0.0$. A maximum of 50.8% and 4.8% increase in $C_f$ and $Nu$ is obtained and a minimum of 27.6% and 2.3% increase in $C_f$ and $Nu$ is obtained, respectively. Through this Table it is easy to identify the role of surface roughness and of nanofluid towards heat transfer enhancement. This study reveals that $Al_2O_3$ nanoparticle have the capacity to produce a coolant (nanofluid) with higher rate of heat transfer.

Numerical values of magnitude of ${C_f}_{avg}$ and $Nu_{avg}$ for different nanoparticle ($MWCNT$, $SWCNT, Al_2O_3, TiO_2\ \ Ag$) when $Pr = 7.0, M = 0.5, \alpha = 0.2, \phi = 0.1$ are tabulated in Tables 4.7 and 4.8. It is observed that the $Nu_{avg}$ and magnitude of ${C_f}_{avg}$ increases with the increase of number of waves $n$.

Table 4.9 shows percent change in magnitude of ${C_f}_{avg}$ for different nanoparticle ($MWCNT,\ SWCNT, Al_2O_3, TiO_2\ \ Ag$) when $Pr = 7.0, M = 0.5, \alpha = 0.2, \phi = 0.1$, in comparison to the cases of pure fluid flow past a flat plate and the pure fluid flow past a wavy plate. It is observed that maximum increase of about 51.9% in magnitude of ${C_f}_{avg}$ is obtained for $Ag$ with 10% concentration in the base fluid and minimum increase of about 17.48% in the value of ${C_f}_{avg}$ is obtained for $MWCNT$ with 10% concentration when the present results are compared with the value ${C_f}_{avg} = 0.69938$ at $\alpha = 0.2$ and $\phi = 0.0$ for one wave length. It is also noted that percentage in decrease in ${C_f}_{avg}$ remains almost the same by increasing number of waves. On the other hand maximum reduction of 151.27% in ${C_f}_{avg}$ is obtained for $Ag$ and minimum of 85.18% for $MWCNT$ with 10% concentration in the base fluid when the present results are compared with ${C_f}_{avg} = 0.4437$ at $\alpha = 0.0$ and $\phi = 0.0$ for one wave length. Furthermore, the Tables reveal that the rise in magnitude of ${C_f}_{avg}$ increases by increasing the number of waves. Also percent change in $Nu_{avg}$ for different nanoparticle in comparison to the cases of pure fluid flow past a flat plate and the pure fluid flow past a wavy plate is listed in Table 4.10. It is observed that maximum gain of about 10.52% in $Nu_{avg}$ is obtained for $Al_2O_3$ and minimum of 8.9% for $TiO_2$ with 10% concentration in the base fluid when the present results are compared with $Nu_{avg} = 1.5597$ at $\alpha = 0.2$ and $\phi = 0.0$ for one wave length. The Table 4.10 also

**Table 4.4:** Values of $C_f$ and $Nu$ for different values of $\alpha$ and $\phi$ when $Pr = 7.0, M = 0.5$ for alumina ($Al_2O_3$).

<table>
<tr><th>$\xi$</th><th>$\phi$</th><th>$\alpha$</th><th>$-C_f$</th><th>$Nu$</th></tr>
<tr><td rowspan="5">0.5 (Crest)</td><td rowspan="2">0.1</td><td>0.0</td><td>1.1175</td><td>1.0575</td></tr>
<tr><td>0.1</td><td>1.1243</td><td>1.0415</td></tr>
<tr><td>0.0</td><td rowspan="3">0.2</td><td>0.87458</td><td>0.90201</td></tr>
<tr><td>0.05</td><td>1.0014</td><td>0.9503</td></tr>
<tr><td rowspan="3">0.1</td><td>1.1440</td><td>0.9914</td></tr>
<tr><td rowspan="5">1.0 (Node)</td><td>0.0</td><td>0.9856</td><td>1.4446</td></tr>
<tr><td>0.1</td><td>0.89303</td><td>1.4385</td></tr>
<tr><td>0.0</td><td rowspan="3">0.2</td><td>0.52946</td><td>1.2823</td></tr>
<tr><td>0.05</td><td>0.60696</td><td>1.3505</td></tr>
<tr><td>0.1</td><td>0.69547</td><td>1.4188</td></tr>
<tr><td rowspan="5">1.5 (Trough)</td><td rowspan="2">0.1</td><td>0.0</td><td>0.95052</td><td>1.7091</td></tr>
<tr><td>0.1</td><td>0.96164</td><td>1.6845</td></tr>
<tr><td>0.0</td><td rowspan="3">0.2</td><td>0.75731</td><td>1.4777</td></tr>
<tr><td>0.05</td><td>0.86805</td><td>1.5482</td></tr>
<tr><td>0.1</td><td>0.99431</td><td>1.6182</td></tr>
</table>

**Table 4.5:** Percent increase in magnitude of $C_f$ and $Nu$ for alumina ($Al_2O_3$) in comparison to pure fluid ($\phi = 0$) and flat plate case $\alpha = 0$ when $Pr = 7.0, M = 0.5$.

<table>
<tr><th>$\xi$</th><th>$\alpha$</th><th>$\phi$</th><th>% increase in magnitude of $C_f$</th><th>% increase in $Nu$</th></tr>
<tr><td rowspan="5">0.5 (Crest)</td><td>0.0</td><td rowspan="2">0.1</td><td>30.9</td><td>10.6</td></tr>
<tr><td>0.1</td><td>30.9</td><td>10.9</td></tr>
<tr><td rowspan="3">0.2</td><td>0.0</td><td>0.0</td><td>0.0</td></tr>
<tr><td>0.05</td><td>14.5</td><td>5.4</td></tr>
<tr><td rowspan="3">0.1</td><td>30.8</td><td>10.8</td></tr>
<tr><td rowspan="5">1.0 (Node)</td><td>0.0</td><td>31.3</td><td>10.3</td></tr>
<tr><td>0.1</td><td>31.3</td><td>10.4</td></tr>
<tr><td rowspan="3">0.2</td><td>0.0</td><td>0.0</td><td>0.0</td></tr>
<tr><td>0.05</td><td>14.6</td><td>5.3</td></tr>
<tr><td rowspan="3">0.1</td><td>31.4</td><td>10.6</td></tr>
<tr><td rowspan="5">1.5 (Trough)</td><td>0.0</td><td>31.5</td><td>9.5</td></tr>
<tr><td>0.1</td><td>31.4</td><td>9.5</td></tr>
<tr><td rowspan="3">0.2</td><td>0.0</td><td>0.0</td><td>0.0</td></tr>
<tr><td>0.05</td><td>14.6</td><td>4.8</td></tr>
<tr><td>0.1</td><td>31.3</td><td>91.5</td></tr>
</table>

predicts that percentage in increase in $Nu_{avg}$ remains almost the same by increasing number of waves. On the other hand maximum increase of 24.92% in $Nu_{avg}$ is obtained for $Al_2O_3$ and minimum of 20.65% for $Ag$ with 10% concentration in the base fluid when the present results are compared with $Nu_{avg} = 1.3871$ at $\alpha = 0.0$ and $\phi = 0.0$ for one wave length.

Furthermore, the Table reveals that enhancement in $Nu_{avg}$ increases by increasing number of waves. Through this Table it is easy to identify the role of surface roughness and of nanofluid towards heat transfer enhancement. This study reveals that $Al_2O_3$ nanoparticle have the capacity to produce a coolant (nanofluid) with higher rate of heat transfer.

**Table 4.6:** Percent change in $C_f$ and $Nu$ for different nanoparticle when $M = 0.0, Pr = 7.0,\ \alpha = 0.2,\ \phi = 0.1$.

| $\xi$ | Nano particle material | % increase in magnitude of $C_f$ | | % increase in $Nu$ | |
|---|---|---|---|---|---|
| | | Versus $f''(0) = 0.8539$ at $\alpha = \phi = 0.0$ | Versus $f''(0.5,0) = 0.87458$ at $\alpha = 0.2,\ \phi = 0.0$ | Versus $Nu = 0.9531$ at $\alpha = \phi = 0.0$ | Versus $Nu = 0.90201$ at $\alpha = 0.2,\ \phi = 0.0$ |
| 0.5 | $Al_2O_3$ | 34.0 | 30.8 | 4.8 | 10.8 |
| | $Ag$ | 50.8 | 47.3 | 2.3 | 8.1 |
| | $TiO_2$ | 34.7 | 31.5 | 2.9 | 8.7 |
| | $SWCNT$ | 30.3 | 27.2 | 2.9 | 8.7 |
| | $MWCNT$ | 27.6 | 24.6 | 3.5 | 9.4 |

**Table 4.7:** Numerical values of ${C_f}_{avg}$ for different nanoparticle for different waves when $M = 0.0, Pr = 7.0,\ \alpha = 0.2,\ \phi = 0.1, \xi = 1.0$ **.**

| Nano particle material | ${C_f}_{avg}$ | | |
|---|---|---|---|
| | $n = 1$ | $n = 2$ | $n = 3$ |
| $Al_2O_3$ | 0.90902 | 1.7168 | 2.4703 |
| $Cu$ | 1.0691 | 2.0197 | 2.9057 |
| $Ag$ | 1.11490 | 2.1058 | 3.0302 |
| $TiO_2$ | 0.91877 | 2.7353 | 2.4969 |
| $SWCNT$ | 0.85959 | 1.6234 | 2.3360 |
| $MWCNT$ | 0.82164 | 1.5517 | 2.2328 |

**Table 4.8:** Numerical values of $Nu_{avg}$ for different nanoparticle for different waves when $M = 0.0, Pr = 7.0,\ \alpha = 0.2,\ \phi = 0.1, \xi = 1.0$ **.**

| Nano particle material | $Nu_{avg}$ | | |
|---|---|---|---|
| | $n = 1$ | $n = 2$ | $n = 3$ |
| $Al_2O_3$ | 1.7328 | 2.0562 | 2.2869 |
| $Cu$ | 1.7092 | 2.0197 | 2.2428 |
| $Ag$ | 1.6736 | 1.9748 | 2.1916 |
| $TiO_2$ | 1.6992 | 2.0166 | 2.2431 |
| $SWCNT$ | 1.7072 | 2.0270 | 2.2551 |
| $MWCNT$ | 1.7212 | 2.0460 | 2.2771 |

**Table 4.9:** Percent change in magnitude of ${C_f}_{avg}$ for different nanoparticles when $M = 0.0, Pr = 7.0,\ \alpha = 0.2,\ \phi = 0.1, \xi = 1.0$ **.**

| Nano particle material | % increase in magnitude of ${C_f}_{avg}$ | | | | | |
|---|---|---|---|---|---|---|
| | Versus ${C_f}_{avg} = 0.4437$ at $\alpha = \phi = 0.0$ | | | Versus ${C_f}_{avg} = 0.69938$ at $\alpha = 0.2,\ \phi = 0.0$ | Versus ${C_f}_{avg} = 1.3209$ at $\alpha = 0.2,\ \phi = 0.0$ | Versus ${C_f}_{avg} = 1.9006$ at $\alpha = 0.2,\ \phi = 0.0$ |
| | $n = 1$ | $n = 2$ | $n = 3$ | $n = 1$ | $n = 2$ | $n = 3$ |
| $Al_2O_3$ | 104.87 | 225.38 | 456.77 | 29.98 | 29.97 | 29.98 |
| $Cu$ | 140.95 | 355.10 | 554.87 | 5.28 | 5.28 | 5.28 |
| $Ag$ | 151.27 | 374.60 | 582.94 | 59.41 | 59.42 | 59.43 |
| $TiO_2$ | 107.07 | 291.10 | 462.75 | 31.37 | 31.37 | 31.37 |
| $SWCNT$ | 93.73 | 265.88 | 426.48 | 22.91 | 22.90 | 22.90 |
| $MWCNT$ | 85.18 | 249.72 | 403.22 | 17.48 | 17.47 | 17.47 |

**Table 4.10:** Percent change in magnitude of $Nu_{avg}$ for different nanoparticles when $M = 0.0, Pr = 7.0,\ \alpha = 0.2,\ \phi = 0.1, \xi = 1.0$ .

| Nano particle material | % increase in $Nu_{avg}$ | | | | | |
|---|---|---|---|---|---|---|
| | Versus $Nu_{avg} = 1.3871$ at $\alpha = \phi = 0.0$ | | | Versus $Nu_{avg} = 1.5597$ at $\alpha = 0.2,\ \phi = 0.0$ | Versus $Nu_{avg} = 1.8573$ at $\alpha = 0.2,\ \phi = 0.0$ | Versus $Nu_{avg} = 2.0686$ at $\alpha = 0.2,\ \phi = 0.0$ |
| | $n = 1$ | $n = 2$ | $n = 3$ | $n = 1$ | $n = 2$ | $n = 3$ |
| $Al_2O_3$ | 24.92 | 48.24 | 64.87 | 10.52 | 10.70 | 10.60 |
| $Cu$ | 23.22 | 45.60 | 614.69 | 9.58 | 8.74 | 8.42 |
| $Ag$ | 20.65 | 42.37 | 58.00 | 7.30 | 6.3 | 5.9 |
| $TiO_2$ | 22.50 | 45.38 | 61.71 | 8.90 | 8.58 | 8.43 |
| $SWCNT$ | 23.08 | 46.13 | 62.58 | 9.5 | 9.1 | 9.1 |
| $MWCNT$ | 24.09 | 47.50 | 64.16 | 10.35 | 10.16 | 10.10 |

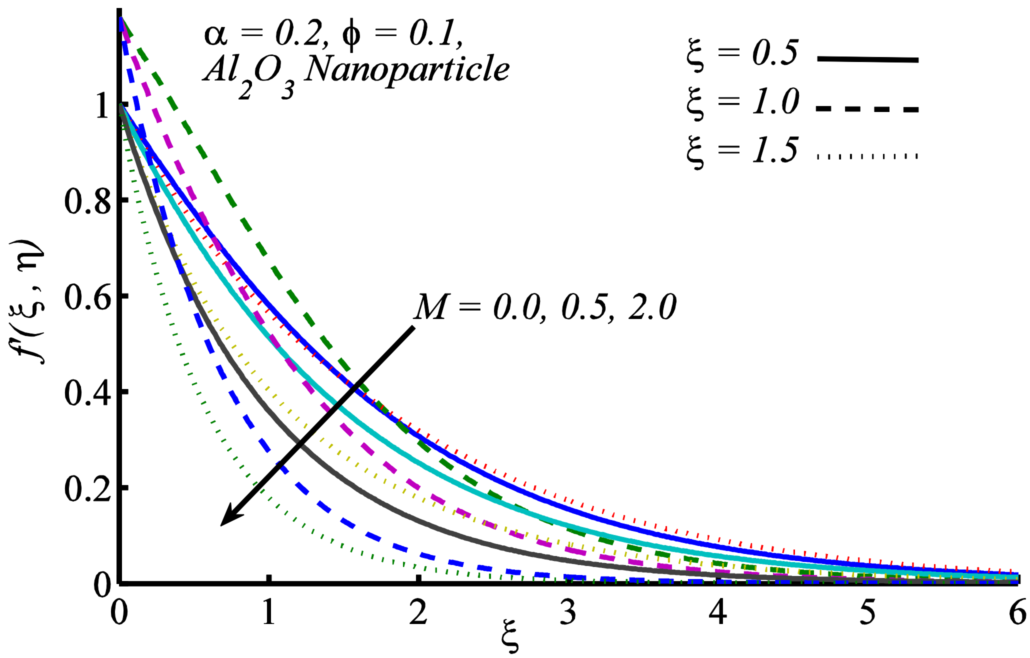


**Figure 4.2:** Effect of magnetic field on velocity profile.

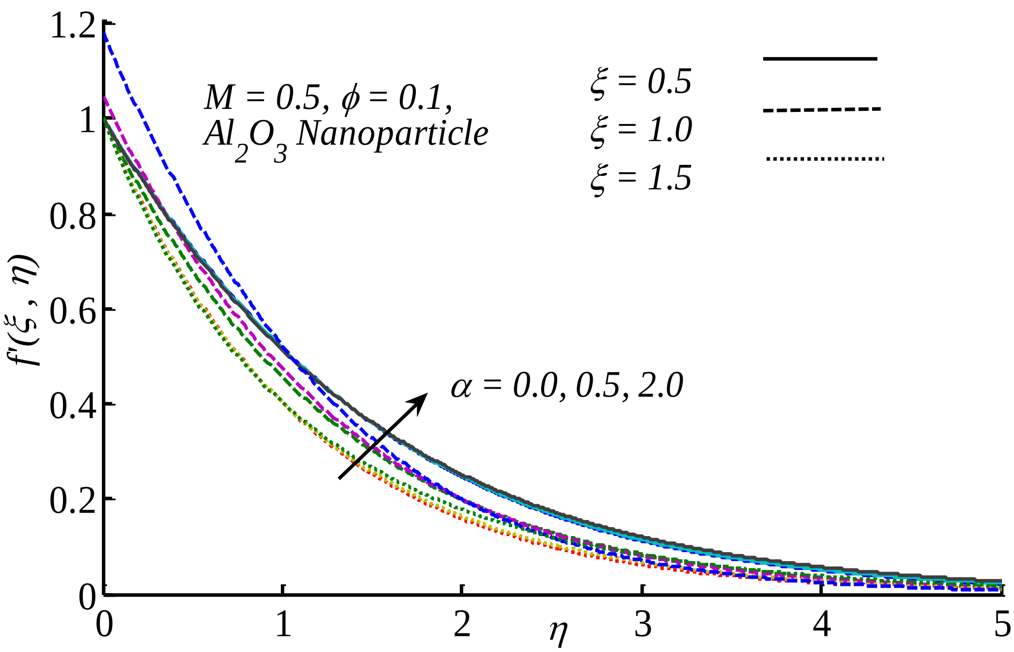


**Figure 4.3:** Effect of amplitude to wavelength ratio α on velocity profile.

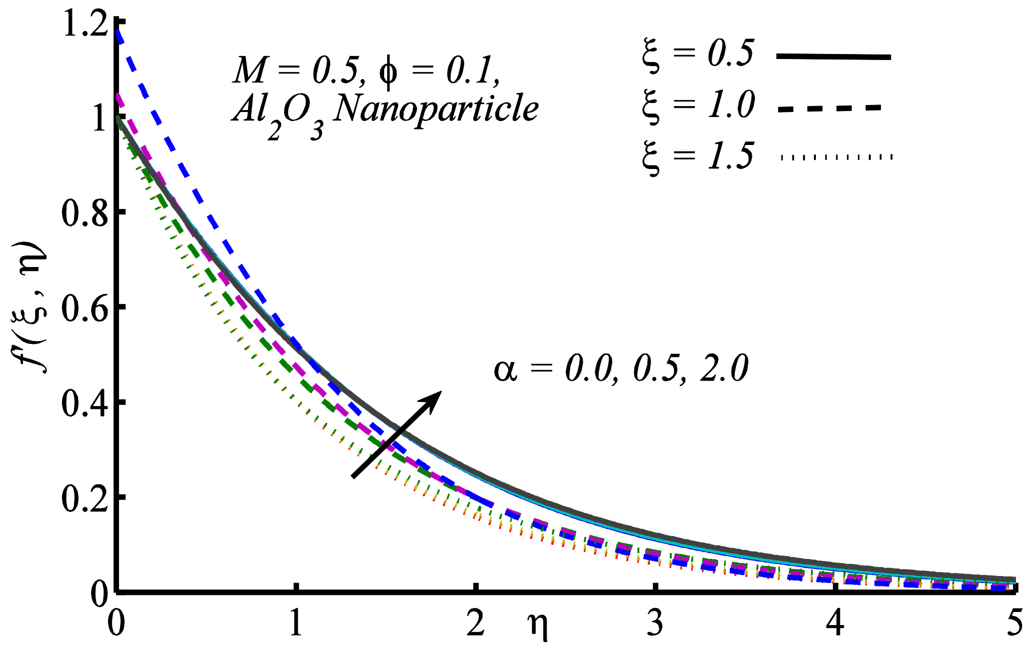


**Figure 4.4:** Temperature profile for different values of α.

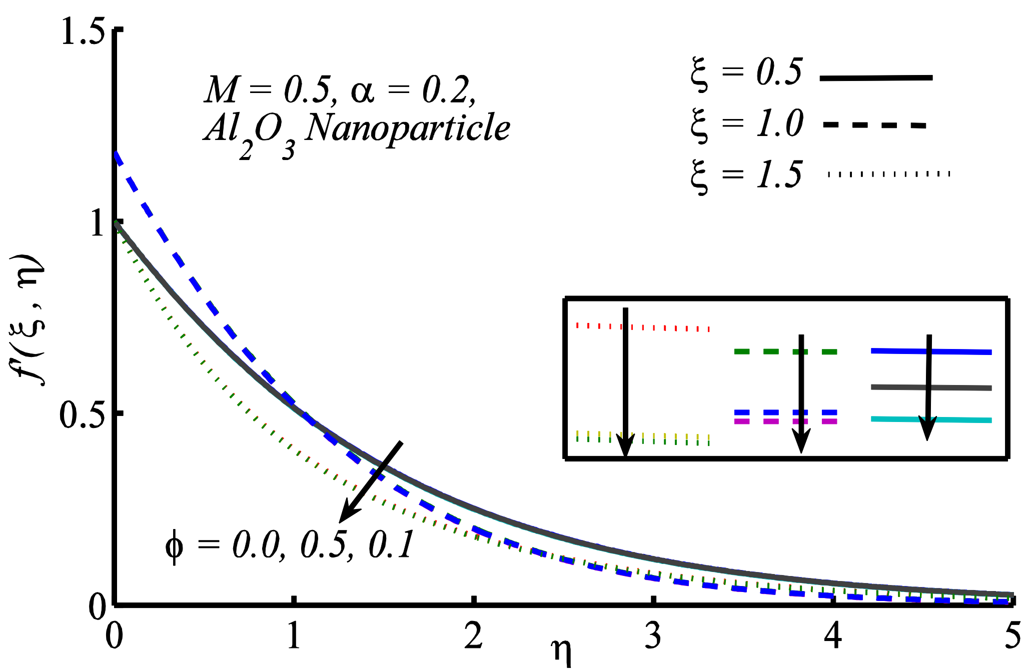


**Figure 4.5:** The effect of volume fraction parameter $\phi$ on velocity profile.

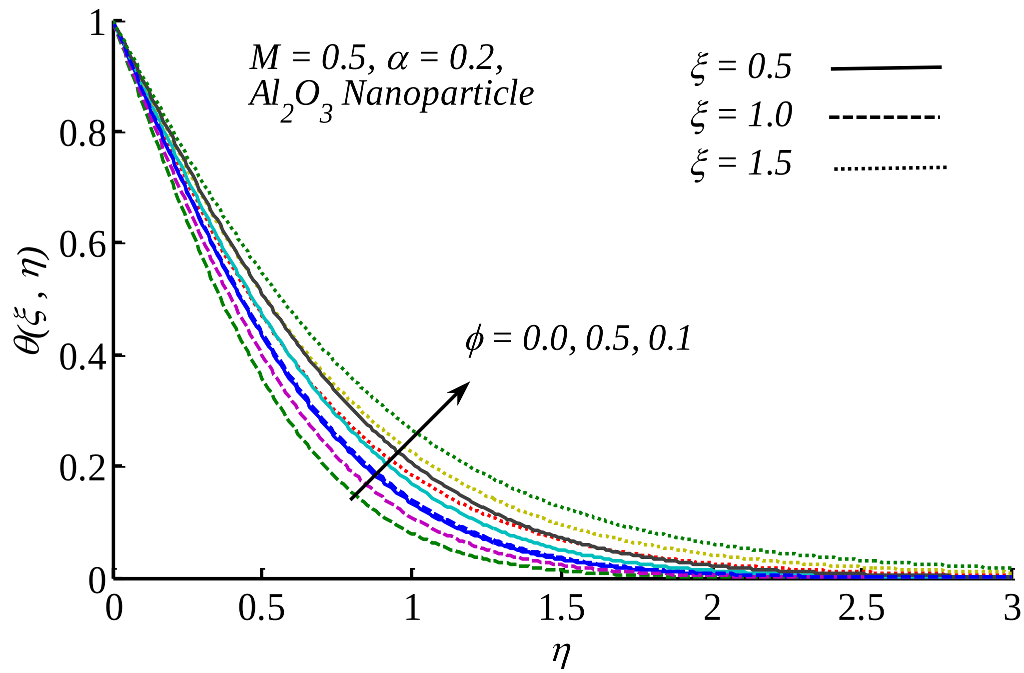


**Figure 4.6:** The effect of $\phi$ on temperature profile.

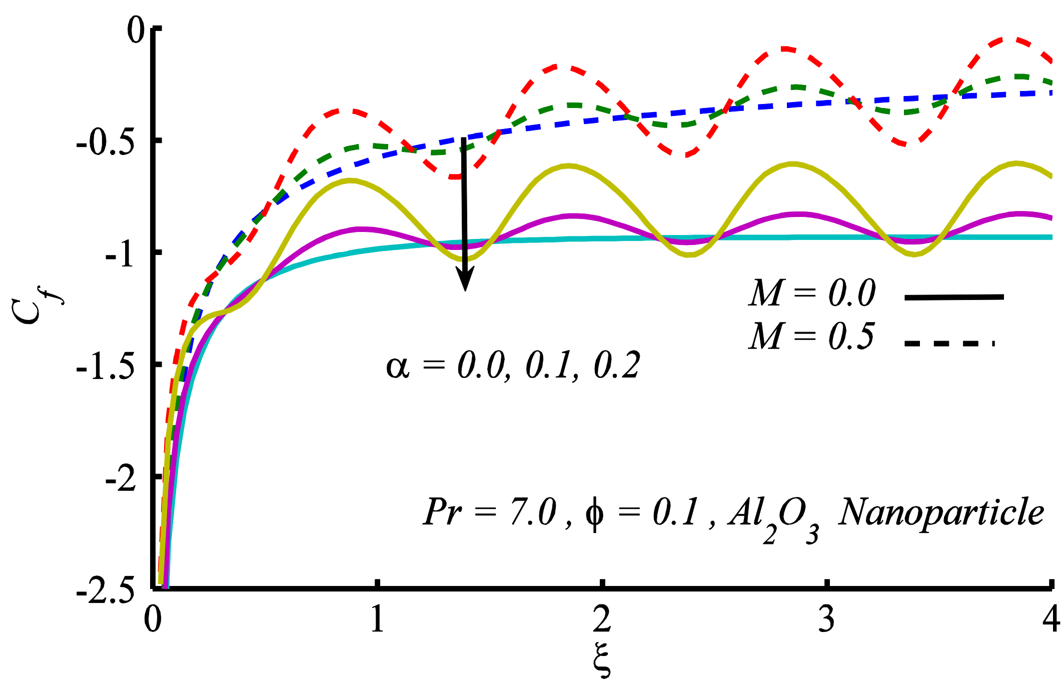


**Figure 4.7:** Skin friction plotted against ξ for different α.

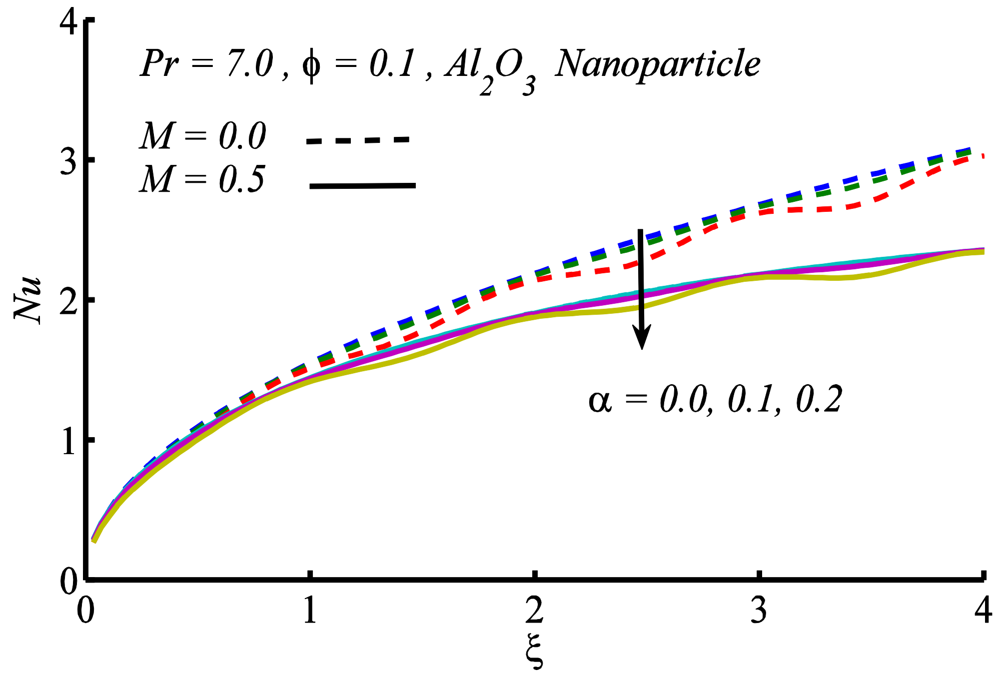


**Figure 4.8:** Nusselt number graph for different α.

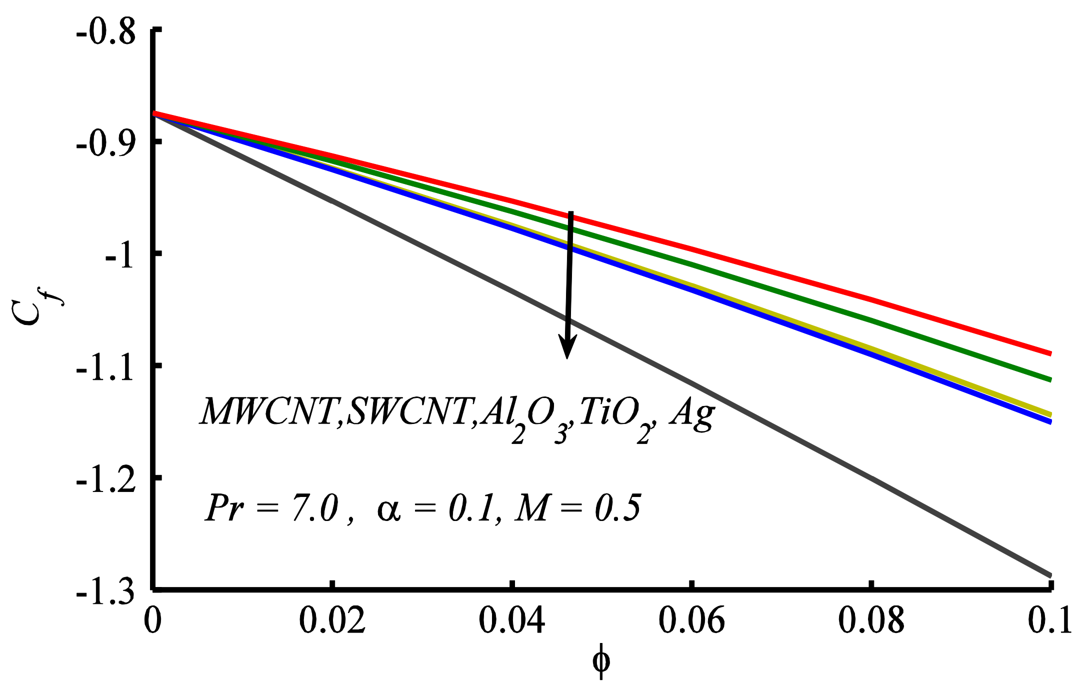


**Figure 4.9:** Skin-friction plotted against $\phi$ for different nanoparticle.

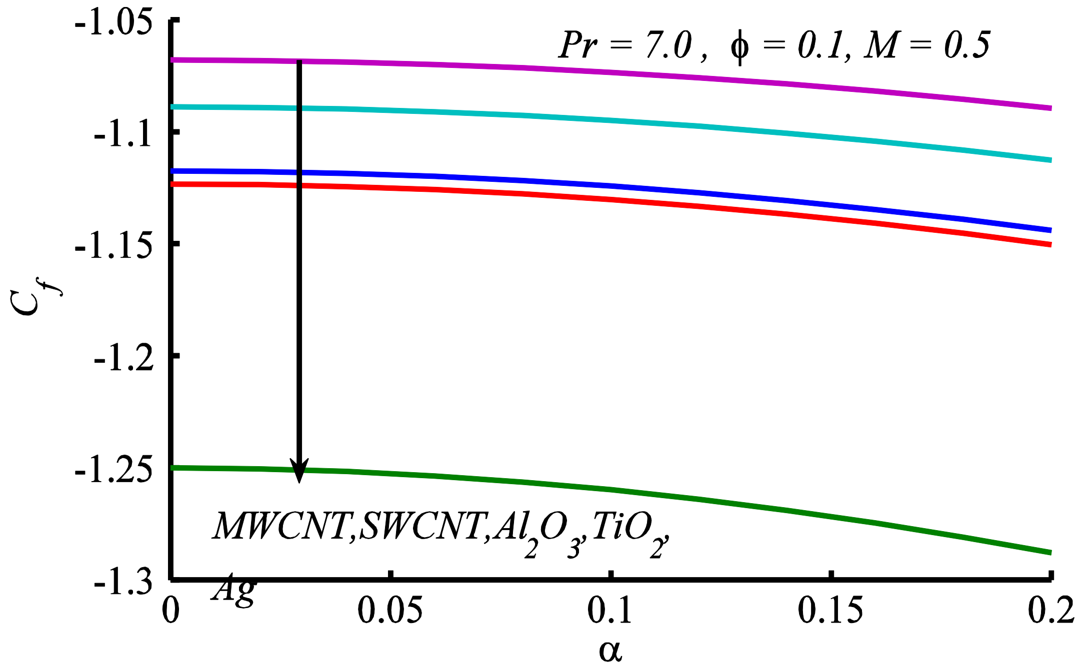


**Figure 4.10:** Skin friction behavior for different nanoparticle against $\alpha$.

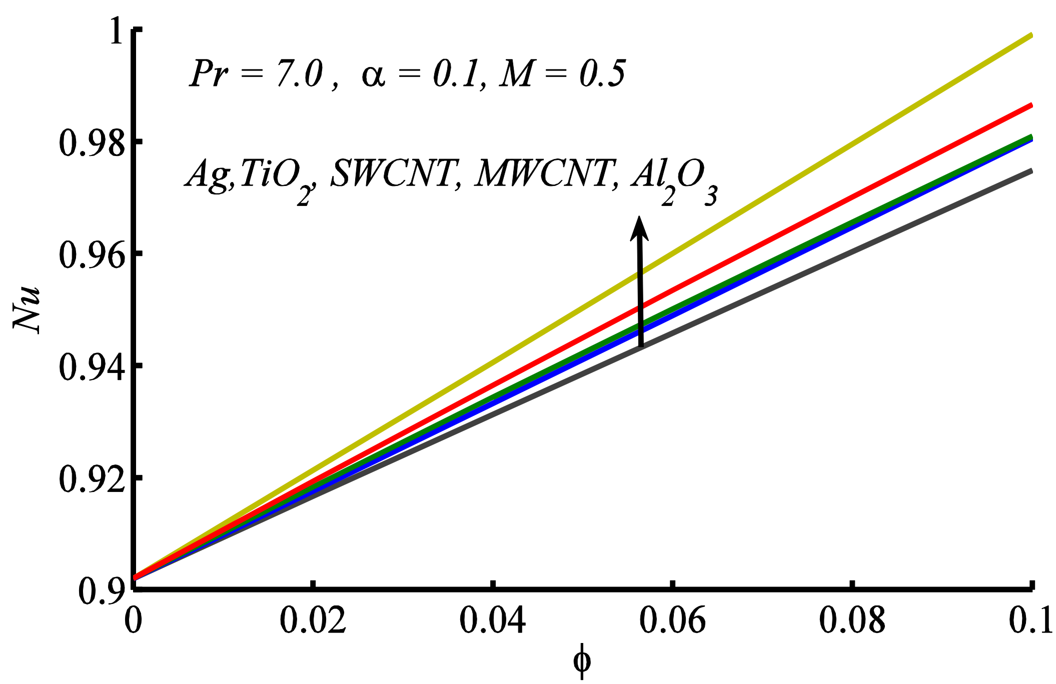


**Figure 4.11:** Nusselt number behavior against $\phi$ for different nanoparticle.

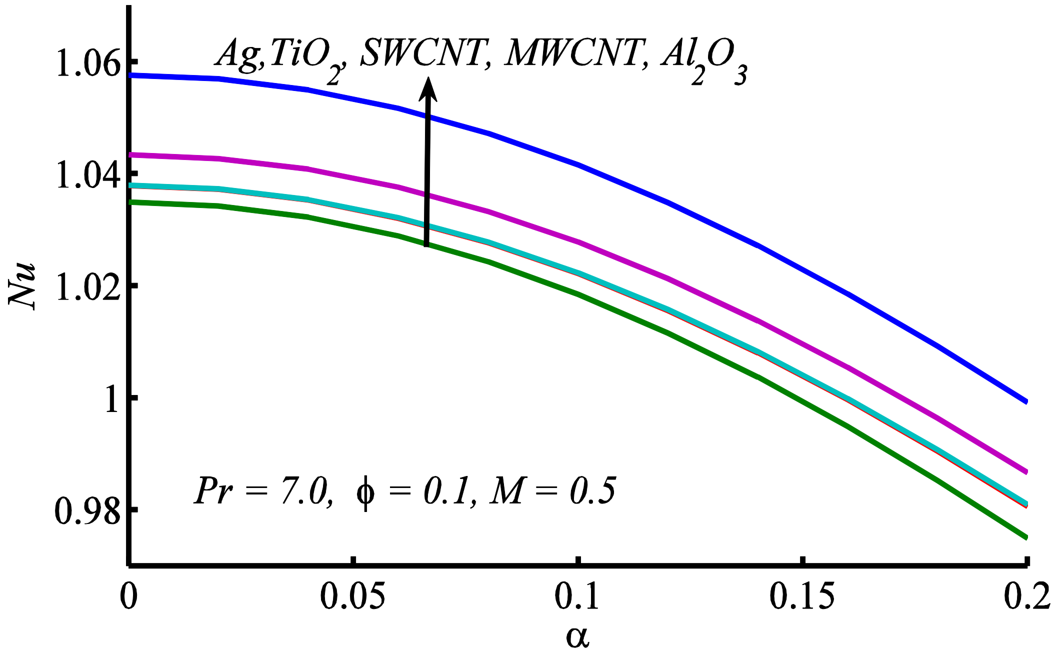


**Figure 4.12:** Nusselt number plotted against $\alpha$ for different nanoparticle.

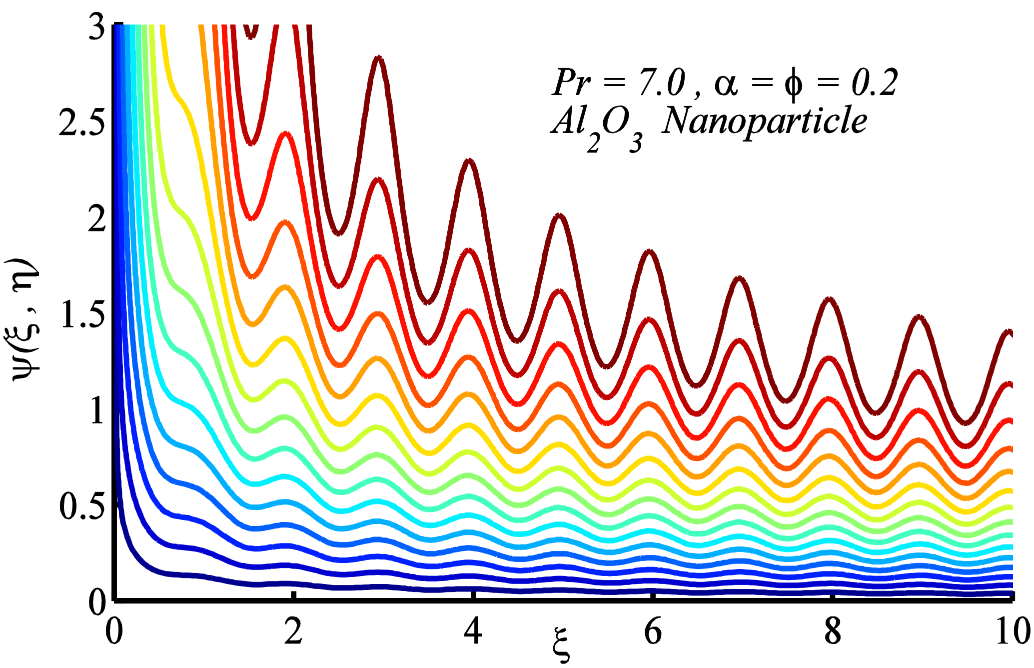


**Figure 4.13:** Stream function plotted at α = 0.2.

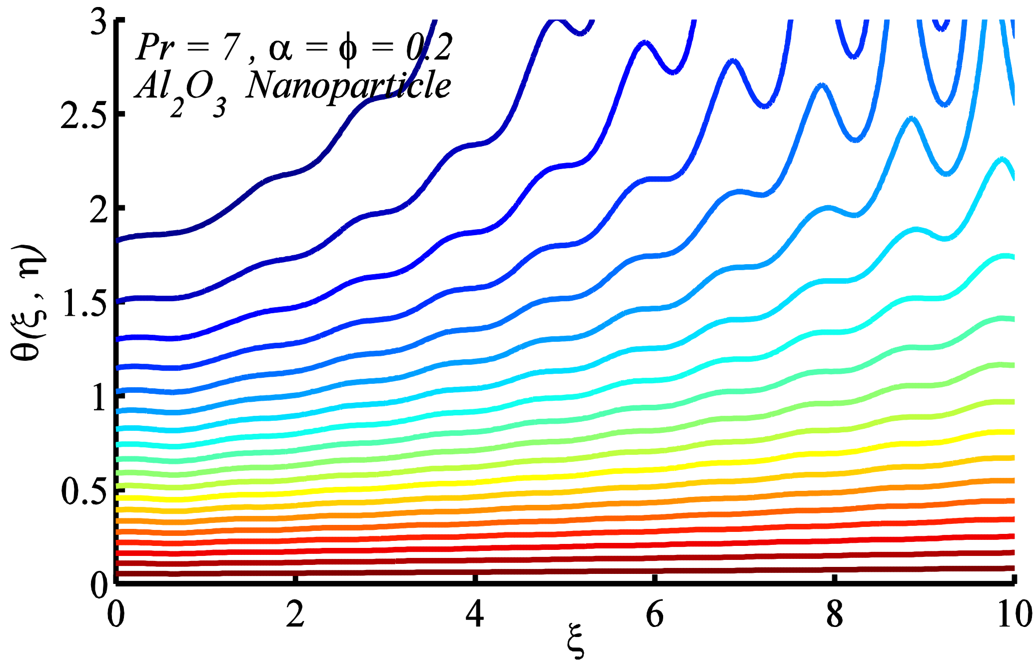


**Figure 4.14:** Isotherms plotted at $\alpha = 0.2$.

## 4.4 Conclusion

In this chapter, heat transfer enhancement due to nanofluid and surface texture of the moving rough plate has been computed. Governing non-similar equations have been solved numerically. The accuracy and validity of numerical procedure is ensured with published results. It is observed that the velocity and temperature grow within the boundary layer by increasing the parameter $\alpha$. Consequently, the skin friction increases and Nusselt number decreases by increasing the values of $\alpha$. It is noted that the skin friction increases by increasing the solid volume fraction of nanoparticle. Similar trend of Nusselt number is noted for increasing values of $\phi$, this observation highlights the fact that by increasing the nanoparticle concentration the momentum and thermal transport is also enhanced and provides the reason for recommending the nanofluid as a preferred coolant. Nanoparticle of five different metals are used and percent increase in the rate of heat transfer is calculated. Maximum gain of about 10.8% is obtained for $Al_2O_3$ nanoparticle with 10% concentration and minimum of 8.1% increase is noted for $Ag$ with 10% concentration in the nanofluid. For average rate of heat transfer maximum gain of about 10.52% is obtained for $Al_2O_3$ nanoparticle with 10% concentration and minimum of 7.3% increase is noted for $Ag$ with 10% concentration in the nanofluid for one wavelength. Our study reveals that the Alumina ($Al_2O_3$) forms good coolant in comparison to the other four nanoparticles.

# Chapter 5

# Heat transfer analysis in non-similar natural convection flow of nanofluid along a vertical wavy surface

Heat transfer characteristic in natural convection flow of water-based nanofluid near a vertical rough wall is presented in this chapter. The analysis considers five different nanoparticles, namely, silver ($Ag$), copper ($Cu$), alumina ( $Al_2O_3$), magnetite ($Fe_3O_4$) and silica ($SiO_2$). The concentration has been limited to the range $0-10\%$ for all types of nanoparticles. The governing equations are modeled using the Boussinesq approximation where by the Tiwari and Das model is utilized to represent the nanofluid. The analysis examines the effects of nanoparticle volume fraction, type of nanoparticle and the wavy surface geometry parameter on the skin friction and Nusselt number. It is observed that for a given nanofluid the skin friction and Nusselt number can be maximized via an appropriate tuning of the wavy surface geometry parameter along with the selection of suitable nanoparticle. Particular to this study copper ($Cu$) is observed to be more productive towards the flow and heat transfer enhancement. In total the metallic oxides are found to be less beneficial as compared to the pure metals.

## 5.1 Formulation of the problem

Consider a non-flat vertical surface with transverse undulations following the sinusoidal patterns. The surface texture of the vertical wavy surface is depicted in Fig. 5.1 and described in equation (1.18). The origin of the coordinate system lies on the leading edge of the vertical surface as shown in Fig. 5.1. It is assumed that the surface temperature of the vertical wavy surface $T_w$ is uniform and $T_w > T_\infty$, where $T_\infty$ denotes the ambient temperature. The flow is assumed to be caused due to temperature difference between the wavy plate and the ambient fluid. Accordingly the flow is steady and two-dimensional in nature. The study of convective transport in nanofluid requires a suitable model that can successfully capture the contribution of nanoparticle in the flow and heat transfer phenomena. The aforementioned Tiwari and Das model [32] considers the improved material properties of the nanofluid.

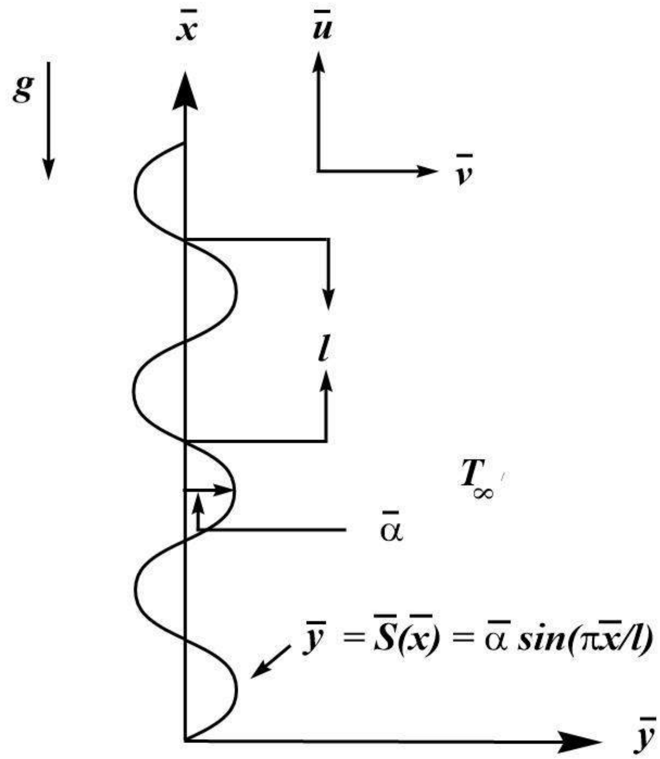


**Figure 5.1:** Physical model and coordinate system.

According to this model the two-dimensional mass; momentum and energy conservation laws with the consideration of Boussinesq approximation are furnished as

$$\frac{\partial \bar{u}}{\partial \bar{x}} + \frac{\partial \bar{v}}{\partial \bar{y}} = 0, \tag{5.1}$$

$$\bar{u}\frac{\partial \bar{u}}{\partial \bar{x}} + \bar{v}\frac{\partial \bar{u}}{\partial \bar{y}} = -\frac{1}{\rho_{nf}}\frac{\partial \bar{p}}{\partial \bar{x}} + \nu_{nf}\nabla^2\bar{u} + \frac{1}{\rho_{nf}}g(\rho\beta)_{nf}(T - T_\infty), \tag{5.2}$$

$$\bar{u}\frac{\partial \bar{v}}{\partial \bar{x}} + \bar{v}\frac{\partial \bar{v}}{\partial \bar{y}} = -\frac{1}{\rho_{nf}}\frac{\partial \bar{p}}{\partial \bar{y}} + \nu_{nf}\nabla^2\bar{v}, \tag{5.3}$$

$$\bar{u}\frac{\partial T}{\partial \bar{x}} + \bar{v}\frac{\partial T}{\partial \bar{y}} = \alpha_{nf}^*\nabla^2 T. \tag{5.4}$$

According to the coordinate system along with the assumed flow conditions, the appropriate boundary conditions for the velocity components and temperature function are described as

$$\left.\begin{array}{l}\bar{y}=\bar{S}(\bar{x}):\bar{u}=0, \qquad \bar{v}=0, \qquad T=T_w\,,\\ \bar{y}\to\infty:\bar{u}=0, \qquad \bar{p}=p_\infty, \qquad T=T_\infty\,.\end{array}\right\} \tag{5.5a}$$

Since the boundary layer starts to develop at $\bar{x}>0$ therefore at the leading edge $\bar{x}=0$ the ambient flow conditions are assumed to be valid which are given by

$$\bar{x}=0,\ \bar{p}=p_\infty, T=T_\infty\text{ , for all }\ \bar{y}\neq 0\,. \tag{5.5b}$$

Let us introduce dimensionless variables of the form

$$\begin{gathered}\xi=x=\frac{\bar{x}}{l}\,, y=\frac{\bar{y}-\bar{S}(\bar{x})}{l}Gr^{\frac{1}{4}}\,, u=\frac{\rho_f l}{\mu_f}Gr^{-\frac{1}{2}}\,\bar{u}\ , v=\frac{\rho_f l}{\mu_f}Gr^{-\frac{1}{4}}\left(\bar{v}-S_\xi\bar{u}\right),\\ S=\frac{\bar{S}(\bar{x})}{l}, \qquad \theta(\xi\,,\eta)=\frac{T-T_\infty}{T_w-T_\infty}\,,\end{gathered} \tag{5.6}$$

here $Gr$ is the Grashof number. Using the argument that the pressure gradient along $\bar{x}$ −axis is zero while eliminating $\partial\bar{p}/\partial\bar{y}$ from Eqs. (5.2) and (5.3), Eqs. (5.2) – (5.4) in non-dimensionalized come out of the form

$$u\frac{\partial u}{\partial x}+v\frac{\partial u}{\partial y}+\frac{\omega_\xi}{\omega}u^2=\frac{\omega^2}{d_1}\frac{\partial^2 u}{\partial y^2}+\frac{d_5}{\omega^2 d_2}\theta, \tag{5.7}$$

$$u\frac{\partial\theta}{\partial x}+v\frac{\partial\theta}{\partial y}=\frac{d\omega^2}{d_3 Pr}\frac{\partial^2\theta}{\partial y^2}\,. \tag{5.8}$$

In order to re-cast the system (5.7) − (5.8) in to more convenient form we introduce the following new variables;

$$\xi=x, \qquad \psi(\xi\,,\eta)=\xi^{\frac{3}{4}}f(\xi\,,\eta)\ , \qquad \eta=\xi^{-\frac{1}{4}}y\ , \qquad \theta=\theta(\xi\,,\eta)\,, \tag{5.9}$$

due to which the Eqs. (5.7) & (5.8) are transformed as

$$\frac{\omega^2}{d_1}f'''+\frac{3}{4}\,ff''-\frac{1}{2}f'^2+\frac{d_5}{d_2}\theta=\xi\left[f'\frac{\partial f'}{\partial\xi}-f''\frac{\partial f}{\partial\xi}\right], \tag{5.10}$$

$$\frac{d\omega^2}{d_3 Pr}\theta''+\frac{3}{4}\,f\theta'=\xi\left[f'\frac{\partial\theta}{\partial\xi}-\theta'\frac{\partial f}{\partial\xi}\right]. \tag{5.11}$$

The material parameters $d\,, d_1, d_2\,, d_3$ are given in Eq. (4.11) and $d_5$ is given by

$$d_5=\left[1-\phi+\phi\left({}^{(\rho\beta)_p}\!\big/_{(\rho\beta)_f}\right)\right]. \tag{5.12}$$

Following Eq. (5.9), the boundary conditions in dimensionless form are described as

$$\begin{gathered}f(\xi\,,0)=0, \qquad f'^{(\xi\,,0)}=0, \qquad \theta(\xi\,,0)-1=0,\\ f'(\xi\,,\infty)=0, \qquad \theta(\xi\,,\infty)=0.\end{gathered} \tag{5.13}$$

The local skin friction coefficient the local Nusselt number are defined in equations (1.20) and (1.23). After using equation (5.6) in equations (1.20) and (1.23), the local skin friction coefficient and local Nusselt number take the form

$$
\begin{aligned}
C_f &= C_{fx}\left(\frac{Gr}{x}\right)^{\frac{1}{4}} = \frac{\omega}{(1-\phi)^{2.5}}\, f''^{(\xi\ ,0)},\\
Nu &= Nu_x (Grx^3)^{-1/4} = -\omega d\theta'(\xi\ ,0).
\end{aligned}
\tag{5.14}
$$

The mean values of the these quantities are respectively defined as

$$
\begin{aligned}
C_{f\,avg} &= \frac{1}{\mathbb{S}}\int_0^{\xi} \frac{x^{\frac{1}{4}}\omega^2}{(1-\phi)^{2.5}}\, f''(\xi\ ,0)d\xi,\\
Nu_{avg} &= -\frac{1}{\mathbb{S}}\int_0^{\xi} dx^{\frac{3}{4}}\omega^2\theta'(\xi\ ,0)d\xi.
\end{aligned}
\tag{5.15}
$$

## 5.2 Numerical procedure

The governing non-similar equations (5.10) – (5.11) subject to the boundary conditions (5.13) are solved numerically using an implicit finite difference scheme known as Keller-box method [178-185]. The details of this scheme have already been explained in Chapter 4. In order to validate the solution procedure for the current problem, already existing results by Alim et al. [130], Kabir et al. [133] and Hossain et al. [190] have been reproduced. A comparison between the present results and already existing data is given in Table 5.1 where the results are in excellent agreement. This authenticates our present solution scheme and allows its utilization in the solution of current equations.

## 5.3 Results and discussion

The effects of nanoparticle volume fraction and wavy amplitude on the velocity and temperature profiles of the $Cu$ water nanofluid are plotted in Figs. 5.2 and 5.3 for different values of $\alpha$ and $\phi$. From Fig. 5.2 it is observed that the velocity increases at crest and trough locations on the wavy surface but decreases at node. This fact is due to the increase in values of $\alpha$ which highlights the role of surface undulation towards enhanced convection. Figure 5.3 displays the influence of various values of the nanoparticle volume fraction $\phi$ on velocity and temperature profiles. It can be seen from Fig. 5.3 that the velocity profile decreases at crest, node and trough locations on the wavy surface on increasing $\phi$ but velocity is minimum at node as compared to crest and trough. The temperature profiles under the influence of same values of $\alpha$ $(= 0.0, 0.1, 0.2)$ and $\phi$ $(= 0.0, 0.05, 0.1)$ are also plotted in Figs. 5.2 and 5.3, respectively. The effect of $\alpha$ on temperature profile is shown in Fig. 5.2. It is seen that variation in $\alpha$ does not bring significant change in the temperature profile at crest and trough positions but an increase at the node. Figure 5.3 shows the influence of various values of the nanoparticle volume fractions $\phi$ on temperature distribution. It is seen that by increasing $\phi$, thickness of thermal boundary layer enhances. Since the $Cu$ has high thermal conductivity therefore the maximum increase in thickness is observed for $Cu$-water nanofluid. Figures 5.4 and 5.5 depict the variation of the $C_f$ and $Nu$ with an increasing values of wavy amplitude $\alpha$ for $Cu$-water nanoparticle. An increase in $\alpha$ results in increasing the wavy amplitude of the curves which further grows downstream keeping the wavelengths constant in both graphs. The variation of $C_f$ and $Nu$ with $\phi$ is shown in Figs. 5.6 and 5.7, respectively. Evidently the volume fraction parameter does not effect the $C_f$ significantly as compared to the $Nu$. This fact highlights the direct impact of nanoparticle concentration on the heat transfer rate.

The current analysis has been carried out for five different types of nanoparticles, namely, silver ($Ag$), copper ($Cu$), alumina ($Al_2O_3$), magnetite ($Fe_3O_4$) and silica ($SiO_2$). Table 1.2 shows the thermophysical properties of water and the said five elements $Ag, Cu, Al_2O_3, Fe_3O_4$ and $SiO_2$. Here we investigate the effects of different nanoparticles on $C_f$ and $Nu$. It is worth mentioning here that this study reduces the governing Eqs. (5.10) – (5.11) to those of a pure or regular fluid for $\phi = 0$. The $C_f$ and $Nu$ are plotted against the solid volume fraction $\phi$ and wavy amplitude $\alpha$ for different types of nanoparticles ($Ag, Cu, Al_2O_3, Fe_3O_4, SiO_2$) in Figs. 5.8 – 5.11. Figures 5.8 and 5.9 illustrate the variations of the $C_f$ and $Nu$ with nanoparticle volume fraction parameter $\phi$. These figures show that these quantities increase almost linearly with $\phi$ and maximum increase in $C_f$ is observed for silver ($Ag$) and in $Nu$ for copper ($Cu$). This shows that the presence of the nanoparticles in the base fluid increases the effective thermal conductivity of the fluid quite appreciably which consequently enhances the heat transfer characteristics as seen in these figures. Similarly the variation in $C_f$ and $Nu$ against wavy amplitude is shown in Figs. 5.10 and 5.11 for different nanoparticles. Clearly, the variation due to these parameters is almost linear but the nature of nanoparticle does matter. Maximum increase in skin friction is observed for silver ($Ag$) and in $Nu$ for copper ($Cu$). It is worth mentioning that according to Eq. (5.14) the Nusselt number is a product of the temperature gradient and the thermal conductivity ratio (conductivity of the nanofluid to the conductivity of the base fluid). Increasing $\phi$ leads to an increase in the thermal conductivity ratio which in turn increases the Nusselt number. Isotherms are plotted for some values of $\alpha$ $(= 0.0, 0.1, 0.2)$ and $\phi$ ($= 0.0, 0.05, 0.1$ in Figs. 5.12 and 5.13 respectively. The wavy pattern can easily be seen in the isotherm graphs.

Numerical data of $C_f$ and $Nu$ for different values of $\alpha$ and $\phi$ when $Pr = 7.0$ for copper ($Cu$) at the locations $x = 0.5$, $x = 1.0$ and $x = 1.5$ are presented in Table 5.2. It is observed that both $C_f$ and $Nu$ increase with the increase of $\phi$ and the $C_f$ increases and $Nu$ decreases with the increase of $\alpha$. Table 5.3 shows percent change in $C_f$ and $Nu$ for copper ($Cu$) nanoparticle for different values of $\alpha$ and $\phi$ when $Pr = 7.0$ in comparison to wavy and flat vertical plate situations at three different locations; crest, node and trough on the vertical wavy surface. It is observed that at crest $C_f$ increases and $Nu$ decreases by increasing the wavy amplitude at fixed concentration of nanoparticle. Similarly for a fixed value of $\alpha$ both $C_f$ and $Nu$ increase by increasing the nanoparticle concentration. The similar behavior is followed by the $C_f$ and $Nu$ at the trough location but at the node both $C_f$ and $Nu$ increase with the increase of wavy amplitude and concentration of nanoparticle. The nature of nanoparticle has a fundamental role in enhancing the convective heat transfer phenomena. Nanoparticle of five different materials ($Ag, Cu, Al_2O_3, Fe_3O_4, SiO_2$) including two metals and three oxides have been considered in Table 5.4 towards the calculation of percent increase in the magnitude of $C_f$ and $Nu$. It is observed that maximum increase due to metals of about $10.9\%$ in $C_f$ is obtained for $Ag$ with $10\%$ concentration in the base fluid and minimum increase in metals of about $8.9\%$ in the value of $C_f$ is obtained for $Cu$ with $10\%$ concentration when the present results are compared with the value $f''(0.5,0) = 0.6460$ at $\alpha = 0.2$ and $\phi = 0.0$. Similarly for oxides, maximum increase of about $6.1\%$ in $C_f$ is obtained for $Al_2O_3$ with $10\%$ concentration in the base fluid and minimum increase of about 2.2 % in the value of $C_f$ is obtained for $SiO_2$ with the same concentration. On the other hand for metals, maximum gain in metal of about 11.1% in $Nu$ is obtained for $Cu$ and minimum of 10.3% for $Ag$ with 10% concentration in the base fluid when the present results are compared with $Nu = 0.7337$ at $\alpha = 0.2$ and $\phi = 0.0$. Similarly, for oxides, maximum increase of about 10.2% in Nusselt number is obtained for $Al_2O_3$ with 10% concentration in the base fluid and minimum decrease of about 5.2% in the value of Nusselt number is obtained for $SiO_2$ with same concentration. The percent increase in skin friction and Nusselt number is also calculated in comparison to$f''(0) = 0.6375$ and $Nu = 0.7455$ at $\alpha = 0.0$ and $\phi = 0.0$. For metals, maximum of 12.2% and 9.3% increase in $C_f$ and $Nu$ is obtained and a minimum of 1.6% and 3.3% increase in $C_f$ and $Nu$ is obtained, respectively. Similarly for oxides, maximum of 7.6% and 8.5% increase in $C_f$ and $Nu$ is obtained and a minimum of 3.6% increase in $C_f$ and 6.7% decrease in $Nu$ is obtained, respectively. Through Table 5.4 it is easy to identify the role of surface roughness and of nanofluid towards heat transfer enhancement.

Numerical values of ${C_f}_{avg}$ and $Nu_{avg}$ for five different materials ($Ag, Cu, Al_2O_3, Fe_3O_4, SiO_2$) including two metals and three oxides are presented in Table 5.5. Table 5.6 shows percent change in ${C_f}_{avg}$ and $Nu_{avg}$ of five different materials ($Ag, Cu, Al_2O_3, Fe_3O_4, SiO_2$) in comparison to wavy and flat vertical plate when $Pr = 7.0$, $\alpha = 0.2$, $\phi = 0.1, \xi = 1.0$. It is observed that maximum increase due to metals of about 11% in ${C_f}_{avg}$ is obtained for $Ag$ with 10% concentration in the base fluid and minimum increase due to metals of about 0.6% in the value of ${C_f}_{avg}$ is obtained for $Au$ with 10% concentration when the present results are compared with the value ${C_f}_{avg} = 0.4560$ at $\alpha = 0.2$, $\phi = 0.0$. Similarly for oxides, maximum increase of about 6.2% in ${C_f}_{avg}$ is obtained for $Al_2O_3$ with 10% concentration in the base fluid and minimum increase of about 2.2 % in the value of ${C_f}_{avg}$ is obtained for $SiO_2$ with same concentration. On the other hand for metals, maximum gain due to metals of about 11.3% in $Nu_{avg}$is obtained for $Cu$ and minimum of 5.3% for $Ag$ with 10% concentration in the base fluid when the present results are compared with $Nu_{avg} = 0.6469$ at $\alpha = 0.2$, $\phi = 0.0$ .

**Table 5.1:** Comparison of present results with existing data at $\alpha = 0$.

| $Pr$ | $f''(0,0)$ | | | | $-\theta'(0,0)$ | | | |
|---|---|---|---|---|---|---|---|---|
| | Present | Hossain et al. [190] | Alim et al. [130] | Kabir et al. [133] | Present | Hossain et al. [190] | Alim et al. [130] | Kabir et al. [133] |
| 1 | 0.9082 | 0.9080 | 0.90814 | 0.90813 | 0.4010 | 0.401 | 0.40101 | 0.40102 |
| 10 | 0.5928 | 0.5910 | 0.59269 | 0.59270 | 0.8268 | 0.825 | 0.82663 | 0.82662 |
| 25 | 0.4876 | 0.4850 | 0.48733 | 0.48732 | 1.0690 | 1.066 | 1.06847 | 1.06848 |
| 50 | 0.4176 | 0.4850 | 0.41727 | 0.41728 | 1.2896 | 1.066 | 1.28879 | 1.28878 |
| 100 | 0.3559 | 0.3520 | 0.35559 | 0.35558 | 1.5495 | 1.542 | 1.54827 | 1.54828 |

**Table 5.2:** Variation in $C_f$ and $Nu$ for different values of $\alpha$ and $\phi$ when $Pr = 7.0$ for copper ($Cu$).

| $\xi$ | $\phi$ | $\alpha$ | $C_f$ | $Nu$ |
|---|---|---|---|---|
| 0.5 (Crest) | 0.1 | 0.0 | 0.6945 | 0.8286 |
| | | 0.1 | 0.6969 | 0.8250 |
| | 0.0 | 0.2 | 0.6460 | 0.7337 |
| | 0.05 | | 0.6729 | 0.7746 |
| | 0.1 | | 0.7035 | 0.8151 |
| 1.0 (Node) | | 0.0 | 0.6945 | 0.8286 |
| | | 0.1 | 0.6435 | 0.8135 |
| | 0.0 | 0.2 | 0.4914 | 0.6971 |
| | 0.05 | | 0.5121 | 0.7365 |
| | 0.1 | | 0.5358 | 0.7756 |
| 1.5 (Trough) | 0.1 | 0.0 | 0.6945 | 0.8286 |
| | | 0.1 | 0.6959 | 0.8239 |
| | 0.0 | 0.2 | 0.6437 | 0.7312 |
| | 0.05 | | 0.6698 | 0.7713 |
| | 0.1 | | 0.66975 | 0.8111 |

**Table 5.3:** Percent increase in $C_f$ and $Nu$ for copper ($Cu$) in comparison to pure fluid ($\phi = 0$) with wavy ($\alpha \neq 0$) and flat plate ($\alpha = 0$) case when $Pr = 7.0$.

| $\xi$ | $\alpha$ | $\phi$ | % increase in $C_f$ | | % increase in $Nu$ | |
|---|---|---|---|---|---|---|
| | | | Versus wavy plate at $\phi = 0.0$ | Versus flat plate at $\phi = 0.0$ | Versus wavy plate at $\phi = 0.0$ | Versus flat plate at $\phi = 0.0$ |
| 0.5 (Crest) | 0.0 | 0.1 | $-$ | 1.9 | $-$ | 11.1 |
| | 0.1 | | 8.9 | 9.3 | 11.1 | 10.7 |
| | 0.2 | 0.0 | 0.0 | 1.3 | 0.0 | $-1.6$ |
| | | 0.05 | 4.1 | 5.6 | 5.6 | 3.9 |
| | | 0.1 | 8.9 | 10.3 | 11.1 | 9.3 |
| 1.0 (Node) | 0.0 | | $-$ | 1.9 | $-$ | 11.1 |
| | 0.1 | | 8.7 | 0.9 | 11.1 | 9.1 |
| | 0.2 | 0.0 | 0.0 | $-22.9$ | 0.0 | $-6.5$ |
| | | 0.05 | 4.2 | $-10.2$ | 5.6 | $-1.2$ |
| | | 0.1 | 9.0 | $-15.9$ | 11.2 | 4.0 |
| 1.5 (Trough) | 0.0 | | $-$ | 1.9 | $-$ | 11.1 |
| | 0.1 | | 8.9 | 9.1 | 11.1 | 10.5 |
| | 0.2 | 0.0 | 0.0 | $-0.4$ | 0.0 | $-1.9$ |
| | | 0.05 | 4.0 | 5.0 | 5.4 | 3.4 |
| | | 0.1 | 8.7 | 9.8 | 10.9 | 8.8 |

**Table 5.4:** Percent change in $C_f$ and $Nu$ for different nanoparticle when $Pr = 7.0,\ \alpha = 0.2,\ \phi = 0.2$.

| ξ | Nano particle material | % increase in $C_f$ | | % increase in $Nu$ | |
|---|---|---|---|---|---|
| | | Versus $f''(0) = 0.6375$ at $\alpha = \phi = 0.0$ | Versus $f''(0.5,0) = 0.6460$ at $\alpha = 0.2,\ \phi = 0.0$ | Versus $Nu = 0.7455$ at $\alpha = \phi = 0.0$ | Versus $Nu = 0.7337$ at $\alpha = 0.2,\ \phi = 0.0$ |
| 0.5 | $Au$ | 1.6 | 0.2 | 3.3 | 5.0 |
| | $Ag$ | 12.2 | 10.8 | 8.6 | 10.3 |
| | $Cu$ | 10.3 | 8.9 | 9.3 | 11.1 |
| | $Fe_3O_4$ | 5.8 | 4.4 | 5.6 | 7.3 |
| | $Al_2O_3$ | 7.6 | 6.1 | 8.5 | 10.2 |
| | $SiO_2$ | 3.6 | 2.2 | $-6.7$ | $-5.2$ |

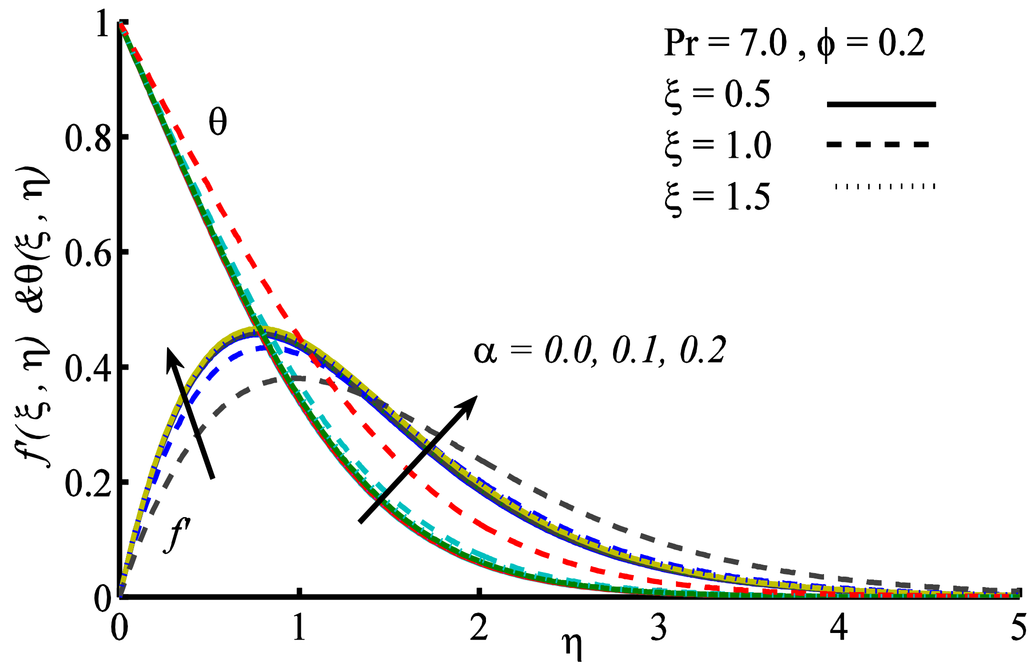


**Figure 5.2:** The effect of α on velocity and temperature profile.

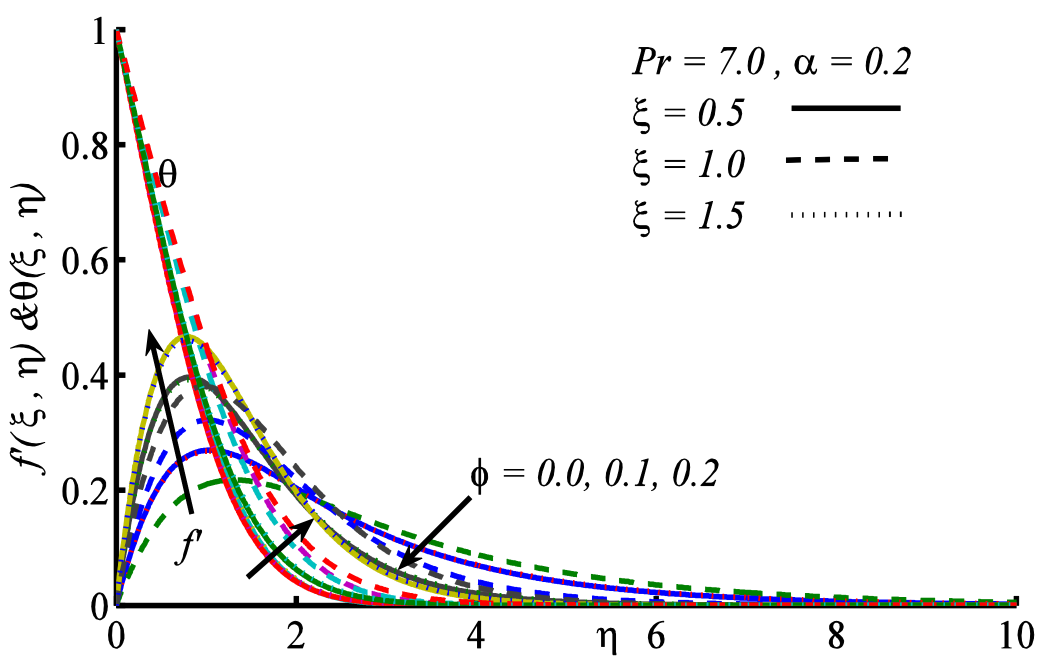


**Figure 5.3:** The effect of $\phi$ on velocity and temperature profile.

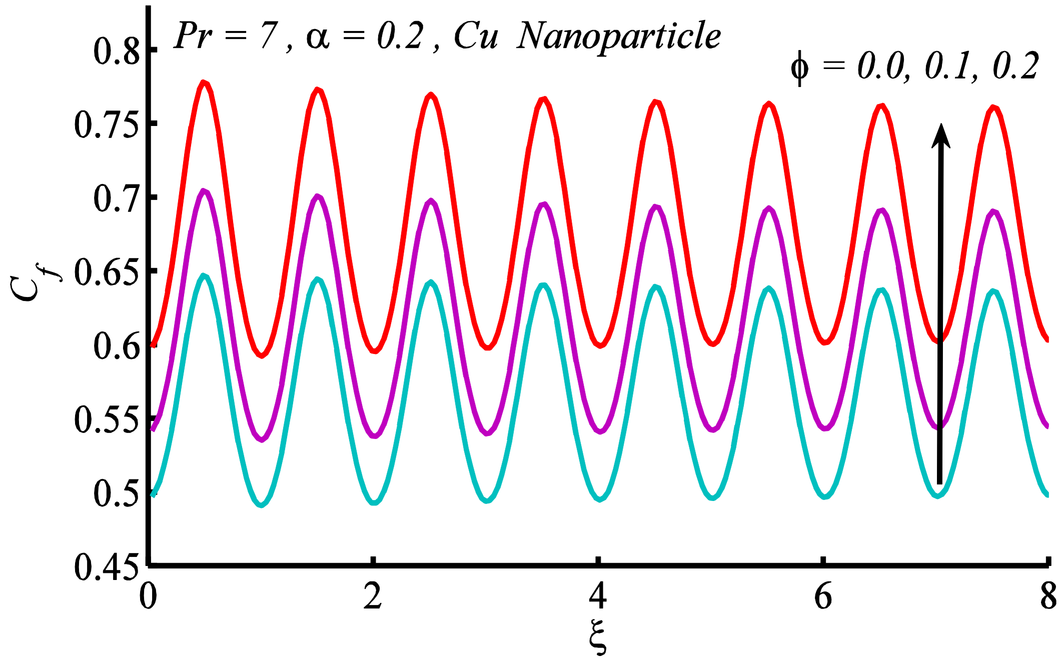


**Figure 5.4:** Skin friction coefficient plotted for different value of $\phi$.

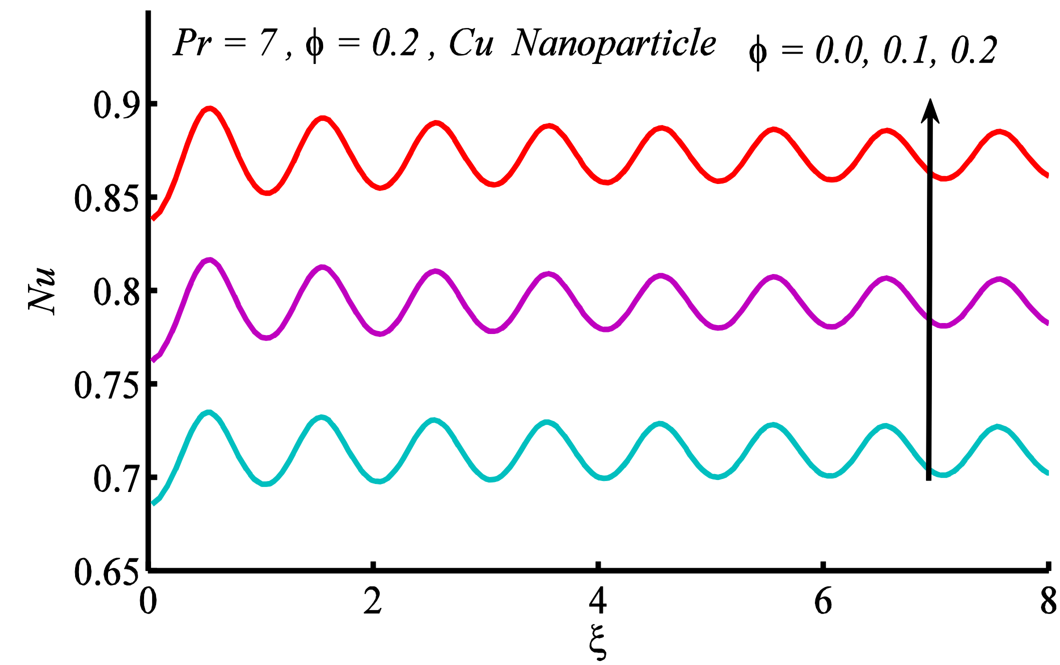


**Figure 5.5:** Nusselt number plotted against $\xi$ for different values of $\phi$.

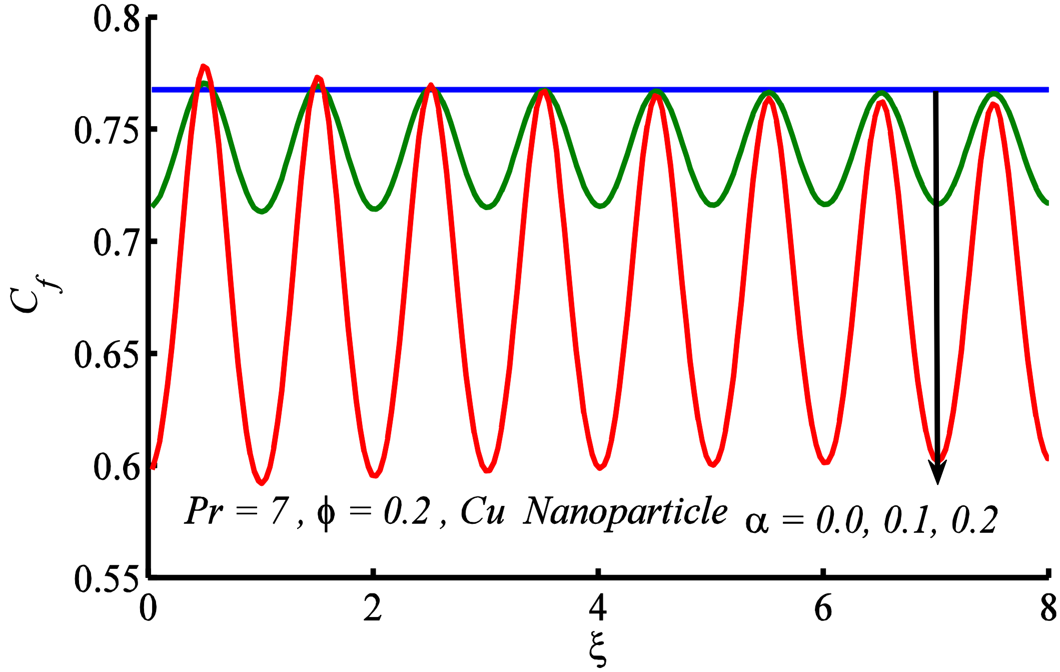


**Figure 5.6:** Wall skin friction coefficient plotted for different values of $\alpha$.

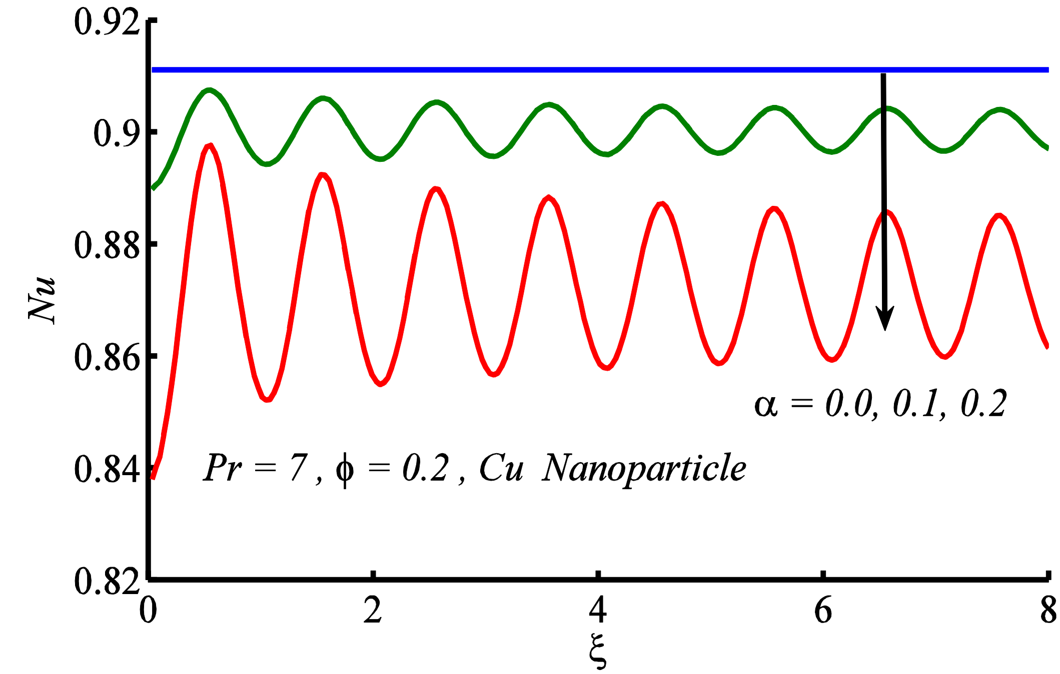


**Figure 5.7:** Nusselt number graph for different values of $\alpha$.

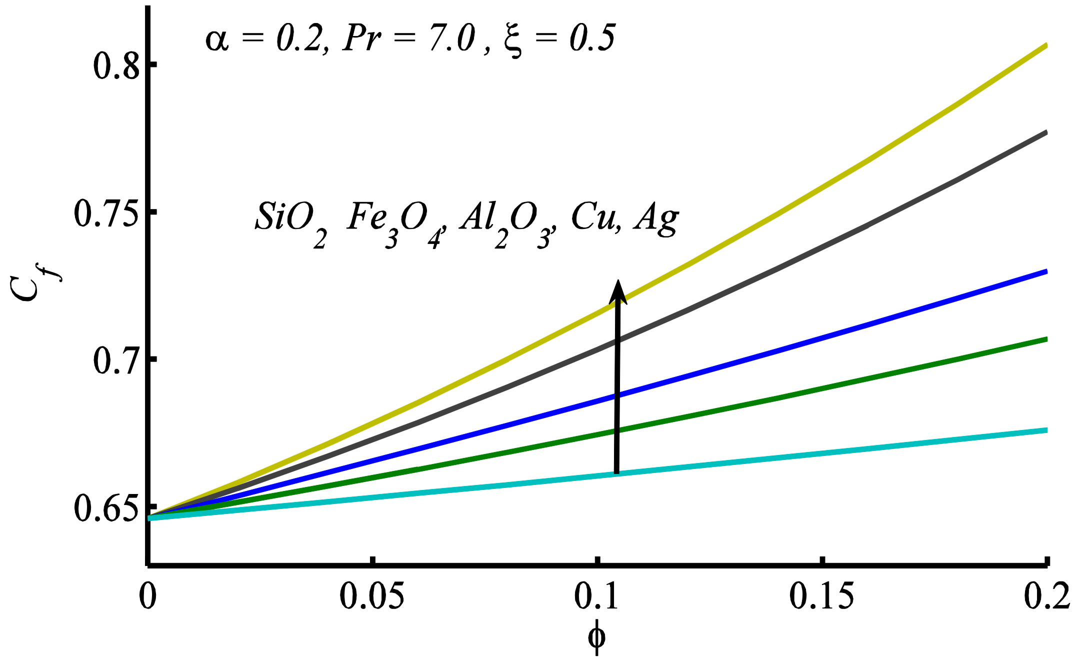


**Figure 5.8:** Variation in skin friction coefficient due to $\phi$ for different nanoparticles.

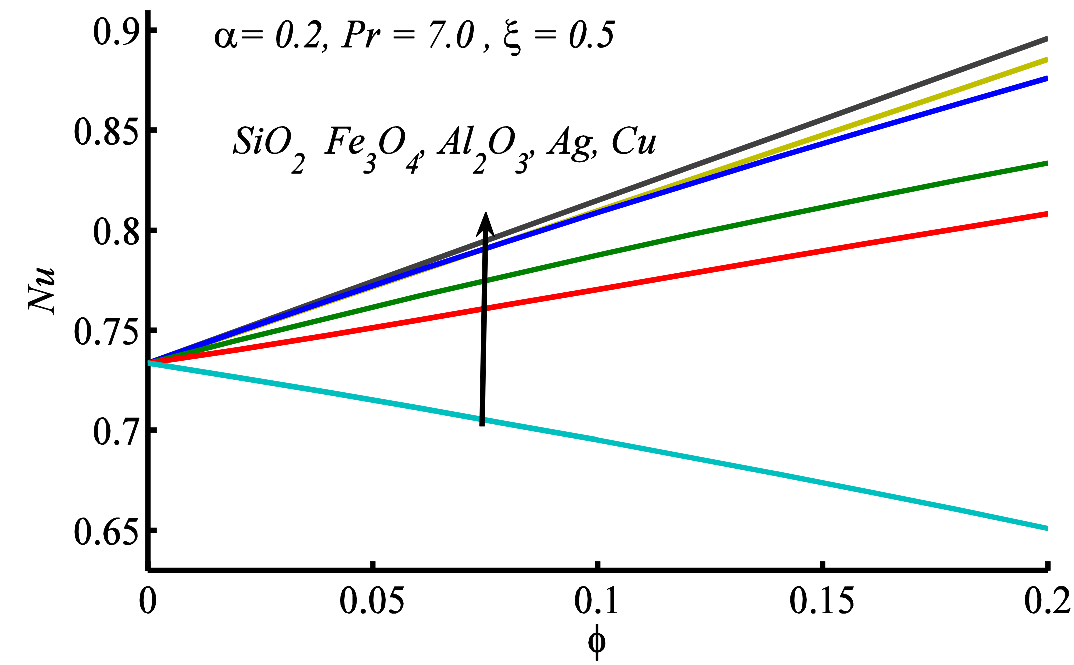


**Figure 5.9:** Variation of Nusselt number due to $\phi$ for different nanoparticles.

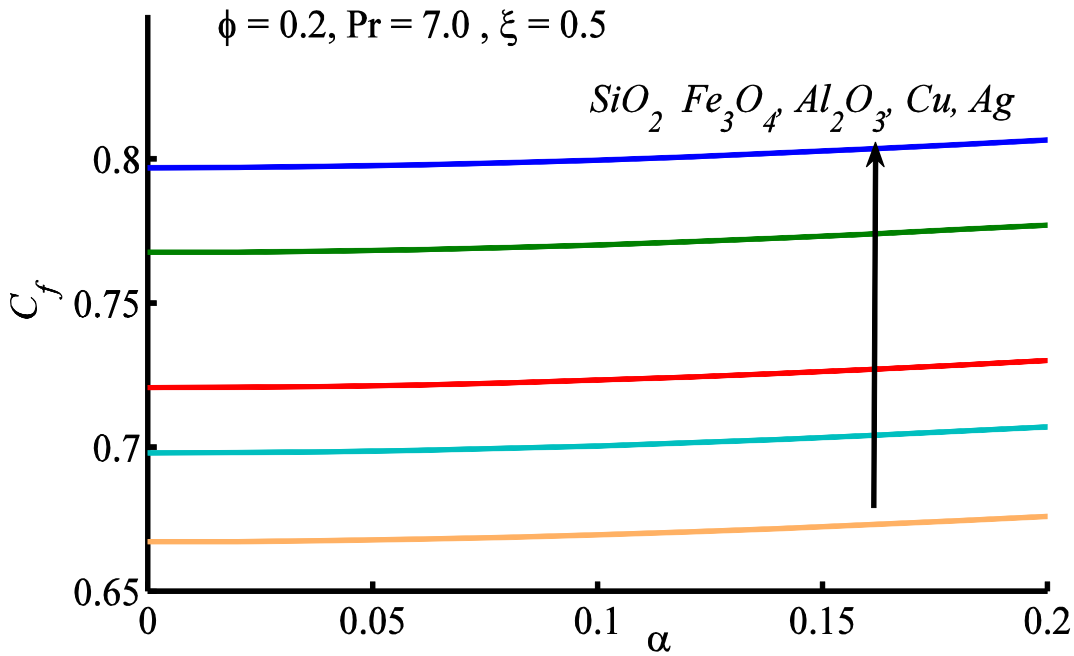


**Figure 5.10:** Variation of skin friction due to $\alpha$ for different nanoparticles.

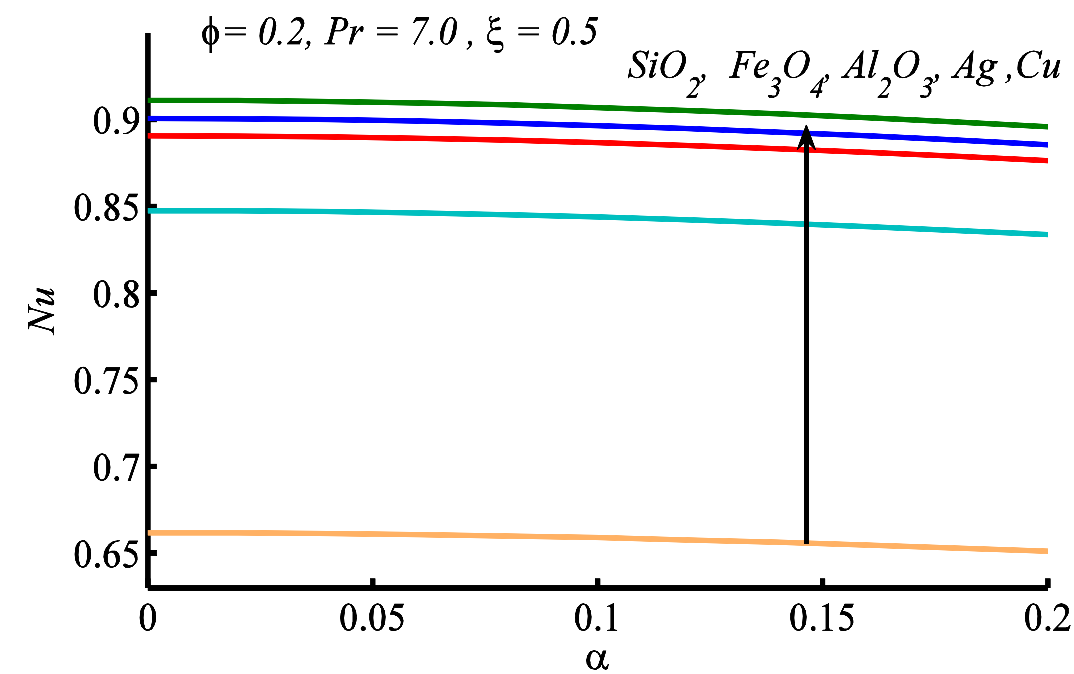


**Figure 5.11:** Plot of Nusselt number against $\alpha$ for different nanoparticles.

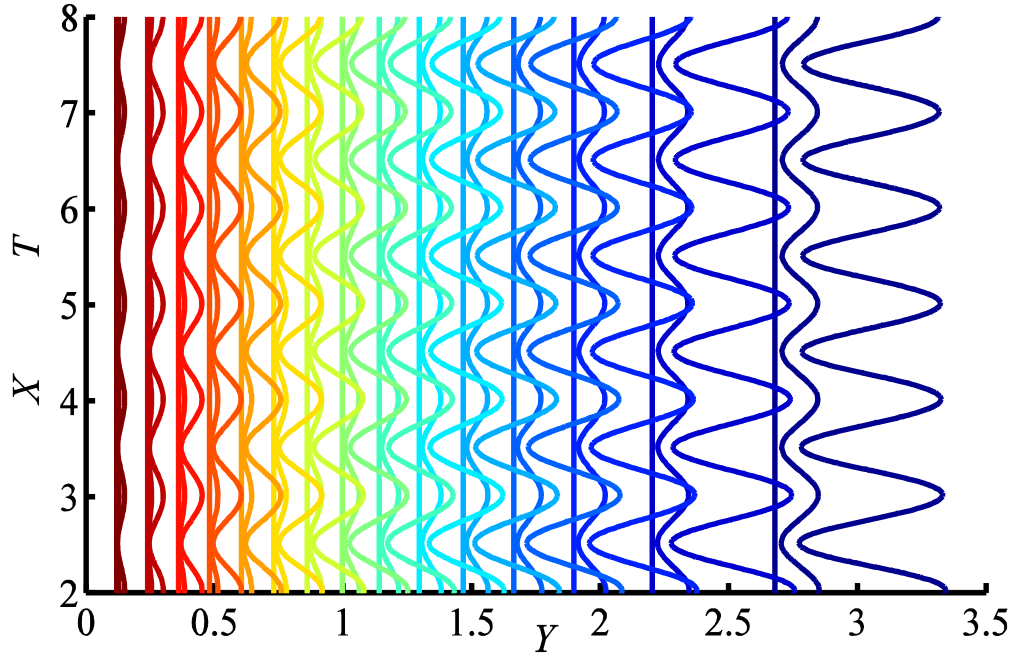


**Figure 5.12:** Isotherms plotted at different $\alpha$.

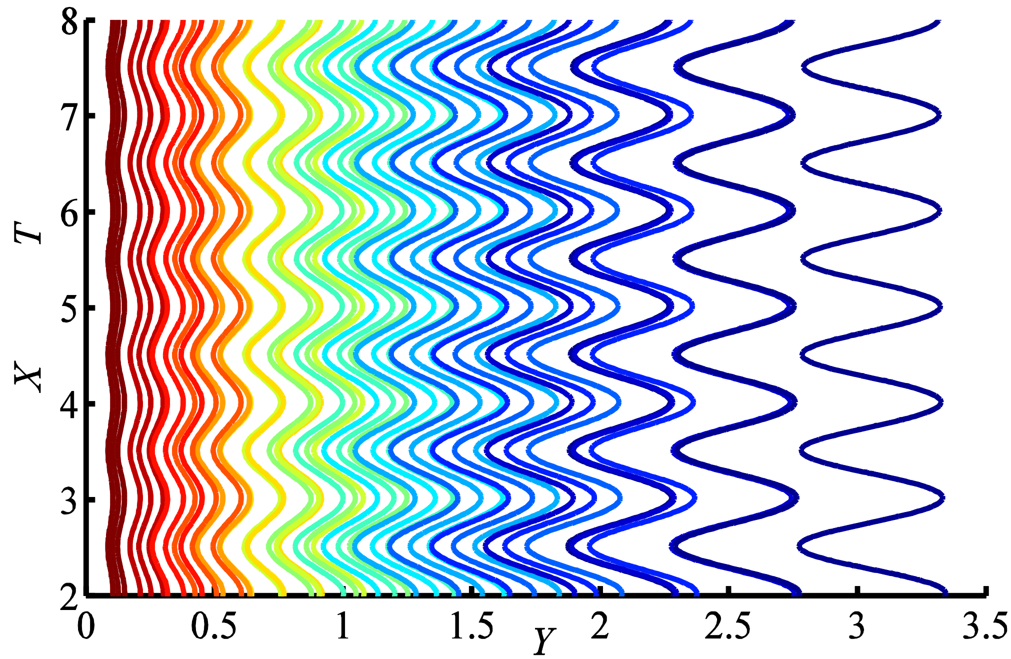


**Figure 5.13:** Effect of different $\phi$ on isotherms.

Similarly for oxides, maximum increase of about 10.3% in $Nu_{avg}$ is obtained for $Al_2O_3$ with 10% concentration in the base fluid and minimum decrease of about 5.2% in the value of $Nu_{avg}$ is obtained for $SiO_2$ with same concentration. The percent increase in $C_{f\,avg}$ and $Nu_{avg}$ is also calculated in comparison to $C_{f\,avg} = 0.6375$, $Nu_{avg} = 0.7455$ at $\alpha = \phi = 0.0$. For metals, maximum of 10.8% and 11.1% increase in $C_{f\,avg}$ and $Nu_{avg}$ is obtained and a minimum of 0.3% and 5.1% increase in $C_{f\,avg}$ and $Nu_{avg}$ is obtained, respectively. Similarly for oxides, maximum of 6.2% and 10.3% increase in $C_{f\,avg}$ and $Nu_{avg}$ is obtained and a minimum of 2.2% increase in $C_{f\,avg}$and 5.2% decrease in $Nu_{avg}$ is obtained, respectively. Through Table 5.6 it is easy to identify the role of surface roughness and of nanofluid towards heat transfer enhancement.

**Table 5.5:** Numerical values of $C_{f\,avg}$ and $Nu_{avg}$ for different nanoparticle when $Pr = 7.0,\ \alpha = 0.2,\ \phi = 0.1, \xi = 1.0$ .

| Nano particle material | $C_{f\,avg}$ | $Nu_{avg}$ |
|---|---|---|
| $Cu$ | 0.4973 | 0.7199 |
| $Au$ | 0.4588 | 0.6816 |
| $Ag$ | 0.5061 | 0.7155 |
| $Al_2O_3$ | 0.4845 | 0.7138 |
| $Fe_3O_4$ | 0.4765 | 0.6951 |
| $SiO_2$ | 0.4662 | 0.6130 |

**Table 5.6:** Percent change in $C_{f\,avg}$ and $Nu_{avg}$for different nanoparticles when $Pr = 7.0$, $\alpha = 0.2,\ \phi = 0.1, \xi = 1.0$ .

| Nano particle material | % increase in $C_{f\,avg}$ | | % increase in $Nu_{avg}$ | |
|---|---|---|---|---|
| | Versus $C_{f\,avg} = 0.6375$ at $\alpha = \phi = 0.0$ | Versus $C_{f\,avg} = 0.4560$ at $\alpha = 0.2, \phi = 0.0$ | Versus $Nu_{avg} = 0.7455$ at $\alpha = \phi = 0.0$ | Versus $Nu_{avg} = 0.6469$ at $\alpha = 0.2,\ \phi = 0.0$ |
| $Au$ | 0.3 | 0.6 | 5.1 | 5.3 |
| $Ag$ | 10.8 | 11.0 | 10.4 | 10.6 |
| $Cu$ | 8.9 | 9.1 | 11.1 | 11.3 |
| $Fe_3O_4$ | 4.4 | 4.5 | 7.4 | 7.5 |
| $Al_2O_3$ | 6.2 | 6.2 | 10.3 | 10.3 |
| $SiO_2$ | 2.2 | 2.2 | $-5.2$ | $-5.2$ |

## 5.4 Conclusion

Present chapter investigates the natural convection flow of nanofluid for five different types of nanoparticles, namely, copper ($Cu$), silver ($Ag$), alumina ($Al_2O_3$), magnetite ($Fe_3O_4$) and silica ($SiO_2$) with a valid range of nanoparticle concentration ($0-10\%$) by taking water as base fluid. An excellent agreement between the present results and already published data proves the validity of present results. Our analysis reveals that:

- The skin friction increases and the Nusselt number decreases by increasing the values of wavy amplitude $\alpha$.
- An increase in concentration of nanoparticles in the base fluid produces an increase in the skin friction coefficient and the local Nusselt number.
- Maximum increase in skin friction of about 10.9% for $Ag$ and in local Nusselt number of about 11.1% is obtained for $Cu$ with 10% concentration.
- Minimum increase in skin friction of about 2.2% and decrease in local Nusselt number of about 5.2% is observed for $SiO_2$ with 10% concentration.
- Maximum increase in average skin friction of about 11.0% for $Ag$ and in average Nusselt number of about 11.3% is obtained for $Cu$ with 10% concentration.

# Chapter 6

# Effect of heat generation/absorption on non-similar natural convection nanofluid flow along a vertical wavy surface

This chapter is the extension of problem in previous chapter towards the investigation of heat generation/absorption effect on natural convection heat transfer from a vertical wavy surface. Transport equations have been solved numerically by the same implicit finite difference scheme as utilized in the previous chapters. The result in the form of Nusselt number and skin friction coefficient are calculated and presented through graphs against the dimensionless constants for two types of nanoparticles, namely, alumina ($Al_2O_3$) and magnetite ($Fe_3O_4$). The impact of nanoparticle concentration on flow and heat transfer process in the problem under investigation has been studied in detail. The results indicate that $Al_2O_3$-water nanofluid exhibits higher skin friction and the heat transfer rate in comparison to $Fe_3O_4$ water based nanofluid. The influence of heat generation / absorption parameter is to decrease / increase (respectively) the heat transfer rate and increase / decrease (respectively) the skin friction coefficient. For heat generation / absorption cases percent change in the skin friction and Nusselt number for two nanoparticles is shown in tabular form where comparison to the flat plate (pure fluid) and wavy surface (pure fluid) cases has also been made. The present results have been validated by producing the results available in literature where a very good agreement is obtained.

## 6.1 Mathematical formulation

Similar to the previous chapter the two-dimensional incompressible, steady, natural convective flow of nanofluid along vertically fixed wavy plate has been considered. The configuration of the wavy sheet is described by the sinusoidal function described in Eq. (1.18) as already shown in Figure 5.1. It is assumed that all material properties of the fluid are constant except the density which varies with temperature. The wall temperature is denoted by $T_w$ where $T_\infty$ denotes the ambient temperature such that $T_w > T_\infty$. Temperature dependent heat generation / absorption is described as $Q(T - T_\infty)$ with $T \geq T_\infty$; the amount generated / absorbed per unit volume and $Q \gtrless 0$ is the heat generation / absorption constant. Due to the presence of temperature gradient near the wavy surface the flow is driven by the bouncy force. In view of the above flow assumptions the appropriate boundary conditions read as:

$$\begin{aligned} &\bar{y} = \bar{S}(\bar{x}): \bar{u} = 0, \bar{v} = 0, T = T_w, \quad \text{for all} \quad \bar{x} > 0, \\ &\bar{y} \to \infty: \bar{u} = 0, \bar{p} = p_\infty, T = T_\infty, \quad \text{for all} \quad \bar{x} > 0. \end{aligned} \tag{6.1}$$

### 6.1.1 Nanofluid: thermo-physical properties

The material properties such as density, effective dynamic viscosity, heat capacity, thermal expansion coefficient, effective thermal conductivity of pure fluid and nanoparticles are given in Table 1.2. In this chapter, we consider the alumina and magnetite nanoparticles. Alumina is the strongest and stiffest of the oxide ceramics and widely used material in engineering ceramics. Alumina has a relatively high thermal conductivity in ceramic. It has acceptable price therefore, its cost is less in fabricating alumina shapes. Magnetite is normal and one of the three common natural oxides of iron. It has great significance such as, magnetic recording media, high density digital recording disc, in drug delivery system, cancer therapy and medical diagnostic etc.

Based on theoretical and experimental findings, there are several different expressions for the calculation of the thermo-physical properties of the nanofluid given in Sec. 1.2.5 which have been utilized in the present analysis.

### 6.1.2 Governing equations

According to the flow assumptions discussed in Sec. 6.1 the flow is two-dimensional and steady in nature. The base fluid is assumed to be water at normal temperature which allows the utilization of boundary layer assumptions. The convective transport of the nanoparticles has been described by the famous Tiwari and Das model [32]. According to this model the mass, momentum and energy conservation laws read as

$$\frac{\partial \bar{u}}{\partial \bar{x}}+\frac{\partial \bar{v}}{\partial \bar{y}}=0, \qquad (6.2)$$

$$\bar{u}\frac{\partial \bar{u}}{\partial \bar{x}}+\bar{v}\frac{\partial \bar{u}}{\partial \bar{y}}=-\frac{1}{\rho_{nf}}\frac{\partial \bar{p}}{\partial \bar{x}}+\nu_{nf}\nabla^2\bar{u}+\frac{1}{\rho_{nf}}g(\rho\beta)_{nf}(T-T_\infty), \qquad (6.3)$$

$$\bar{u}\frac{\partial \bar{v}}{\partial \bar{x}}+\bar{v}\frac{\partial \bar{v}}{\partial \bar{y}}=-\frac{1}{\rho_{nf}}\frac{\partial \bar{p}}{\partial \bar{y}}+\nu_{nf}\nabla^2\bar{v}, \qquad (6.4)$$

$$\bar{u}\frac{\partial T}{\partial \bar{x}}+\bar{v}\frac{\partial T}{\partial \bar{y}}=\alpha_{nf}^{*}\nabla^2 T+(1/\left(\rho c_p\right)_{nf})Q(T-T_\infty), \qquad (6.5)$$

where $\boldsymbol{\nabla}^2$ is the Laplacian operator, $\bar{u}$ and $\bar{v}$ represent components of the velocity vector, $\rho$ represents the density, $c_p$ represents the specific heat, $\beta$ represents the thermal expansion coefficient, $\alpha$ is thermal diffusivity and subscripts "$f$", "$nf$" and "$p$" refer to fluid, nanofluid and nanoparticle, respectively.

To transform the transport equations to the dimensionless form where the domain of interest is, $0 \leq y<\infty;\ x>0$. We utilize the same variables and parameters defined in equation (5.7). Thus, eliminating the term $\partial\bar{p}/\partial\bar{y}$ by using the same argument as in Chapters 4 and 5 from equation (6.3). The system (6.2) – (6.4) in non-dimensionalized form reads as

$$u\frac{\partial u}{\partial x}+v\frac{\partial u}{\partial y}+\frac{\omega_\xi}{\omega}u^2=\frac{\omega^2}{d_1}\frac{\partial^2 u}{\partial y^2}+\frac{d_5}{\omega^2 d_2}\theta, \qquad (6.6)$$

$$u\frac{\partial \theta}{\partial x}+v\frac{\partial \theta}{\partial y}=\frac{d\omega^2}{d_3 Pr}\frac{\partial^2 \theta}{\partial y^2}+\frac{H}{d_3}\theta, \qquad (6.7)$$

where $H=Ql^2/\mu_f\, Gr^{\frac{1}{2}}\left(\rho c_p\right)_f$ is the heat generation/absorption parameter. Now we use the transformations given in equation (5.9) to render the governing equations to a more convenient form. In this way the governing equations in dimensionless form transform to the following non-linear partial differential equations

$$\frac{\omega^2}{d_1}f'''+\frac{3}{4}\,ff''-\xi(\frac{1}{2}+\frac{\omega_\xi}{\omega})f'^2+\frac{d_5}{\omega^2 d_2}\theta=\xi\left[f'\frac{\partial f'}{\partial \xi}-f''\frac{\partial f}{\partial \xi}\right], \qquad (6.8)$$

$$\frac{d\omega^2}{d_3 Pr}\theta''+\frac{3}{4}\,f\theta'+\xi^{1/2}\frac{H}{d_3}\theta=\xi\left[f'\frac{\partial \theta}{\partial \xi}-\theta'\frac{\partial f}{\partial \xi}\right], \qquad (6.9)$$

where $H \gtrless 0$ is the heat source/sink parameter. Boundary conditions in non-dimensional form read as

$$\left.\begin{array}{ll} f(\xi,0)=0,\ \ f'(\xi,0)=0, & \theta(\xi,0)=1, \\ f'(\xi,\infty)=0, & \theta(\xi,\infty)=0. \end{array}\right\} \tag{6.10}$$

The surface shear stress in terms of local friction factor, the local heat transfer rate in term of Nusselt number, average skin friction coefficient and average Nusselt number have been defined in the similar manner as did in Chapter 5.

## 6.2 Computational procedure and validation of results

The governing equations (6.8) – (6.10) which are non-similar in nature have been integrated through a finite difference scheme which is commonly referred as the Keller-box scheme. The detailed procedure of this method is presented in Chapter 4. For solving the system (6.8) – (6.10) the same procedure has been followed. It is well established that this technique gives quite exact results for boundary layer equations. The value $\eta_\infty = 20$ is taken sufficiently large for the convergence of solution. A uniform grid having step size $\Delta\eta = \Delta\xi = 0.005$ is utilized. Also, for the accuracy of solution the difference between the current and the previous iteration was fixed at $10^{-5}$ in order to stop the iteration process. For the validation of present solution computed data is compared with the already published results present in the open literature and is displayed in Tables 6.1, 6.2 and 6.3. The calculated values of $C_f$, $Nu$, $f''(0,0)$, and $\theta'(0,0)$ are compared with those of Alim et al. [112], Kabir et al. [115] and Hossain et al. [165]. It is obvious from these Tables that the values of $C_f$, $Nu$, $f''(0,0)$, and $\theta'(0,0)$ are very well matched with the already existing results.

**Table 6.1:** Comparison of $C_f$ and $Nu$ values when $\phi = 0, \alpha = 0.2, H = 0.0,\ \xi = 2.0$.

| $Pr$ | $C_f$ | | $Nu$ | |
|---|---|---|---|---|
| | present | Alim et al.[130] | Present | Alim et al.[130] |
| 0.72 | 0.74643 | 0.74641 | 0.33683 | 0.33715 |
| 1.5 | 0.66054 | 0.6690 | 0.43354 | 0.43391 |
| 3.0 | 0.58201 | 0.58220 | 0.54120 | 0.54159 |
| 4.5 | 0.53822 | 0.53827 | 0.61241 | 0.61277 |
| 7.0 | 0.49270 | 0.49260 | 0.69782 | 0.69810 |

**Table 6.2:** Comparison of values $C_f$ and $Nu$ when $\phi = 0, \alpha = 0.2, H = 0.5,\ \xi = 2.0$.

| $Pr$ | $C_f$ | | $Nu$ | |
|---|---|---|---|---|
| | present | Alim et al.[130] | Present | Alim et al.[130] |
| 0.72 | 0.96720 | 0.96548 | −0.31579 | −0.31624 |
| 1.5 | 0.92711 | 0.92773 | −0.62468 | −0.62799 |
| 3.0 | 0.90460 | 0.90585 | −1.2180 | −1.22414 |
| 4.5 | 0.90353 | 0.90512 | −1.8157 | −1.82501 |
| 7.0 | 0.91563 | 0.91769 | −2.8271 | −2.84207 |

**Table 6.3:** Comparison of $f''(0, 0)$ and $-\theta'(0, 0)$ values when $\phi = 0, \alpha = 0.2, H = 0$.

| $Pr$ | $f''(0,0)$ | | | | $-\theta'(0,0)$ | | | |
|---|---|---|---|---|---|---|---|---|
| | Present | Hossain et al. [165] | Alim et al. [112] | Kabir et al. [115] | Present | Hossain et al. [165] | Alim et al. [112] | Kabir et al. [115] |
| 1 | 0.9082 | 0.908 | 0.90814 | 0.90813 | 0.4010 | 0.401 | 0.40101 | 0.40102 |
| 10 | 0.5928 | 0.591 | 0.59269 | 0.59270 | 0.8268 | 0.825 | 0.82663 | 0.82662 |
| 25 | 0.4876 | 0.485 | 0.48733 | 0.48732 | 1.0690 | 1.066 | 1.06847 | 1.06848 |
| 50 | 0.4176 | 0.485 | 0.41727 | 0.41728 | 1.2896 | 1.066 | 1.28879 | 1.28878 |
| 100 | 0.3559 | 0.352 | 0.35559 | 0.35558 | 1.5495 | 1.542 | 1.54827 | 1.54828 |

## 6.3 Results and discussion

In this section we have analyzed the effects of heat source/sink ($H \gtrless 0$) parameter; waviness parameter ($\alpha$) and nanoparticle concentration ($\phi$) on the free convection flow of nanofluid over a vertical wavy surface. The physical parameters of primary interest are the skin friction ($C_f$) and the Nusselt number ($Nu$). These quantities are obtained and shown in Eq. (5.15). The computations are carried out for two kinds of nanoparticles assuming water as base fluid; range of nanoparticle concentration ($\phi$) is taken from 0 to 0.1. The nanoparticles used in this study are alumina ($Al_2O_3$) and magnetite ($Fe_3O_4$). The distributions of the $C_f$ and $Nu$ in the case of $Al_2O_3$-water and $Fe_3O_4$-water are plotted in Figs. 6.2 to 6.10. Numerical values of $C_f$ and $Nu$ are tabulated in Tables 6.4 and 6.5 for heat generation/absorption parameter $H(\gtrless 0)$.

The influence of heat source/sink ($H \gtrless 0$); waviness parameter ($\alpha$), and nanoparticle concentration ($\phi$) on $C_f$ and $Nu$ are presented in Figs. 6.2 to 6.6 for two nanoparticles alumina and magnetite. The Figs. 6.2 and 6.3 illustrate the behavior of heat source/sink parameter, *($H \gtrless 0$)*, on the $C_f$ and $Nu$. Decrease in $Nu$ and increase in $C_f$ is observed by increase in the value of heat source ($H > 0$), whereas the inverse behavior is captured for the value of heat absorption ($H < 0$). Because the increase in heat source ($H > 0$) enhances temperature inside the boundary layer which results in decrease in $Nu$ and the increase in heat absorption ($H < 0$) forms a layer of cold fluid near the heated surface which results in increase in $Nu$. It is noted that for the case of alumina more increment in the values of $C_f$ and $Nu$ are attained as compared to magnetite. The Fig. 6.4 illustrates the effects of wavy amplitude on $C_f$ in the presence of heat generation/absorption ($H = \pm 2$). It is observed that $C_f$ decreases with the increase of waviness parameter. Effects of nanoparticle concentration on $C_f$ and $Nu$ in the presence of heat generation / absorption ($H = \pm 2$) are shown in Figs. 6.5 and 6.6. It is noted from these graphs that as the nanoparticle concentration increases, the viscous force of the nanofluid increases. Rate of flow is decreased due to more resistive fluid and $C_f$ is increased. Also, it is noted that the heat transfer rate reduces with the increment in the nanoparticles concentration at heat source ($H = +2$) whereas, heat transfer rate rises with the increment in the nanoparticles concentration in the heat absorption situation ($H = -2$). Obviously, the $Nu$ is higher in case of $Al_2O_3$-nanoparticle as compared to $Fe_3O_4$-nanoparticle.

Dimensionless $C_f$ and $Nu$ as a function of wavy amplitude, nanoparticle concentration, and heat generation parameter for two nanoparticles alumina and magnetite water based nanofluid are plotted in Figs. 6.7 to 6.10 at fixed $\xi = 0.5$ and $Pr = 7.0$. Figure 6.7 illustrates the variation in the $Nu$ as function of waviness parameter $\alpha$ for the said two nanoparticles. Upon increasing the values of waviness parameter the $Nu$ decreases and is greater for alumina nanoparticle as compared to magnetite nanoparticle. Figure 6.8 depicts the variation in the $Nu$ as a function of nanoparticle concentration for two nanoparticles. Here, we see that the $Nu$ rises for denser concentration of the nanoparticles. Figures 6.9 and 6.10 show the behavior of $C_f$ and $Nu$ as function of heat generation/absorption ($H \gtrless 0$) parameter. From these Figures it is observed that $C_f$ increases and $Nu$ decreases with increasing the heat source parameter ($H > 0$) whereas $C_f$ decreases and $Nu$ increases with increasing the heat absorption parameter ($H < 0$) . Also, these Figures reveal that $Al_2O_3$-nanoparticles exhibits better enhancement as compared to $Fe_3O_4$-nanoparticle.

In Tables 6.4 and 6.5 percent change in $C_f$ and $Nu$ are calculated for heat generation/absorption $(H \gtreqless 0)$ at different positions, i.e. $\xi = 0.5$, $\xi = 1.0, \xi = 1.5$ and $\xi = 2.0$ on the wavy surface by comparing the values with flat plate (pure fluid) and wavy surface (pure fluid) results. Table 6.4 reveals that the overall maximum increase in $C_f$ and decrease in $Nu$ is found in comparison to flat surface (pure fluid). In comparison to flat surface maximum increase in $C_f$ is 34.4% for alumina nanoparticle at $\xi = 1.5$ and highest decrease in $Nu$ is 169.6% for magnetite nanoparticle at $\xi = 2.0$. Also, in comparison to (pure fluid) wavy surface highest increase in $C_f$ is 8.3% for alumina nanoparticle at $\xi = 2.0$ and highest decrease in $Nu$ is 89.1% for magnetite nanoparticle at $\xi = 1.5$. Table 6.5 shows that the overall maximum decrease in $C_f$ and increase in $Nu$ is found in comparison to flat surface (pure fluid). In comparison to flat surface highest decrease in $C_f$ is 36.4% for magnetite nanoparticle at $\xi = 2.0$ and highest increase in $Nu$ is 119.9% for alumina nanoparticle at $\xi = 2.0$. Also, in comparison to (pure fluid) wavy surface highest increase in $C_f$ is 5.4% for alumina nanoparticle at $\xi = 0.5$ and highest increase in $Nu$ is 14.3% for alumina nanoparticle at $\xi = 2.0$.

**Table 6.4:** Percent change in $C_f$ and $Nu$ for different nanoparticles when $Pr = 7.0$, $\alpha = 0.2, \phi = 0.1, H = 0.2, \xi = 1.0$.

| $\xi$ | Nano particle material | % increase in $C_f$ | | % increase in $Nu$ | |
|---|---|---|---|---|---|
| | | Versus<br>$f''(0,0) = 0.6375$,<br>$f''(0,0) = 0.6375$,<br>at $\alpha = \phi = 0.0$,<br>$H = 0.0$. | Versus<br>$f''(0.5,0) = 0.7279$,<br>$f''(1.0,0) = 0.5840$,<br>$f''(1.5,0) = 0.7948$,<br>$f''(2.0,0) = 0.6309$,<br><br>at $\alpha = 0.2$, $\phi = 0.0$,<br>$H = 0.2$. | Versus<br>$Nu(0,0) = 0.7455$,<br>at $\alpha = \phi = 0.0$,<br>$H = 0.0$. | Versus<br>$Nu(0.5,0) = 0.2651$,<br>$Nu(1.0,0) = 0.0024$,<br>$Nu(1.5,0) = -0.1575$<br>$Nu(2.0,0) = -0.3427$,<br><br>at $\alpha = 0.2$, $\phi = 0.0$,<br>$H = 0.2$. |
| 0.5 | $Al_2O_3$ | 22.2 | 7.1 | −67.6 | −8.8 |
| | $Fe_3O_4$ | 20.5 | 5.6 | −70.0 | −15.7 |
| 1.0 | $Al_2O_3$ | −17.2 | 7.6 | −110.8 | −32.4 |
| | $Fe_3O_4$ | −2.8 | 6.0 | −113.0 | −39.2 |
| 1.5 | $Al_2O_3$ | 34.3 | 7.8 | −137.6 | −77.8 |
| | $Fe_3O_4$ | 32.6 | 6.3 | −140.0 | −89.1 |
| 2.0 | $Al_2O_3$ | 8.1 | 8.3 | −167.4 | −46.6 |
| | $Fe_3O_4$ | 5.9 | 7.0 | −169.6 | −51.4 |

**Table 6.5:** Percent change in $C_f$ and Nu for different nanoparticle when $Pr = 7.0,$ $\alpha = 0.2, \phi = 0.1, H = -0.2, \xi = 1.0.$

| $\xi$ | Nano particle material | % increase in $C_f$ | | % increase in $Nu$ | |
|---|---|---|---|---|---|
| | | Versus $f''(0,0) = 0.6375,$ at $\alpha = \phi = 0.0,$ $H = 0.0.$ | Versus $f''(0.5,0) = 0.5768,$ $f''(1.0,0) = 0.4175,$ $f''(1.5,0) = 0.5302,$ $f''(2.0,0) = 0.3934,$ at $\alpha = 0.2, \phi = 0.0,$ $H = -0.2.$ | Versus $Nu(0,0) = 0.7455,$ at $\alpha = \phi = 0.0,$ $H = 0.0.$ | Versus $Nu(0.5,0) = 0.1.1259,$ $Nu(1.0,0) = -1.2456,$ $Nu(1.5,0) = -1.3806$ $Nu(2.0,0) = -1.4340,$ at $\alpha = 0.2, \phi = 0.0,$ $H = -0.2.$ |
| 0.5 | $Al_2O_3$ | $-4.5$ | 5.4 | 71.0 | 13.2 |
| | $Fe_3O_4$ | $-6.3$ | 3.5 | 67.6 | 11.0 |
| 1.0 | $Al_2O_3$ | $-31.0$ | 5.3 | 90.0 | 13.7 |
| | $Fe_3O_4$ | $-32.3$ | 3.3 | 86.3 | 11.6 |
| 1.5 | $Al_2O_3$ | $-12.6$ | 5.0 | 111.1 | 14.0 |
| | $Fe_3O_4$ | $-14.3$ | 3.0 | 107.2 | 11.9 |
| 2.0 | $Al_2O_3$ | $-35.1$ | 5.0 | 119.9 | 14.3 |
| | $Fe_3O_4$ | $-36.4$ | 3.0 | 115.9 | 12.2 |

Numerical values of ${C_f}_{avg}$ and $Nu_{avg}$ are tabulated in Table 6.6 and the Table 6.7 while Table 6.8 shows percent change in ${C_f}_{avg}$ and $Nu_{avg}$ for $Al_2O_3$ and $Fe_3O_4$ nanoparticles when $Pr = 7.0,\ \alpha = 0.2, \phi = 0.1,\ \xi = 1.0$ , in comparison to pure flat and wavy plate for heat generation absorption parameter ($H \gtrless 0$). Table 6.7 reveals that the overall maximum increase of about 5.3% in ${C_f}_{avg}$ is obtained for $Al_2O_3$ with 10% concentration in the base fluid and minimum increase of about 3.3% in the value of average skin friction is obtained for $Fe_3O_4$ with 10% concentration when the present results are compared with the value ${C_f}_{avg} = 0.3876$ at $\alpha = 0.2, H = -0.2$ and $\phi = 0.0$. On the other hand maximum increase of 76.3% in ${C_f}_{avg}$ is obtained for $Al_2O_3$ and minimum of 73% for $Fe_3O_4$ with 10%

concentration in the base fluid when the present results are compared with $Nu_{avg} = 1.1537$, at $\alpha = 0.2$, $\phi = 0.0$, $H = -0.2$. Table 6.8 shows that an overall increase in $C_{f\,avg}$ and $Nu_{avg}$ is found in comparison to wavy surface (pure fluid) and flat surface (pure fluid). In comparison to wavy surface highest increase in $C_{f\,avg}$ is 7.8% and highest increase in $Nu_{avg}$ is 46.2% for alumina nanoparticle at $H = 0.2$. Also, in comparison to (pure fluid) flat surface highest decrease in $C_{f\,avg}$ is 22.9% and highest increase in $Nu_{avg}$ is 2.06% for magnetite nanoparticle at $H = 2.0$.

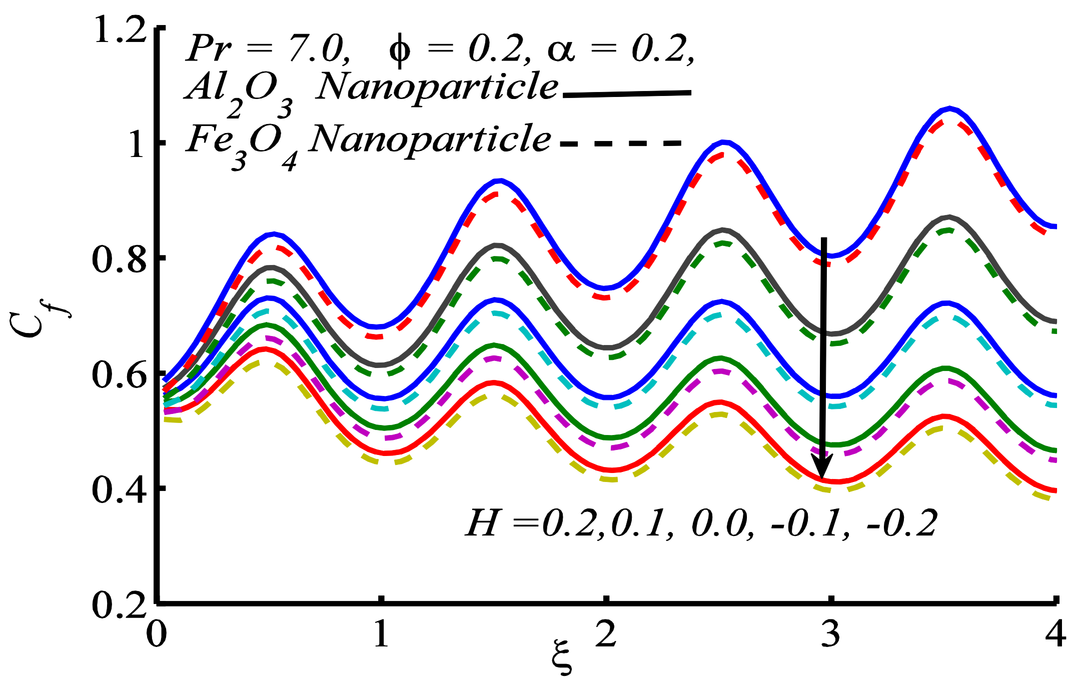


**Figure 6.2:** Heat generation/absorption effects on skin friction.

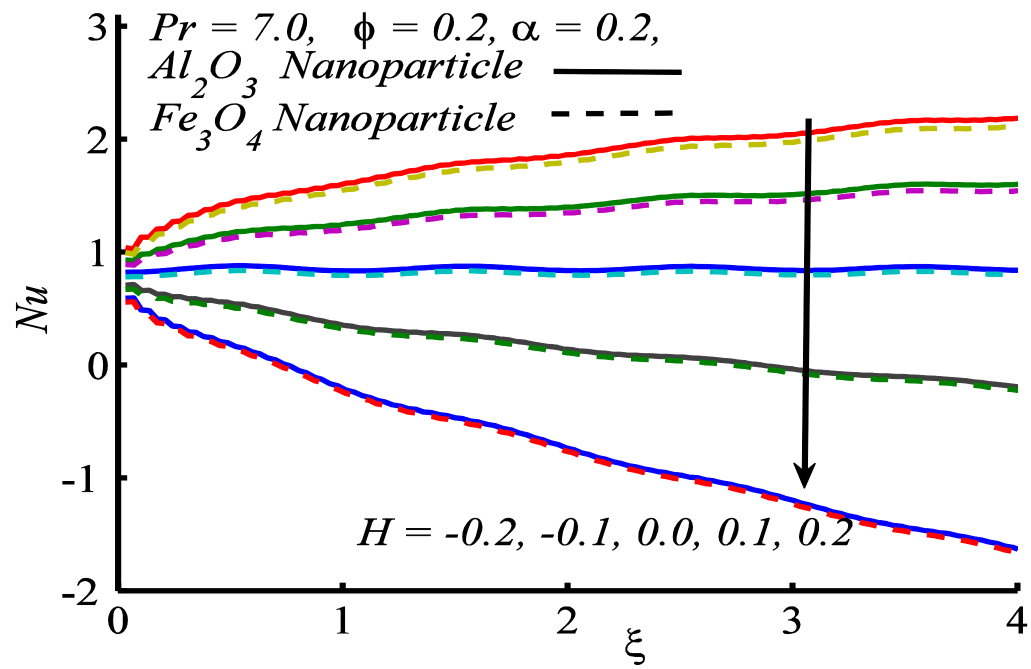


**Figure 6.3:** Heat generation/absorption effects on Nusselt number.

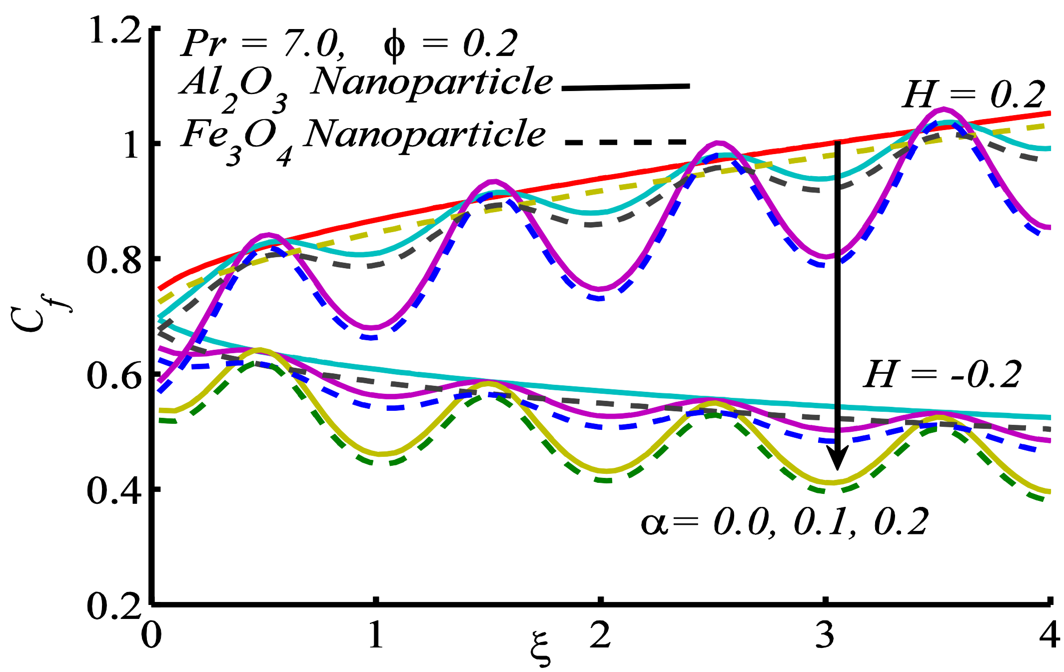


**Figure 6.4:** Effect of $\alpha$ on $C_f$.

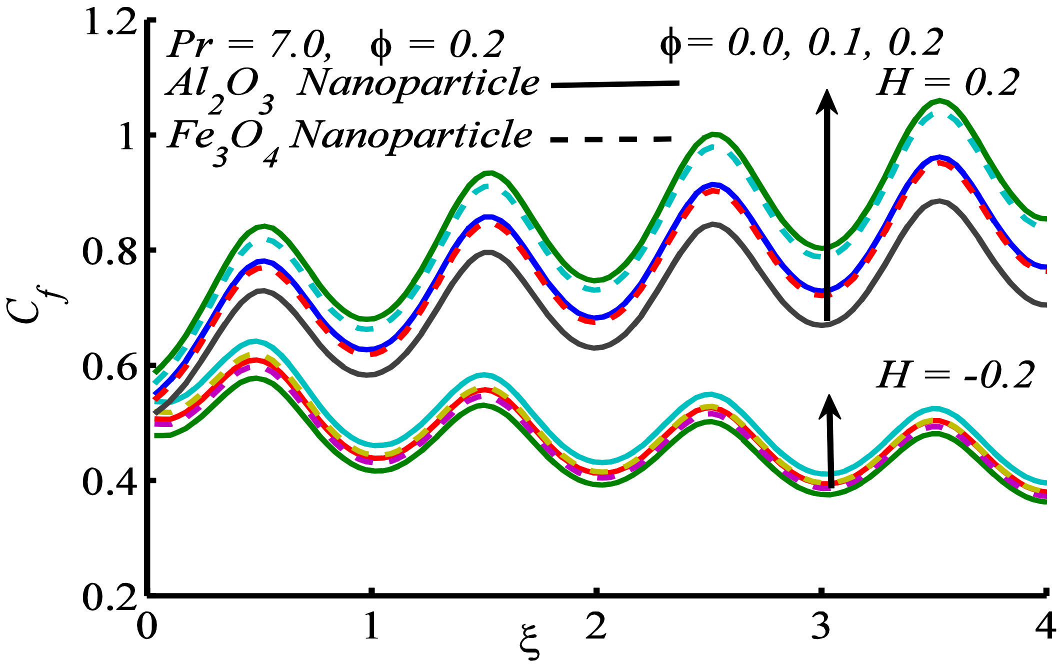


**Figure 6.5:** Graph of $C_f$ influenced by $\phi$.

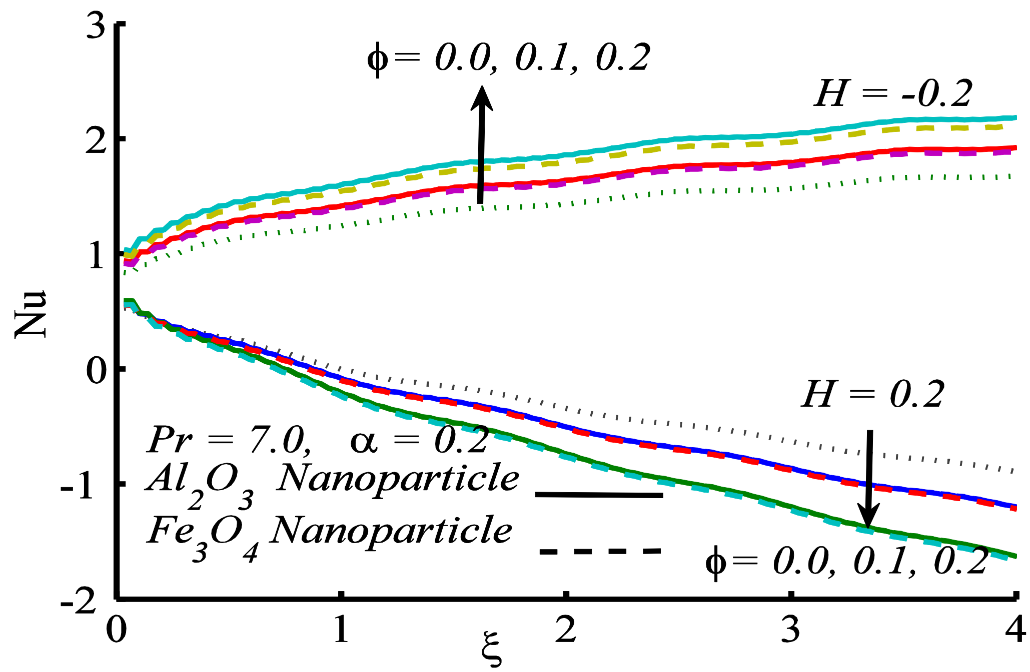


**Figure 6.6:** Impact of $\phi$ on Nusselt number.

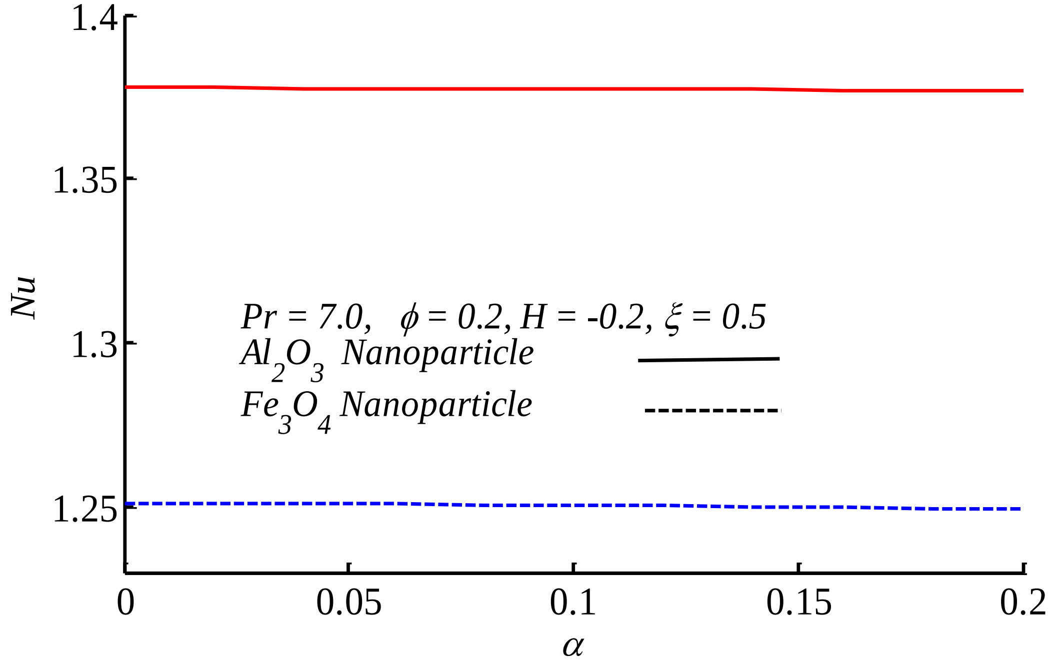


**Figure 6.7:** Variation of Nusselt number against $\alpha$.

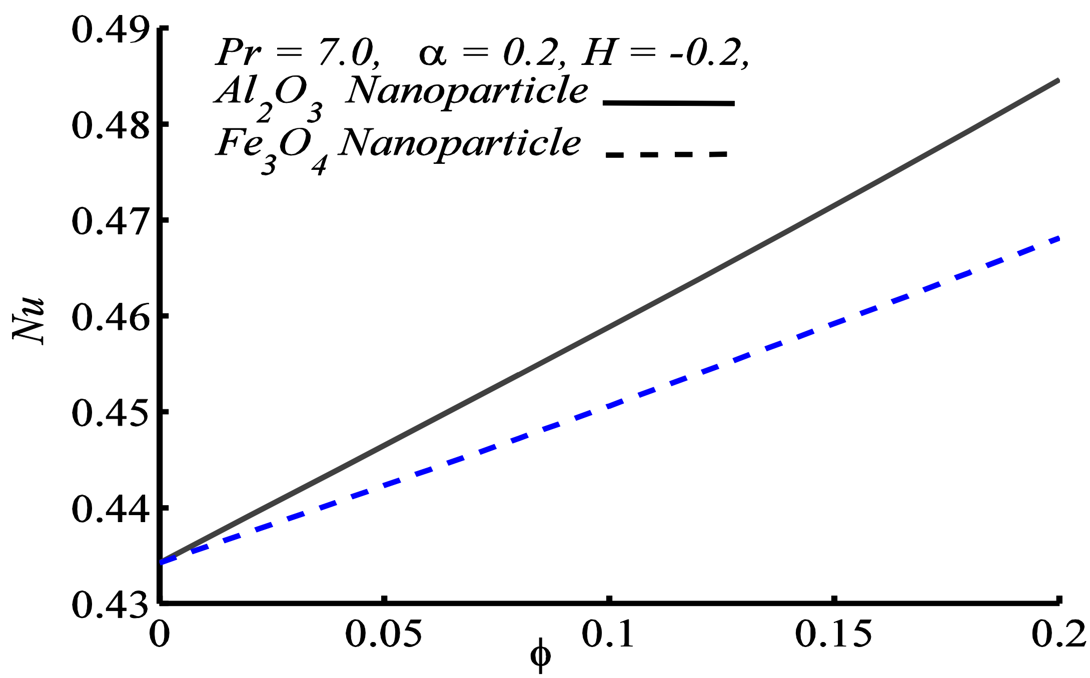


**Figure 6.8:** Nusselt Number variation against $\phi$.

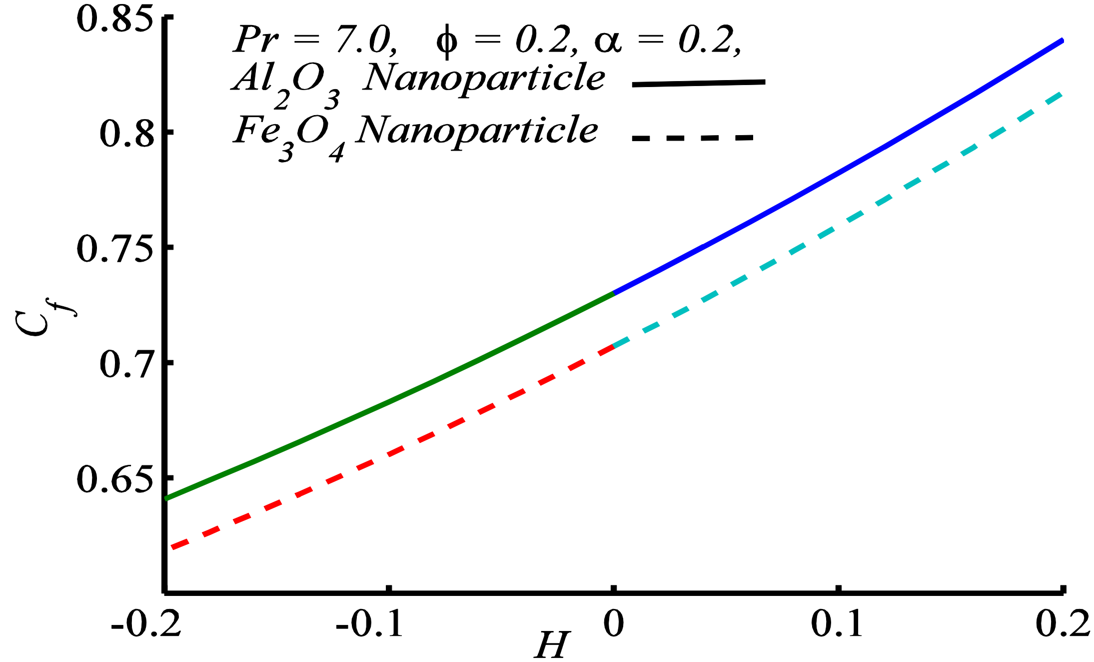


**Figure 6.9:** $C_f$ versus $H$.

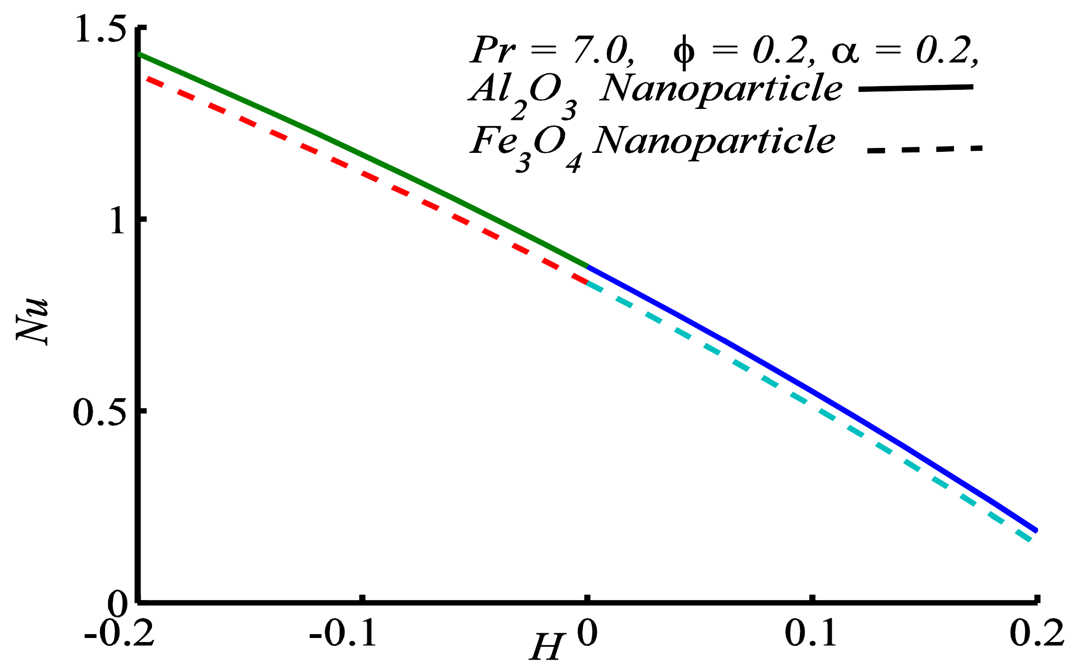


**Figure 6.10:** Nusselt number behavior against $H$.

**Table 6.6:** Numerical values of ${C_f}_{avg}$ and $Nu_{avg}$ for different nanoparticles when $Pr = 7.0,\ \alpha = 0.2,\ \phi = 0.1, \xi = 1.0$.

| Nanoparticle material | ${C_f}_{avg}$ | $Nu_{avg}$ | ${C_f}_{avg}$ | $Nu_{avg}$ |
|---|---|---|---|---|
| | at $H = -0.2$. | | at $H = 0.2$. | |
| $Al_2O_3$ | 0.4082 | 1.3143 | 0.5843 | $-0.0744$ |
| $Fe_3O_4$ | 0.4005 | 1.2897 | 0.5751 | $-0.0897$ |

**Table 6.7:** Percent change in ${C_f}_{avg}$ and $Nu_{avg}$ for different nanoparticles when $Pr = 7.0$, $\alpha = 0.2,\ \phi = 0.1, \xi = 1.0, H = -0.2$ .

| Nano particle material | % increase in ${C_f}_{avg}$ | | % increase in $Nu_{avg}$ | |
|---|---|---|---|---|
| | Versus ${C_f}_{avg} = 0.6375$, at $\alpha = \phi = 0.0$, $H = 0.0$. | Versus ${C_f}_{avg} = 0.3876$, at $\alpha = 0.2$, $\phi = 0.0$, $H = -0.2$. | Versus $Nu_{avg} = 0.7455$, at $\alpha = \phi = 0.0$, $H = 0.0$. | Versus $Nu_{avg} = 1.1537$, at $\alpha = 0.2$, $\phi = 0.0$, $H = -0.2$. |
| $Al_2O_3$ | $-36.0$ | 5.3 | 76.3 | 13.9 |
| $Fe_3O_4$ | $-37.2$ | 3.3 | 73.0 | 11.8 |

**Table 6.8:** Percent change in ${C_f}_{avg}$ and $Nu_{avg}$ for different nanoparticles when $Pr = 7.0$, $\alpha = 0.2,\ \phi = 0.1, \xi = 1.0, H = 0.2$.

| Nano particle material | % increase in ${C_f}_{avg}$ | | % increase in $Nu_{avg}$ | |
|---|---|---|---|---|
| | Versus ${C_f}_{avg} = 0.7463$, at $\alpha = \phi = 0.0$, $H = 0.2$. | Versus ${C_f}_{avg} = 0.5420$, at $\alpha = 0.2$, $\phi = 0.0$, $H = 0.2$. | Versus $Nu_{avg} = 0.0846$, at $\alpha = \phi = 0.0$, $H = 0.2$. | Versus $Nu_{avg} = -0.0019$, at $\alpha = 0.2$, $\phi = 0.0$, $H = 0.2$. |
| $Al_2O_3$ | $-21.7$ | 7.8 | $-1.8$ | 38.1 |
| $Fe_3O_4$ | $-22.9$ | 6.1 | $-2.06$ | 46.2 |

## 6.4 Concluding remarks

In this chapter, the impact of heat generation/absorption for two types of nanoparticles on natural convection boundary layer flow along vertical wavy surface has been investigated. For this problem the Tiwari and Das model which includes the nanoparticle concentration, viscosity and thermal conductivity has been adapted. Natural convective flow and heat transfer along the vertical wavy surface in nanofluid containing two types of nanoparticles, namely, alumina ($Al_2O_3$) and magnetite ($Fe_3O_4$) have been studied. Influence of emerging parameters such as, nanoparticle volume fraction ($\phi$), heat generation/absorption ($H \gtrless 0$) and wavy amplitude ($\alpha$) on Nusselt number ($Nu$) and skin friction coefficient ($C_f$) for both the nanofluids have been examined. The important results of the current study are summarized as follows:

- $C_f$ is an increasing/decreasing function of heat generation/absorption parameter and the local Nusselt number is decreasing/increasing function of heat generation/absorption parameter, respectively.
- $Nu$ increases and $C_f$ decreases with increasing amplitude of wavy surface for fixed value of heat absorption parameter.
- On increasing nanoparticle concentration the $C_f$ and $Nu$ increase for heat absorption parameter.
- $C_f$ and $Nu$ are observed higher for Alumina in comparison to Magnetite nanoparticle.
- ${C_f}_{avg}$ and $Nu_{avg}$ are observed higher for Alumina in comparison to Magnetite nanoparticle.
- Highest increase in $Nu_{avg}$ is 46.2% for alumina nanoparticle at $H = 0.2$.

# Chapter 7

# Heat transfer phenomena in natural convection flow of nanofluid past a vertical wavy cone

The problem of natural convective heat transfer phenomenon due to water-based nanofluid from a wavy cone is investigated in this chapter. Analysis is performed to study the heat transfer augmentation due to five types of nanoparticles, namely, alumina ($Al_2O_3$), copper ($Cu$), silver ($Ag$), copper oxide ($CuO$) and titania ($TiO_2$). The flow has been assumed to be steady and fluid properties have been supposed to be constant except for the density depending upon temperature giving rise to the buoyancy force. Famous Tiwari and Das model of nanofluid has been utilized in this study. The effects of cone half angle $\gamma$ and amplitude of the waviness $\alpha$ on the Nusselt number ($Nu$) and skin friction coefficient ($C_f$) are studied. A comparison is made with the case of pure fluid flow past a wavy cone at different values of $\alpha$. It has been observed that the $TiO_2$-nanoparticles have happened to show the maximum cooling performance and $Cu$-nanoparticle appeared to have maximum heating performance in this study. The results shown in this research could serve as a reasonable source of reference for taming the natural convection heat transfer enhancement along wavy cone. Present results are matched with the already published work for pure fluid and are shown to be in good agreement.

## 7.1 Mathematical formulation

Consider the natural convection flow adjacent to a vertical cone with transverse wavy surface having constant temperature $T_w$ where the constant ambient temperature is denoted by $T_\infty$. It is supposed that the cone surface is hotter than the ambient fluid, i.e. ($T_w > T_\infty$). The coordinate system is selected in such a way that $\bar{x}$ −axis runs from the apex of the non-wavy cone and the $\bar{y}$ −axis is measured normally out word as depicted in Fig. 7.1. The density of fluid depends upon temperature while other properties are supposed to be constant. Different empirical mathematical models are available for the modeling of nanofluid based on the homogeneous distribution of the nanoparticle, see for instance Sec.1.5. The most popular models are due to Buongiorno [31] and Tiwari and Das [32]. Because of mathematical convenience the Tiwari and Das model is preferred by most of the researchers dealing with nanofluids. In this model only the volume fraction, the particle dimensions and the material properties are important.

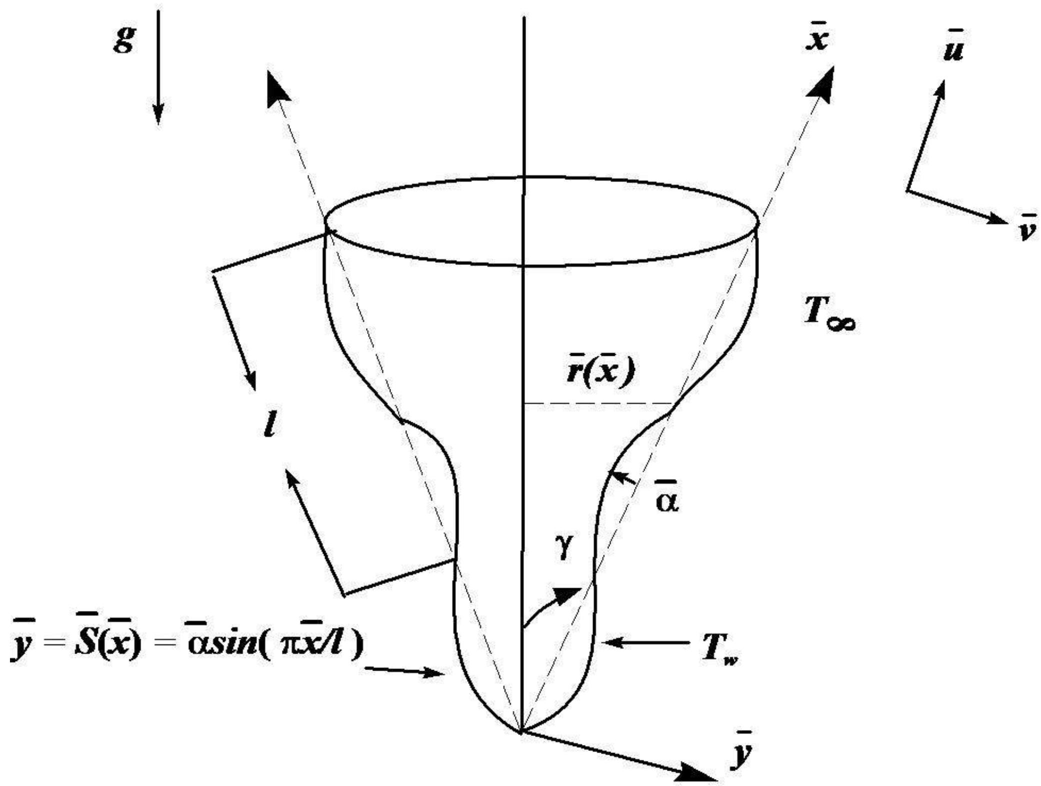


**Figure 7.1:** Flow geometry and coordinate system.

This improved density of the nanofluid plays important role in the free convection flow which is mainly established due to the gravitational body force. Because of the absence of circular component of velocity the flow is essentially two-dimensional. According to the Tiwari and Das Model [32] the mass, momentum and energy conservation laws after the consideration of above assumptions read as:

Mass

$$\frac{\partial(\bar{r}\bar{u})}{\partial\bar{x}} + \frac{\partial(\bar{r}\bar{v})}{\partial\bar{y}} = 0, \tag{7.1}$$

Momentum

$$\bar{u}\frac{\partial \bar{u}}{\partial \bar{x}}+\bar{v}\frac{\partial \bar{u}}{\partial \bar{y}}=-\frac{1}{\rho_{nf}}\frac{\partial \bar{p}}{\partial \bar{x}}+\nu_{nf}\nabla^2\bar{u}+\frac{1}{\rho_{nf}}g(\rho\beta)_{nf}(T-T_\infty)cos\gamma, \tag{7.2}$$

$$\bar{u}\frac{\partial \bar{v}}{\partial \bar{x}}+\bar{v}\frac{\partial \bar{v}}{\partial \bar{y}}=-\frac{1}{\rho_{nf}}\frac{\partial \bar{p}}{\partial \bar{y}}+\nu_{nf}\nabla^2\bar{v}-\frac{1}{\rho_{nf}}g(\rho\beta)_{nf}(T-T_\infty)sin\gamma, \tag{7.3}$$

Energy

$$\bar{u}\frac{\partial T}{\partial \bar{x}}+\bar{v}\frac{\partial T}{\partial \bar{y}}=\alpha_{nf}^{*}\nabla^2 T, \tag{7.4}$$

where $\gamma$ is cone half angle. The local radius $\bar{r}$ of the corresponding cone flat surface is described as $\bar{r}(\bar{x}) = \bar{x}sin\gamma$ and the sinusoidal wavy surface is shown in Fig. 7.1.

The applicable boundary conditions in the perspective of the flow assumptions read as

$$\begin{aligned} &\bar{y}=\bar{S}(\bar{x}): \bar{u}=0, \bar{v}=0, T=T_w\,, \\ &\bar{y}\to\infty: \bar{u}=0, \bar{p}=p_\infty, T=T_\infty\,. \end{aligned} \tag{7.5}$$

In accordance with the cone geometry we use stream function related to the velocity components as $rv=-\partial\psi/\partial x$ , $ru=\partial\psi/\partial y$, due to which the equation of continuity is satisfied identically. In order to normalize the system, we utilize the suitable set of new variables given by

$$\xi=x=\frac{\bar{x}}{l}\,, y=\frac{\bar{y}}{l}, r=\frac{\bar{r}}{l}=\ \xi\ sin\gamma, \eta=\xi^{-\frac{1}{4}}\frac{\bar{y}-\bar{S}(\bar{x})}{l}Gr^{\frac{1}{4}}\,, u=\frac{\rho_f\,l}{\mu_f}Gr^{-\frac{1}{2}}\,\bar{u}\ ,$$

$$v=\frac{\rho_f\,l}{\mu_f}Gr^{-\frac{1}{4}}\big(\bar{v}-S_\xi\bar{u}\big), S=\frac{\bar{S}(\bar{x})}{l}, \theta(\xi\,,\eta)=\frac{T-T_\infty}{T_w-T_\infty}, \tag{7.6}$$

$$\psi(\xi\,,\eta)=\xi^{\frac{3}{4}}f(\xi\,,\eta), p=\frac{l^2}{\nu^2\rho_f}Gr^{-\frac{1}{4}}\,\bar{p}\,, Gr=\frac{g\beta_f(T_w-T_\infty)l^3}{\nu_f^2},$$

which transform the system (7.2) – (7.5) to the following form

$$\frac{\omega^2}{\mathrm{d}_1}f'''+\frac{7}{4}\,ff''-(\frac{1}{2}+\frac{\omega_\xi}{\omega}\xi)f'^2+\frac{\mathrm{d}_5(1-\omega_\xi Tan\xi)}{\mathrm{d}_2\omega^2}\theta=\xi\left[f'\frac{\partial f'}{\partial\xi}-f''\frac{\partial f}{\partial\xi}\right], \tag{7.7}$$

$$\frac{\mathrm{d}\omega^2}{\mathrm{d}_3 Pr}\theta''+\frac{7}{4}\,f\theta'=\xi\left[f'\frac{\partial\theta}{\partial\xi}-\theta'\frac{\partial f}{\partial\xi}\right], \tag{7.8}$$

$$\left.\begin{aligned} f(\xi\,,0)=\ f'(\xi\,,0)\ =\ \theta(\xi\,,0)-1=0,\\ f'(\xi\,,\infty)=\ \theta(\xi\,,\infty)=0. \end{aligned}\right\} \tag{7.9}$$

Here $\mathrm{d}\,,\mathrm{d}_1,\mathrm{d}_2\,,\mathrm{d}_3$ and $\mathrm{d}_5$ are the material parameters given in equations (4.15) and (5.13), $Gr$ is the Grashof number, $\omega$ is wavy contribution and $Pr$ is the Prandtl number.

The wall shear stress and the surface heat flux are the physical quantities of interest which are necessarily required for the determination of local skin friction coefficient and the local Nusselt number. In view of the non-dimensional transformations (7.6), their final expressions read as:

$$\left.\begin{aligned} C_f &= C_{fx}\left(\frac{Gr}{x}\right)^{\frac{1}{4}} = \frac{\omega}{(1-\phi)^{2.5}}\, f''(\xi\,,0), \\ Nu &= Nu_x(Grx^3)^{-1/4} = -\omega d\theta'(\xi\,,0). \end{aligned}\right\} \tag{7.10}$$

The average skin friction and average Nusselt have been described as

$$\begin{aligned} C_{f_{avg}} &= \frac{1}{\mathbb{S}}\int_0^{\xi} \frac{x^{\frac{1}{4}}\omega^2}{(1-\phi)^{2.5}}\, f''(\xi\,,0)d\xi, \\ Nu_{avg} &= -\frac{1}{\mathbb{S}}\int_0^{\xi} dx^{\frac{3}{4}}\omega^2\theta'(\xi\,,0)d\xi. \end{aligned} \tag{7.11}$$

## 7.2 Solution procedure

Using implicit finite difference numerical scheme as discussed in Chapter 4, the transport equations (7.7) and (7.8) together with the boundary conditions (7.9) have been solved by this procedure. The solution was supposed to have converged and the iterative process was stopped when the comparative difference between the current and the previous iterations reached $10^{-5}$.

In order to validate the precision of the current technique, we have matched our outcomes with those of Hearing [60], Roy [61], Yih [64], Pop and Na [160-161] and Singh et al. [187] for the skin friction coefficient $C_{fx}(Gr/x)^{\frac{1}{4}}$ and local Nusselt number $Nu_x(Grx^3)^{-1/4}$ in Table 3.1. The comparisons are found to be a superb match in all the above cases. After ensuring the accuracy of the current procedure we have employed it to the current problem.

## 7.3 Results and discussion

In this analysis we have shown the effects of amplitude of wavy surface, nanoparticle concentration, and cone half angle on the natural convection flow of nanofluid past a vertical wavy cone. The skin friction coefficient ($C_f$) and the Nusselt number ($Nu$) are the important physical quantities that are necessary to be examined. The $C_f$ and $Nu$ plots are shown in Figs. 7.2 – 7.7 when $Cu$-water based nanofluid is considered. Nanoparticle concentration $\phi$ varies from 0 – 10 % and wavy amplitude $\alpha$ varies from 0 to 0.2, the values of the cone half angle $\gamma$ are taken $\pi/12, \pi/6$ and $\pi/4$ for fixed Prandtl number ($Pr = 7.0$). The computation is performed for different values of the wavy amplitude $\alpha$, nanoparticle concentration parameter $\phi$ and the cone inclination half angle $\gamma$. We used five different nanoparticles viz. alumina ($Al_2O_3$), silver ($Ag$), copper ($Cu$), copper oxide ($CuO$), and titania ($TiO_2$). Figures 7.2 – 7.7 illustrate the change in $C_f$ and $Nu$ for increasing values of wavy amplitude $\alpha$, nanoparticle concentration parameter $\phi$ and the cone inclination half angle $\gamma$ for $Cu$ -water nanofluid. These Figures show that $C_f$ and $Nu$ enhance with the increase of nanoparticle concentration parameter $\phi$ and cone inclination angle $\gamma$ whereas a decrease is depicted with an increase of wavy amplitude $\alpha$. Figures 7.8 – 7.13 depict the variation of the $C_f$ and $Nu$ with the variation of wavy amplitude $\alpha$, nanoparticle volume fraction parameter $\phi$ and cone inclination angle $\gamma$ for the selected types of the nanoparticle. From these Figures it is clear that the $Nu$ enhances with the increase of wavy amplitude $\alpha$; nanoparticle concentration parameter $\phi$ and cone inclination half angle $\gamma$. The $C_f$ enhances with the increase of nanoparticle concentration parameter $\phi$ whereas decreases with the increase of wavy amplitude $\alpha$ and cone inclination angle $\gamma$. Also it is noted that $Nu$ is maximum in the case of $Cu$-nanoparticle whereas $C_f$ is maximum for $Ag$-nanoparticle; $C_f$ and $Nu$ are minimum for $TiO_2$-nanoparticle. Isotherms are plotted for some values of $\alpha$ ($\alpha = 0.0,\ 0.1,\ 0.2$) and $\phi$ ($\phi = 0.0,\ 0.05,\ 0.1$) and $\gamma$ ($\gamma = \pi/12, \pi/6, \pi/4$) in Figs. 7.14 - 7.16. The wavy pattern is prominent and the figures indicate that with the increase of these parameters the thermal boundary layer thickness increases.

Thermo-physical properties of the five nanoparticles $Cu$, $CuO$, $Al_2O_3$, $Ag$ , $TiO_2$ and water are shown in Table 1.2. The results of $C_f$ and $Nu$ are tabulated in Table 7.1. The values are reported for the selected values of $\alpha$, $\phi$ and $\gamma$ when $Pr = 7.0$ for copper ($Cu$) nanoparticle along vertical wavy cone surface at $x = 0.5$, $x = 1.0$ and $x = 1.5$. It is observed that $Nu$ enhances with the increase of $\alpha$, $\phi$ and $\gamma$ whereas $C_f$ reduces with the increase of $\alpha$ and $\gamma$ at crest location and similar behavior is observed at node and trough locations.

The main objective of adding nanoparticles to the classical fluids is to enhance the rate of heat transfer for such fluids, so it is necessary to identify the particular nanoparticle which can be used to achieve the maximum heat transfer rate. Numerical values of average skin friction and average rate of heat transfer for different nanoparticles ($Cu, CuO, Ag$, $Al_2O_3, TiO_2$ ) when $Pr = 7.0$,

**Table 7.1:** $C_f$ and $Nu$ data for different $\alpha, \phi$ and $\gamma$ at $Pr = 7.0$ for copper ($Cu$) nanoparticle.

| $\xi$ | $\phi$ | $\alpha$ | $\gamma$ | $C_f$ | $Nu$ |
|---|---|---|---|---|---|
| 0.5 (Crest) | 0.1 | 0.0 | $\pi/4$ | 0.5766 | 1.0246 |
| | | 0.1 | | 0.5669 | 1.0477 |
| | 0.0 | 0.2 | | 0.5100 | 0.5957 |
| | 0.05 | | | 0.5321 | 0.9996 |
| | 0.1 | | 0 | 0.5812 | 1.0347 |
| | | | $\pi/12$ | 0.5753 | 1.0383 |
| | | | $\pi/6$ | 0.5681 | 1.0434 |
| | | | $\pi/4$ | 0.5572 | 1.0530 |
| 1.0 (Node) | | 0.0 | $\pi/4$ | 0.5766 | 1.0246 |
| | | 0.1 | | 0.6474 | 1.1049 |
| | 0.0 | 0.2 | | 0.5693 | 1.0007 |
| | 0.05 | | | 0.5947 | 1.0592 |
| | 0.1 | | 0 | 0.4438 | 0.9718 |
| | | | $\pi/12$ | 0.4946 | 1.0156 |
| | | | $\pi/6$ | 0.5506 | 1.0611 |
| | | | $\pi/4$ | 0.6233 | 1.1167 |
| 1.5 (Trough) | | 0.0 | $\pi/4$ | 0.5766 | 1.0246 |
| | | 0.1 | | 0.5949 | 1.0382 |
| | 0.0 | 0.2 | | 0.5582 | 0.9156 |
| | 0.05 | | | 0.5857 | 0.9720 |
| | 0.1 | | 0 | 0.5834 | 1.0252 |
| | | | $\pi/12$ | 0.5926 | 1.0251 |
| | | | $\pi/6$ | 0.6027 | 1.0257 |
| | | | $\pi/4$ | 0.6160 | 1.0275 |

$\gamma = \pi/4, \alpha = 0.2, \phi = 0.1, \xi = 1.0$ are presented in Table 7.2 and calculations of percent increase in the magnitude of average skin friction and the average Nusselt number for five different materials ($Cu, CuO, Ag, Al_2O_3, TiO_2$ ) have been shown in Tables 7.3 and 7.4. It is observed that maximum increase of about 12% in average skin friction is obtained for $Ag$ with 10% concentration in the base fluid when compared with the value

${C_f}_{avg} = 0.5260$ at $\alpha = 0.0,\ \phi = 0.0, \gamma = \pi/4$ and minimum increase of about 5.8% in the value of average skin friction is obtained for $TiO_2$ with 10% concentration when the present results are compared with the value ${C_f}_{avg} = 0.5284$ at $\alpha = 0.0,\ \phi = 0.2, \gamma = \pi/4$. On the other hand maximum gain of about 39% in average Nusselt number is obtained for $Cu$ with 10% concentration when the present results are compared with the value $Nu_{avg} = 0.7455$ at $\alpha = \phi = 0.0, \gamma = \pi/2$ and minimum increase of about 6.8% in the value of Nusselt number is obtained for $TiO_2$ with 10% concentration when the present results are compared with the value $Nu_{avg} = 0.9341$ at $\alpha = 0.0,\ \phi = 0.0, \gamma = \pi/4$. The percent increase in average skin friction and average Nusselt number for nanofluid is higher in case of smaller amplitude when compared with the pure fluid results. Overall, it is observed that the nanofluid has a great capacity to serve as the best coolant as compared to the pure fluid.

**Table 7.2:** Numerical values of ${C_f}_{avg}$ and $Nu_{avg}$ for different nanoparticle when $Pr = 7.0,\ \alpha = 0.2, \gamma = \pi/4, \phi = 0.1, \xi = 1.0$ .

| Nano particle material | ${C_f}_{avg}$ | $Nu_{avg}$ |
|---|---|---|
| $Cu$ | 0.5785 | 1.0364 |
| $CuO$ | 0.5731 | 1.0236 |
| $Ag$ | 0.5892 | 1.0306 |
| $Al_2O_3$ | 0.5625 | 1.0262 |
| $TiO_2$ | 0.5589 | 0.9978 |

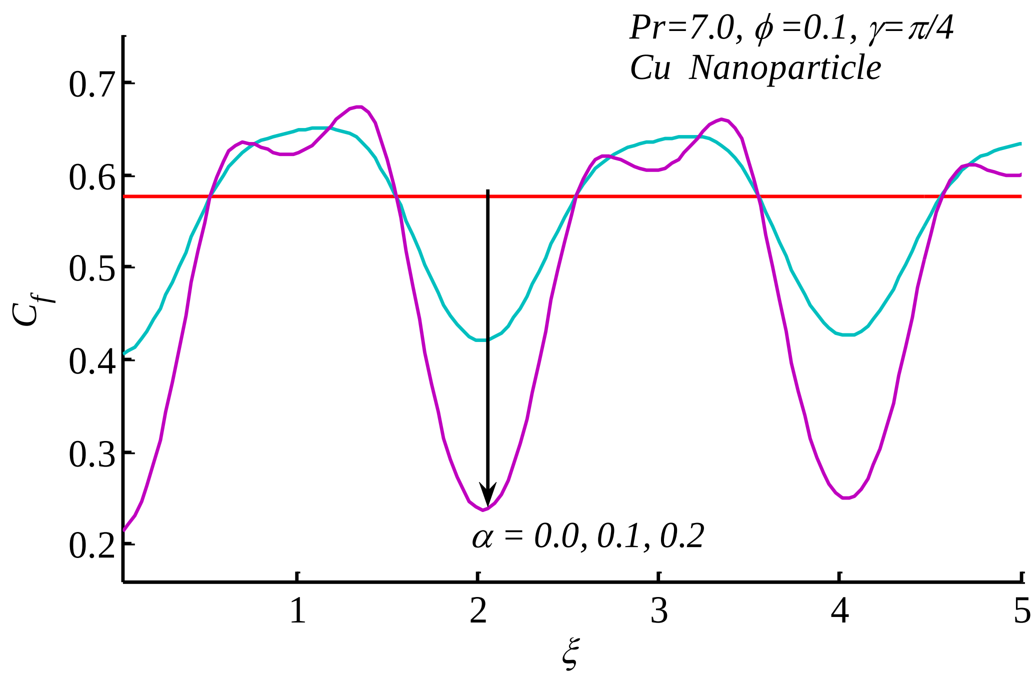


**Figure 7.2:** Effect of $\alpha$ on skin friction profile.

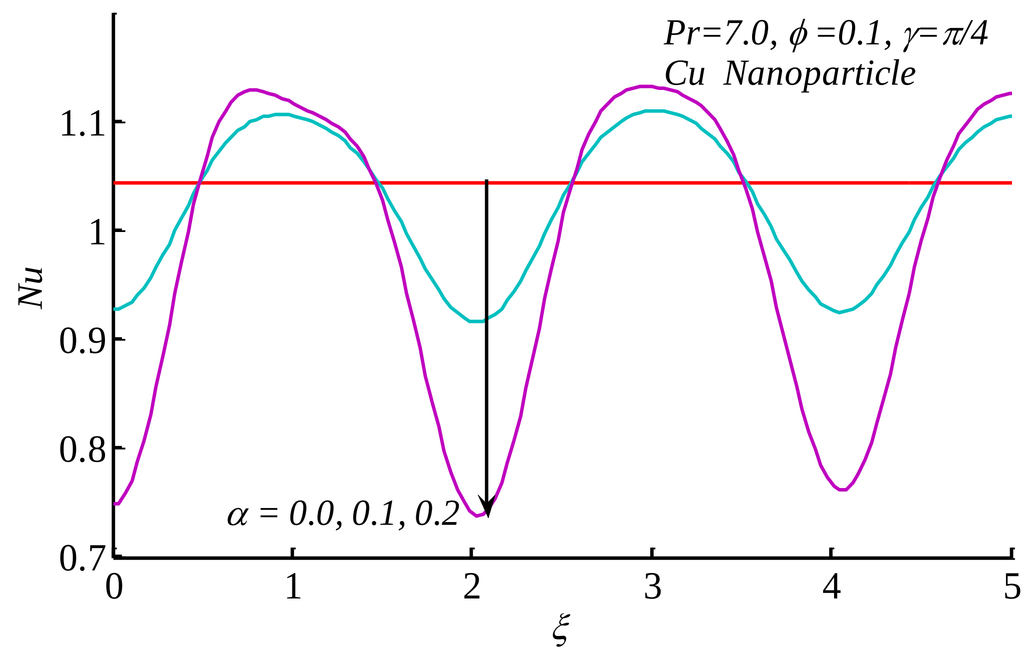


**Figure 7.3:** Nusselt number plotted against $\xi$ for various $\alpha$.

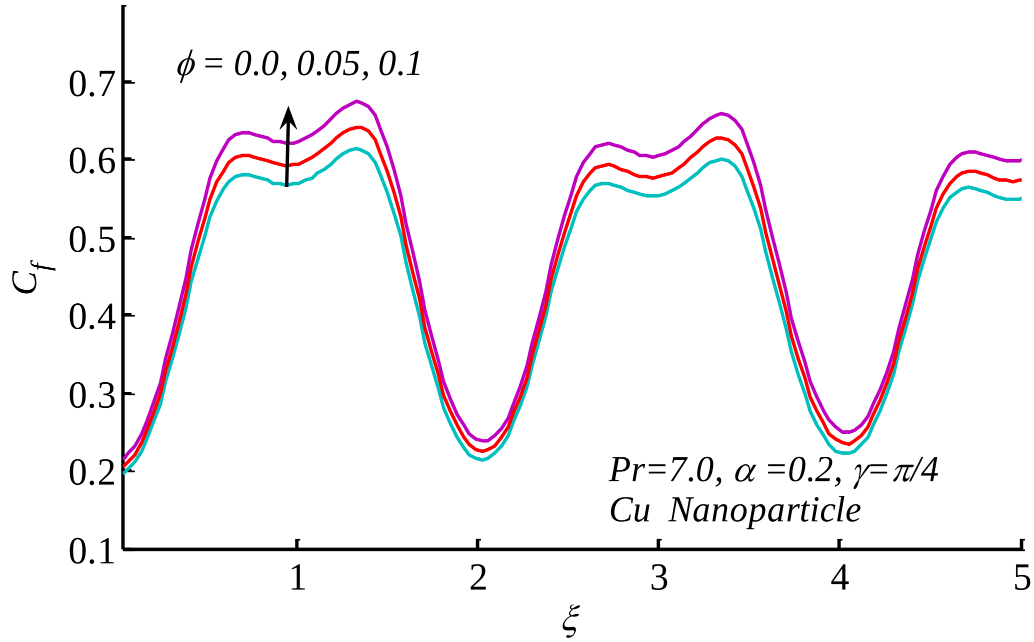


**Figure 7.4:** Influence of $\phi$ on skin friction coefficient.

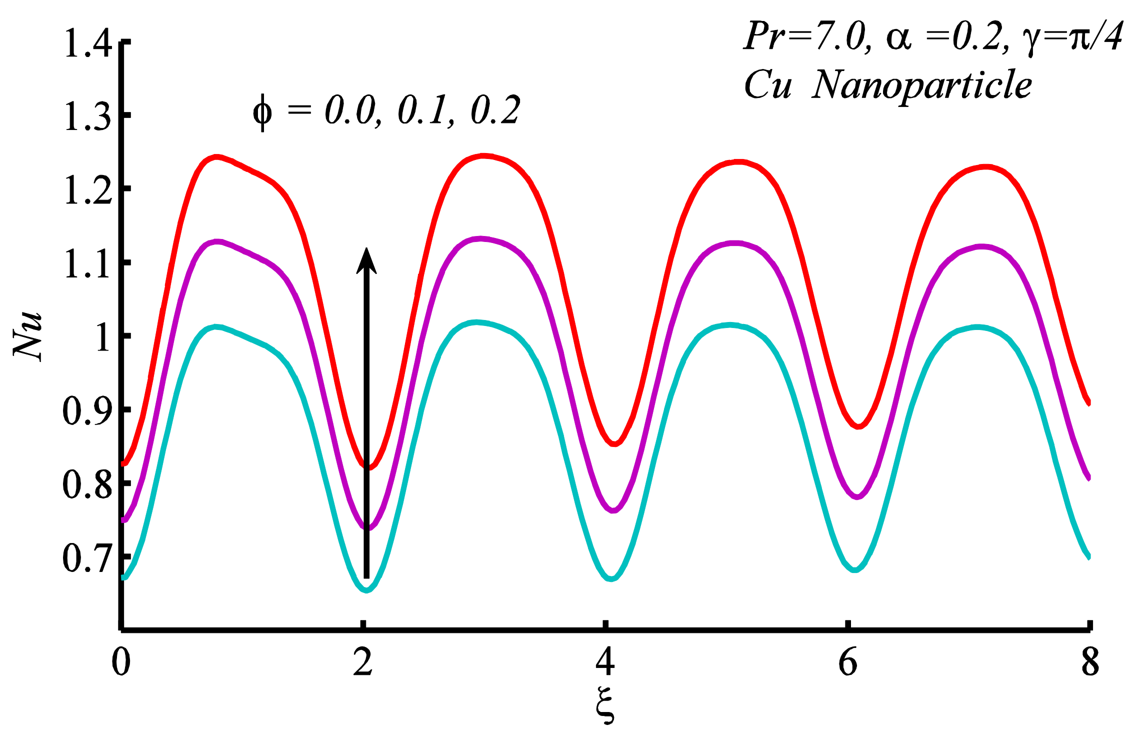


**Figure 7.5:** Variation of Nusselt number due to $\phi$.

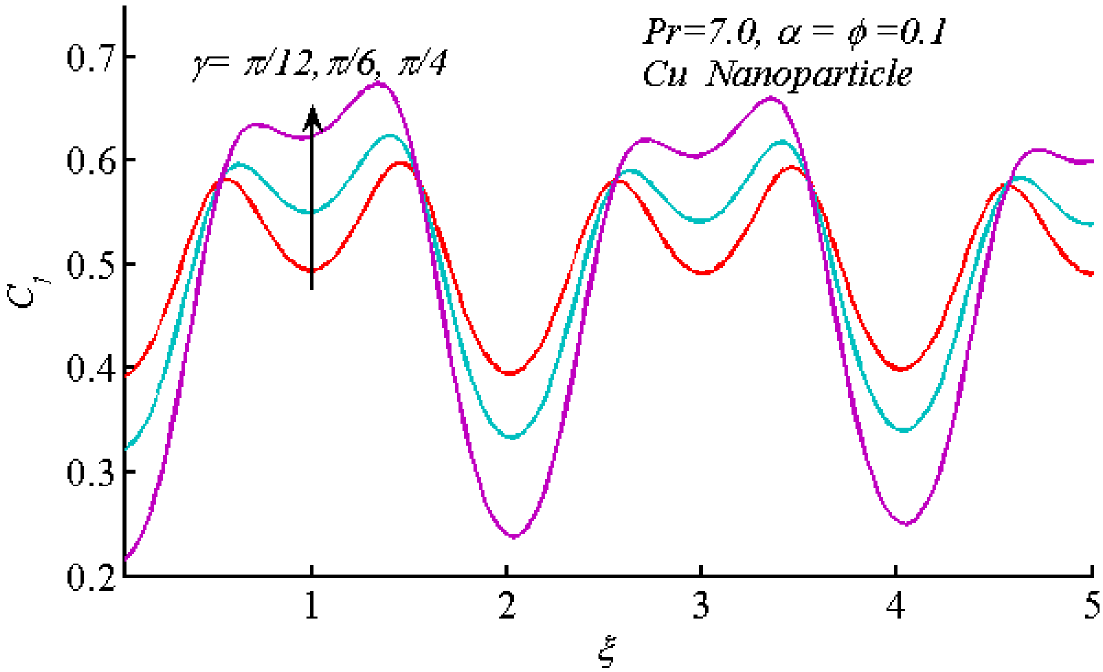


**Figure 7.6:** Change in skin friction for different $\gamma$.

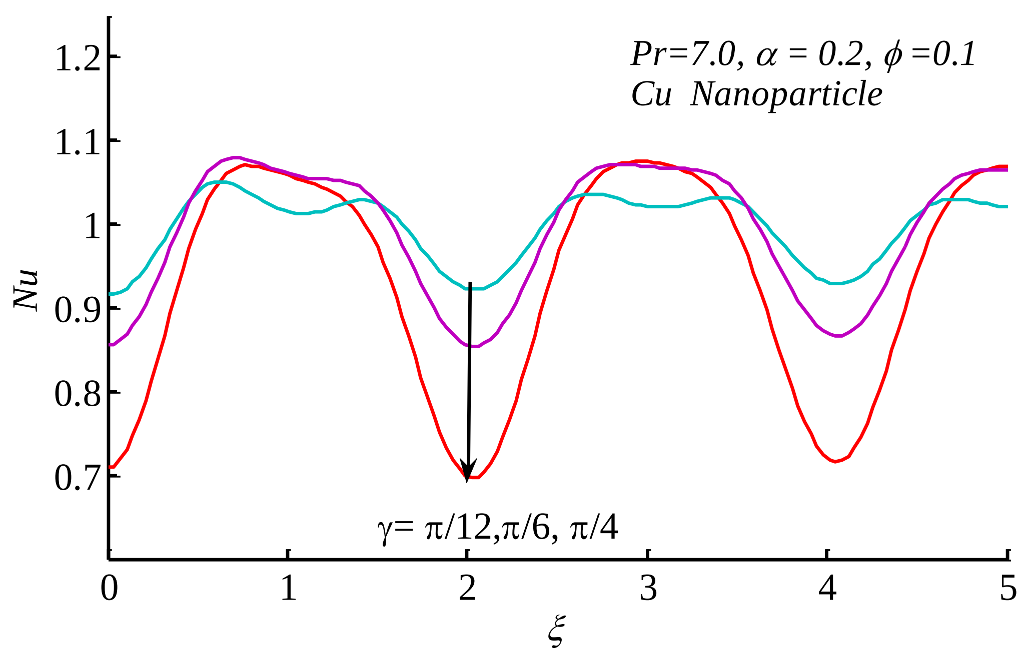


**Figure 7.7:** Nusselt number graph for different $\gamma$.

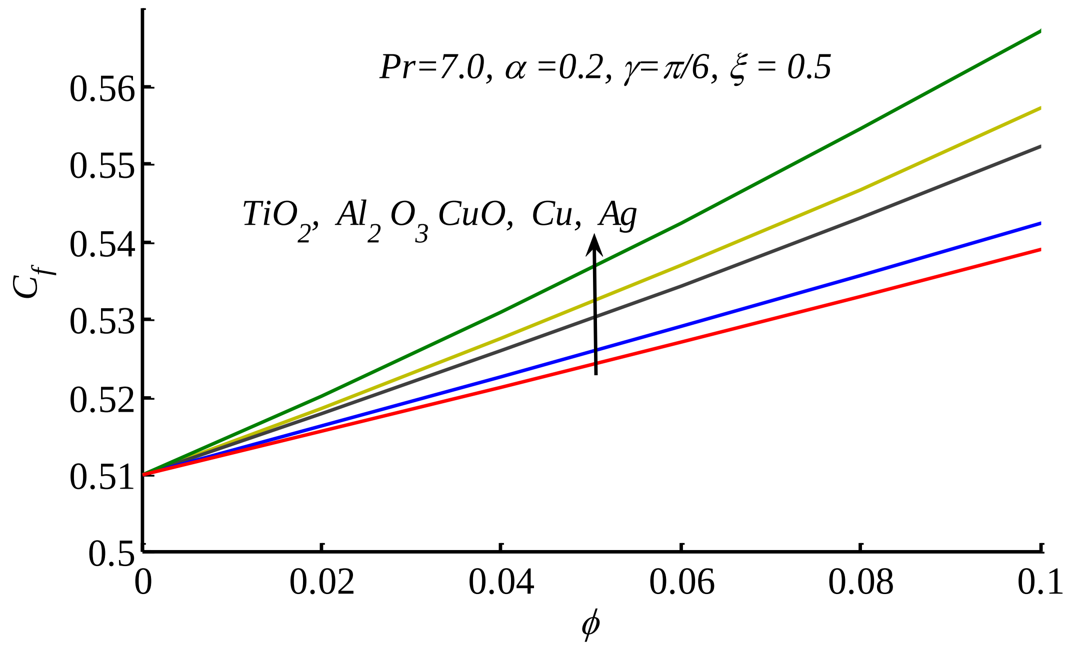


**Figure 7.8:** Behavior of skin friction coefficient against $\phi$ for different nanoparticles.

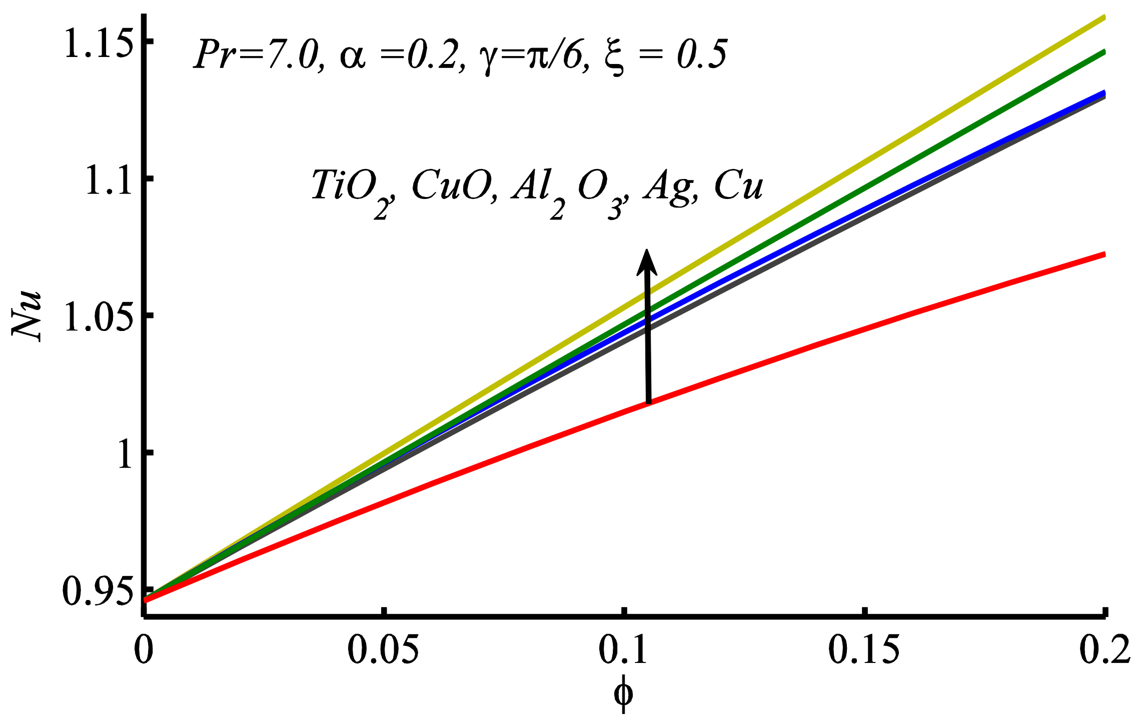


**Figure 7.9:** Nusselt number profile against $\phi$ for different nanoparticles.

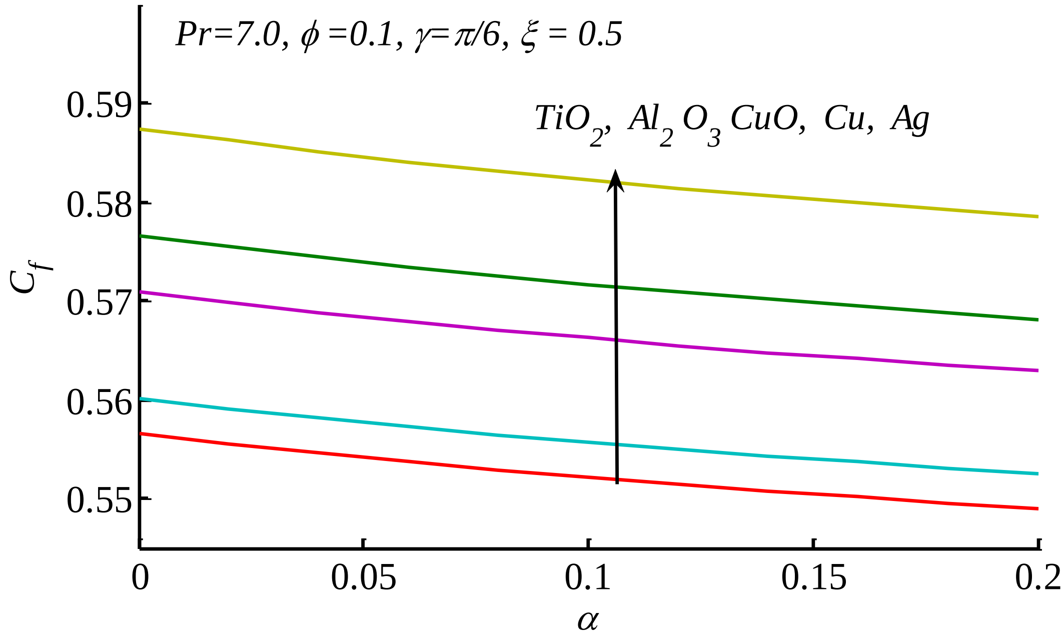


**Figure 7.10:** The effect of $\alpha$ on skin friction coefficient for different nanoparticles.

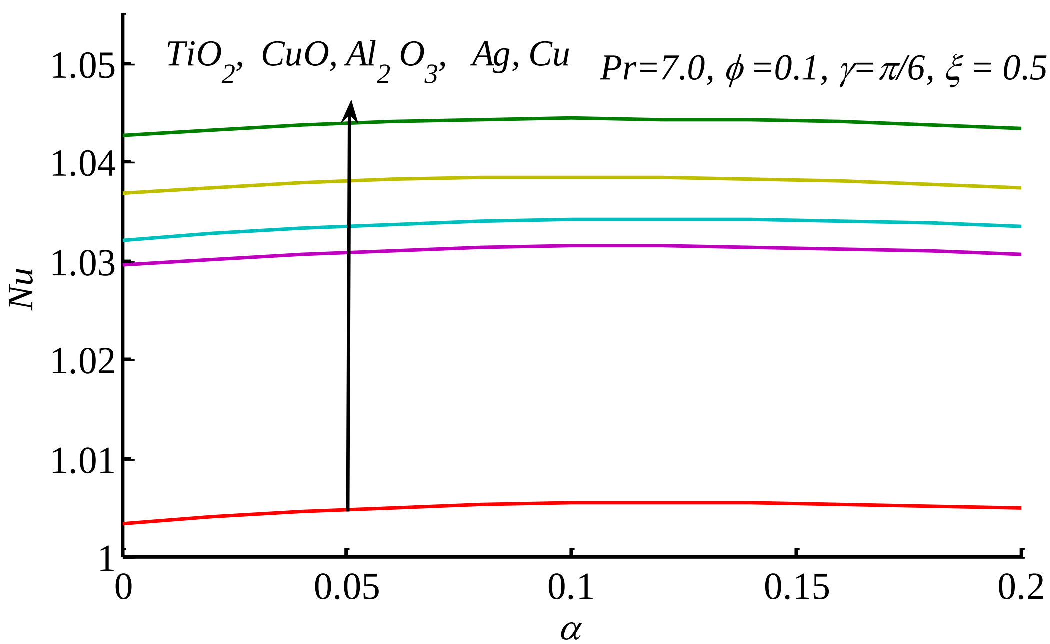


**Figure 7.11:** Nusselt number against $\alpha$ for different nanoparticles.

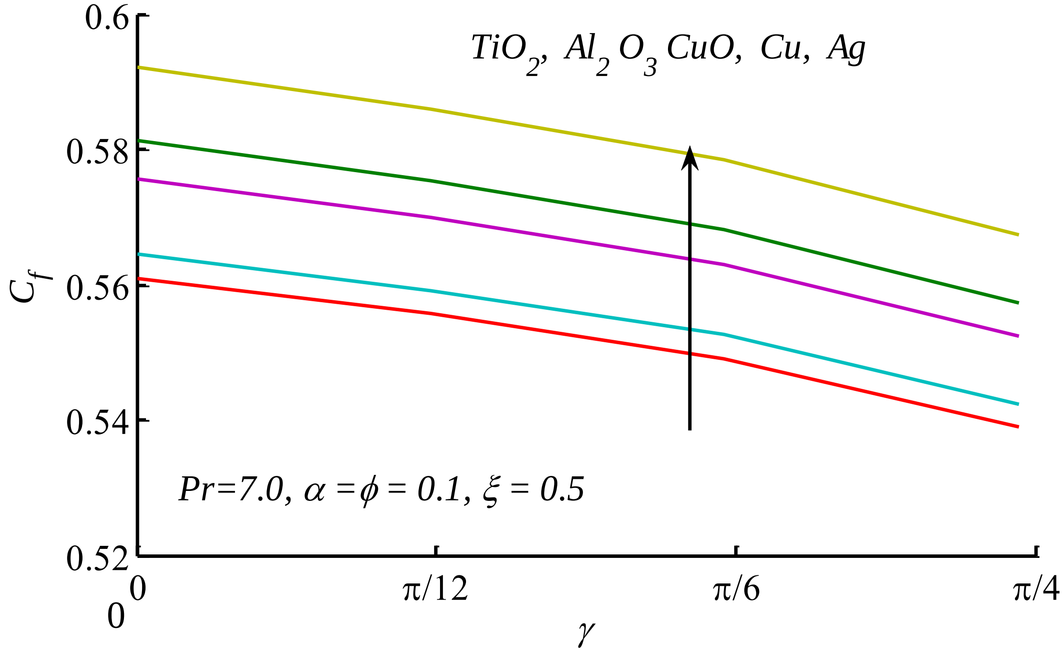


**Figure 7.12:** The effect of $\gamma$ on $C_f$ for different nanoparticles.

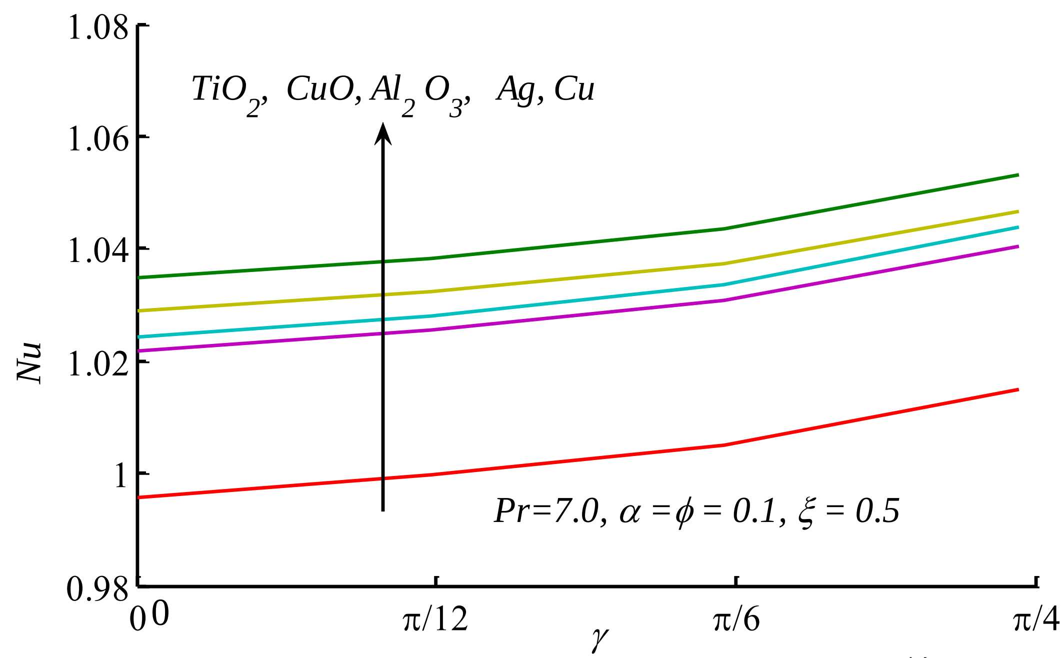


**Figure 7.13:** Change in Nusselt number against $\gamma$ for different nanoparticles.

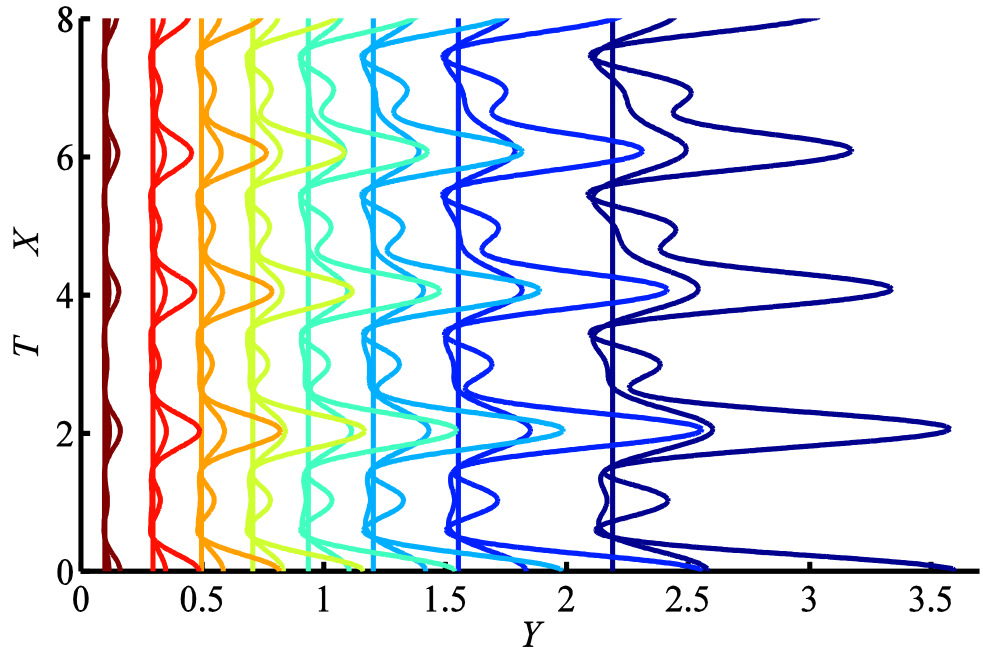


**Figure 7.14:** Isotherms plotted at various $\alpha$ $(= 0.0, 0.1, 0.2)$.

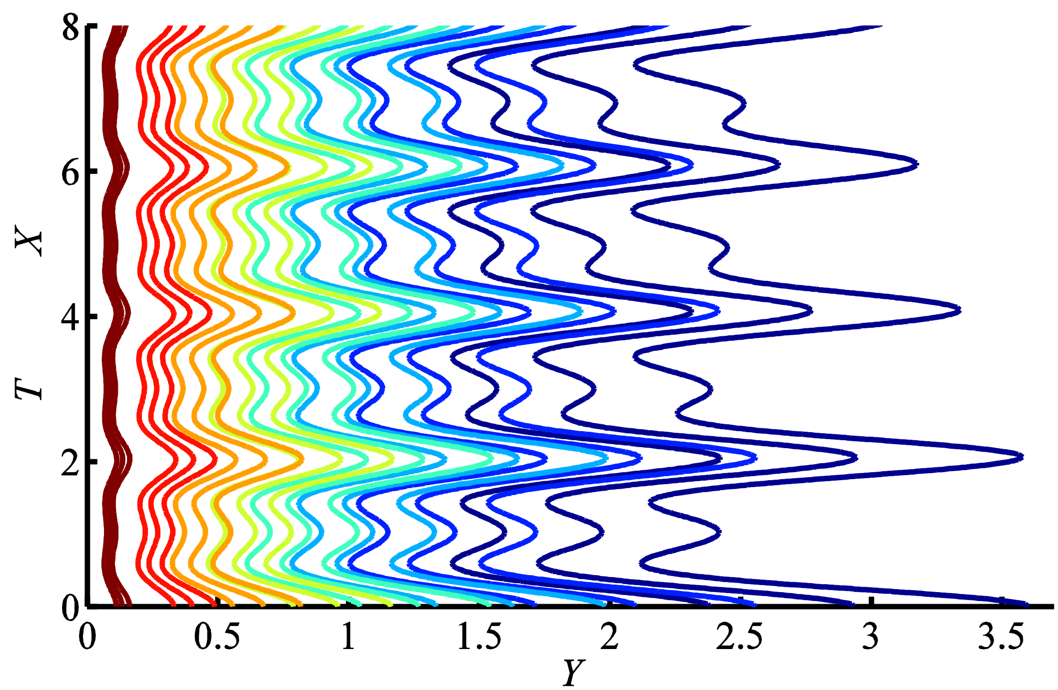


**Figure 7.15:** Effect of different $\phi$ $(= 0.0, 0.05, 0.1)$ on isotherms.

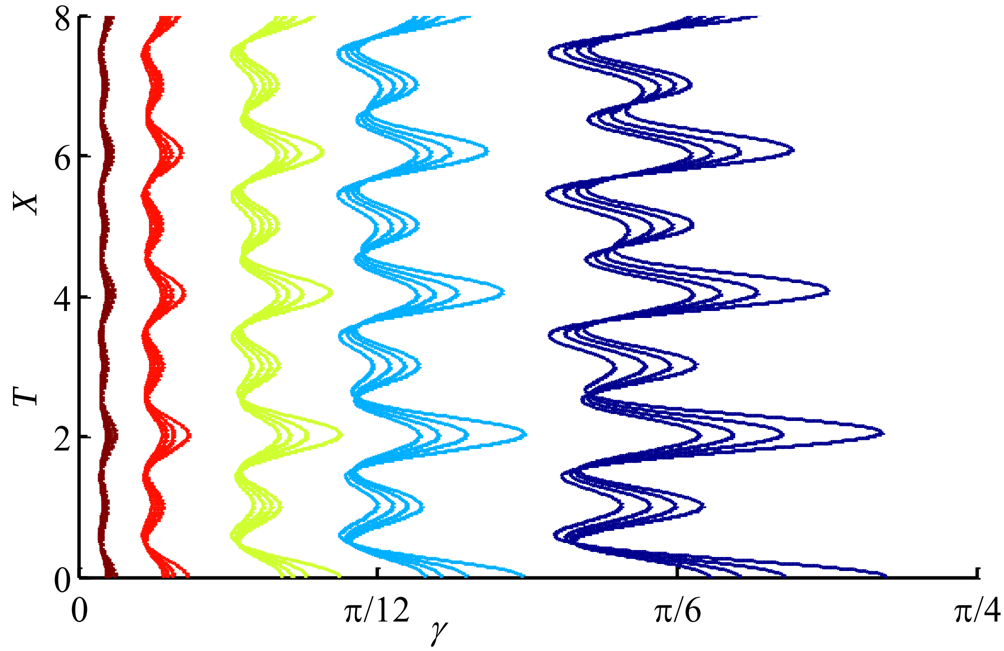


**Figure 7.16:** Isotherms at various values of $\gamma$ $(= 0, \pi/12, \pi/6, \pi/4)$.

**Table 7.3:** Percent change in ${C_f}_{avg}$ and $Nu_{avg}$ for different nanoparticles when $Pr = 7.0,\ \alpha = 0.2,\ \phi = 0.1, \gamma = \pi/4, \xi = 1.0$.

| Nano particle material | % increase in ${C_f}_{avg}$ | | |
|---|---|---|---|
| | Versus ${C_f}_{avg} = 0.6375$ at $\alpha = \phi = 0.0,$ $\gamma = 0.$ | Versus ${C_f}_{avg} = 0.5260$ at $\alpha = \phi = 0.0,$ $\gamma = \pi/4.$ | Versus ${C_f}_{avg} = 0.5284$ at $\alpha = 0.2,\ \phi = 0.0,$ $\gamma = \pi/4.$ |
| $Cu$ | $-9.2$ | 10.0 | 9.5 |
| $CuO$ | $-10.1$ | 9.0 | 8.5 |
| $Ag$ | $-7.6$ | 12.0 | 11.5 |
| $Al_2O_3$ | $-11.8$ | 6.9 | 6.4 |
| $TiO_2$ | $-12.3$ | 6.2 | 5.8 |

**Table 7.4:** Percent change in average Nusselt number $Nu_{avg}$ for different nanoparticles when $Pr = 7.0,\ \alpha = 0.2,\ \phi = 0.1, \gamma = \pi/4\, , \xi = 1.0$ .

| Nano particle material | % increase in $Nu_{avg}$ | | |
|---|---|---|---|
| | Versus $Nu_{avg} = 0.7455$ at $\alpha = \phi = 0.0,$ $\gamma = 0.$ | Versus $Nu_{avg} = 0.9341$ at $\alpha = 0.0,\ \phi = 0.0,$ $\gamma = \pi/4.$ | Versus $Nu_{avg} = 0.9291$ at $\alpha = 0.2,\ \phi = 0.0,$ $\gamma = \pi/4.$ |
| $Cu$ | 39.0 | 11.0 | 11.5 |
| $CuO$ | 37.3 | 9.6 | 10.1 |
| $Ag$ | 38.2 | 10.3 | 10.9 |
| $Al_2O_3$ | 37.7 | 9.6 | 10.4 |
| $TiO_2$ | 33.8 | 6.8 | 7.3 |

## 7.4 Concluding remarks

Heat transfer phenomenon in natural convection flow past a wavy cone has been investigated in this chapter for base fluid water and five nanoparticles, namely, alumina ($Al_2O_3$), copper ($Cu$), copper oxide ($CuO$), silver ($Ag$), and titania ($TiO_2$). The non-linear transport equations have been solved numerically and the accuracy of the solution scheme has been shown by giving comparison with the already existing data. Results show that heat transfer rate is significantly increased by the addition of nanoparticles with respect to the base liquid and heat transfer enhancement is observed to be more prominent with the increase of the nanoparticle concentration. It is shown that Nusselt number is maximum in the case of $Cu$-nanoparticle and decreases, successively, for $Ag$-nanoparticle, $Al_2O_3$-nanoparticle, $CuO$-nanoparticle and $TiO_2$-nanoparticle. Maximum gain of about 39% in average Nusselt number is obtained for $Cu$ with 10% concentration. Furthermore, it is concluded that the nanofluid serves as a very useful fluid in the expeditions of cooling and heating processes.

# Chapter 8

# Conclusion and future work

In this dissertation, we studied similar and non-similar flows of nanofluid with heat and mass transfer. The contribution of nanoparticle towards convective heat transfer enhancement is manifold which requires a suitable model in order to capture the correct physics. There are several empirical and semi-empirical nanofluid models available in the literature. Among these the most popular models are those proposed by Buongiorno and Tiwari and Das. In the Buongiorno nanofluid model, the basic transport equations for fluid flow and heat transfer are appended with a transport equation for nanoparticle concentration. Buongiorno distinguished the succeeding dominating phenomena: the Brownian diffusion (stochastic motion of nanoparticles), thermophoresis (particle diffusion due to the temperature gradient) and the Brownian motion; while the Tiwari and Das model focuses upon the modified thermophysical properties of the nanofluid.

This study is mainly divided into two types of flows, namely, self-similar flows (Chapters 2 and 3) and non-similar flows (Chapters 4 to 7). The laminar incompressible self-similar flows of nanofluid have been considered for the plate and cone geometries subjected to natural convective phenomenon. For the plate geometry two cases, namely, the VWT and VHF, by considering the power-law form of the variable wall temperature, have been investigated. The non-similar flows include the study of forced and natural convection flows of nanofluid past the surfaces involving wavy texture. The steady MHD boundary layer nanofluid flow and heat transfer over the moving wavy plate is examined for different nanoparticles namely, $MWCNT$, $SWCNT$, $Al_2O_3$, $TiO_2$ and $Ag$. Heat transfer analysis of natural convection flow of nanofluid along a vertical wavy surface has been investigated for five different nanoparticles, namely, silver ($Ag$), copper ($Cu$), alumina ($Al_2O_3$), magnetite ($Fe_3O_4$) and silica ($SiO_2$). The influence of heat generation/absorption in nanofluid flow over a vertical wavy surface for two types of nanoparticles namely, alumina ($Al_2O_3$) and magnetite ($Fe_3O_4$) is also investigated. The problem of natural convective heat transfer of water-based nanofluid along wavy cone surface is studied numerically for five different types of nanoparticles, namely, alumina ($Al_2O_3$), copper ($Cu$), silver ($Ag$), copper oxide ($CuO$) and titania ($TiO_2$).

After the utilization of suitable transformations, the constitutive equations of these models are transformed into dimensionless ordinary differential equations for the case of self-similar flows and to the partial differential equations for the case of non-similar flows and results were obtained by employing the implicit finite difference numerical scheme (Keller-box method). Findings of these studies are dependent upon the dimensionless parameters. These dimensionless parameters provide the trend of variation of different physical quantities like temperature, velocity, skin friction coefficient, local Nusselt number and Sherwood number. The results in the absence of different nanoparticle ($MWCNT$, $SWCNT, Cu, CuO,\ Al_2O_3, Fe_3O_4,\ TiO_2, SiO_2$ and $Ag$ considered in this analysis) are also calculated and a comparison of the results with the absence and presence of nanoparticles is made. It is noted that the skin friction $C_f$ increases with the increment in Brownian motion parameter $Nb$, Prandtl number $Pr$, wavy amplitude $\alpha$, concentration of nanoparticles $\varphi$ and thermophoresis parameter $Nt$. However, skin friction reduces as power-law index $m$ and Lewis number $Le$ are increased. Also skin friction coefficient is an increasing/decreasing function of heat generation/absorption parameter. It is observed that the skin friction coefficient is maximum in the case of $Ag$-nanoparticle. For non-flat surface, the percent increase in average skin friction coefficient for nanofluid is higher when compared with the pure fluid results and flat plate results. Moreover, local Nusselt number enhances by increasing the values of concentration of nanoparticles and the cone half angle while it reduces as Brownian motion parameter, thermophoresis parameter and wavy amplitude are increased whereas, local Nusselt number is decreasing/increasing function of heat generation/absorption parameter. It is shown that local Nusselt number is maximum in the case of $Cu$-nanoparticle. For non-flat surface, the percent increase in average Nusselt number for nanofluid is higher when compared with the pure fluid and flat plate results. Sherwood number rises by incrementing $Nb$ and $Nt$ parameters. Also Sherwood number enhances by increasing the power-law index, Prandtl and Lewis numbers.

Overall, it is observed that the nanofluid has a great capacity to serve as the best coolant as compared to the pure fluid. Furthermore, it is concluded that the nanofluid serves as very useful fluid in the expeditions of cooling and heating processes.

Based on these investigations, there are a number of possibilities of research that still needs to be performed, both in terms of theoretical and simulation studies. The steady natural and forced convection flow problems discussed in this dissertation can be extended for the unsteady state problems. Moreover, the study of the non-homogenous nanofluid models in current flow problems would also be a very useful extension of the present work and results in higher values of heat transfer enhancement. Furthermore, different shape factors of nanoparticles and performance of nanoparticles in different types of base fluids would also be a very useful extension of the present work.

# References


[1] A. Bejan, *Convective heat transfer*, (4th Ed.) John Wiley & Sons, New York 2014.

[2] B. Gebhart, Y. Jaluria, R.L. Mahajan, and B. Sammakia, *Buoyancy induced flows and transport*, Hemisphere Cambridge 1988.

[3] G. Gebhart, Natural convection flows and stability, Adv. Heat Transfer, 9 (1973) 273-348.

[4] I. Pop and D.B. Ingham, *Convection heat transfer*, Pergamon Oxford UK 2001.

[5] Y A. Cengel, *Heat Transfer, a practical approach*, (2nd Ed.) McGraw-Hill 2004.

[6] A.J. Smits, *A Physical Introduction to Fluid Mechanics*, (2nd Ed.) Princeton University 2018.

[7] E. Schmidt and W. Beckmann, Das Temperatur-und Geschwindigkeitsfeld vor einer Wärme abgebenden senkrechten Platte bei natürlicher Konvektion, Technische Mechanik und Thermodynamik, 1(11) (1930) 391-406.

[8] S. Ostrach, An analysis of laminar free convective flow and heat transfer about a flat plate parallel to direction of the generating body force, NASA, (1953) 1111.

[9] J.A. Schetz and R. Eichhorn, Natural convection with discontinuous wall-temperature variations, J. Fluid Mech., 18(2) (1964) 167-176.

[10] D. Shang, *Free convection film flows and heat transfer*, Berlin, Heidelberg, New York, Springer 2006.

[11] R.B. Bird, W.E. Stewart, and E.N. Lightfoot, *Transport Phenomena*, Wiley, New York 2007.

[12] M.S. Alam and M.M. Rahman, Dufour and Soret effects on mixed convection flow past a vertical porous flat plate with variable suction, Nonlinear Anal. Model. Control, 11(1) (2006) 3-12.

[13] D.A. Nield, A. Bejan, and Nield-Bejan, *Convection in porous media*, (Vol. 3) springer, New York 2006.

[14] R. Kandasamy and I. Hashim, Nonlinear MHD mixed convection flow and heat and mass transfer of first order chemical reaction over a wedge with variable viscosity in the presence of suction or injection, J. Theor. appl. mech., 34(2) (2007) 111-134.

[15] V.K. Prasad and K. Vajravelu, Heat transfer in the MHD flow of a power-law fluid over a non-isothermal stretching sheet. Int. J. Heat Mass Transfer, 52(21-22) (2009) 4956-4965.

[16] G. Palani, and U. Srikanth, MHD flow past a semi-infinite vertical plate with mass transfer, Nonlinear Anal.: Modell. Control, 14(3) (2009) 345-356.

[17] G. Periyanagounder, G., R.S. Kanniappan and L. Parasuraman, Doubly stratified effects in a free convective flow over a vertical plate with heat and mass transfer, Therm. Sci., 18(2) (2014) 365-376.

[18] G. Periyanagounder, R.S. Kanniappan, and L. Parasuraman, Doubly stratified effects in a free convective flow over a vertical plate with heat and mass transfer. Therm. Sci., 18(2) (2014) 365-376.

[19] I. Mustafa, T. Javed and A. Majeed, Magnetohydrodynamic (MHD) mixed convection stagnation point flow of a nanofluid over a vertical plate with viscous dissipation, Can. J. Phys., 93(11) (2015) 1365-1374.

[20] A. Mehmood and M. Usman, Heat transfer enhancement in rotating disk boundary layer, Therm. Sci., (2017) DOI: TSCI160412293M

[21] S.O. Abah and R.T Abah, Analysis of magnetic and injection effects on unsteady heat and mass laminar flow past a vertical surface, Int. J. Eng. Tech. Res., 1(7) (2013) 116-126.

[22] K. Gangadhar, Soret and Dufour effects on hydro magnetic heat and mass transfer over a vertical plate with a convective surface boundary condition and chemical reaction, J. Appl. Fluid Mech., 6(1) (2013) 95-105.

[23] M. Ali, Mixed convection boundary layer flows induced by a permeable continuous surface stretched with prescribed skin friction. World Acad. Sci., Int. J. Math., Comp., Phys., Elect. Comp. Eng. 7(6) (2013) 1001-1005.

[24] A.J. Chamkha, A.M. Aly and Z.A. Raizah, Double diffusion MHD free convection flow along a sphere in the presence of a homogenous chemical reaction in the presence of a homogenous chemical reaction and soret and Dufour effects, Appl. Math. Comp., 6(1) (2017) 34-44.

[25] A. Buhr, and K. Ehrenfried, High-speed particle image velocimetry of the flow around a moving train model with boundary layer control elements, World Acad. Sci. Eng. Tech., Int. J. Mech., Aerospace, Indus., Mech. Manuf. Eng. 11(3) (2017) 589-597.

[26] A.K. Kareem and S. Gao, Mixed convection heat transfer enhancement in a cubic lid-driven cavity containing a rotating cylinder through the introduction of artificial roughness on the heated wall, Phys. Fluids, 30(2) (2018) 025103.

[27] J.C. Maxwell, *A treatise on electricity and magnetism*, Vol. 1. 2nd Ed. Oxford Clarendon Press 1881.

[28] H. Masuda, A. Ebata, K. Teramae, and N. Hishinuma, Alteration of thermal conductivity and viscosity of liquid by dispersing ultrafine particles (dispersions of Al2O3, SiO2, and TiO2 ultrafine particles), Japan. J. Therm. Prop., 7(4) (1993) 227-233.

[29] S.U.S. Choi, Enhancing thermal conductivity of fluids with nanoparticle in developments and applications of Non-Newtonian flows, eds. D.A. Siginer, H.P. Wang, ASME F.E.D., San Francisco, CA, 231 (1995) 99-103.

[30] J.P. Holman, *Heat transfer*, New York McGraw-Hill 1981.

[31] J. Buongiorno, Convective Transport in Nanofluids, ASME J. Heat Transfer, 128 (2006) 240-250.

[32] R.K. Tiwari and M.K. Das, Heat transfer augmentation in a two-sided lid-driven differentially heated square cavity utilizing nanofluids, Int. J. Heat Mass Transfer, 50 (2007) 2002-18.

[33] V. Bianco, O. Manca and K. Vafai, *Heat transfer enhancement with nanofluids*, CRC Press London, New York 2015.

[34] W.J. Minkowycz, E.M. Sparrow and J.P. Abraham, *Nanoparticle heat transfer and fluid flow*, CRC press London, New York 2013.

[35] M.M.M. Abdou, Effect of radiation with temperature dependent viscosity and thermal conductivity on unsteady a stretching sheet through porous media, Nonlinear Anal., 15(3) (2010) 257-270.

[36] W. Yu, and H. Xie, A review on nanofluids: preparation, stability mechanisms, and applications, J. nanometer., (2012).

[37] S. Dinarvand, A. Abbassi, R. Hosseini, I. Pop, Homotopy analysis method for mixed convective boundary layer flow of a nanofluid over a vertical circular cylinder, Therm. Sci., 19(2) (2015) 549-561.

[38] A.Moradi, A. Alsaedi, and T. Hayat, Investigation of heat transfer and viscous dissipation effects on the Jeffery-Hamel flow of nanofluids, Therm. Sci., 19(2) (2015) 563-578.

[39] F.A. Salama, Effects of radiation on convection heat transfer of Cu-water nanofluid past a moving wedge. Therm. Sci., 20(2) (2016) 437-447.

[40] A.G.M Rahman, Effects of variable viscosity and thermal conductivity on unsteady MHD flow of non-Newtonian fluid over a stretching porous sheet, Therm. Sci.,17(4) (2013) 1035-1047.

[41] L. Parasuraman, N.C. Peddisetty, and G. Periyannagounder, Radiation effects on an unsteady MHD natural convective flow of a nanofluid past a vertical plate, Therm. Sci., 19(3) (2015) 1037-1050.

[42] Y. Yirga and D. Tesfay, Heat and mass transfer in MHD flow of nanofluids through a porous media due to a permeable stretching sheet with viscous dissipation and chemical reaction effects, Int. J. Mech., Aero, Indus, Mech. Manu. Eng., 9 (2015) 674-681.

[43] M. Ramzan and F. Yousaf, Boundary layer flow of three-dimensional viscoelastic nanofluid past a bi-directional stretching sheet with Newtonian heating, AIP Adv., 5(5) (2015) 057132.

[44] K. Vajravelu and J. Nayfeh, Convective heat transfer at a stretching sheet, Acta Mech., 96 (1993) 47-54.

[45] K. Vajravelu, Convection heat transfer at a stretching sheet with suction or blowing, J. Math. Anal. Appl., 188(3) (1994) 1002-1011.

[46] K. Vajravelu and E. Soewono, Fourth order non-linear systems arising in combined free and forced convection flow of a second order fluid, Int. J. Non-Linear Mech., 29(6) (1994) 861-869.

[47] J. Fan, J. Shi and X. Xu, Similarity solution of free convective boundary-layer behavior at a stretching surface, Heat Mass Transfer, 35(3) (1999) 191-196.

[48] S.P.A. Devi and M. Thiyagarajan, Steady nonlinear hydromagnetic flow and heat transfer over a stretching surface of variable temperature, Heat Mass Transfer, 42 (2006) 671-677.

[49] M. Ali and F. Al-Yousef, Laminar mixed convection boundary layers induced by a linearly stretching permeable surface, Int. J. Heat Mass Transfer, 45(21) (2002) 4241-4250.

[50] K. Javaherdeh, M.M. Nejad and M. Moslemi, Natural convection heat and mass transfer in MHD fluid flow past a moving vertical plate with variable surface temperature and concentration in a porous medium, Eng. Sci. Tech. Int. J., 18(3) (2015) 423-431.

[51] A.A. Mehrizi,Y. Vazifeshenas and G. Domairry, New analysis of natural convection boundary layer flow on a horizontal plate with variable wall temperature, J. Theo. Appl. Mech., 50 (2012) 1001-1010.

[52] M. Jashim Uddin and I. Pop, Free convection boundary layer flow of a nanofluid from a convectively heated vertical plate with linear momentum slip boundary condition, Sains Malaysiana, 41(11) (2012) 1475-1482.

[53] M. Qasim, Z.H. Khan, R.J. Lopez and W.A. Khan, Heat and mass transfer in nanofluid thin film over an unsteady stretching sheet using Buongiorno’s model, Europe. Phys. J. Plus, 131(1) (2016) 1-11.

[54] M.J. Uddin, W.A. Khan, and A.M. Ismail, Effect of variable properties, Navier slip and convective heating on hydromagnetic transport phenomena, Indian J. Phys., 90(6) (2016) 627-637.

[55] M. Ghalambaz, A. Noghrehabadi and A. Ghanbarzadeh, Natural convection of nanofluids over a convectively heated vertical plate embedded in a porous medium, Brazilian J. Chem. Eng., 31(2) (2014) 413-427.

[56] M. Ramzan and F. Yousaf, Boundary layer flow of three-dimensional viscoelastic nanofluid past a bi-directional stretching sheet with Newtonian heating, AIP Advances, 5(5) (2015) 057132.

[57] K. Das, P.R. Duari and P.K. Kundu, Numerical simulation of nanofluid flow with convective boundary condition, J. Egypt. Math. Soc., 23(2) (2015) 435-439.

[58] W.A. Khan, M.J. Uddin and A.M. Ismail, Hydrodynamic and thermal slip effect on double-diffusive free convective boundary layer flow of a nanofluid past a flat vertical plate in the moving free stream, Plos One, 8(3) (2013) e54024.

[59] R.G. Hering and R.J. Grosh, Laminar free convection from a non-isothermal cone, Int. Heat Mass Transfer, 5 (1962) 1059-1068.

[60] R.G. Hering, Laminar free convection from a non isothermal cone at low Prandtl numbers, Int. J. Heat Mass Transfer, 8 (1965) 1333-1337.

[61] S. Roy, Free convection over a slender vertical cone at high Prandtl numbers, ASME J. Heat Transfer, 101 (1974) 174–176.

[62] K. Vajravelu and J. Nayfeh, Hydromagnetic convection at a cone and a wedge, Int. Commun., Heat Mass Transfer, 19(5) (1992) 701-710.

[63] N. G. Kafoussias, Effects of mass transfer on free convection flow past a vertical isothermal cone surface, Int. J. Eng. Sci., 30(3) (1992) 273-281.

[64] K.A. Yih, Effect of radiation on natural convection about a truncated cone, Int. J. Heat Mass Transfer, 42(23) (1999) 4299-4305.

[65] M.A. Behrang, M. Ghalambaz, E. Assareh, and A.R. Noghrehabadi, A new solution for natural convection of Darcian fluid about a vertical full cone embedded in porous media prescribed wall temperature by using a hybrid neural network-particle swarm optimization method, W. Acad. Sci. Eng. Tech., 49 (2011) 1098-1103.

[66] C.Y. Cheng, Free convection heat transfer from a non-isothermal permeable cone with suction and temperature dependent viscosity, J. Appl. Sci. Eng., 18(1) (2015) 17-24.

[67] H.M. Duwairi, O.A. Zeid and R.A. Damseh, Viscous and Joule heating effects over an isothermal cone in saturated porous media, Jordan J. Mech. Ind. Eng., 1(2) (2007) 113-118.

[68] E.M.A. Elbashbeshy, T.G. Emam and E.A. Sayed, Effect of pressure work and heat generation / absorption on free convection flow from a vertical circular cone with variable surface heat flux, W. J. Eng. Phys. Sci., 1(2) (2013) 17-25.

[69] W.H. Braun, S. Ostrach and J.E. Heighway, Free convection similarity flows about two dimensional and axisymmetric with closed lower ends, Int. J. Heat Mass Transfer, 2 (1961) 121-135.

[70] T. Grosan, A. Postelnicu and I. Pop, Free convection boundary layer over a vertical cone in a non-Newtonian fluid saturated porous medium with internal heat generation, Technische Mechanik, 24(4) (2004) 91-104.

[71] A.J. Chamkha, A.M. Aly and M.A. Mansour, Effects of chemical reaction and pressure work on free convection over a stretching cone embedded in a porous medium, Int. J. Ind. Math., 4(4) (2012) 319-333.

[72] A.R. Sohouli,D. Domairry, M. Famouri and A. Mohsenzadeh, Analytical solution of natural convection of Darcian fluid about a vertical full cone embedded in porous media prescribed wall temperature by means of HAM, Int. Commun. Heat Mass Transfer, 35(10) (2008) 1380-1384.

[73] A. Mahdy, Natural convection boundary layer flow due to gyrotactic microorganisms about a vertical cone in porous media saturated by a nanofluid, J. Braz. Soc. Mech. Sci. Eng., 38(1), 67-76.

[74] A. Behseresht, A. Noghrehabadi and M. Ghalambaz, Natural convection heat and mass transfer from a vertical cone in porous media filled with nanofluids using the

practical ranges of nanofluids thermo-physical properties, Chem. Eng. Res. Des., 92(3) (2014) 447-452.

[75] A. Noghrehabadi, A. Behseresht, M. Ghalambaz and J. Behseresht, Natural-convection flow of nanofluids over vertical cone embedded in non-Darcy porous media, J. Therm. Phys. Heat Transfer, 27(2) (2013) 334-341.

[76] M.M. Keshtkar and J. Hadizadeh, Boundary layer flow over a porous medium of a nanofluid past from a vertical cone, Int. J. Innov. Res. Sci. Eng., 2347-3207.

[77] E.L.A. Fauzi, S. Ahmad and I. Pop, Mixed convection boundary layer flow from a vertical cone in a porous medium filled with a nanofluid, W. Acad. Sci. Eng. Tech., 70 (2012) 10-25.

[78] F.N. Lin, Laminar free convection from a vertical cone with uniform surface heat flux, Letters Heat Mass Transfer, 3 (1976) 49-58.

[79] P.J. Singh and S. Roy, Unsteady mixed convection flow over a vertical cone due to impulsive motion, Int. J. Heat Mass Transfer, 50(5-6) (2007) 949-959.

[80] B. Pullepu, K. Ekambavanan and A.J. Chamkha, Unsteady laminar free convection from a vertical cone with uniform surface heat flux, Nonlinear Anal. Model. Control, 13(1) (2008) 47-60.

[81] B. Pullepu and A.J. Chamkha, Transient laminar MHD free convective flow past a vertical cone with non-uniform surface heat flux, Nonlinear Anal. Model. Control, 14(4) (2009) 489-503.

[82] C.S. Balla and K. Naikoti, Finite element analysis of magnetohydrodynamic transient free convection flow of nanofluid over a vertical cone with thermal radiation, Proc. Inst. Mech. Eng. N: J. Nanomaterials, Nanoengineering and Nanosystems, 230(3) (2016) 161-173.

[83] A.Majeed, T. Javed and I. Mustafa, Heat transfer analysis of boundary layer flow over hyperbolic stretching cylinder, Alex. Eng. J., 55(2) (2016) 1333-1339.

[84] E.M. Elbashbeshy, T.G. Emam and E.A.A. Sayed, Effect of thermal radiation on free convection flow and heat transfer over a truncated cone in the presence of pressure work and heat generation/absorption. Therm. Sci., 20(2) (2016) 555-565.

[85] S.A. Gaffar, V.R. Prasad, S.K. Reddy, and O.A. Bég, Magnetohydrodynamic free convection boundary layer flow of non-Newtonian tangent hyperbolic fluid from a vertical permeable cone with variable surface temperature, J Braz. Soc. Mech. Sci., 39(1) (2017) 101-116.

[86] M. Bandaru, M.M. Rashidi and H.S. Raju, Influence of nonliner convection and thermophoresis on heat and mass transfer from a rotating cone to fluid flow in porous medium. Therm. Sci., 21(6B) (2017) 2781-2793.

[87] O.A. Bég, J. Zueco, A. Kadir, T.A. Bég and U.F. Khan, Network electro-thermal simulation of non-isothermal magnetohydrodynamic heat transfer from a transpiring cone with buoyancy and pressure work, Int. J. Appl. Comp. Math., 3(2) (2017) 1525-1547.

[88] K. Parand, Z. Delafkar, and F. Baharifard, Rational Chebyshev Tau method for solving natural convection of Darcian fluid about a vertical full cone embedded in porous media whit a prescribed wall temperature, World Acad. Sci. Eng. Tech., 5(8) (2011) 1186-1191.

[89] D.A.S. Rees and I. Pop, Free convection induced by a horizontal wavy surface in a porous medium, Fluid Dyn. Res., 14 (1994) 151-166.

[90] D.A.S. Rees and I. Pop, Boundary layer flow and heat transfer on a continuous moving wavy surface, Acta Mech., 112 (1995) 149-158.

[91] M.A. Hossain and I. Pop, Magneto-hydrodynamic boundary layer flow and heat transfer on a continuous moving wavy surface, Arch. Mech., 48(5) (1996) 813- 823.

[92] M. Narayana, P. Sibanda, S.S. Motsa and P.G. Siddheshwar, On double-diffusive convection and cross diffusion effects on a horizontal wavy surface in a porous medium, Bound. Val. Prob., 88 (2012) 1–22.

[93] H.J. Jang, W.M. Yan, W. M., and H.C. Liu, Natural convection heat and mass transfer along a vertical wavy surface, Int. J. Heat Mass Transfer, 46(6) (2003) 1075-1083.

[94] F.M. Hady, R.A. Mohamed and A. Mahdy, MHD free convection flow along a vertical wavy surface with heat generation or absorption effect. International Commun. Heat Mass Transfer, 33(10) (2006) 1253-1263.

[95] C.Y. Cheng, Non-similar solutions for double diffusive convection near a frustum of a wavy cone in porous media**.** Appl. Math. Comp., 194(1) (2007) 156-167.

[96] A. Rahman, M.M. Molla and M.M.A. Sarker, Natural convection flow along the vertical wavy cone in case of uniform surface heat flux where viscosity is an exponential function of temperature, Int. J. Heat Mass Transfer, 38(6) (2011) 774-780.

[97] N. Parveen and M.A. Alim, Numerical solution of temperature dependent thermal conductivity on MHD free convection flow with joule heating along a vertical wavy surface, J. Mech. Eng., 44(1) (2014) 43-50.

[98] T. Javed, H. Ahmad and A. Ghaffari, Influence of radiation on vertical wavy surface with constant heat flux: Using Keller box scheme. Alex. Eng. J., 55(3) (2016) 2221-2228.

[99] S. Siddiqa, N. Begum, A. Waheed, M.A. Hossain and R.S. Reddy, Numerical solution of contaminated oil along a vertical wavy frustum of a cone, Therm. Sci., (2016) Doi: TSCI160425231S

[100] I. Mustafa, T. Javed and A. Ghaffari, Hydromagnetic natural convection flow of water-based nanofluid along a vertical wavy surface with heat generation, J. Mol. Liq., 229 (2017) 246-254.

[101] A. Mehmood, M.S. Iqbal, S. KHAN and S. Munawar, Entropy analysis in moving wavy surface boundary layer, (2017) DOI: TSCI161029029M

[102] I. Mustafa, T. Javed, Heat transfer in natural convection flow of nanofluid along a vertical wavy plate with variable heat flux. Therm. Sci., (2017) Doi: TSCI161012014M

[103] S. Siddiqa and A.M. Hossain, Heat and mass transfer effects on natural convection flow along a horizontal triangular wavy surface, Therm. Sci., 21(2) (2017), 977-987.

[104] M.S. Abdallah and B. Zeghmati, Effects of the wavy surface on free convection-radiation along an inclined plate, World Acad. Sci. Eng. Tech., Int. J. Phys. Math. Sci. 7(6) (2013) 990-996.

[105] D. Srinivasacharya, B. Mallikarjuna, and R. Bhuvanavijaya, Effects of thermophoresis and variable properties on mixed convection along a vertical wavy surface in a fluid saturated porous medium, Alex. Eng. J., 55(2) (2016) 1243-1253.

[106] D. Ravipati, Free convection along a vertical wavy surface in a nanofluid, MS Thesis, Cleveland State University, 2012.

[107] A.J. Chamkha and S.E. Ahmed, Unsteady MHD heat and mass transfer by mixed convection flow in the forward stagnation region of a rotating sphere at different wall conditions, Chem. Eng. Commun., 199(1) (2012) 122-141.

[108] A.J. Chamkha and S.E. Ahmed, Unsteady MHD heat and mass transfer by mixed convection flow in the forward stagnation region of a rotating sphere in the presence of chemical reaction and heat source, Proc. World Congress Eng., 1 (2011).

[109] N.S. Bondareva, M.A. Sheremet and I. Pop, Magnetic field effect on the unsteady natural convection in a right-angle trapezoidal cavity filled with a nanofluid: Buongiorno's mathematical model, Int. J. Num. Methods Heat Fluid Flow, 25(8) (2015) 1924-1946.

[110] A.Mahdy and S E. Ahmed. Thermosolutal Marangoni boundary layer magnetohydrodynamic flow with the Soret and Dufour effects past a vertical flat plate, Eng. Sci. Tech. Int. J., 18(1) (2015) 24-31.

[111] E. Pohlhausen, Der Wareastausch Zwischen Festen Kor- penn und Flussigkeiten mit Kleineer Reibung und Klein- erwarmeletung, Zeitschrift für Angewandte Mathematik und Mechanik, 2 (1921) 115-121.

[112] S. Ostrach, An analysis of laminar free convective flow and heat transfer about a flat plate parallel to direction of the generating body force, NASA (1953) (1111).

[113] L.S. Yao, Natural convection along a vertical wavy surface, ASME J. Heat Transfer, 105 (1983) 465-468.

[114] S.G. Moulic and L.S. Yao, Natural convection along a wavy surface with uniform heat flux, ASME J. Heat Transfer., 111 (1989) 1106-1108.

[115] D.A.S. Rees and I. Pop, A note on a free convection along a vertical wavy surface in a porous medium, ASME J. Heat Transfer, 115 (1994) 505-508.

[116] M.A. Hossain and D.A.S. Rees, Combined heat and mass transfer in natural convection flow from a vertical wavy surface, Acta. Mech., 136 (1999) 133-141.

[117] C.Y. Cheng, Natural convection heat and mass transfer near a vertical wavy surface with constant wall temperature and concentration in a porous medium, Int. Commun. Heat Mass Transfer, 27 (2000) 1143-1154.

[118] R.S.R. Gorla and M. Kumari, Free convection along a vertical wavy surface in a nanofluid, J. Nano Eng. Nano Sys., 225(3) (2011) 133-142.

[119] S.E. Ahmed and M.A. El-Aziz, Effect of local thermal non-equilibrium on unsteady heat transfer by natural convection of a nanofluid over a vertical wavy surface, Meccanica, 48(1) (2013) 33-43.

[120] J.L. Baker, R.E. Faw and F.A. Kulacki, Post accident heat removal-Part I: Heat transfer within an internally heated non-boiling liquid layer, Nucl. Sci. Eng., 61(2) (1976) 222-230.

[121] M.A. Delichatsios, Air entrainment into buoyant jet flames and pool fires, Comb. Flame, 70(1) (1987) 33-46.

[122] K. Vajravelu and A. Hadjinicolaou, Heat transfer in a viscous fluid over a stretching sheet with viscous dissipation and internal heat generation, Int. Commun. Heat Mass Transfer, 20 (1993) 417-430.

[123] M.M. Molla, M.A. Hossain and M.A. Taher, Magnetohydrodynamic natural convection flow on a sphere with uniform heat flux in presence of heat generation, Acta Mech., 186(1-4) (2006) 75-86.

[124] M.M. Alam, M.A. Alim and M.M. Chowdhury, Viscous dissipation effects on MHD natural convection flow over a sphere in the presence of heat generation, Nonlinear Anal. Model. Control, 12(4) (2007) 447-459.

[125] A.A. Mamun, Z.R. Chowdhury, M.A. Azim and M.A. Maleque, Conjugate heat transfer for a vertical flat plate with heat generation effect, Non-linear Anal. Model. Control, 13(2) (2008) 213-223.

[126] A.A. Mamun, Z.R. Chowdhury, M.A. Azim and M.M. Molla, MHD-conjugate heat transfer analysis for a vertical flat plate in presence of viscous dissipation and heat generation, Int. Commun. Heat Mass Transfer, 35(10) (2008) 1275-1280.

[127] M.A. Mansoor and S.E. Ahmed, A numerical study on natural convection in porous media-filled an inclined triangular enclosure with heat sources using nanofluid in the presence of heat generation effect, Eng. Sci. Tech., Int. J. 18(3) (2016) 485-495.

[128] M.M. Molla, M.A. Hossain and L.S. Yao, Natural convection flow along a vertical wavy surface with heat generation/absorption, Int. J. Therm. Sci., 43(2) (2004) 157-163.

[129] F.M. Hady, R.A. Mohamed and A. Mahdy, MHD free convection flows along a vertical wavy surface with heat generation or absorption effect, Int. Commun. Heat Mass Transfer, 33(10) (2006) 1253-1259.

[130] M.A. Alim, S. Alam and M. Miraj, Effects of temperature dependent thermal conductivity on natural convection flow along a vertical wavy surface with heat generation, Int. J. Eng. Tech., 11(6) (2011) 60-69.

[131] N. Parveen and M.A. Alim, MHD free convection flow in presence of joule heating and heat generation with viscosity dependent on temperature along a vertical wavy surface, Int. J. Energy Tech., 4 (21) (2012) 1-10.

[132] N. Parveen and M.A. Alim, MHD free convection flow with temperature dependent thermal conductivity in presence of heat absorption along a vertical wavy surface, Pro. Eng., 56 (2013) 68-75.

[133] K.H. Kabir, M.A. Alim and L S. Andallah, Effects of viscous dissipation on MHD natural convection flow along a vertical wavy surface with heat generation, Amer. J. Comp. Math., 3 (2013) 91-98.

[134] S. Siddiqa, M.A. Hossain and S.C. Saha, Natural convection flow with surface radiation along a vertical wavy surface, Numer. Heat Transfer, 64 (2013) 400-415.

[135] M.M. Molla, M.A. Taher, M.M. Chowdhury, and M.A. Hossain, Magnetohydrodynamic natural convection flow on a sphere in presence of heat generation, Nonlinear Anal. Model. Control, 10(4) (2005) 349-363.

[136] M.M. Alam, M.A. Alim and M.M. Chowdhury, Viscous dissipation effects on MHD natural convection flow over a sphere in the presence of heat generation, Nonlinear Anal.: Model. Control, 12(4) (2007) 447-459.

[137] A.A. Mamun, Z.R. Chowdhury, Z. R., M.A. Azim, and M.A. Maleque, Conjugate heat transfer for a vertical flat plate with heat generation effect, Nonlinear Anal. Model. Control, 13(2) (2008) 213-223.

[138] C.Y. Cheng, Natural convection heat transfer from a horizontal isothermal elliptical cylinder with internal heat generation, International Commun. Heat Mass Transfer, 36(4) (2009) 346-350.

[139] C.Y. Cheng, Natural convection boundary layer on a horizontal elliptical cylinder with constant heat flux and internal heat generation, Int. Commun. Heat Mass Transfer, 36(10) (2009) 1025-1029.

[140] T. Thumma, O.A. Bég, and A. Kadir, Numerical study of heat source/sink effects on dissipative magnetic nanofluid flow from a non-linear inclined stretching/shrinking sheet, J. Mol. Liq., 232 (2017) 159-173.

[141] M. Bhavana, D.C. Kesavaiah, and A. Sudhakaraiah, The Soret effect on free convective unsteady MHD flow over a vertical plate with heat source, International Journal of Inno. Res. Sci., Eng. Tech., 2(5) (2013) 1617-1628

[142] R. Choudhury, P. Dhar and D. Dey, Viscoelastic MHD boundary layer flow with heat and mass transfer over a continuously moving inclined surface in presence of energy dissipation, Heat Mass Transfer, 8(4) (2013) 146-155.

[143] O.D. Makinde, F. Mabood and M.S. Ibrahim, Chemically reacting on MHD boundary layer flow of nanofluid over a non-linear stretching sheet with heat source/sink and thermal radiation, Therm. Sci. 22(1B) (2018) 495-506.

[144] B. Shankar and Y. Yirga, Unsteady heat and mass transfer in MHD flow of nanofluids over stretching sheet with a non-uniform heat source/sink, Int. J. Math., Comp. Sci. Eng.,7 (2013) 1267-1275.

[145] R.A. Mohamed, S.M. Abo-Dahab and T.A. Nofal, Thermal radiation and MHD effects on free convective flow of a polar fluid through a porous medium in the presence of internal heat generation and chemical reaction, Math. Prob. Eng., 804719, 5(1) (2010) 9-10.

[146] P.M. Krishna, V. Sugunamma, and N. Sandeep, Effects of radiation and chemical reaction on MHD boundary layer flow over a moving vertical porous plate with heat source, Adv. Phys. Theor. Appl., 26 (2013) 109-128.

[147] C.A. Reddy and B. Shankar, Magneto hydrodynamics stagnation point flow of a nanofluid over an exponentially stretching sheet with an effect of chemical reaction, heat source and suction/injunction, W. J. Mech., 5(11) (2015) 211-221.

[148] H.J. Merk and J.A. Prins, Thermal convection in laminar boundary layer-I, Int. Appl. Sci. Res., A4 (1953) 11-24.

[149] H.J. Merk and J.A. Prins, Thermal convection in laminar boundary layer-II, Int. Appl. Sci. Res., A4 (1954) 195-206.

[150] S. Roy, Free convection from a vertical cone at high Prandtl numbers, ASME J. Heat Transfer, 96 (1974) 115-117.

[151] F.N. Lin, Laminar convection from a vertical cone with uniform surface heat flux, Letts. Heat Mass Transfer, 3 (1976) 49-58.

[152] M. Alamgir, Overall heat transfer from vertical cones in laminar free convection an approximate method, ASME, J. Heat Transfer, 101(1) (1979) 174-176.

[153] I. Pop and H.S. Takhar, Compressibility effects in laminar free convection from a vertical cone, Appl. Sci. Res., 48 (1991) 71-82.

[154] K.Y. Yih, The effect of uniform lateral mass flux on free convection about a vertical cone embedded in porous media, Int. Commun. Heat Mass Transfer, 24 (1997) 1195-1205.

[155] C.Y. Cheng, Natural convection boundary layer flow of a micro polar fluid over a vertical permeable cone with variable wall temperature, Int. Commun. Heat Mass Transfer, 38 (2011) 429-433.

[156] M.A. Hossain and S.C. Paul, Free convection from a vertical permeable cone with non-uniform surface temperature, Acta. Mech., 151 (2001) 103-114.

[157] M.A. Hossain and S.C. Paul, Free convection from a vertical permeable circular cone with non-uniform surface heat flux, Heat Mass Transfer, 37 (2001) 167-173.

[158] C.Y. Cheng, Free convection heat transfer from a non-isothermal permeable cone with suction and temperature dependent viscosity, J. App. Sci. Eng., 18(1) (2015) 17-24.

[159] B. Pullepu, K. Ekambavanan and A.J. Chamkha, Unsteady laminar free convection from a vertical cone with uniform surface heat flux, Non-linear Anal. Model. Control, 13 (1) (2008) 47-60.

[160] I. Pop and T.Y. Na, Natural convection of a Darcian fluid about a wavy cone, Int. Commun. Heat Mass Transfer, 21 (1994) 891-899.

[161] I. Pop and T.Y. Na, Natural convection from a wavy cone, Appl. Sci. Res., 54 (1995) 125-136.

[162] I. Pop and T.Y. Na, Natural convection over a frustum of a wavy cone in a porous medium, Mech. Res. Commun., 22 (1995) 81-190.

[163] C.Y. Cheng, Natural convection heat and mass transfer near a wavy cone with constant wall temperature and concentration in a porous medium, Mech. Res. Commun., 27 (2000) 613-620.

[164] M.A. Hossain , M.S. Munir and I. Pop, Natural convection flow of a viscous fluid with viscosity inversely proportional to linear function of temperature from a vertical wavy cone, Int. J. Therm. Sci., 40 (2001) 366-371.

[165] A. Rahman, M.M. Molla and M.M.A. Sarker, Natural convection flow along the vertical wavy cone in case of uniform surface heat flux where viscosity is an exponential function of temperature, Int. Commun. Heat Mass Transfer, 38 (2011) 774-780.

[166] D.J. Acheson, *Elementary fluid dynamics*, Oxford University Press 1990.

[167] G.K. Batchelor, *An introduction to fluid dynamics*, Cambridge University Press 1967.

[168] Y. Jaluria, *Computer Methods for Engineering*, Allyn Bacon Inc., Boston 1988.

[169] I.A. Mudunkotuwa and V.H. Grassian, Impact of surface structure and surface energetics on understanding the behavior of nanomaterials in the environment, J. Environ. Monit., 13 (5) (2011) 1135-1144.

[170] B.C. Pak, and Y. I. Cho, Hydrodynamic and heat transfer study of dispersed fluids with submicron metallic oxide particles, Exp. Heat Transfer Int. J., 11(2) (1998) 151-170.

[171] K.S. Hwang, S.P. Jang and S.U.S. Choi, Flow and convective heat transfer characteristics of water-based Al2O3 nanofluids in fully developed laminar flow regime, Int. J. Heat Mass Transfer, 52 (2009) 193-199.

[172] S.P. Jang and S. U. S. Choi. Role of Brownian motion in the enhanced thermal conductivity of nanofluids, Appl. Phys. Letts., 84(21) (2004) 4316–4318.

[173] S.P. Jang and S.U.S. Choi, Effects of various parameters on nanofluid thermal conductivity, ASME J. Heat Transfer, 129(5) (2007) 617-623.

[174] A. Einstein, A new determination of the molecular dimensions, Ann. Phys., 19(2) (1906) 289-306.

[175] A. Einstein, The theory of the Brownian motion, Ann. Phys., 19(2) (1906) 371-381.

[176] A. Einstein, Correction of my work: A new determination of the molecular dimensions, Ann. Phys., 34(3) (1911) 591-592.

[177] H.C. Brinkman, The viscosity of concentrated suspensions and solution, J. Chem. Phys., 20 (1952) 571-581.

[178] H.B. Keller, Numerical methods in boundary layer theory, Ann. Rev. Fluid Mech., 10 (1988) 793-796.

[179] T. Cebeci and P. Bradshaw, *Physical and computational aspects of convective heat transfer*, Springer New York 1988.

[180] T.Y. Na, *Computational methods in engineering boundary value problems*, Academic Press New York 1979.

[181] S. Siddiqui, On convection flow of viscous fluid along a surface with and without radiation effect, PhD. Dissertation, COMSATS Institute of Information Technology Islamabad, 2011.

[182] G. Saha, Heat transfer performance investigation of nanofluids flow in pipe, Doctoral dissertation, University of Glasgow, 2016.

[183] I. Mustafa, Study of fluid flows around a stretching cylinder, PhD. Dissertation, IIUI, 2016.

[184] A. Ghaffari, Numerical study of oblique stagnation point flow of non-linear fluids, PhD. Dissertation, IIUI, 2016.

[185] A. Majeed, Study of fluid flows around a stretching cylinder, PhD. Dissertation, IIUI, 2017.

[186] I. Pop and D.B. Ingham, *Convection heat transfer*, Pergamon Oxford UK 2001.

[187] P. Singh, V. Radhakrishnan and K.A. Narayan, Non-similar solutions of free convection flow over a frustum of a cone. Ingen. Arch., 59 (1989) 382-389.

[188] H.M. Elshehabey, F.M. Hady, S.E. Ahmed and R.A. Mohamed, Numerical investigation for natural convection of a nanofluid in an inclined L-shaped cavity in the presence of an inclined magnetic field, Int. Commun. Heat Mass Transfer, 57 (2014) 228-238.

[189] T.C. Chiam, Magnetohydodynamic heat transfer over a non-isothermal stretching sheet, Acta Mech., 122 (1997) 169-179.

[190] M.A. Hossain, S. Kabir, D.A.S. Rees, Natural convection of fluid with temperature dependent viscosity from heated vertical wavy surface, ZAMP, 53 (2002) 48-52.